

UC Irvine

UC Irvine Electronic Theses and Dissertations

Title

Oxygen, pH, and antibiotics drive changes in cystic fibrosis bacterial physiology

Permalink

<https://escholarship.org/uc/item/8bz4j5jv>

Author

Gallagher, Tara

Publication Date

2020

License

<https://creativecommons.org/licenses/by/4.0/> 4.0

Peer reviewed|Thesis/dissertation

UNIVERSITY OF CALIFORNIA,
IRVINE

Oxygen, pH, and antibiotics drive changes in cystic fibrosis bacterial physiology

DISSERTATION

submitted in partial satisfaction of the requirements
for the degree of

DOCTOR OF PHILOSOPHY

in Biological Sciences

by

Tara Gallagher

Dissertation Committee:
Assistant Professor Katrine Whiteson, Chair
Associate Professor Michelle Digman
Dr. Felix Grun
Associate Professor Allon Hochbaum
Assistant Professor Albert Siryaporn

2020

Portion of introduction © 2018 American Society for Microbiology
Chapter 1 © 2018 American Society for Microbiology
Chapter 2 © 2019 American Society for Microbiology
All other materials © 2020 Tara Gallagher and Katrine Whiteson

DEDICATION

To

The Gallagher clan:
Susan, Mike, Rach, and Alexsh Gallagher

&

The newest member of my clan:
Simon Leemans

TABLE OF CONTENTS

	Page
LIST OF FIGURES	iv
LIST OF TABLES	vi
ACKNOWLEDGEMENTS	vii
VITA	viii
ABSTRACT OF THE DISSERTATION	xiii
INTRODUCTION	1
CHAPTER 1: Tracking Polymicrobial Metabolism in Cystic Fibrosis Airways: <i>Pseudomonas aeruginosa</i> Metabolism and Physiology Are Influenced by <i>Rothia mucilaginosa</i> -Derived Metabolites	16
CHAPTER 2: Cystic Fibrosis-Associated <i>Stenotrophomonas maltophilia</i> Strain-Specific Adaptations and Responses to pH	31
CHAPTER 3: Visualization of <i>Pseudomonas aeruginosa</i> pyocyanin reduction at the surface of biofilms	69
CHAPTER 4: LC-MS detection of antibiotic agents in sputum from persons with cystic fibrosis	105
Summary and future directions	158
APPENDIX A: Method for DNA extraction from human saliva and sputum	163
APPENDIX B: Methods for Wound genome analyses	165
REFERENCES	174

LIST OF FIGURES

	Page
Figure i Cystic fibrosis microbiome schematic	11
Figure ii Dissertation aims schematic	12
Figure 1.1 <i>R. mucilaginosa</i> metabolism of ¹³ C glucose	26
Figure 1.2 Cross-feeding interactions between <i>R. mucilaginosa</i> and <i>P. aeruginosa</i>	27
Figure S1.1 Abundances of isotope-enriched metabolites for <i>R. mucilaginosa</i> grown in artificial-sputum medium	29
Figure S1.2 Abundances of isotope-enriched glutamate ions	30
Figure 2.1 <i>S. maltophilia</i> genomics	57
Figure 2.2 <i>S. maltophilia</i> growth in different pH	59
Figure 2.3 <i>S. maltophilia</i> metabolomics in different pH	63
Figure 2.4 <i>S. maltophilia</i> transcriptomics in different pH	64
Figure 2.5 <i>S. maltophilia</i> sputum metatranscriptomes	65
Figure 2.6 <i>S. maltophilia</i> gene categories expression	66
Figure 2.7 Acidic stress response genes	67
Figure 2.8 Proposed model for <i>S. maltophilia</i> colonization of CF airways	68
Figure 3.1 Phasor schematic	87
Figure 3.2 FLIM and HIM phasor components	88
Figure 3.3 <i>P. aeruginosa</i> culture phasor coordinates and fractional contribution images	89
Figure 3.4 <i>P. aeruginosa</i> phasors	91
Figure 3.5 Comparison of FLIM and HIM predictions	92
Figure 3.6 Fractional contributions and lifetime images of metabolites in biofilms	93
Figure 3.7 Fractional contributions of pyocyanin in biofilms	94

Figure S3.1	Emission spectra of fluorophores	95
Figure S3.2	Emission spectra and FLIM of chemically and electrochemically reduced pyocyanin	96
Figure S3.3	<i>P. aeruginosa</i> in M9 glucose FLIM phasor	98
Figure S3.4	Poster figure: Examples of FLIM images	101
Figure S3.5	Poster figure: FLIM phasor of <i>P. aeruginosa</i> in different conditions	102
Figure S3.6	Poster figure: Variation in G coordinates	103
Figure 4.1	Chromatograms of antibiotics	128
Figure 4.2	Comparison of LC-MS limits of detection	129
Figure 4.3	Comparison of extraction methods	130
Figure 4.4	Antibiotics detected in sputum replicates	132
Figure 4.5	Subject antibiotic usage	133
Figure 4.6	Concentrations of detected antibiotics	134
Figure S4.1	Antibiotic combinations on same day	139
Figure S4.2	LC-MS run information	140
Figure S4.3	Subject metadata correlations with LC-MS detection rates	141
Figure S4.4	Daily metrics for individual subjects	143

LIST OF TABLES

		Page
Table i	Introduction: Cystic fibrosis lung microbiome & antibiotics studies	XX
Table S3.1	Poster table: PERMANOVA analyses	103
Table 4.1	Multiple reaction monitoring parameters for antibiotics	131
Table 4.2	Survey options	136
Table 4.3	Contingency tables comparing LC-MS data to subject usage	137
Table S4.1	Antibiotics properties	153
Table S4.2	Comparison of mobile phases	154
Table S4.3	Comparison of LC-MS limits of detection to minimum inhibitory concentrations	155
Table S4.4	Limit of detections for different extraction methods	156

ACKNOWLEDGEMENTS

First and foremost, thank you to my advisor, Katrine Whiteson, who is one of the most dedicated scientists I know. Thank you for teaching me how to think holistically about a biological problem. Thank you for being patient with me as you've helped me grow to become a better scientist.

Thank you to my committee members, Michelle Digman, Felix Grun, Allon Hochbaum, and Albert Siryaporn. I respect all of you to the utmost degree. It means a lot to me that you are all always so willing to help me, and I am grateful and appreciative of your support.

To Joann, Andrew, Julio, Jason, and Whitney: you're the best lab mates anyone could ever ask for. I can't imagine getting my PhD without you guys.

To my research buddies: Amanda, Clark, Miki, Joe, Josh, Erika, Miranda, and Christina – thank you so much for all your support. None of this would have been possible without your help.

Thank you to Vasan Venugopalan for being my biophotonics mentor and giving me the opportunity to be part of the NSF IGERT BEST program. Thank you for giving me financial support for two years. Thank you for unintentionally introducing me to my husband and fellow IGERTee, Simon.

Thank you to John LiPuma, Linda Kalikin, Lindsay Caverly, and Lisa Carmody from University of Michigan for your support throughout my PhD. I appreciate our collaboration

and time spent working together. I feel lucky to be part of such an effective and caring team.

Thank you to all my longstanding friends & family, both in science and not in science, who have continuously uplifted me throughout this process... My friends: Jenna, Jesse, Lee, & Aaron --- you are the reason why I love CMB. My fellow Dukes: Kevin and Steve. My family: Susan, Mike, Rachel, Brian, Alex, Simon, Wim, Annette, Eline, Richie, Nico, and Nelia! I love you all and am so blessed to have your love and support.

Financial support was also provided by the NIH, Gilead, and the CCBS Department. Thank you to the Mortazavi lab for generously allowing us to use their sequencer. Thank you to UCI's HPC staff for doing an amazing job running the HPC and helping irritating users like me!

Portions of the introduction, Chapter 1, and Chapter 2 were published with the permission of American Society for Microbiology. One part of the introduction is a reprint of excerpts from the publication in Journal of Bacteriology. The text of chapter 1 is a reprint of the material as it appears in the journal mSphere. The text of Chapter 2 is a reprint of the material as it appears in the Journal of Bacteriology.

Curriculum vitae of Tara Gallagher

Education:

University of California, Irvine, Irvine, CA
M.S./Ph.D. in Molecular Biology & Biochemistry (anticipated Spring 2020) GPA: 3.97/4.0

James Madison University, Harrisonburg, VA
M.S. in Biological Sciences (June 2015) GPA: 3.96/4.0

Virginia Tech Blacksburg, VA
B.S. in Biology (May 2013) Summa Cum Laude GPA: 3.89/4.0

Research Experience:

Ph.D. Student Researcher, University of California, Irvine (Irvine, CA) August 2015-present

- Developed high throughput LC-MS assay to fulfill unmet need of incorporating antibiotics data into microbiome studies (submitting manuscript to JAAC)
- Determined acidic pH is stressful and increases antibiotic tolerance in an opportunistic pathogen, *Stenotrophomonas maltophilia*, using genomics, transcriptomics, and metatranscriptomics (published in JBact)
- Invited to give a talk at the 2018 Pacific AAAS meeting and write a commentary on utilizing stable isotopes to probe bacterial metabolism (published in mSphere and JBact)
- Awarded a seed grant (\$11K) and travel grant (\$500) for my research on visualizing bacterial metabolism with cutting-edge fluorescence lifetime and spectral microscopy (manuscript in prep)

M.S. Student Researcher, James Madison University (Harrisonburg, VA)
2013-2015

- Collaborated with interdisciplinary team to make novel antimicrobials to kill antibiotic-resistant organisms, resulting in two publications and a poster presentation award
- Awarded teaching fellowships for instructing 100 students in four biology laboratories

Undergraduate Student Researcher, Virginia Tech (Blacksburg, VA) 2012-13

- Determined the surface protein, type four pili, is necessary for the pathogen *Clostridium perfringens* to adhere to muscle (published in BMC Genomics)

Grants & Fellowships

Dr. William F. Holcomb Scholarship (\$1K) June 2019

- Achieved recognition for excellence in biomedical research at the 2019 Department of Molecular Biology and Biochemistry Graduate Honors Convocation at University of California, Irvine

- American Society for Microbiology Student Travel Award (\$500) May 2019
- Selected by the American Society for Microbiology to present my dissertation work on a cutting-edge imaging approach at the national Microbe 2019 meeting: "Bacterial Metabolism in Infection-Relevant Conditions with Label-Free Fluorescence and Metabolomics"
- Center for Complex Biological Systems Opportunity Award(\$11K) Summer 2016
- Awarded a seed grant for my proposal on "Microscale biogeography of phage-infection and antibiotic resistance in biofilms", and invited to present this work at the American Society for Microbiology national 2019 meeting and Center for Complex Biological Systems symposium
- National Science Foundation IGERT Fellowship (\$80K) 2016-2018
- Awarded the NSF-funded Integrative Graduate Education and Research Traineeship (IGERT) in Biophotonics for two years and gained experience in optics and biomedical devices
- Sigma Xi Grants in Aid of Research (\$760) Spring 2014
- Awarded by Sigma Xi Scientific Research Society for my research proposal: "Antibacterial activities of novel cationic amphiphiles"

Professional Publications:

First author publications:

T. Gallagher, J. Phan, A. Oliver, A.B. Chase, W.E. England, S. Wandro, C. Hendrickson, S.F. Riedel, K. Whiteson, 2019. *Stenotrophomonas maltophilia* strain-specific adaptations and responses to pH. *Journal of Bacteriology* 201: e00478-18.

T. Gallagher, J. Phan, K. Whiteson. Getting our fingers on the pulse of slow-growing bacteria in hard-to-reach places. *Journal of Bacteriology* 200 (24), e00540-18. *Commentary

*B. Gao, *T. Gallagher, Y. Zhang, M. Elbadawi-Sidhu, Z. Lai, O. Fiehn, K.L. Whiteson. 2018. Tracking Polymicrobial Metabolism in Cystic Fibrosis Airways: *Pseudomonas aeruginosa* Metabolism and Physiology Are Influenced by *Rothia mucilaginosa*-Derived Metabolites. *mSphere* 3(2):e00151-18.
*Co-first authors

T.M. Gallagher, J.N. Marafino, B.K. Wimbish, B. Volkers, G. Fitzgerald, K. McKenna, J. Floyd, N.T. Minahan, B. Walsh, K. Thompson, D. Bruno, M. Paneru, S. Djikeng, S. Masters, S. Haji, K. Seifert, K.L. Caran "Hydra Amphiphiles: Using Three Heads and One Tail to Influence Aggregate Formation and to Kill Pathogenic Bacteria." *Colloids and Surfaces B: Biointerfaces*. 2017, 157, 440-448.

Co-author publications:

S.R. Murray, A.H. Hartman, T.M. Gallagher, G.J. Camper, R.V. Jensen, S.B. Melville. 2020. "Clostridium perfringens grown in liquid or on plates have large-scale differences in gene expression levels, including genes encoding type IV pili-associated proteins." BMC Genomics 21(45).

J. Phan, T. Gallagher, A. Oliver, W.E. England, K. Whiteson. 2018. Fermentation products in the cystic fibrosis airways induce aggregation and dormancy-associated expression profiles in a CF clinical isolate of *Pseudomonas aeruginosa*. FEMS microbiology letters 365 (10), fny082

C.Q. Nguyen, W.J. Thrift, A. Bhattacharjee, S. Ranjbar, T. Gallagher, M. Darvishzadeh-Varcheie, R.N. Sanderson, F. Capolino, K. Whiteson, P. Baldi, A. Hochbaum, R. Ragan. et al. 2018. Longitudinal Monitoring of Biofilm Formation via Robust Surface-Enhanced Raman Scattering Quantification of *Pseudomonas aeruginosa*-Produced Metabolites. ACS applied materials & interfaces 10(15): 12364-12373.

S. Wandro, A. Oliver, T. Gallagher, C. Weihe, W. England, J.B.H. Martiny, K. Whiteson. 2018. Predictable molecular adaptation of coevolving *Enterococcus faecium* and lytic phage EfV12-phi1. Frontiers in microbiology 9: 3192

S. Wandro, L. Carmody, T. Gallagher, J.J. LiPuma, K. Whiteson. 2017. Making it last: Storage time and temperature have differential impacts on metabolite profiles of airway samples from cystic fibrosis patients. mSystems 2(6), e00100

J.N. Marafino, T.M. Gallagher, J. Barragan, B.L. Volkers, J.E. LaDow, K. Bonifer, G. Fitzgerald, J.L. Floyd, K. McKenna, N.T. Minahan, B. Walsh, K. Seifert, K.L. Caran. 2015. "Colloidal and Antibacterial Properties of Novel Triple-Headed, Double-Tailed Amphiphiles: Exploring Structure- Activity Relationships and Synergistic Mixtures." Bioorg. Med. Chem. 23, 3566-3573

Presentations:

American Society for Microbiology Microbe 2019 annual meeting, San Francisco, CA. 2019

- Awarded a travel grant (\$500) to present my poster: "Bacterial Metabolism in Infection-Relevant Conditions with Label-Free Fluorescence and Metabolomics"

Pacific AAAS 2018 Annual Meeting, California State Polytechnic University, Pomona, CA. 2018

- Invited to give a talk on "Tracking metabolic interactions between the cystic fibrosis pathogen, *Pseudomonas aeruginosa* and the oral microbe, *Rothia mucilaginosa*."

Cystic Fibrosis: Ecology, Evolution & Eradication, Telluride Scientific Research Center, CO. 2017

- Gave a talk on “Stable isotope metabolomics and non-invasive imaging of sputum” and discussed improving treatment of cystic fibrosis lung infections with researchers and clinicians.

Prokaryotic Group Research presentation, University of California, Irvine, CA.
2016

- Talk: “Transcriptomic Analysis of a Cystic Fibrosis Isolate”

Pathways to Cures: Clinical Translational Research Day, University of California, Irvine, CA. 2016

- Poster: “A Stenotrophomonas Story: Characterizing an Understudied Cystic Fibrosis Isolate”

American Society for Microbiology, Virginia Branch 2014 meeting, Harrisonburg, VA. 2014

- 1st place poster: “Antibacterial activity of novel triscationic amphiphiles”

Skills:

Spectroscopy:

- Fluorescence lifetime imaging microscopy
- Hyperspectral microscopy
- Liquid Chromatography Mass Spectrometry

Bioinformatics:

- Computational languages: Python, R, Unix (GitHub: github.com/tgallagh)
- Statistical analyses in R
- Metagenomics, transcriptomics and metabolomics

Wet-lab:

- Genetics and cloning in bacteria
- Anaerobic bacterial culturing
- Mouse work, tissue culture and toxicity assays

Community Outreach and Volunteer Experience:

- Coordinated and prepared slides with nationwide directors of microbiome cores for the National Conference of Microbiome Centers in Irvine, CA (2019)
- Tutored math at Turtle Rock Elementary and Middle School (2017)
- Participated in cleanups of nature preserves and beaches in Orange County with the CCBS outreach group (2017-2018)

ABSTRACT OF THE DISSERTATION

Oxygen, pH, and antibiotics drive changes in cystic fibrosis bacterial physiology

by

Tara Gallagher

Doctor of Philosophy in Biological Sciences

University of California, Irvine, 2020

Assistant Professor Katrine Whiteson, Chair

Cystic fibrosis (CF) is a genetic disease that results in the accumulation of dense, dehydrated mucus in the airways. Unclearable mucus contributes to the establishment of long-term microbial communities in the CF airways. Opportunistic pathogens damage the airways by inducing the host inflammatory response and generating toxic metabolites, contributing to decreased quality of life and lifespan (~40 years) for persons with CF. In order to improve treatment of lung infections, it is necessary to understand the role of microbes and microbial metabolism in triggering CF pulmonary exacerbations (CFPE), periods of worsening lung function. While antibiotics ease CFPE symptoms, infections are almost never fully eradicated. To elucidate antibiotic failure, we must first understand how relevant conditions in the airways, particularly around the time of CFPE, shape the microbiome and its antibiotic sensitivity.

CFPE may be characterized by increases in acidity (1), fermentation metabolites (2), and anaerobic bacteria (3). We characterized CF polymicrobial metabolic interactions between the fermenting microbe, *Rothia muciliganosa*, and the opportunistic pathogen,

Pseudomonas aeruginosa (**Chapter 1**). Even in nutrient-rich medium designed to mimic sputum content, *P. aeruginosa* utilized *Rothia*-derived fermentation products to produce amino acids. As both host inflammation and microbial fermentation often result in drops in pH, we next determined that acidic pH is stressful for another CF opportunistic pathogen, *Stenotrophomonas maltophilia*, using transcriptomics and metabolomics (**Chapter 2**). *S. maltophilia* coped with low pH by expressing stress response genes and catabolizing amino acids to synthesize polyamines. Fermentation and subsequent drops in pH can be the result of hypoxia, which is a predominant condition in CF sputum (4). We used a combination of fluorescence lifetime imaging and spectral microscopy to study bacterial metabolism in oxygen gradients (**Chapter 3**).

To tackle the question of how antibiotics impact the microbiome, we need objective information about which antibiotics are reaching the infection-site. Given the diverse properties of antibiotics, the type and concentration of each antibiotic should be incorporated. We developed an LC-MS method to detect 18 antibiotics in 171 sputum samples and assessed the specificity of our LC-MS assay relative to subject self-reported usage (**Chapter 4**).

INTRODUCTION

Cystic fibrosis pulmonary exacerbations are complex, debilitating periods of lung decline

Cystic fibrosis (CF) is a genetic disease that affects 30,000 people in the U.S. (5). People with CF have a mutation in the CF transmembrane receptor (CFTR), resulting in reduced ion transport across epithelial cells and production of misfolded mucin protein (6, 7). Dense, dehydrated mucus impairs mucociliary clearance, contributing to long-term bacterial colonization of the CF airways. The majority of individuals with CF die as a result of respiratory failure caused by chronic bacterial colonization and inflammation in the airways (8). CF lung microbial communities are individualized (9–13), and there remains little understanding of how microbes affect CF clinical status, especially during periods of lung decline known as cystic fibrosis pulmonary exacerbations (CFPE). The majority of adult patients experience CFPE annually, and the cost of a single CFPE was estimated to be \$12,000 in 2017 (14). Although most patients take additional antibiotics during exacerbations which ease symptoms, the damage of exacerbations can be irreversible. Up to 25% of patients fail to return to baseline lung function after an exacerbation event (15). Characterization of microbial structure and metabolism around exacerbations can be used to improve clinical decision-making for antibacterial treatment of CF lung infections and exacerbations.

Understanding *in vivo* bacterial physiology can improve antibiotic treatment of chronic infections and exacerbations

Excerpts from: "Getting Our Fingers on the Pulse of Slow-Growing Bacteria in Hard-To-Reach Places"

Authors: Tara Gallagher, Joann Phan, Katrine Whiteson

**Our full commentary, which reviews Nebeuer et al.'s "Refining the application of microbial lipids as tracers of *Staphylococcus aureus* growth rates in cystic fibrosis sputum" (16), can be found at: DOI: 10.1128/JB.00540-18 (17).*

Pulmonary exacerbations cause irreversible and life-shortening lung damage (15).

Understanding whether and how microbes are involved in triggering exacerbations is a central mystery in the world of CF microbiology, and yet culturing, quantitative PCR (qPCR), and amplicon sequencing of sputum samples have so far largely failed to yield clear signatures associated with exacerbations (18). In fact, there is no measurable increase in abundance of bacteria in general or the common CF pathogen *Pseudomonas* spp. specifically, as measured by culturing or qPCR (19, 20). There are two clearly physiologically distinct populations of bacteria colonizing the airways of CF patients (21): the opportunistic pathogens, including *Pseudomonas* spp. and other Gram negatives that come to dominate the infections as the disease progresses, and the anaerobes that are likely derived from the oral cavity and may themselves be important indicators or even triggers of some exacerbations (3, 11, 22–25). Moving toward active measurements of bacterial metabolic output in the CF

airway environment is an exciting and important step toward understanding the conditions surrounding exacerbations, to enable earlier and more specific diagnosis and treatment.

The inability to discriminate between physiologically active and dead bacteria limits our understanding of the role of bacterial members in a polymicrobial community, including in airway infections (26). Measuring the growth rates of infecting bacteria has always been challenging. Standard clinical microbiology approaches are biased by nutrient-rich, aerobic culture conditions used to isolate bacteria from clinical samples, favoring the growth of bacteria suited to those conditions (27). Improvements were sought using culture independent DNA sequencing-based approaches (28), but many of these studies are stymied by misrepresentation of the community composition. For example, DNA sequencing approaches include the extracellular DNA that is produced by biofilm forming bacteria (29) and do not distinguish DNA from actively dividing microbes. Furthermore, physiologically active bacteria may not be actively dividing and would thus have abundances so low that DNA sequencing-based approaches would not be useful for determining their role in infection. Hence, the basic and central question goes unanswered: what is the growth rate of infecting bacteria *in situ*?

STABLE ISOTOPES: FROM PROBING HUMAN HEALTH TO EXPLORING THE SPECTACULAR DIVERSITY OF MICROBIAL METABOLISM

Stable isotopes—nonradioactive forms of atoms with the same number of protons but a different number of neutrons—were first discovered in the early 20th century. Natural

abundances of stable isotopes vary geographically and biologically, and both natural and spiked isotope-enriched tracers have since been used to probe growth, nutrition, and metabolism in diverse contexts (30). The very early applications of isotope tracers followed the fate of a specific labeled substrate in animals in the 1930s (31, 31).

In microbial ecology, stable isotopes have been used to track the flow of a labeled metabolite through an ecosystem. For example, stable-isotope probing (SIP) involves administering an isotope-labeled substrate *in situ* and utilizing ultracentrifugation to separate and sequence light (nonlabeled) nucleic acids and heavy (labeled) nucleic acids (32). Radajewski *et al.* first used DNA-based SIP to identify soil bacteria that metabolize labeled methanol by sequencing the 16S rRNA amplicons from the heavy DNA fractions (32). Stable isotopes have since proven to be a powerful tool for exploring the central tenets of microbial ecology, that microbes are the most numerous and diverse entities on the planet and that most molecules can be used by microbes.

This idea is also especially important in the context of human health, where bacterial metabolites may play an underappreciated role in disease progression. McLean *et al.* used a combination of RNA- and DNA-based SIP to identify oral microbes that metabolize carbohydrates at a low pH, potentially important drivers of dental plaque formation (33). Another example, the urea breath test, tracks hydrolysis of ¹³C-labeled urea into ¹³C carbon dioxide to diagnose gut infections by *Helicobacter pylori* (34).

There are enormous numbers of microbial metabolites in the human body—as many as one-half of the many thousands of molecules in a drop of blood are thought to be produced or modified by microbial metabolism—leaving an immense and undiscovered frontier in terms of understanding the impact of microbial metabolism on human health (35–38).

Stable-isotope approaches for following active microbial metabolism can be designed to track specific compounds or to globally follow metabolism with mass spectroscopy and Raman spectroscopy (39).

WHAT IS LIMITING MICROBIAL GROWTH?

The CF airway environment is rich in nutrients, including carbon and nitrogen sources (40). However, access to oxygen and other electron acceptors may be quite limiting (4, 41) and may be responsible for the low growth rates observed in this study and others, with doubling times averaging days to weeks. Furthermore, local gradients of pH (4) and toxic molecules of human immune (42) or microbial origin may also alter growth (43–46). Creating realistic culture conditions for clinical microbiology research—beyond recapitulating the nutrient composition in artificial sputum medium recipes that are based in part on metabolite analysis of sputum—should also involve representing the physiological conditions that result in realistic growth rates. Manipulating oxygen access or growing samples under conditions that enable the formation of pH and oxygen gradients is an important step forward (47, 48).

CAVEATS IN THE CONTEXT OF CF MICROBIOLOGY

Sputum samples are local representatives of a heterogeneous airway environment, which is a continuous system with contributions from the upper and lower airways (49). Any individual sputum sample cannot globally represent the heterogeneous lung. In the future,

breath testing may allow for a more global sampling of the airways and the microbial metabolites being produced there (3, 50).

On the opposite end of the spectrum, any bulk method using a heterogeneous sputum sample will not yield spatial resolution at the smaller scales that microbes occupy, or at larger scales, in terms of where in the lung the microbes are located. Approaches for clarifying and imaging microbes from human samples (51) and then resolving the location of the different bacterial species with specific probes are also becoming more feasible (52).

Another layer of complexity is the heterogeneity in single-cellular metabolism that can arise from genomic variants or the complicated microenvironments found in CF sputum. In fact, Neubauer *et al.* noted that single-cell growth rate visualization methods could elucidate whether the observed low growth rates are arising from a subpopulation. In previous work, the authors showed that *S. aureus* replication varied at a single-cell level in a chemostat (29, 45). The oxygen, pH, and metabolite gradients found within CF sputum make it difficult to recapitulate all relevant conditions that dictate bacterial metabolism in an experiment. Sputum is characterized by steep oxygen gradients (53, 54), but the role of anaerobes in CF infection is an active area of debate (25). Nonetheless, the nutrient-rich, aerobic conditions used in research and clinical microbiology labs may select for an unrepresentative subset of the community. Using both anaerobic and aerobic conditions may help in identifying bacterial contributors of CF disease.

EXPANDING OUR KNOWLEDGE OF IN VIVO BACTERIAL PHYSIOLOGY WILL IMPROVE TREATMENT STRATEGIES

Insight into *in vivo* bacterial activity not only affects our clinical measurements but also translates to better representative *in vitro* model systems. The use of poorly representative lab models is particularly detrimental to the assessment of antibiotic susceptibility. In the case of CF and other infections, treatment often involves antibiotics that target replication processes. As a result, slower-replicating bacteria in infection are better able to tolerate antibiotic treatment.

Improved treatment strategies and *in vitro* model systems that are more representative of the low *in vivo* growth rates of cystic fibrosis bacteria are needed. As our knowledge of *in vivo* bacterial growth and metabolism expands, clinical decision-making can also evolve to tackle these slow-growing, hard-to-reach bacterial infections.

ACKNOWLEDGMENTS: We thank Heather Maughan, Andrew Oliver, and Stephen Wandro for their assistance in editing and revising the commentary.

Exacerbation resolution requires studying antibiotic presence in the CF airways

Improving antibacterial treatment of exacerbations requires determining if antibiotics are reaching the CF airways. Most individuals with CF take maintenance antibiotics regularly and additional treatment antibiotics for exacerbations. Out of the dozens of studies describing the CF lung microbiome, ten included information about antibiotics (9, 15, 55–62) (**Table i**). Antibiotic usage was incorporated through medical

charts (56–61); self-reported usage information (9, 62, 63); or LC-MS detection of antibiotics in patient sera (64). Medical charts and self-reported usage are marginally unreliable (65), and the lack of objective antibiotic information may contribute to contradictory findings concerning shifts in the CF microbiome following antibacterial treatment (**Table i**).

The levels of antibiotics in the airways are often unknown, as most pharmacokinetic studies measure antibiotics in serum (66–87) with a smaller number measuring antibiotics at the infection-site (74, 78, 88, 89). Bacterial survival and gene expression are affected by the type of antibiotic and the local concentration (90). Ideally, microbiome models will include information about the local concentration of each antibiotic.

Goals and scope of this dissertation

More knowledge on *in vivo* CF bacterial activity and local availability of antibiotics at the infection-site can be used to improve clinical decision-making about diagnosis and treatment of exacerbations. This dissertation characterizes CF bacterial physiology in exacerbation-relevant conditions (**Aim 1**) and determines which antibiotics are reaching the CF airways and their impact on the microbial community (**Aim 2**).

Aim 1: Exacerbation-relevant environments affect CF pathogen physiology (Chapters 1-3)

Microbial colonization of the CF airways is the biggest contributor of mortality in CF patients, yet we have little understanding of the role of microbial community biogeography and activity on CFPE. It is likely that CF microbes contribute to, or are at least impacted by, exacerbations. CFPE are characterized by increased inflammation, acidity and fermentation (1–3). These conditions could be the result of microbial activity and also impact antibiotic efficacy.

How do CF opportunistic pathogens respond to changes in pH, oxygen, and fermentation metabolites (**Figure ii**)? We first determined that *Rothia*-derived fermentation products are utilized by *P. aeruginosa* to synthesize amino acids, even in a nutrient-rich background (**Chapter 1**). The product of most fermentation pathways are acids with low pKa, reducing the local pH. The airways of persons with CF are more acidic than those of healthy individuals, and the pH drops further during CFPE (2). Most gram-negative opportunistic pathogens grow optimally at neutral pH, and must survive acidic environments in the CF airways (91, 92). We found that CF isolates of *Stenotrophomonas maltophilia*, an understudied pathogen, were not better adapted to low pH than environmental or other human isolates. Rather, *S. maltophilia* responds to acidic pH by expression of stress pathways *in vitro* and in CF sputum (**Chapter 2**).

The CF airways are also characterized by steep drops in oxygen (4), which can drive fermentation from bacteria such as *Rothia* and *Streptococcus* and limits the replication of aerobic opportunistic pathogens such as *P. aeruginosa*. We used fluorescence lifetime imaging microscopy (FLIM) and hyperspectral imaging to characterize *P. aeruginosa* redox activity throughout a biofilm, in aerobic and low oxygen environments (**Chapter 3**).

Aim 2: Antibiotic levels measured in CF sputum impact microbial communities (Chapter 4)

Accurate antibiotics information is important to determine the link between microbiome and disease. Most persons with CF take maintenance antibiotics throughout their lives. Additional antibiotics are prescribed if the patient experiences worsening symptoms. The majority of CF microbiome studies that included antibiotic information depended on medical charts (**Table i**) (57, 59, 62, 64, 93–98), which can be unreliable (65, 99). We developed two LC-MS methods to detect 18 antibiotics in CF sputum and assessed the detection of these antibiotics relative to subject-reported use. We found that the detection of certain antibiotics did not agree with self-reported use, underlining the need for objective methods to account for antibiotics in microbiome studies (**Chapter 4**).

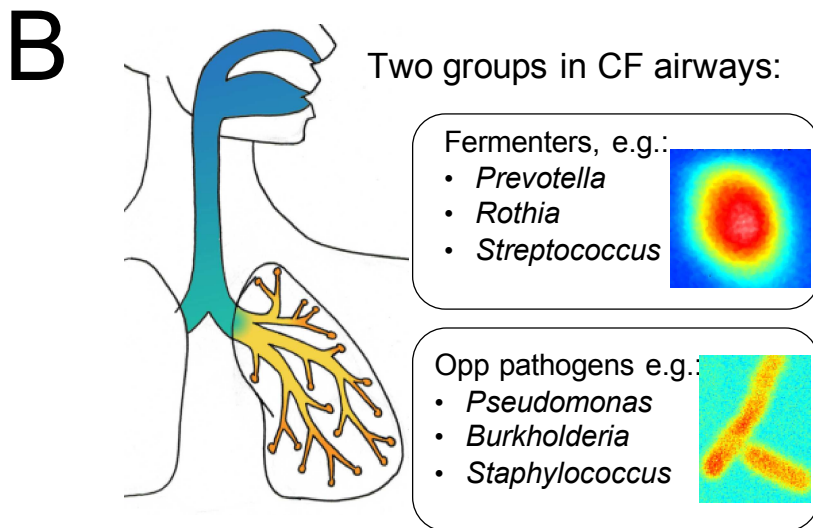
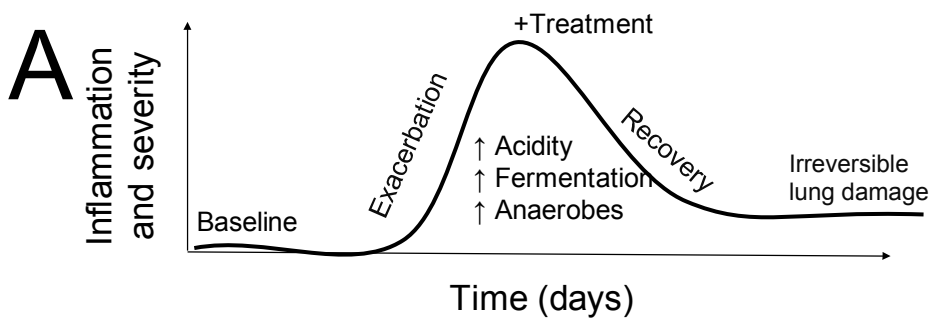
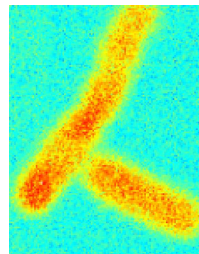


Fig. i. (A) Persons with CF periodically experience exacerbations, which can be characterized by increases in acidity (1), fermentation (2), inflammation (42), and anaerobes (25). Many exacerbation events result in irreversible lung damage (15). **(B)** The microbial contribution to exacerbations is not well-understood, even though the microbial composition of the CF lungs has been characterized. The CF microbial community consists of two populations: the fermenters, which can also be found in the oral cavities of healthy and diseased individuals, and a dominant opportunistic pathogen (11). The species composition of the microbial communities are personalized. Lung illustration by Bryan Ramirez, adapted from Whiteson *et al.* (21). Opp=opportunistic.

Aim 1: Impact of exacerbation-relevant conditions on pathogens?

Acidic pH
Fermentation
Low O₂



Aim 2: Impact of antibiotics on microbes?

Abx in sputum → Community structure & function

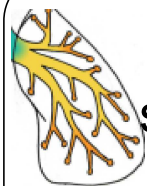


Figure ii. By expanding our knowledge of CF lung microbe activity, we can improve antibacterial treatment of chronic infections and acute pulmonary exacerbations. This involves understanding how bacteria survive and live in CF- and exacerbation-relevant conditions (**Aim 1**). Antibacterial resolution of exacerbations also requires determining if antibiotics are reaching the airways at adequate concentrations and their impact on the microbial community (**Aim 2**). Abx=antibiotics. Lung illustration by Bryan Ramirez, adapted from Whiteson *et al.* (21)

Table i: Summary of CF microbiome studies which included antibiotics data. The subject age, disease state, and method of antibiotics reported differed for every study. Contradicting trends are highlighted by different colors. Studies that report the microbiome community is not affected by antibiotics are shaded in purple, while studies that report drops in bacterial diversity following antibiotic treatment are shaded in orange. (57, 59, 62, 64, 93–98)

Publication	# of subjects	Age of subjects	Disease State	Microbiome Method	Method of antibiotics reporting	Findings
*Caverly, et al. Annals ATS 2019	6	30-51	Early, intermediate, severe	16S of longitudinal sputum from baseline periods	Self-reported usage.	Maintenance antibiotics were a significant driver of day-to-day variation in subjects' microbial communities during baseline periods.
Jorth, et al. Cell Reports. 2019.	22	2-21	Not reported	16S of low-volume BAL.	Medical charts	Classical CF pathogens dominated the lung microbiome in pediatric patients. Overall, no major change with antibiotics but there was a slightly higher abundance of <i>Streptococcus</i> , <i>Veillonella</i> , and <i>Prevotella</i> in antibiotic-treated subjects.
Bacci, et al. bioRxiv. 2019.	22	14-55	Moderate-severe	Shotgun sequencing of sputum before and after exacerbation	Medical charts	Microbiome was stable during exacerbations. Functional genes in bacteria were conserved across patients. Antibiotic resistance genes were not affected by antibiotic intake.
Heirali, et al. JCF 2019.	37	≥18	Early, intermediate, severe	16S of sputum before, during, and after inhaled aztreonam	Medical charts	Overall, inhaled aztreonam had little impact on CF microbiome but trended towards decreased diversity. On an individual level, patients with high levels of <i>Streptococcus</i> and <i>Staphylococcus</i> and lower levels of <i>Haemophilus</i> at baseline responded clinically to aztreonam.
Hahn, et al. Scientific Reports 2019.	20	2-21	Early and intermediate	16S of sputum, BAL, or oropharangeal swabs during BETR	LC-MS to determine levels of beta-lactams in plasma.	Individuals with therapeutic levels of the antibiotic had more dramatic drops in lung microbiome diversity than in patients who received subtherapeutic levels.

*Carmody, et al. PLoS One. 2018.	24	6-53	Early, intermediate, severe	16S of sputum during baseline, exacerbation, treatment, and recovery	Noted beginning of treatment antibiotics for exacerbations based on subject self-reported usage.	Disease stage (early, intermediate, or severe) affects the trends with microbial composition across different clinical states (baseline, exacerbation, treatment, and recovery). In early and intermediate disease stage patients, the abundance of anaerobes increased during exacerbation onset. In early disease stage patients, the diversity and relative abundance of anaerobes decreased after treatment for pulmonary exacerbations.
Whelan, et al. PLoS One 2017.	6	26-36	Early and intermediate	16S of sputum during stable, treatment, and intermediate timepoints.	Self-reported usage.	The diversity within the lung microbiome did not consistently change with IV antibiotic treatment. The lung microbiome is patient- specific.
Cuthbertson, et al. ISME 2016.	10	17-55	Not reported	Sputum from pre- exacerbation baseline, exacerbation, treatment, recovery, post-exacerbation baseline. Extracellular DNA removed with propidium monazide treatment. 16S sequencing.	Recorded antibiotics prescribed for exacerbation treatment.	As a whole, the microbiome did not change across clinical state. While <i>P. aeruginosa</i> abundance remained stable across all five clinical states, some bacterial groups changed. <i>Porphyromonas catoniae</i> decreased in abundance from baseline to treatment.
Goddard, et al. PNAS. 2012.	10	NR	Severe (5 transplant)	16S of pre-transplant sputum and explanted lungs.	Medical charts	Non-typical bacteria varied daily in abundance in CF sputum. Different microbiomes in pre- transplant sputum than explanted lungs. Most patients were given additional antibiotics during transplant, so difficult to determine if antibiotics affected lung microbiome.

Fodor, et al. PLOS One. 2012.	23	18-41	Not reported	16S of sputum at exacerbation onset, after IV antibiotics treatment, and during stable period	Medical charts	The microbial community composition remained relatively stable during exacerbation and treatment. Decrease in total bacterial load immediately after treatment. Slight decrease in species richness after treatment. <i>Streptococcus, Oribacterium, Neisseria</i> abundance dropped followed treatment
*Zhao, et al. PNAS. 2012.	6	18-30	Early, intermediate, severe	16S of sputum from decade-long sampling.	Medical charts	Antibiotics were a stronger driver of changes in the bacterial diversity than lung function or subject disease stage.

CHAPTER 1:

Tracking Polymicrobial Metabolism in Cystic Fibrosis

Airways: *Pseudomonas aeruginosa* Metabolism and Physiology Are Influenced by *Rothia mucilaginosa*-Derived Metabolites

Authors: *Bei Gao, *Tara Gallagher, Ying Zhang, Mona Elbadawi-Sidhu, Zijuan Lai, Oliver Fiehn, Katrine L. Whiteson

*B.G. and T.G. contributed equally to this work

**All supplemental tables contain datasets which can be found at:*

DOI: 10.1128/mSphere.00151-18 (100)

ABSTRACT

Due to a lack of effective immune clearance, the airways of cystic fibrosis patients are colonized by polymicrobial communities. One of the most widespread and destructive opportunistic pathogens is *Pseudomonas aeruginosa*; however, *P. aeruginosa* does not colonize the airways alone. Microbes that are common in the oral cavity, such as *Rothia mucilaginosa*, are also present in cystic fibrosis patient sputum and have metabolic capacities different from those of *P. aeruginosa*. Here we examine the metabolic interactions of *P. aeruginosa* and *R. mucilaginosa* using stable-isotope-assisted metabolomics. Glucose-derived ¹³C was incorporated into glycolysis metabolites, namely, lactate and acetate, and some amino acids in *R. mucilaginosa* grown aerobically and anaerobically. The amino acid glutamate was unlabeled in the *R. mucilaginosa* supernatant but incorporated the ¹³C label after *P. aeruginosa* was cross-fed the *R. mucilaginosa* supernatant in minimal medium and artificial-sputum medium. We provide evidence

that *P. aeruginosa* utilizes *R. mucilaginosa*-produced metabolites as precursors for generation of primary metabolites, including glutamate.

IMPORTANCE

Pseudomonas aeruginosa is a dominant and persistent cystic fibrosis pathogen. Although *P. aeruginosa* is accompanied by other microbes in the airways of cystic fibrosis patients, few cystic fibrosis studies show how *P. aeruginosa* is affected by the metabolism of other bacteria. Here, we demonstrate that *P. aeruginosa* generates primary metabolites using substrates produced by another microbe that is prevalent in the airways of cystic fibrosis patients, *Rothia mucilaginosa*. These results indicate that *P. aeruginosa* may get a metabolic boost from its microbial neighbor, which might contribute to its pathogenesis in the airways of cystic fibrosis patients.

OBSERVATION

Cystic fibrosis (CF) patients experience persistent polymicrobial colonization of their airways. *Rothia mucilaginosa* and *Pseudomonas aeruginosa* are microbes frequently detected in CF patient airways, and their co-occurrence has been observed in CF patient sputum (13, 60, 101, 102). Microbes within polymicrobial infections display complex interactions, such as metabolite cross-feeding (103). For example, *P. aeruginosa* inefficiently metabolizes host-derived mucins. Rather, *P. aeruginosa* utilizes mucin degradation products from oral anaerobes to support its growth (46, 104). Still, many studies of CF-associated microbes are conducted under artificial conditions that fail to take into account the nutrient and oxygen gradients found in CF patient airways (4, 105).

The lack of overlap between laboratory conditions and CF patient airways is reflected by the differences in growth rates, with estimates of bacterial doubling times being 100-fold times lower in sputum than in standard medium (53). Furthermore, most CF studies focus on single microbes. One primary reason for this is the lack of a robust model to examine the microbial interactions. Stable-isotope-assisted metabolomics analyzes the fate of heavy atoms from stable-isotope-labeled precursors to products, which makes it a suitable approach for monitoring metabolites produced by one microbe when cross-fed to a second microbe. In order to further explore cross-feeding interactions between two CF microbes in a relevant environment, we cross-fed labeled glycolysis products from *R. mucilaginosa* to *P. aeruginosa*. Both strains were isolated from the sputa of CF patients. We believe that our *P. aeruginosa* strain is representative of CF strains, as its core genome is similar to that of *P. aeruginosa* strain PA17 and other CF isolates (43). In an effort to mimic the CF airway environment, *R. mucilaginosa* was fed labeled glucose in anaerobic and aerobic artificial-sputum media, and the *R. mucilaginosa* supernatant was fed to *P. aeruginosa* in nutrient-rich (artificial-sputum medium) under low-nutrient (M9 minimal medium) conditions. As *P. aeruginosa* lacks some glucose utilization capacities, including a key enzyme involved in glycolysis, phosphofructokinase, we postulated that cross-feeding metabolites from *R. mucilaginosa* impacts the metabolism of *P. aeruginosa* (106).

***R. mucilaginosa* metabolism under aerobic and anaerobic conditions.**

R. mucilaginosa was grown aerobically and anaerobically in artificial-sputum medium (**Text S1**). Under both anaerobic and aerobic conditions, glucose-derived ¹³C was incorporated into glycolysis metabolites, namely, lactate and acetate, and some amino acid

biosynthesis pathways in *R. mucilaginosa* (**Fig. 1.1**; [Table S1](#)). The labeled glucose was not incorporated into the tricarboxylic acid (TCA) cycle, pentose phosphate pathway, or long-chain fatty acid biosynthesis pathways. For most metabolites, ¹³C incorporation rates were different under different oxygen conditions. For pyruvate, alanine, valine, and acetate, greater label ratios were observed under anaerobic conditions at 24 h. In contrast, lactate, glycine, serine, and isoleucine had greater label ratios under aerobic conditions at 24 h. The incorporation of [U-¹³C₆]glucose into leucine biosynthesis was not impacted by oxygen conditions. Carbon fate in *R. mucilaginosa* diverged after 3-phosphoglycerate. The ¹³C label was incorporated into serine and glycine, or into pyruvate, the precursor for lactate, acetate, and some amino acids.

Cross-feeding interactions between *R. mucilaginosa* and *P. aeruginosa*.

In order to study the impact of *R. mucilaginosa* metabolites on *P. aeruginosa*, we cross-fed supernatant from an aerobic 48-h *R. mucilaginosa* culture to *P. aeruginosa* grown under low-nutrient conditions (M9 minimal medium) and nutrient-rich conditions (artificial-sputum medium). *P. aeruginosa* was grown for 120 h before the cells were harvested in order to recapitulate the low growth rates of bacteria in CF patient sputa (53). The *R. mucilaginosa* supernatant included labeled lactate, pyruvate, and alanine (**Fig. 1.2A**; [Fig. S1.1](#); [Table S2](#)). *P. aeruginosa* utilized *R. mucilaginosa*-derived metabolites to produce metabolites in M9 minimal medium and artificial-sputum medium. For example, although labeled lactate was found in the *R. mucilaginosa* supernatant, it was not detected in *P. aeruginosa* cultures, suggesting that *P. aeruginosa* consumed *R. mucilaginosa*-derived lactate (**Fig. 1.2A**; [Fig. S1.1](#); [Table S2](#)). *P. aeruginosa* utilization of lactate and other

fermentation products has been observed in other studies (46, 107). Since lactate levels have been reported as an indicator of CF patient response to antibiotic therapy, the finding that *P. aeruginosa* consumes lactate derived from another CF microbe may have clinical implications (2).

Labeled metabolites detected in *P. aeruginosa* cells grown in minimal medium included pyruvate, alanine, valine, serine, glycine, leucine, and isoleucine (**Fig. 1.2A; Fig. S1.1; Table S2**). In addition, isotope enrichment for serine, glycine, leucine, and isoleucine was greater in *P. aeruginosa* cells than in the supernatant of *R. mucilaginosa*, indicating that *P. aeruginosa* biosynthesized those metabolites. In contrast, when *P. aeruginosa* was grown in artificial-sputum medium, *P. aeruginosa* had higher levels of a single isotope-enriched amino acid (isoleucine) than occurred in the *R. mucilaginosa* supernatant (**Fig. 1.2A; Fig. S1.1; Table S2**). Interestingly, although the *R. mucilaginosa* supernatant contained only unlabeled glutamate (**Fig. 1.2B and C; Fig. S1.2; Table S3**), labeled glutamate was detected in both *P. aeruginosa* cultures (**Fig. 1.2B, D, and E; Fig. S1.2; Table S3**). This suggests that *P. aeruginosa* biosynthesized glutamate from ^{13}C sources in the *R. mucilaginosa* supernatant even in a nutrient-rich background with initially freely available glutamate (**Text S1**).

Glutamate provides a link between nitrogen and carbon metabolism by serving as a major amine group donor in transamination reactions for the synthesis of additional amino acids and nucleosides. In *Escherichia coli*, up to 88% of the total nitrogen that ends up in a biomass comes from glutamate, and the cellular glutamate pool needs to be kept high to drive the transamination reactions (108). In *P. aeruginosa* specifically, glutamate is a

component of the cell wall and may play a role in *P. aeruginosa* virulence (109). Glutamate enhanced the yield of a virulence factor, exotoxin A (109), and induced swarming motility in *P. aeruginosa* on semisolid surfaces (110). More recently, glutamate-induced dispersion via c-di-GMP signaling pathways has been suggested (111). Glutamate might be derived from glutamine or alpha-ketoglutarate (112). However, the abundance of these two compounds was below the limit of quantification in this study. Future studies are needed to examine the biosynthesis pathways of glutamate and its role in the metabolism and physiology of *P. aeruginosa*. In summary, this study provides evidence that metabolite cross-feeding exists between *R. mucilaginosa* and *P. aeruginosa*, two common microorganisms found in polymicrobial communities in CF patient airways. The results from our study provide evidence that the physiology of CF pathogens can be influenced by the metabolic capabilities of other nearby microorganisms, even in a nutrient-rich environment, which can be tracked with stable-isotope-labeled metabolomics.

Culture conditions and metabolomics.

The bacterial strains chosen for this study were isolated from CF patients at the UCSD Adult CF Clinic: *Pseudomonas aeruginosa* PaFLR01 and *Rothia mucilaginosa* RmFLR01 (43, 113). First, we took time points from *R. mucilaginosa* cultures to examine the kinetics of metabolites in glycolysis, the TCA cycle, amino acid biosynthesis, short- and long-chain fatty acid biosynthesis, and the pentose phosphate pathway in *R. mucilaginosa*, which was grown in triplicate in artificial-sputum medium (48) spiked with 100 mM [$U-^{13}C_6$]d-glucose (Sigma-Aldrich and Cambridge Isotope Laboratory) under anaerobic and aerobic oxygen conditions (5% CO₂) at 37°C. *R. mucilaginosa* cells were

harvested at 4 h, 8 h, and 24 h. For the metabolite cross-feeding study, *R. mucilaginosa* was grown in the same medium aerobically for 48 h. The *R. mucilaginosa* supernatant was collected by filtering the culture, and the supernatant was diluted 10-fold in M9 minimal medium supplemented with succinate and in fresh artificial-sputum medium. *P. aeruginosa* was grown in triplicate aerobically, and the cells were harvested at 120 h. Metabolite extraction and data acquisition were carried out by following West Coast Metabolomics Center standard operating procedures ([Text S1](#)). Agilent MassHunter quantitative analysis software (v. B.07.00) was used for raw data processing. Natural abundance was corrected when isotope enrichment was calculated.

ACKNOWLEDGMENTS

This work was supported as a pilot project by the NIH (grant DK097154). K.L.W. is supported by a Gilead CF Research Scholars Award (app_00b072). T.G. is supported through the National Science Foundation's Integrative Graduate Education and Research Traineeship (IGERT) program (grant DGE-1144901).

Text S1: Supplemental experimental details

1. Bacterial Cultural Media

1.1 Artificial sputum media recipes for *Rothia mucilaginosa* culture

Pig mucin 2%

KCl 0.22mg/mL

NaCl 5mg/mL

Egg Yolk Emulsion 0.25%

Salmon sperm DNA 1.4mg/mL

Ferritin 0.004mg/mL

Essential amino acid mix 0.375x

Non-essential amino acid mix 0.5x

MgSO₄ 1mM

BME vitamin stock 1x

Trace metals stock 1x

U-13C₆ glucose 40mM

Essential amino acid components:

Ingredient and stock concentration (50x):

L-Arginine HCl (6.32 g/l)

L-Cystine • 2HCl (1.564 g/l)

L-Histidine•HCl•H₂O (2.1 g/l)

L-Isoleucine (2.625 g/l)

L-Leucine (2.62 g/l)

L-Lysine•HCl (3.625 g/l)

L-Methionine (0.755 g/l)

L-Phenylalanine (1.65 g/l)

L-Threonine (2.38 g/l)

L-Tryptophan (0.51 g/l)

L-Tyrosine (1.8 g/l)

L-Valine (2.34 g/l)

Non-essential amino acid components:

Ingredient and stock concentration (100x):

L-Alanine (free base) (0.89 g/l)

L-Asparagine•H₂O (1.5 g/l)

L-Aspartic Acid (1.33 g/l)

L-Glutamic Acid (1.47 g/l)

Glycine (0.75 g/l)

L-Proline (1.15 g/l)

L-Serine (1.05 g/l)

1.2 M9 minimal media recipes for *Pseudomonas aeruginosa* culture

Na₂HPO₄ 7H₂O 64g/L

KH₂PO₄ 15g/L

NaCl 2.5g/L

NH₄Cl 5g/L

MgSO₄ 1mM

CaCl₂ 0.1mM

Succinate 40mM

2. Sample Preparation and Data Acquisition

2.1 Bacterial strains *Pseudomonas aeruginosa* FLR19 and *Rothia mucilaginosa* RmFLR01

were isolated from the sputum of an adult CF patient. The genomes from both of these strains are publicly available on the PATRIC database to anyone with a PATRIC account:

<https://www.patricbrc.org/workspace/tgallagh@patricbrc.org/Genomes/FLR01>

<https://www.patricbrc.org/workspace/tgallagh@patricbrc.org/Genomes/Rm>

2.2 Glycolysis, TCA cycle metabolites and amino acids

50 uL of bacterial cells or supernatant were used for extraction. Polar metabolites were extracted with 1mL acetonitrile, isopropanol and water (3:3:2) and dried down in the

speed vacuum concentration system, followed by methoximation and tert.butyldimethylsilylation. Agilent 5977A GC-quadrupole mass spectrometer was used for data acquisition in electron ionization mode.

2.3 Pentose phosphate pathway metabolites

50uL bacterial cells or media were used for extraction. Metabolites were extracted with 1mL acetonitrile, isopropanol and water (3:3:2) and dried down in the speed vacuum concentration system, followed by methoximation and trimethylsilylation. Agilent 7200 GC-accurate-mass QTOF was used for data acquisition in methane chemical ionization mode.

2.4 Short Chain Fatty Acids

50uL bacterial cells or media were used for short chain fatty acid analysis. Metabolites were extracted with 700uL of water, hydrochloric acid and methyl tert-butyl ether (5:1:1), followed by dehydration by anhydrous sodium sulfate and tert.butyldimethylsilylation. Agilent 5977A GC- quadrupole mass spectrometer was used for data acquisition in electron ionization mode.

2.5 Long Chain Fatty Acids 50uL bacterial cells or media were used for lipidomics analysis. 225uL methanol, 750uL methyl tert-butyl ether and 188uL water were used as extraction buffers. Samples were dried down in the speed vacuum concentration system and re-suspended with 110uL of methanol and toluene (9:1) with 50ng/mL CUDA (N-cyclohexyl-N'-dodecanoic acid urea). Data was acquired by Agilent 6550 Accurate-Mass QTOF LC/MS with CSH column in negative mode.

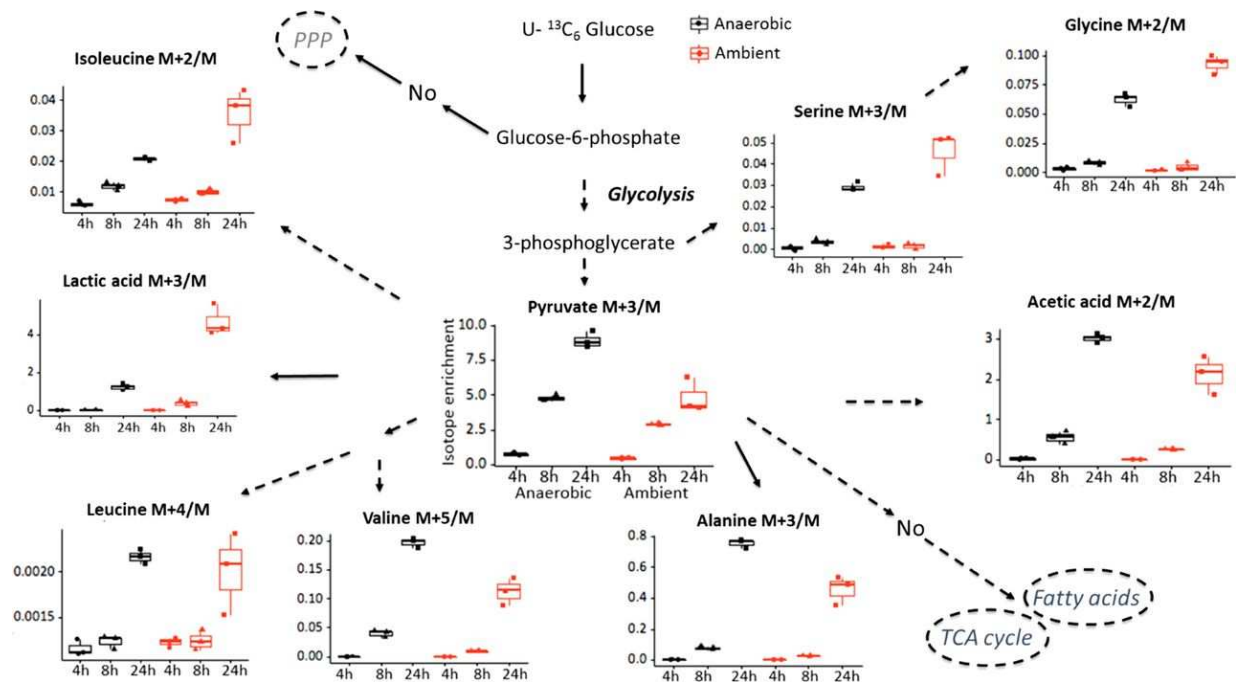


Figure 1.1: Glucose-derived ^{13}C was incorporated into pyruvate, lactate, acetate, alanine, valine, serine, glycine, leucine, and isoleucine in *R. mucilaginosa* under both anaerobic and ambient-oxygen conditions. M+2, M+3, M+4, and M+5 indicate compounds that contained 2, 3, 4, and 5 ^{13}C atoms, respectively. Isotope enrichment means an abundance of labeled ion/unlabeled ion (corrected for natural abundance). Isotope enrichment was greater at 24 h than at 8 h or 4 h. For pyruvate, alanine, valine, and acetate, greater isotope enrichment was observed under anaerobic conditions at 24 h. For lactate, glycine, serine, and isoleucine, greater isotope enrichment was observed under ambient-oxygen conditions at 24 h. The incorporation of glucose-derived ^{13}C into leucine biosynthesis was not affected by oxygen conditions. Dashed lines and solid lines indicate multiple steps and one metabolic step(s) needed to obtain the metabolite, respectively. Error bars, means \pm standard deviations (SD) ($n = 3$ bacterial cultures per group); TCA, citric acid cycle; PPP, pentose phosphate pathway.

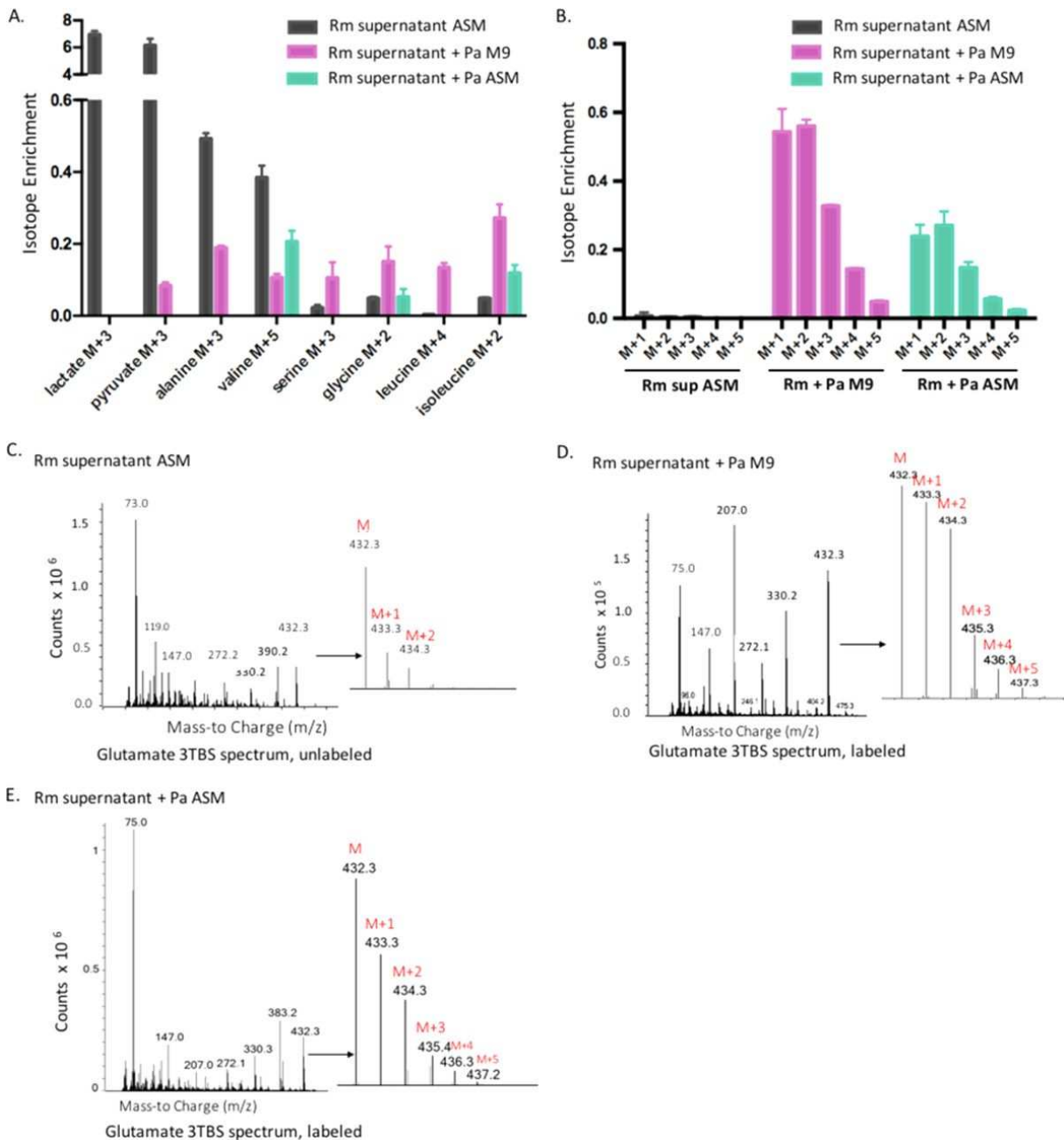


Figure 1.2: Cross-feeding interactions between *R. mucilaginosa* and *P. aeruginosa*. M+1, M+2, M+3, M+4, and M+5 indicate compounds that contained 1, 2, 3, 4, and 5 ^{13}C atoms, respectively. Error bars, means \pm SD ($n = 3$ bacterial cultures per group). (A) Labeled lactate was found in the *R. mucilaginosa* (Rm) supernatant but not in *P. aeruginosa* (Pa) cells. In M9 minimal medium, *P. aeruginosa* cells contained isotopically enriched pyruvate, alanine, valine, serine, glycine, leucine, and isoleucine. In artificial-sputum medium, *P. aeruginosa* cells contained isotopically enriched valine, glycine, and isoleucine. (B) Although the *R. mucilaginosa* supernatant contained only unlabeled glutamate, labeled glutamate was detected in the *P. aeruginosa* cells grown in artificial-sputum medium and

M9 minimal medium. (C to E) Glutamate spectrum for the *R. mucilaginosa* supernatant (C), *P. aeruginosa* grown in M9 minimal medium spiked with the *R. mucilaginosa* supernatant (D), and *P. aeruginosa* grown in artificial-sputum medium spiked with the *R. mucilaginosa* supernatant (E).

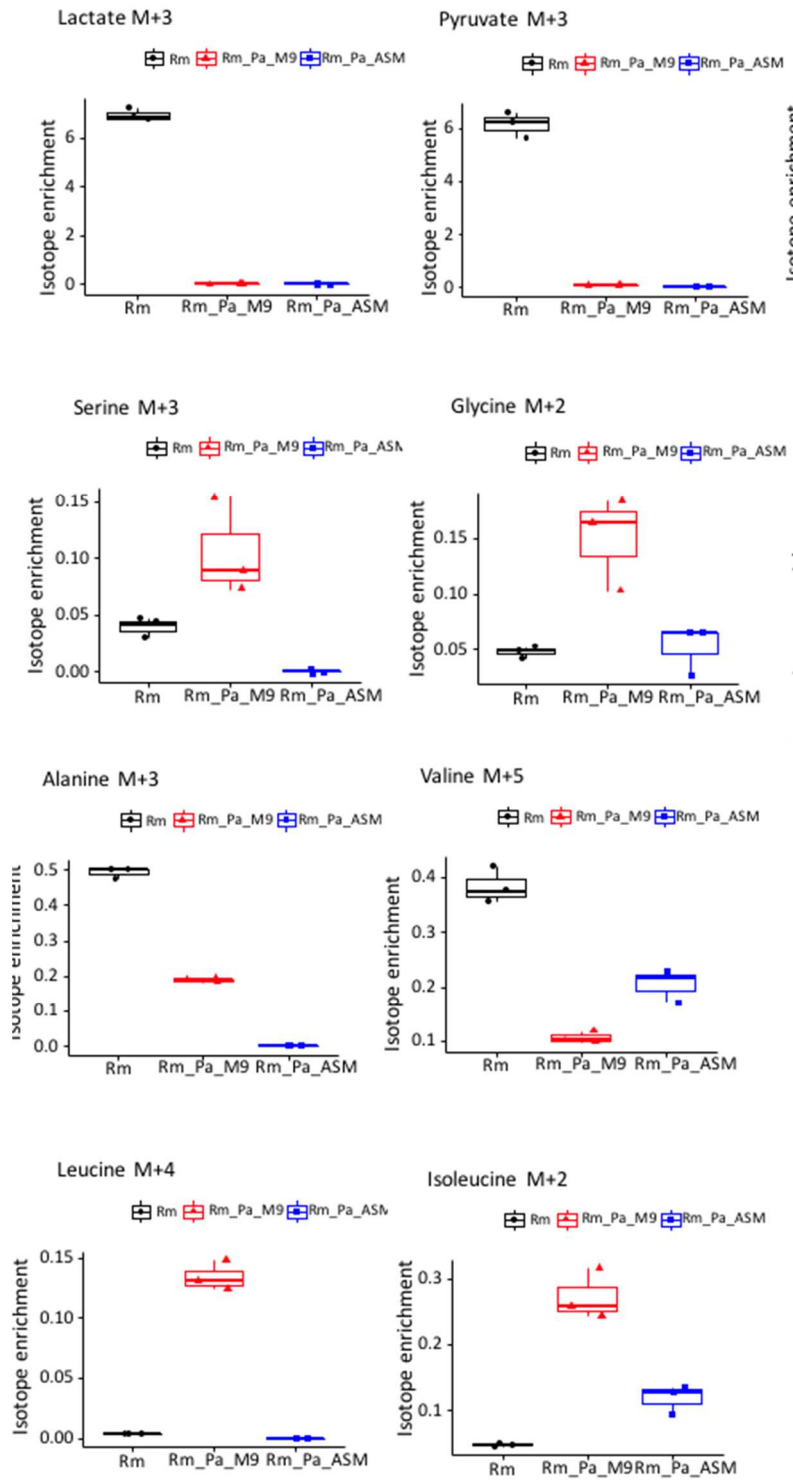


Figure S1.1: Abundances of isotope-enriched metabolites for *R. mucilaginosa* grown in artificial-sputum medium (Rm), *P. aeruginosa* grown in M9 minimal medium spiked with the *R. mucilaginosa* supernatant (Rm_Pa_M9), and *P. aeruginosa* grown in artificial-sputum medium spiked with the *R. mucilaginosa* supernatant (Rm_Pa_ASM)

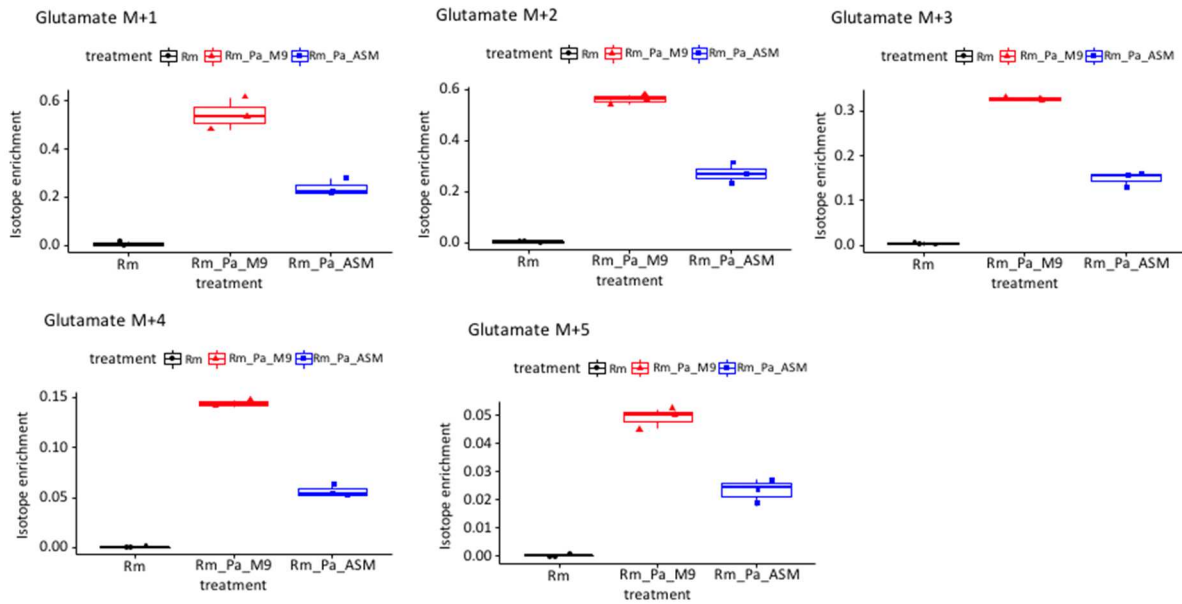


Figure S1.2: Abundances of isotope-enriched glutamate ions for *R. mucilaginosa* grown in artificial-sputum medium (Rm), *P. aeruginosa* grown in M9 minimal medium spiked with the *R. mucilaginosa* supernatant (Rm_Pa_M9), and *P. aeruginosa* grown in artificial-sputum medium spiked with the *R. mucilaginosa* supernatant (Rm_Pa_ASM)

CHAPTER 2:

Cystic Fibrosis-Associated *Stenotrophomonas maltophilia* Strain-Specific Adaptations and Responses to pH

Authors: Tara Gallagher, Joann Phan, Andrew Oliver, Alexander B. Chase, Whitney E. England, Stephen Wandro, Clark Hendrickson, Stefan F. Riedel, Katrine Whiteson

Supplemental data sets for this article may be found at <https://doi.org/10.1128/JB.00478-18>.(114)

ABSTRACT

The airway fluids of cystic fibrosis (CF) patients contain local pH gradients and are more acidic than those of healthy individuals. pH is a critical factor that is often overlooked in studies seeking to recapitulate the infection microenvironment. We sought to determine the impact of pH on the physiology of a ubiquitous yet understudied microbe, *Stenotrophomonas maltophilia*. Phylogenomics was first used to reconstruct evolutionary relationships between 74 strains of *S. maltophilia* (59 from CF patients). Neither the core genome (2,158 genes) nor the accessory genome (11,978 genes) distinguish the CF and non-CF isolates; however, strains from similar isolation sources grouped into the same subclades. We grew two human and six CF *S. maltophilia* isolates from different subclades at a range of pH values and observed impaired growth and altered antibiotic tolerances at pH 5. Transcriptomes revealed increased expression of both antibiotic resistance and DNA repair genes in acidic conditions. Although the gene

expression profiles of *S. maltophilia* in lab cultures and CF sputum were distinct, we found that the same genes associated with low pH were also expressed during infection, and the higher pH cultures were more similar to sputum metatranscriptomes. Our findings suggest that *S. maltophilia* is not well adapted to acidity and may cope with low pH by expressing stress response genes and colonizing less acidic microenvironments. As a whole, our study underlines the impact of microenvironments on bacterial colonization and adaptation in CF infections.

IMPORTANCE

Understanding bacterial responses to physiological conditions is an important priority for combating opportunistic infections. The majority of CF patients succumb to inflammation and necrosis in the airways, arising from chronic infection due to ineffective mucociliary clearance. Steep pH gradients characterize the CF airways but are not often incorporated in standard microbiology culture conditions. *Stenotrophomonas maltophilia* is a prevalent CF opportunistic pathogen also found in many disparate environments, yet this bacterium's contribution to CF lung damage and its response to changing environmental factors remain largely understudied. Here, we show that pH impacts the physiology and antibiotic susceptibility of *S. maltophilia*, with implications for the development of relevant *in vitro* models and assessment of antibiotic sensitivity.

INTRODUCTION

The ability of a microbe to successfully colonize and persist in a new environment depends on its tolerance of various conditions (115–118). pH is a central environmental factor that imposes selective pressure on bacterial phyla and species , drives shifts in

microbial metabolism (117, 119), and affects microbial interactions (117, 120). pH response is considered a deeply conserved trait (118), where different bacteria have specific pH ranges at which they reach dense growth. For example, Gram-negative opportunistic pathogens, including *Pseudomonas aeruginosa*, grow optimally at neutral pH, yet must survive at growth-limiting pH in the environment and infections (91, 92).

One example of infection-relevant pH shifts concerns the airway secretions of cystic fibrosis (CF) patients, which are characterized by steep pH gradients that can suppress bacterial growth. The pH of CF sputum ranges from 2.9 to 6.5 (4), although transient microenvironments of alkaline pH likely exist, arising from bacterial metabolism of amino acids (121, 122). pH is decreased by the CFTR (cystic fibrosis transmembrane conductance regulator) bicarbonate channel defect [1], and the pH can be further reduced during periods of decline in CF lung function, known as pulmonary exacerbations (1–3), potentially due to both host and microbial production of acidic molecules, such as lactic acid (2).

Chronic bacterial colonization in the airways can result in up to a 95% mortality rate in CF patients (8); antibiotics are rarely capable of eradicating established bacterial infections. To better inform treatment, it is imperative to understand the mechanisms opportunistic pathogens use to persist in the airways. The effect of pH on CF bacteria is vastly understudied despite its importance as a major environmental factor in microbial communities. One such CF microbe is *Stenotrophomonas maltophilia*, which is estimated to infect 10% to 18% of patients (123, 124) and is intrinsically resistant to multiple antibiotic classes. *S. maltophilia* is unable to use nitrate as an alternative electron acceptor (125), a

trait that likely impacts its growth and colonization location in the airways (126). One recent retrospective study found that baseline chronic *S. maltophilia* infection is associated with a 3-fold increased risk of mortality or lung transplant in CF patients (127). Two recent studies found that CF-associated *S. maltophilia* has a wide pangenome (128), and human-associated *S. maltophilia* forms core genome clades that are distinct from environmental strains (129). In both studies, there was little correlation between genetic potential and observed phenotypes in *S. maltophilia* (128, 129), including antibiotic susceptibility, which further emphasizes a need to improve the link between genetic information and bacterial physiology in the CF airways. Our knowledge of how opportunistic pathogens behave in CF sputum is limited. To date, only a few studies have looked at changes in CF bacterial gene expression *in vivo* (12, 130, 131). The lack of overlap between experimental conditions and CF sputum is an important factor in the observed differences in bacterial physiology *in vitro* versus *in vivo* (130).

Here, we used a combination of core genome phylogenetics, pangenome analyses, and CF sputum metatranscriptomics, along with transcriptomics, growth curves, and antibiotic assays in a range of pH. We hypothesized that *S. maltophilia* responds to acidic conditions in the CF airways by acquiring and expressing stress response genes. Our phylogenomics analyses did not support that *S. maltophilia* CF strains acquire a specific universal adaptation to acidic pH. Rather, our combined phylogenomic and transcriptomic analyses indicate *S. maltophilia* utilizes both conserved and strain-specific stress responses in lower pH. Furthermore, higher pH cultures had more similar transcriptomes to those of sputum than those of acidic pH cultures, suggesting that *S. maltophilia* may avoid or have limited growth in the lower-pH microenvironments in CF sputum. Our study highlights a

need for better *in vitro* systems, as well as showing the impact of pH on the localization and adaptation of CF bacteria.

***S. maltophilia* cystic fibrosis accessory genes.**

In order to identify genes unique to *S. maltophilia* FLR19 and/or other CF isolates, we analyzed the pangenome, genes that make up the core and accessory genomes (Data Set S2). *S. maltophilia* has an open pangenome consisting of 14,136 genes (**Fig. 2.1B**). The average number of genes in each *S. maltophilia* genome was 4,285 (minimum = 3,908 genes in strain UBA905, maximum = 4,733 genes in strain GC 2009) (**Fig. S2.1**). The CF accessory genome (genes found only in the 59 CF strains) consisted of 4,457 genes, although no gene was found across all 59 CF genomes. Only five of the CF-specific genes, which had no known function, were shared in at least half of the CF isolates (Data Set S2; **Fig. 2.1C**). Our analyses suggest that the genes comprising the CF accessory genome are strain specific, with nearly half ($n = 2,157$ CF-specific accessory genes) being unique to one strain (**Fig. 2.1C**). Accessory genome content was better explained by patient identifier ($R^2 = 37\%$) than CF status ($R^2 = 5.5\%$) (nested permutational multivariate analysis of variance [PERMANOVA]; $P < 0.001$). In accordance with this, the accessory gene content ($n = 11,978$ genes) moderately separated strains into CF and non-CF groups (analysis of similarity [ANOSIM]; $R = 0.55$, $P < 0.05$) (**Fig. 2.1D**).

We next examined whether the overall functional potential of CF strains differed from that of non-CF strains. In particular, we hypothesized that CF strains of *S. maltophilia* would be enriched for stress response genes to cope with acidic pH in the CF airways. We grouped total (core and accessory) gene content into 26 functional categories

based on the combined Rapid Annotation using Subsystem Technology (RAST) SEED annotations of a non-CF type strain (K279a) and a CF isolate (FLR19) (132) (Data Set S3). CF strains did not contain significantly more genes in the “stress response” category but did have greater proportions of genes in the “virulence” and “cofactors” categories (**Fig. S2.1B**; Data Set S4) (two-sample *t* test; $P < 0.05$). The annotated functions of genes in the virulence category included metal and antibiotic resistance (Data Set S3).

***S. maltophilia* growth in acidic, neutral, and basic pH with antibiotics.**

Because the pH of CF airways is acidic and further reduced during pulmonary exacerbations, we wanted to determine how *S. maltophilia* responds to changes in pH. We grew six CF isolates (from San Diego, CA, and from Italy) (128) and two non-CF strains in phosphate-buffered pH 5, 7, and 9 Todd-Hewitt broth. All eight strains had impaired growth in acidic pH relative to that in neutral pH (analysis of variance [ANOVA] with *post hoc* pairwise comparisons; $P < 0.05$) (**Fig. 2.2A**). Similar results were obtained in nonbuffered acidic media spiked with citric, lactic, or sulfuric acid (**Fig. S2.2A**). Cells recovered from a medium at a specific pH were not more tolerant to growth at that pH, suggesting that their growth was due to a physiological response rather than to mutational adaptation to acidic tolerance (**Fig. S2.2B**). In addition, strain FLR19 increased its local pH in the pH 5 buffered Todd-Hewitt broth over a 24-h growth period (**Fig. S2.2C**). The growth of strain FLR19 growth was also impaired in acidic artificial sputum media (ASM) (**Fig. S2.2D**).

***S. maltophilia* cystic fibrosis accessory genes.**

In order to identify genes unique to *S. maltophilia* FLR19 and/or other CF isolates, we analyzed the pangenome, genes that make up the core and accessory genomes (Data Set S2). *S. maltophilia* has an open pangenome consisting of 14,136 genes (**Fig. S2.1b**). The average number of genes in each *S. maltophilia* genome was 4,285 (minimum = 3,908 genes in strain UBA905, maximum = 4,733 genes in strain GC 2009) (**Fig. S2.1**). The CF accessory genome (genes found only in the 59 CF strains) consisted of 4,457 genes, although no gene was found across all 59 CF genomes. Only five of the CF-specific genes, which had no known function, were shared in at least half of the CF isolates (Data Set S2; **Fig. 2.1C**). Our analyses suggest that the genes comprising the CF accessory genome are strain specific, with nearly half ($n = 2,157$ CF-specific accessory genes) being unique to one strain (**Fig. 2.1C**). Accessory genome content was better explained by patient identifier ($R^2 = 37\%$) than CF status ($R^2 = 5.5\%$) (nested permutational multivariate analysis of variance [PERMANOVA]; $P < 0.001$). In accordance with this, the accessory gene content ($n = 11,978$ genes) moderately separated strains into CF and non-CF groups (analysis of similarity [ANOSIM]; $R = 0.55$, $P < 0.05$) (**Fig. 2.1D**).

We next examined whether the overall functional potential of CF strains differed from that of non-CF strains. In particular, we hypothesized that CF strains of *S. maltophilia* would be enriched for stress response genes to cope with acidic pH in the CF airways. We grouped total (core and accessory) gene content into 26 functional categories based on the combined Rapid Annotation using Subsystem Technology (RAST) SEED annotations of a non-CF type strain (K279a) and a CF isolate (FLR19) (132) (Data Set S3). CF strains did not contain significantly more genes in the “stress response” category but did have greater proportions of genes in the “virulence” and “cofactors” categories (**Fig. S2.1B**;

Data Set S4) (two-sample *t* test; $P < 0.05$). The annotated functions of genes in the virulence category included metal and antibiotic resistance (Data Set S3).

***S. maltophilia* growth in acidic, neutral, and basic pH with antibiotics.**

Because the pH of CF airways is acidic and further reduced during pulmonary exacerbations, we wanted to determine how *S. maltophilia* responds to changes in pH. We grew six CF isolates (from San Diego, CA, and from Italy) (128) and two non-CF strains in phosphate-buffered pH 5, 7, and 9 Todd-Hewitt broth. All eight strains had impaired growth in acidic pH relative to that in neutral pH (analysis of variance [ANOVA] with *post hoc* pairwise comparisons; $P < 0.05$) (**Fig. 2.2A**). Similar results were obtained in non-buffered acidic media spiked with citric, lactic, or sulfuric acid (**Fig. S2.2A**). Cells recovered from a medium at a specific pH were not more tolerant to growth at that pH, suggesting that their growth was due to a physiological response rather than to mutational adaptation to acidic tolerance (**Fig. S2.2B**). In addition, strain FLR19 increased its local pH in the pH 5 buffered Todd-Hewitt broth over a 24-h growth period (**Fig. S2.2C**). The growth of strain FLR19 growth was also impaired in acidic artificial sputum media (ASM) (**Fig. S2.2D**).

Beyond observing pH-driven changes in growth, we assayed tolerance to antibiotics prescribed to CF patients (gentamicin, tobramycin, and meropenem) across the pH gradient (**Fig. 2.2B**). The bacterial susceptibility to meropenem and gentamicin in different pH varied at the strain level (ANOVA with *post hoc* comparisons and Bonferroni correction; $P < 0.05$, $n = 6$ to 9). Five of the CF strains (FLR19, FMa 2012, CV 2008, GC 2011, and ZC 2006) were more susceptible to meropenem in acidic pH than in neutral pH (**Fig. 2.2C**) (*t* test with Bonferroni correction; $P < 0.05$, $n = 6$ to 9). The reverse pH effect was

observed with gentamicin for four strains (FLR19, GC 2011, ZC 2005, and K279a), which were more susceptible in basic pH than in neutral pH. Strain NCTC 10257 had significantly increased tolerance of gentamicin, and strain FLR19 trended toward increased tolerance of gentamicin in acidic conditions. These findings align with those of previous antibiotic assays, which showed that β -lactams (meropenem) have increased activity at lower pH, while aminoglycosides (gentamicin) show decreased activity (133).

***S. maltophilia* FLR19 metabolome under acidic, neutral, and basic pH conditions.**

We next wanted to determine how *S. maltophilia* responds metabolically and transcriptionally to changes in pH. We chose FLR19 for the metabolomics and transcriptomics because it is a CF strain not yet characterized but is still closely related evolutionarily to 27 other CF strains from our core genome phylogenetics (**Fig. 2.1A**). Metabolites that were produced or consumed in different conditions were identified using untargeted metabolomics. The metabolomes had little separation based on pH but had distinct metabolic profiles from uninoculated media (**Fig. 2.3A**). *S. maltophilia* FLR19 produced 226 metabolites in at least one of the experimental conditions; 40 metabolites were produced in all three conditions (Data Set S4).

S. maltophilia FLR19 produced 28 metabolites in acidic medium only. These included hydroxyglutaric acid, a by-product of glutamate catabolism (134), and hydroquinone and acetophenone, weak acids with high pK_a. Notably, metabolites involved in polyamine synthesis, *N*-acetylglutamate, putrescine, and spermidine, were consumed by FLR19 in acidic conditions (Data Set S4). The acidic metabolome had significantly less putrescine and more of a nonannotated metabolite (X129225) compared to the neutral

metabolome (Kruskal-Wallis ANOVA with *post hoc* Dunn comparisons; $n = 3$, $P < 0.05$, \log_2 fold change [$\log_2\text{FC}$] > 1 or < -1) (**Fig. 2.3b**; **Fig. S2.4**). The production of polyamines via decarboxylation of amino acids is a well-documented acidic stress response in bacteria (135). The FLR19 strain's consumption of *N*-acetylglutamate, spermidine, and putrescine in acidic pH could be indicative of higher turnover of those intermediates in this polyamine pathway.

Metabolites produced by *S. maltophilia* FLR19 in alkaline pH included weak acids, such as ribonic acid, salicylic acid, urea, glycolic acid, glyceric acid, and isothreonic acid. The basic metabolome had significantly less methionine and more organic acids (Kruskal-Wallis ANOVA with *post hoc* Dunn comparisons; $P < 0.05$, $n = 3$, $\log_2\text{FC} > 1$ or < -1) (**Fig. 2.3C**, **Fig. S2.4**).

***S. maltophilia* FLR19 transcriptome in acidic, neutral, and basic pH.**

In order to determine how our CF isolate responds transcriptionally to changes in pH, we sequenced ribosome-depleted RNA from FLR19 cultures grown in acidic ($n = 2$), neutral ($n = 3$), or basic pH ($n = 2$). The numbers of quality-filtered reads that aligned to the FLR19 genome were 2.2 to 5.1 million, with mean genome-wide coverages ranging from 27 \times to 67 \times (**Fig. 2.4A**, Data Set S6). The transcriptomes separated based on pH, and the acidic transcriptomes are more distinct from the neutral than the basic transcriptomes (axis 1) (**Fig. 2.4B**). The acidic transcriptome had 86 upregulated genes and 84 downregulated genes (negative binomial test; false-discovery rate [FDR] < 0.05 , $\log_2\text{FC} > 1$ or < -1) (**Fig. 2.4C**; Data Set S6). The basic transcriptome only had five upregulated genes and two downregulated genes (**Fig. 2.4D**; Data Set S6). These results suggest that *S.*

maltophilia FLR19 is better suited to grow in basic pH than in acidic pH, which is consistent with the growth curve data.

Comparison of *S. maltophilia* gene expression profiles *in vitro* and in CF sputum.

In order to identify genes actively transcribed by *S. maltophilia* in CF airways, we mapped metatranscriptome reads from sputum (taken from 7 CF patients infected with *P. aeruginosa* (130)) to the *S. maltophilia* pangenome (all coding sequences from 74 strains). Before aligning the metatranscriptome reads to the *S. maltophilia* pangenome, the reads were mapped to a custom-made CF database consisting of 1,812 non-*Stenotrophomonas* CF bacterial genomes from the Pathosystems Resource Integration Center (PATRIC) (136). While this approach reduced the number of false-positive hits to the *S. maltophilia* pangenome from other bacterial RNAs, it also omitted multispecies genes. Two of the sputum samples (E and F) had reads that aligned to *S. maltophilia* genes (3,403 and 28,992 reads, respectively) (Data Set S5).

To compare transcription of *S. maltophilia* FLR19 grown *in vitro* to that of *S. maltophilia* in sputum, we first processed the *in vitro* RNA sequencing reads through the same pipeline as the metatranscriptome reads. Fewer genes were detected in the CF metatranscriptomes than in the *in vitro* transcriptomes (**Fig. 2.5A**; Data Set S6). Since the CF airways are primarily acidic (4), we hypothesized *a priori* that the acidic transcriptomes would be similar to the sputum metatranscriptomes. However, the gene expression profiles of the acidic transcriptomes were least similar to the CF sputum metatranscriptomes (**Fig 2.5B**). The source of the RNA (*in vitro* versus *in vivo*) explained more variance in the gene

expression profiles ($R^2 = 0.79$) than did the experimental pH ($R^2 = 0.14$) (nested PERMANOVA; $P < 0.05$).

Determining the proportion of metatranscriptome and transcriptome reads that aligned to functional categories (132) showed that “protein metabolism” was the most abundant category across all samples (**Fig. 2.6A**). Overall, there were few changes in the rankings of the categories except for minor differences (Data Set S3; **Fig. 2.6A**). Notably, the sputum metatranscriptomes had a higher proportion of reads that aligned to genes involved in iron acquisition (sputum E = 1.2%, sputum F = 0.5%) than did the *in vitro* transcriptomes (0.02% to 0.08%) (Data Set S3). Hierarchical clustering of the enriched categories indicated that the sputum samples were functionally more similar to the alkaline and neutral cultures than to the acidic cultures (**Fig. 2.6B**).

Identification of pH response genes expressed *in vitro* and in CF sputum.

By combining our pangenome analyses and transcriptomics, we identified a DNA glycosylase that was unique to FLR19 and upregulated in acidic pH (**Fig. 2.7A**), suggesting that the expression of this DNA glycosylase may be a strain-specific response to low pH. This gene was in a region containing additional genes that were also expressed at higher levels in acidic pH than in neutral pH, but not at statistically significant levels. This included a hypothetical protein and sulfoxide reductase (**Fig. 2.7A**).

Two additional accessory genes were upregulated by FLR19 in acidic conditions (relative to neutral pH conditions). The first gene, which was also expressed in sputum F (**Fig. 2.7B, left**), encodes a radical *S*-adenosyl-L-methionine (SAM) domain protein. A

SmartBLAST search of the amino acid sequence indicated that this protein is closely related to bacterial photolyases involved in DNA repair. The second gene, also expressed in CF sputum samples, was a multidrug efflux pump gene, *cmeB* (**Fig. 2.7B**, right). The gene for the RND CmeB efflux pump was also found in *S. maltophilia* environmental strains.

Twenty core genes were upregulated by strain FLR19 at low pH and expressed in sputum, including the coding sequences for alkyl hydroperoxide reductases (AhpF and AhpC), the SOS response regulator LexA, and the tripartite multidrug resistance system (**Fig. 2.7C, 2.7D**; Data Set S7). In a similar study, the same stress response genes were also expressed by *P. aeruginosa* at high levels in CF sputum (130). None of the seven differentially expressed genes from when FLR19 was grown at basic pH were found to be expressed by *S. maltophilia* in sputum.

DISCUSSION

In order to improve treatment strategies, we need to better understand how opportunistic pathogens are capable of living in the dynamic, stressful environments found in the CF airways. The pH of CF sputum ranges from 2.9 to 6.5 (4), and further drops during periods of pulmonary exacerbation (1). Interestingly, many of the common Gram-negative opportunistic pathogens that persist in CF infections have impaired growth at lower pH (91, 92), which motivated us to determine how *S. maltophilia* copes in nonoptimal, acidic pH. We hypothesized that because the pH of the CF airways is largely acidic, *S. maltophilia* copes by acquiring and prioritizing expression of stress response genes.

CF strains of *S. maltophilia* adapt to patient-specific factors and are not better adapted to low pH.

We first analyzed all publicly available *S. maltophilia* genomes, along with a clinically relevant isolate unique to this study. For the phylogenomics analysis, we used a 95% AAI cutoff, which allowed us to look at finer-scale relationships between closely related strains but which also potentially overestimated the number of genes in the pangenome. Most of the *S. maltophilia* CF strains were part of four tight subclades on the phylogenetic tree. Steinmann et al. found that core single-nucleotide polymorphism (SNP) phylogenomics separated *Stenotrophomonas* spp. into human-associated and environmental clades (129). However, we cannot confirm this trend due to the limited number of environmental genomes that made it through our initial genome-filtering step. The open pangenome of *S. maltophilia* suggests that this species has diverse capabilities. This is in accordance with results of another study, which looked at the longitudinal phenotypic and genotypic heterogeneity of 91 *S. maltophilia* isolates from 10 CF patients, where the CF strains had a narrow core genome that made up a fraction of a large pangenome (1,911 core genes out of a total 16,486 genes) (128).

We hypothesized *a priori* one mechanism that *S. maltophilia* uses to survive low pH is acquiring stress response genes in the CF airways. However, we were unable to identify a CF-specific signal of adaptation to low pH. Our phylogenomics analyses suggest that *S. maltophilia* adapts to specific niches within a patient's airways. As such, a single strain cannot be considered representative of the entire CF population for a species. The lack of clonal epidemiology in isolates among CF patients is also seen in *P. aeruginosa* (137, 138). CF opportunistic pathogens are thought to be acquired from the environment and to colonize the airways of a patient throughout the patient's life, driving patient-specific adaptation (137–140). Only when analyzing the accessory genome at the functional level

(achieved by binning genes into cellular categories) were we able to find that nonessential genes, including those canonically defined as virulence genes, were enriched in CF strains. Furthermore, there was no significant increase in stress response genes in CF isolates. While we did not find a universal genomic adaptation to acidic pH stress in CF strains, the data from the *in vitro* growth experiments suggest that acidic conditions are stressful for *S. maltophilia*. All eight strains, including six CF isolates and two human strains, had impaired growth at lower pH.

***S. maltophilia* can cope with low pH by expressing both strain-specific and conserved stress response genes.**

Based on our transcriptomics and metatranscriptomics analyses, *S. maltophilia* copes with acidic pH by utilizing both universal responses (expression of core genes) and strain-specific responses. One possible mechanism is by increasing transcription of DNA repair genes, as we observed from our transcriptomics analysis. Strain FLR19 contained both strain-specific and core repair genes. The expression of DNA repair genes has been previously identified in sputum metatranscriptomes and likely reflects bacterial response to stressful conditions in the cystic fibrosis airways that can damage DNA, including the presence of reactive oxygen species and antibiotics (119). Consistent with this was FLR19's increased transcription of alkyl hydroperoxide reductase genes and the stress response gene *lexA*. In a similar study, these stress response genes were upregulated by *P. aeruginosa* in sputum and conferred resistance to antibiotics that included gentamicin (130). Taken together, the findings of Cornforth et al. and our own

findings suggest that CF strains survive in CF-relevant conditions, including acidic pH, with both conserved and adaptive traits.

Transcriptomics suggest that *S. maltophilia* may avoid lower pH.

We used a conservative approach to align the sputum metatranscriptomes to the pangenome to ensure that we only included *S. maltophilia* RNA in our study, which may have resulted in the loss of multispecies signals. We also recognize that the differences in sequencing depth between the *in vitro* transcriptomes and sputum metatranscriptomes bias the identification and quantification of gene expression, and we sought to reduce this bias by calculating the proportion of reads that mapped to functional annotation categories. Overall, the gene expression profiles of the *in vitro* FLR19 cultures were distinct from the *S. maltophilia* transcriptomes in CF sputum.

In contrast to our gene level analysis, the functional profiles of *S. maltophilia* in sputum and under the different pH conditions were similar. A couple of categories were more enriched in the sputum transcriptomes than in the *in vitro* transcriptomes, including iron acquisition. While ferritin is abundant in CF sputum, free iron may be scarce, and bacteria utilize scavengers to obtain iron (141, 142). Although expression of iron uptake genes appears to be a priority for *S. maltophilia* in sputum, we did not see significant enrichment of iron genes from our pangenome analyses in the CF strains, suggesting that *S. maltophilia* utilizes core genes to acquire iron. The acidic transcriptomes had expressed more stress response genes, indicating that the experimental acidic conditions were stressful for FLR19. Perhaps the pH 5 buffered medium was more stressful for strain

FLR19 than sputum, in which *S. maltophilia* may be capable of increasing local pH and colonizing the higher-pH regions (reported to be as high as 6.5 in pediatric sputum) (4).

We originally hypothesized that the acidic transcriptome would be more similar than the neutral and alkaline transcriptomes to that of *S. maltophilia* in sputum, because the pH of CF sputum is acidic (with gradients of 2.9 to 6.5) (4). However, clustering the samples by their functional categories indicated that the basic and neutral transcriptomes were more closely related than the acidic transcriptome to that of sputum. The lack of similarities in functional activity between the acidic and sputum transcriptomes, in addition to dissimilar gene expression profile in sputum compared to all *in vitro* conditions, emphasizes our need to better understand how the local environment impacts *S. maltophilia* colonization. Perhaps the neutral and alkaline transcriptomes were more similar to CF metatranscriptomes because *S. maltophilia* avoids lower pH microenvironments in CF sputum. In accordance with this, we did not find a strong signal of CF-specific or low-pH adaptations from our phylogenomics analysis. As *S. maltophilia* is unable to undergo nitrate respiration (125), oxygen is another factor that can determine the success and location of *S. maltophilia* colonization in the CF airways. In anaerobic environments, bacterial and host cells undergo fermentation, further decreasing the local pH. Cowley et al. reported drops in oxygen and pH with sputum plug depth (4). A recent study finding that Gram-negative opportunistic pathogens prefer regions with higher pH and oxygen levels in sputum mesocosm supports our idea that *S. maltophilia* colonizes microenvironments that are less acidic and more aerobic (92).

Another possibility for the differences in gene expression in sputum compared to that *in vitro* is the lack of overlap in bacterial behavioral studies *in vitro* versus in sputum. Cornforth et al. highlighted this need, finding a discordance in the expression of gene classes when *P. aeruginosa* is grown *in vitro* in comparison to that of *P. aeruginosa* found in human samples, including the same CF sputum samples used in this study (130).

pH affects *S. maltophilia* antibiotic tolerances.

One of very few studies that have looked at the effect of pH on cystic fibrosis strains showed that reductions in the pH of airway secretions inhibited its antibacterial function (143). We saw changes in expression of antibiotic resistance genes by strain FLR19 and in antibiotic susceptibility depending on the strain, antibiotic used, and pH. Both CF and non-CF strains were more sensitive to meropenem in acidic conditions. One non-CF strain (NCTC 10257) and on CF strain (FLR19) had higher tolerance of gentamicin at low pH. We also saw increased expression of antibiotic resistance genes (both core and accessory) when FLR19 was grown at low pH. The same antibiotic resistance genes were expressed by *S. maltophilia* in CF sputum. As CF patients take antibiotics throughout their lives, it is not surprising that a CF isolate expresses antibiotic resistance genes in sputum. While it is known that pH affects antibacterial activity (133), our findings have clinical implications for the treatment of CF infections, especially during pulmonary exacerbations, when the pH of CF airways becomes more acidified (1).

Conclusion.

Our results suggest that *S. maltophilia* is not well-adapted to low pH and uses stress response mechanisms and location to cope with pH gradients characteristic of the CF

airways (**Fig. 2.8**). Tools that spatially resolve bacteria *in vivo* will be indispensable in understanding where and how bacteria adapt to clinical infections (51).

MATERIALS AND METHODS

S. maltophilia FLR19 genome.

S. maltophilia FLR19 was isolated from the sputum of an adult CF patient. The genome was sequenced on an Illumina MiSeq instrument and assembled using A5 (06-04-2016 version) with default parameters. Short scaffolds (<5,000 bp) containing repeated nucleic acid sequences were removed from the genome for downstream analyses.

Phylogenetic analyses.

To examine the phylogenetic relatedness of our isolate, we constructed an initial *S. maltophilia* phylogeny using 21 conserved single-copy marker genes. Specifically, we downloaded 153 strains designated *S. maltophilia* from the PATRIC genome database that contained corresponding metadata (see Data Set S1 in the supplemental material) (136). Next, we screened each downloaded genome for the presence of 21 marker genes with HMMER (144) and built the initial phylogenetic tree with FastTree2 (the Interactive Tree Of Life [iTOL] input for which can be downloaded from the following GitHub repository: <https://github.com/tgallagh/Stenotrophomonas>) (145). Based on the robustness of the resulting phylogeny, we calculated whole-genome pairwise comparisons (both nucleotide and amino acid identity [AAI]) across all genomes and selected a subset of strains ($n = 74$) that were closely related to our strain (>97% AAI) for downstream

analysis. Coding regions from the resulting 74 genomes were translated using Prodigal (146) with predicted functional annotation assigned by Prokka (147). We assigned orthologous protein groups (orthologs) based on a reciprocal protein BLAST search using Roary and clustered orthologs at 95% AAI (148). Single-copy orthologs conserved across all isolates ($n = 2,158$) were used to build a core genome phylogeny. Specifically, each core ortholog was independently aligned using Clustal Omega v1.2.0 (149) and used to create a concatenated core genome alignment (714,427 amino acids). Finally, we constructed a maximum likelihood phylogenetic tree using RAxML v8.0.0 (150) under the “PROTGAMMWAG” model for 100 replicates. We mapped all isolation source data retrieved from the PATRIC metadata onto the tree using iTOL (151). To identify genes unique to *S. maltophilia* FLR19 and other CF isolates, we compared total gene profiles across the 74 closely related genomes. Geneparser was used to determine the presence or absence of genes within the pangenome for each genome. These pangenome data were visualized using a script developed for the Roary pipeline (148). A cumulative gene plot was made using the “specaccum” function from the R package “vegan.” To determine if accessory gene content is a strong predictor of a strain’s isolation environment, a Jaccard dissimilarity matrix of the accessory genome presence-absence matrix was calculated with the “vegdist” function from the R package “vegan.” The dissimilarity matrix was visualized with a nonmetric multidimensional scaling (NMDS) plot constructed with the “metaMDS” function from “vegan.” An ANOSIM and nested PERMANOVA of the Jaccard dissimilatory matrix were conducted using the “anosim” and “adonis” functions from “vegan.”

***S. maltophilia* culture conditions.**

Strain FLR19 was isolated from the sputum of an adult CF patient in San Diego, CA. Strains CV 2008, FMa 2012, GC 2011, ZC 2005, and ZC 2006 were isolated from the sputum of four adult CF patients in Italy (128). Strains K279a and NCTC 10257 were also included to represent non-CF human isolates. For the growth curves, all eight strains of *S. maltophilia* were grown in pH 5, 7, and 9 phosphate-buffered Todd-Hewitt broth (THB). The strains were also grown in pH 5 THB spiked with citric acid, lactic acid, or sulfuric acid. In order to determine how pH affects antibiotic resistance, we also grew *S. maltophilia* cultures under the same conditions but with a concentration gradient of gentamicin (200, 400, or 800 mg/liter), meropenem (64, 128, or 256 mg/liter), and tobramycin (16, 32, or 64 mg/liter) for 24 h. An ANOVA with *post hoc* pairwise comparisons and Bonferroni corrections was conducted in R to compare growth in pH 5 or pH 9 to that in pH 7 medium with and without antibiotics. The fold change in *S. maltophilia* growth with antibiotics compared to growth without antibiotics was calculated, and a two-sample *t* test with Bonferroni corrections was used to identify significant changes in the fold change values of acidic and basic pH relative to neutral pH. Growth curves were collected using a SpectraMax 190 spectrometer from Molecular Devices. All three antibiotics were purchased from Fisher Scientific. For the transcriptomics and metabolomics experiments, *S. maltophilia* FLR19 was grown in pH 5, pH 7, or pH 9 phosphate-buffered THB for 24 h. For the FLR19 experiments, culture pH was measured with colorPhast pH strips from EMD Millipore. FLR19 was also grown in phosphate-buffered pH 5, 7, and 9 artificial sputum media (ASM) based on a recipe from Palmer et al. (40, 100). For the ASM growth curves, colony counts of spot dilution plates were used to calculate FLR19 concentration.

Preparation of *S. maltophilia* FLR19 transcriptomes and metabolomes.

The cells were centrifuged and pellets were stored in TRIzol at -80°C for RNA sequencing. RNA was extracted using the Zymo Direct-zol miniprep kit and concentrated with the Zymo RNA Clean and Concentrate kit. An Illumina Ribo-Zero rRNA removal kit was used to remove rRNA. The RNA libraries were prepared for sequencing with the TruSeq RNA sample preparation kit. Paired-end reads (250 bp) were sequenced on an Illumina HiSeq instrument. For metabolomics analysis, the supernatant was stored at -80°C (152). Triplicates of the uninoculated media and supernatants of acidic, neutral, and basic FLR19 cultures were sent to the West Coast Metabolomics Center for untargeted metabolomics analysis performed with gas chromatography-time of flight mass spectrometry (GC-TOF-MS). Metabolites were extracted from the bacterial supernatants with a 3:3:2 mixture of isopropanol, acetonitrile, and water. The GC-MS analysis followed Fiehn lab standard operating procedures (153).

***S. maltophilia* FLR19 metabolomics analysis.**

The Bray-Curtis distances of the metabolite intensities for all samples were calculated using the “vegdist” function from the R package vegan and visualized with a principal coordinate analysis (PCoA) plot using the “pcoa” function from the R package “ape.” In order to identify metabolites that were shared among or unique to the *S. maltophilia* FLR19 acidic, neutral, and basic metabolomes, the average normalized intensity for the metabolites in the three uninoculated replicates was calculated. The uninoculated media averages were subtracted from the metabolite intensities from the acidic, neutral, and basic metabolomes. A metabolite was considered to be produced in a certain condition

if the blank-subtracted metabolite intensity was positive for all three replicates and consumed if the blank-subtracted metabolite intensity was negative for all three replicates. Metabolites with significantly different levels in the acidic or basic metabolomes, compared to the neutral metabolome, were identified with a Kruskal-Wallis ANOVA and *post hoc* Dunn comparisons in R. Volcano plots were made in R to depict the fold change in metabolite abundances and *P* values of the *post hoc* Dunn comparisons of the metabolites considered to be significant from the Kruskal-Wallis ANOVA.

Transcriptomic analysis.

All RNA sequencing preprocessing was performed on the UC Irvine High Performance Computer Cluster in a Linux environment. Reads were quality-filtered using Trimmomatic version 0.35. (154). Specifically, adaptors were trimmed from the ends of reads, and the parameters used for filtering were as follows: minimum read length of 50 bp and a 4-bp sliding window average Phred quality score of 20. Overlapping reads were combined using Paired-End reAd mergeR (PEAR) and processed as single-end reads, separate from the remaining paired-end reads (155). The preprocessed reads were then aligned to the *S. maltophilia* FLR19 genome using Bowtie 2 in single-end or paired-end mode (156). In order to identify differentially expressed genes in the acidic versus basic transcriptomes (using the neutral transcriptome as a reference), HTSeq-Count (157) and the R package edgeR (158) were used to count the number of reads aligned to a gene. The sum counts of the overlapping reads processed as single-end reads and paired-end reads were calculated for each gene. Genes with \log_2 fold changes greater than 1 or less than -1 and FDR values of <0.05 were considered to be differentially expressed.

***S. maltophilia* metatranscriptome and transcriptome comparison.**

In order to identify genes that were expressed by *S. maltophilia* in cystic fibrosis sputum, seven cystic fibrosis metatranscriptomes (130) were quality filtered using Trimmomatic version 0.35 with the following parameters: minimum read length of 35 and a 4-bp sliding window with an average Phred score of 20 (154). The metatranscriptome reads were then dereplicated with Prinseq-lite version 0.20.4 (159). To ensure that stringent alignment parameters were used, the quality filtered metatranscriptome reads were first aligned using Bowtie 2 (156) to a custom-made database consisting of all non-*S. maltophilia* bacterial genomes associated with cystic fibrosis patients from PATRIC (1,812 genomes) (136). Reads that did not align to the CF bacterial database were then mapped to the *S. maltophilia* pangenome consisting of all the coding sequences from the 74 strains from our phylogenomics with Bowtie 1.

In order to compare gene expression of the *in vitro* *S. maltophilia* FLR19 transcriptomes to that of the metatranscriptomes, we processed the *in vitro* reads using a similar pipeline as that for the metatranscriptomes. Briefly, overlapping paired-end reads from the transcriptomes were aligned to the pangenome as a single read. The number of reads that aligned to a gene was then counted in R and the RPKM (reads per kilobase of transcript per million mapped reads) values were calculated. Reads that mapped to multiple genes were included in the quantification, since the same read often mapped to core genes across multiple genomes. The RPKM values from genes expressed in all nine samples were used to build a Euclidean distance matrix with the “vegdist” function from the R package vegan. The distance matrix coordinates were plotted on a principal-

coordinate analysis (PCoA) plot. A nested PERMANOVA was used to compare the gene RPKM values using the “adonis” function in vegan. For the PERMANOVA, the design structure nested experimental condition (acidic, basic, or neutral pH or sputum) in the source of the sample (*in vitro* versus *in vivo*). The proportion of CF database-filtered reads that aligned to a functional category was determined by counting the reads that mapped to genes found in the RAST SEED cellular categories (132). The *in vitro* FLR19 transcriptome reads were filtered using the same pipeline to compare the proportion of reads that mapped to the SEED categories *in vitro* to CF sputum.

Data availability.

The assembled FLR19 genome is publicly available on the PATRIC website under accession number 40324.190 (136). The metabolomics data are available in Data Set S4. The RNA sequencing reads are deposited in the NCBI GEO database under accession number [GSE121347](#), and the analyses can be found in Data Sets S5 to S7. The metatranscriptome reads can be found in the Sequence Read Archive under accession number [SRP135669](#) (130).

ACKNOWLEDGMENTS

We acknowledge the help of several people from the West Coast Metabolomics Center at UC Davis, including Megan Showalter and Oliver Fiehn. We appreciate the UCI High Performance Cluster staff, who go above and beyond maintaining the cluster and providing support to users. We thank Heather Maughan for help writing and editing the manuscript. We also thank Marvin Whiteley and Daniel Cornforth (Georgia Tech) for sharing their metatranscriptomes. Finally, we thank Matthew Wargo (University of

Vermont), Olivier Jousson (University of Trento), and Alfonso Esposito (University of Trento) for generously sharing their *S. maltophilia* strains with us.

This work was supported as a pilot project from the UC Davis West Coast Metabolomics Center (NIH grant DK097154) and NIH NHLBI (R56HL126754-01A1). K.W. is supported by a Gilead CF Research Scholars Award (app_00b072). T.G. is supported through the National Science Foundation's Integrative Graduate Education and Research Traineeship (IGERT) program (grant DGE-1144901).

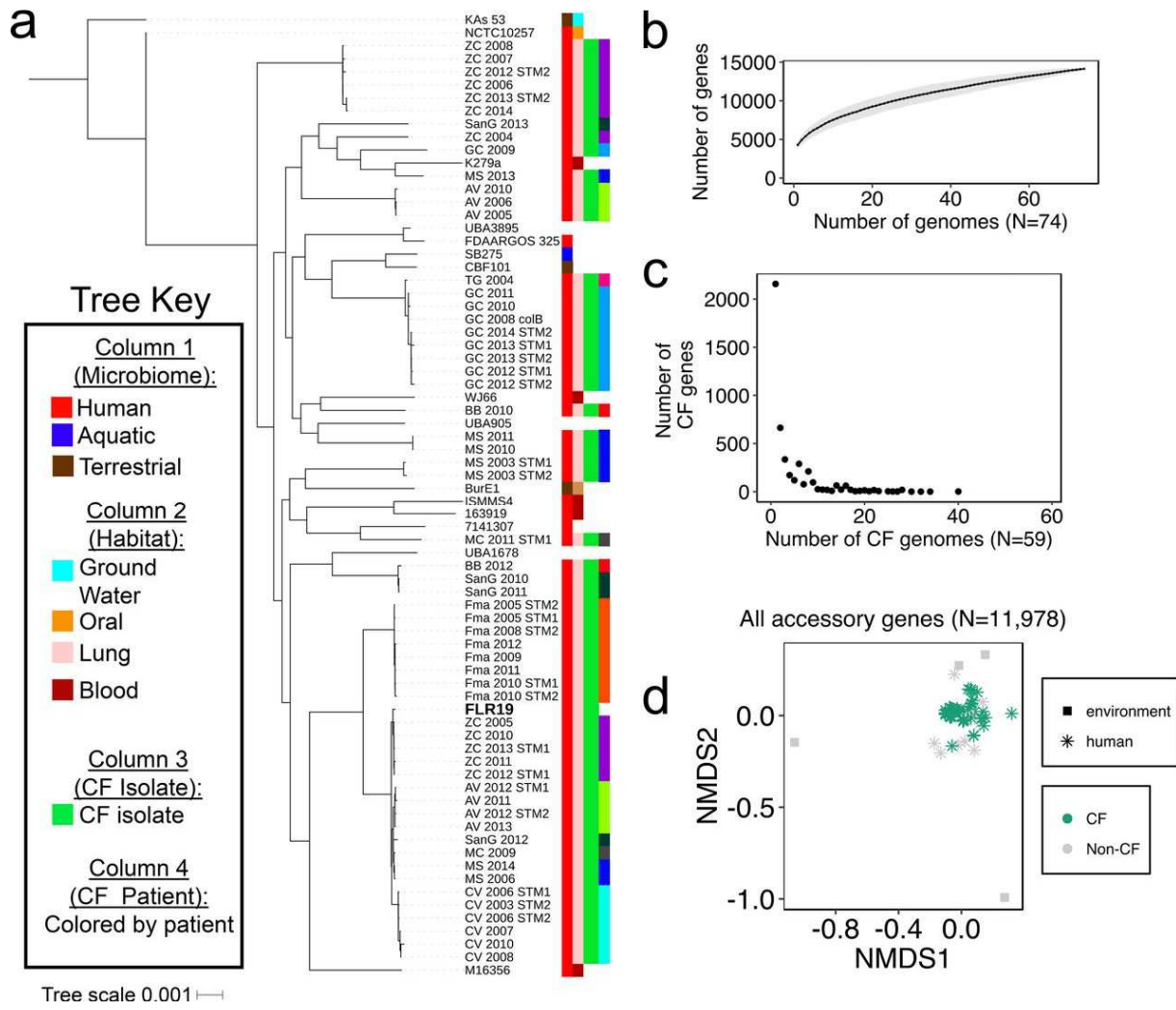
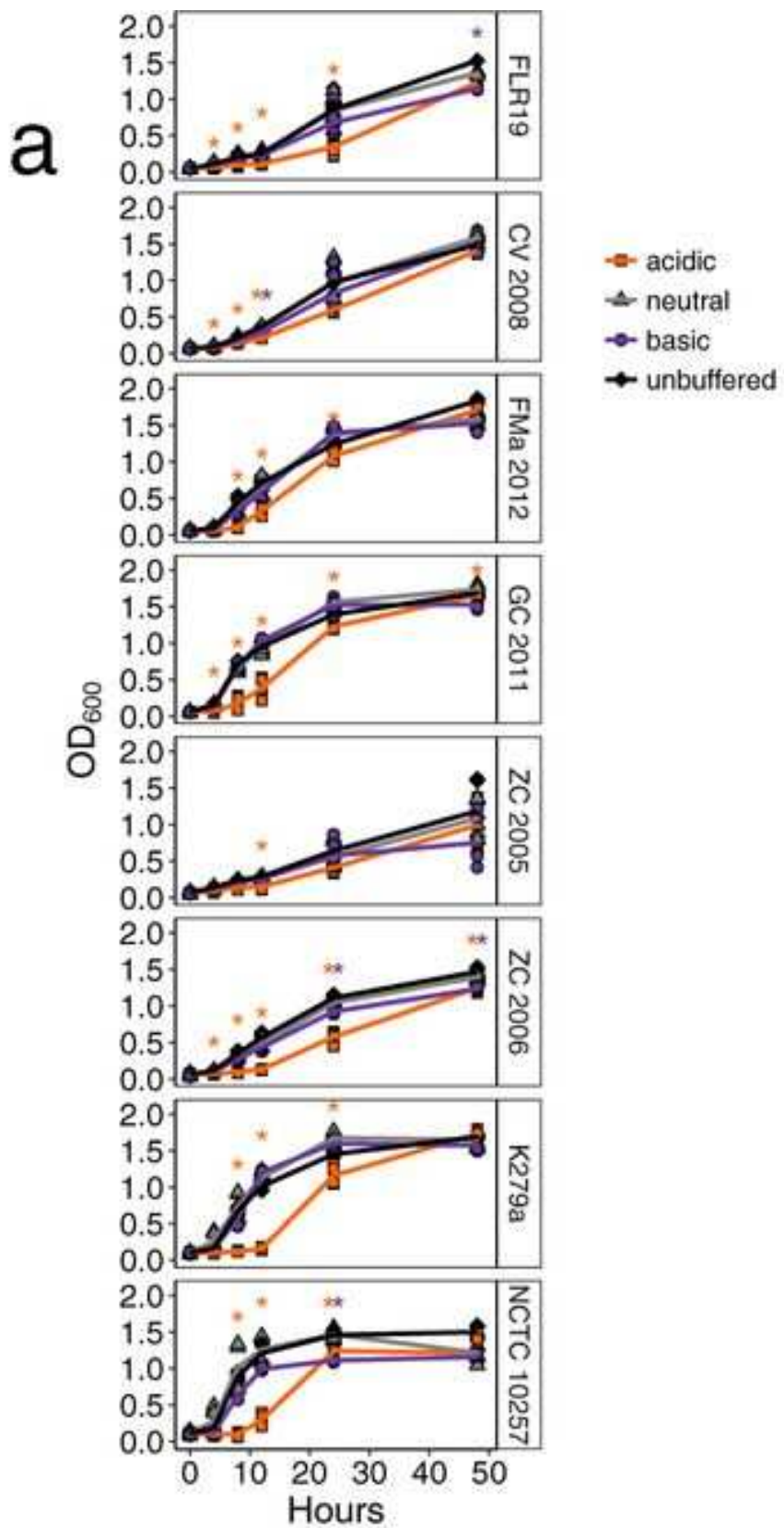
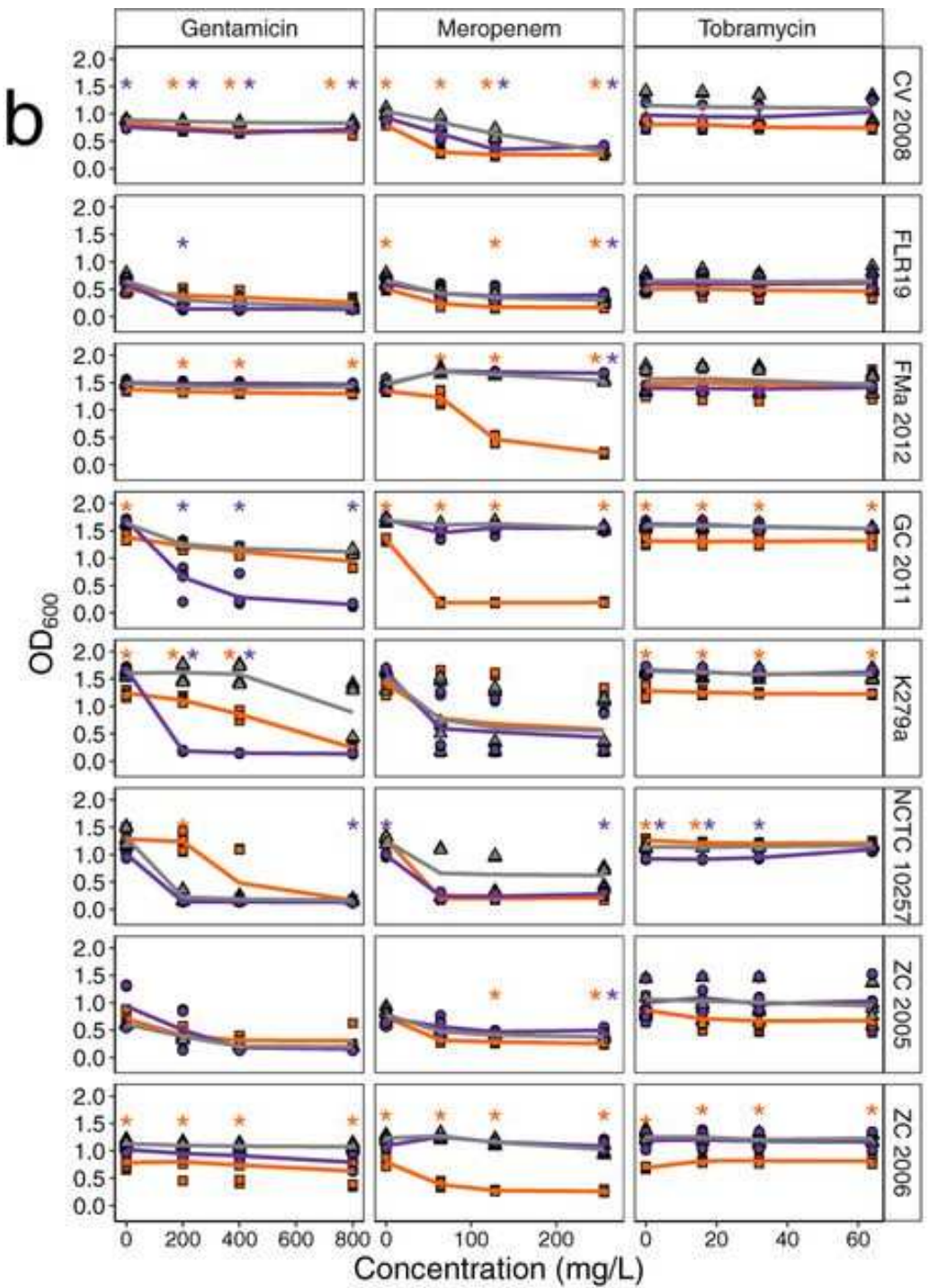


Fig. 2.1. *S. maltophilia* core and pangenome analyses. (a) Phylogenetic tree for 74 *S. maltophilia* strains constructed using 2,158 genes conserved across all strains. Information about the strains' isolation source is represented by the colored blocks in the four columns next to the tree. The last column highlights clonal strains isolated from the sputum of ten CF patients from Esposito et al.'s 2017 study (24), where each patient is designated by a different color and by the first portion of the genome name. (b) *S. maltophilia* pangenome accumulation plot (14,136 gene clusters, $n = 100$ permutations). (c) The distribution of genes found only in CF genomes (4,457 genes). No CF-specific genes were shared in all 59 CF isolates. In accordance with this, the accessory gene content ($n = 11,978$ genes) did not strongly separate strains into CF and non-CF groups. (d) NMDS of Jaccard dissimilarity matrix of accessory genome content ($n = 11,978$ genes, stress = 0.16), where the color indicates if strains were isolated from CF patients ($n = 59$) or were non-CF strains ($n = 15$). The shape indicates if a strain came from a human ($n = 70$) or was environmental ($n = 4$).

sample. An ANOSIM of the Jaccard dissimilarity matrix suggested that the accessory genome is not a strong indicator of whether a strain is CF or non-CF ($R = 0.55$, $P < 0.05$). A nested PERMANOVA of the Jaccard dissimilarity matrix indicated that the patient from whom a strain originates explains more of the variation ($R^2 = 37\%$) in accessory genome content than whether the strain originated from a CF patient ($R^2 = 5.5\%$) ($P < 0.001$).





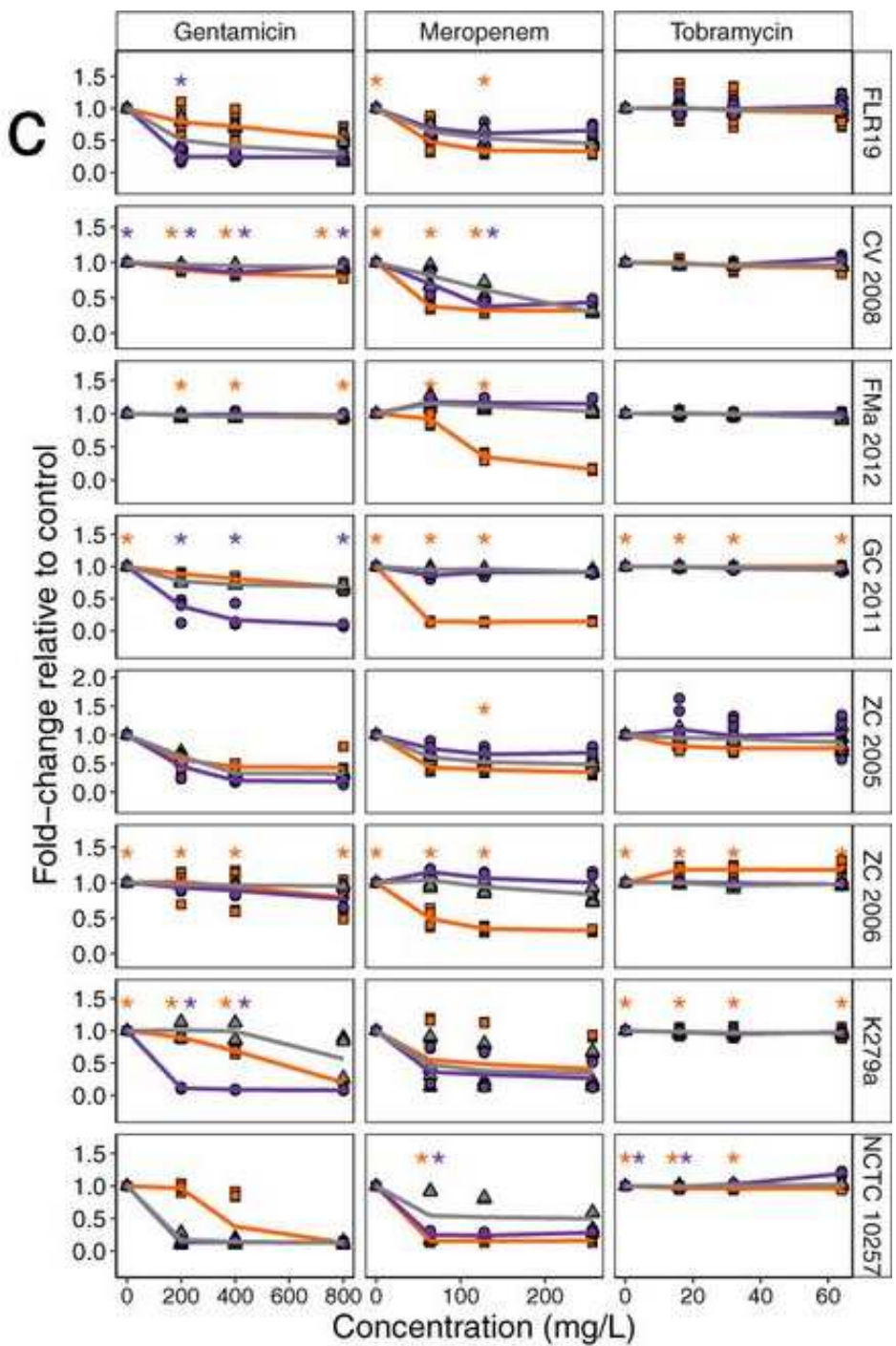


Fig. 2.2: Growth curves of eight *S. maltophilia* strains, consisting of six CF isolates (FLR19, CV 2008, FMa 2012, GC 2011, ZC 2005, and ZC 2006) and two non-CF human strains (K279a and NCTC 10257). Orange asterisks indicate a significant pairwise comparison in acidic to neutral pH, while purple asterisks indicate a significant comparison in basic to neutral pH. (a) The strains were cultured in acidic (initial pH 5), neutral (initial pH 7), and basic (initial pH 9) buffered media ($n = 6$ to 9 replicates; the line represents averages of

replicates). As a comparison, the strains were also cultured in unbuffered media (initial pH, 7.8). Asterisks indicate significant results with an ANOVA and post hoc pairwise comparisons, ($P < 0.05$). (b) Growth of *S. maltophilia* strains in pH-buffered media with different concentrations of gentamicin, tobramycin, and meropenem after 24 h of incubation. The line represents averages from replicates ($n = 6$ to 9 replicates). Asterisks represent $P < 0.05$ from ANOVA with post hoc comparisons and Bonferroni correction. (c) Fold change in the growth of each strain with antibiotics compared to growth without antibiotics. Asterisks represent $P < 0.05$ from two-sample t tests with Bonferroni corrections of the fold change values for acidic and basic pH compared to neutral pH.

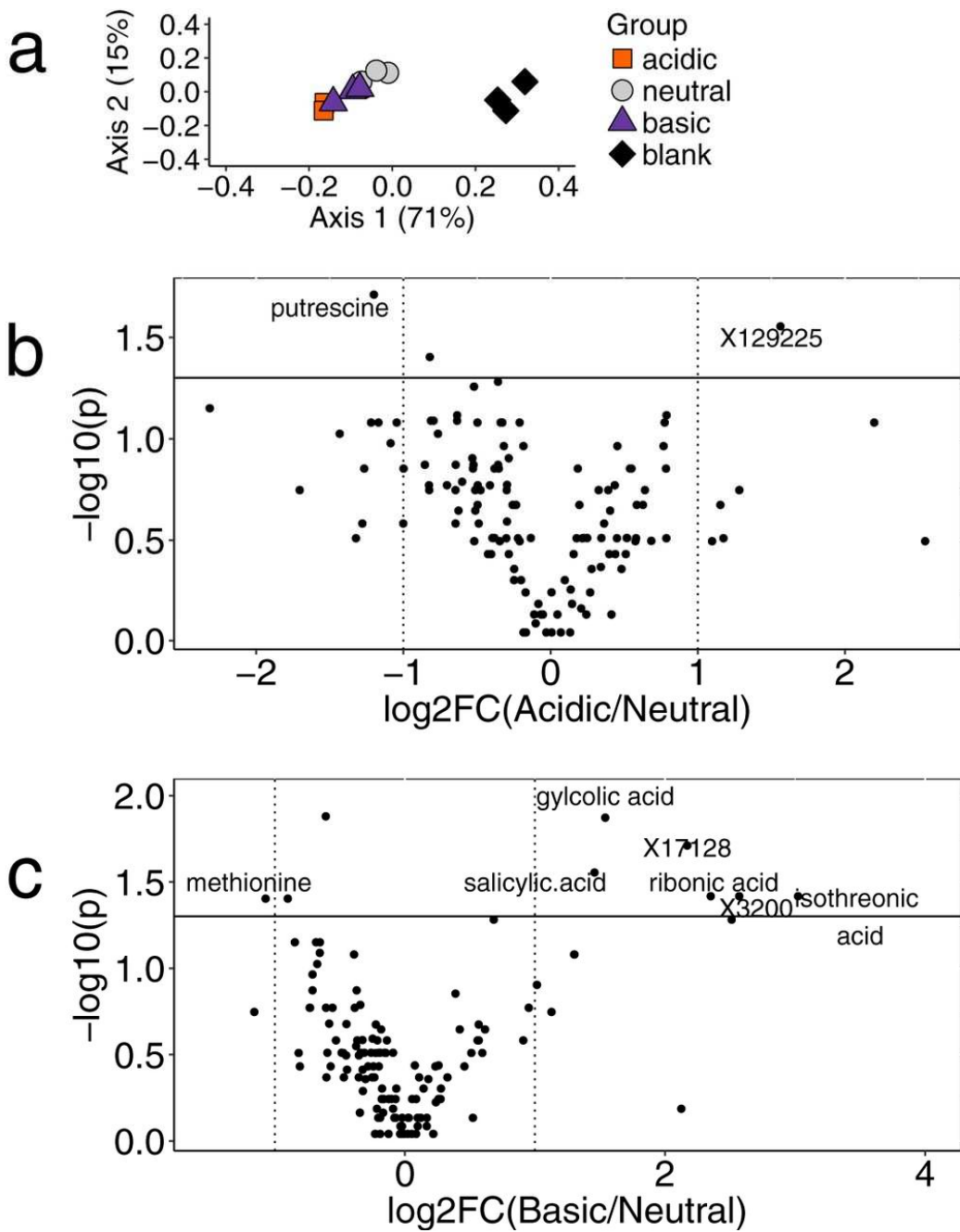


Fig. 2.3: Metabolomics of strain FLR19 under different pH conditions. (a) Principal coordinate ordination analysis (PCoA) of Bray-Curtis distances of the metabolite abundances for the uninoculated medium blank and *S. maltophilia* FLR19 grown in acidic pH, neutral pH, and basic pH ($n = 3$ replicates). (b and c) Volcano plots of the \log_2 fold change ($\log_2\text{FC}$) difference in metabolite abundance for the acidic metabolome (b) and basic metabolome (c) relative to the neutral metabolome. Negative $\log_{10}(p)$ is the P value from the post hoc Dunn analysis, where a P value of < 0.05 and a $\log_2\text{FC}$ value of > 1 or < -1 were considered to be significant. Metabolites with an "X" prefix were nonannotated.

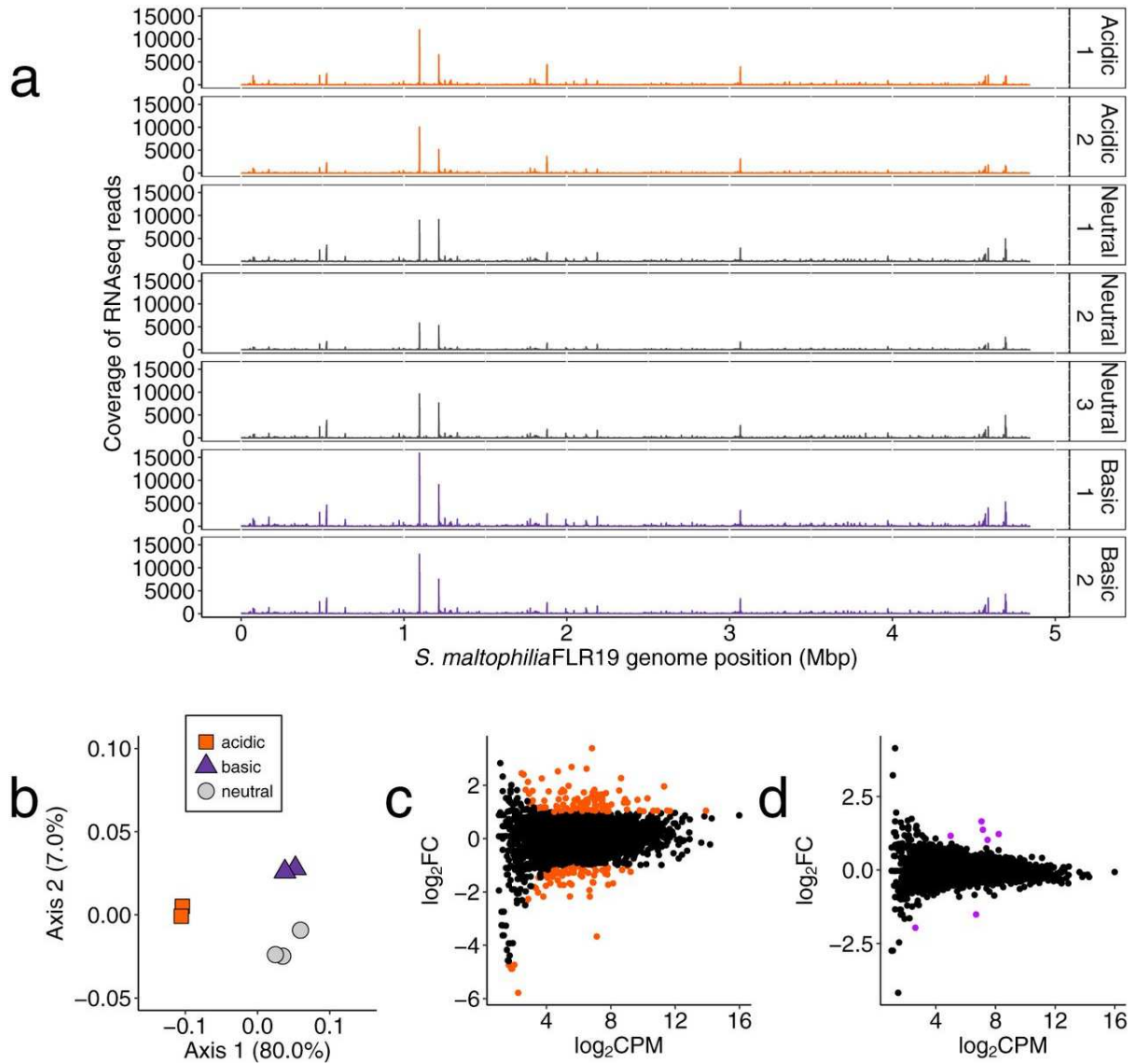


Fig. 2.4: Differential gene expression analyses of FLR19 grown under a range of pH conditions. (a) Coverage of transcriptome reads (counts per million) across the *S. maltophilia* FLR19 genome. (b) Principal-coordinate analysis (PCoA) of the Bray-Curtis distance matrix of the *in vitro* *S. maltophilia* transcriptomes ($n = 2$ for acidic and basic transcriptomes and $n = 3$ for neutral transcriptomes). (c and d) Smear plots of genes in the acidic transcriptome compared to the neutral transcriptome (c) and basic transcriptome compared to the neutral transcriptome (d). Each dot represents the \log_2 counts per million ($\log_2\text{CPM}$) average from both the replicates (x axis) and the average $\log_2\text{FC}$ of the acidic or basic CPM divided by neutral CPM (y axis). Colored dots indicate a $\log_2\text{FC}$ of >1 or <-1 and an FDR of <0.05 .

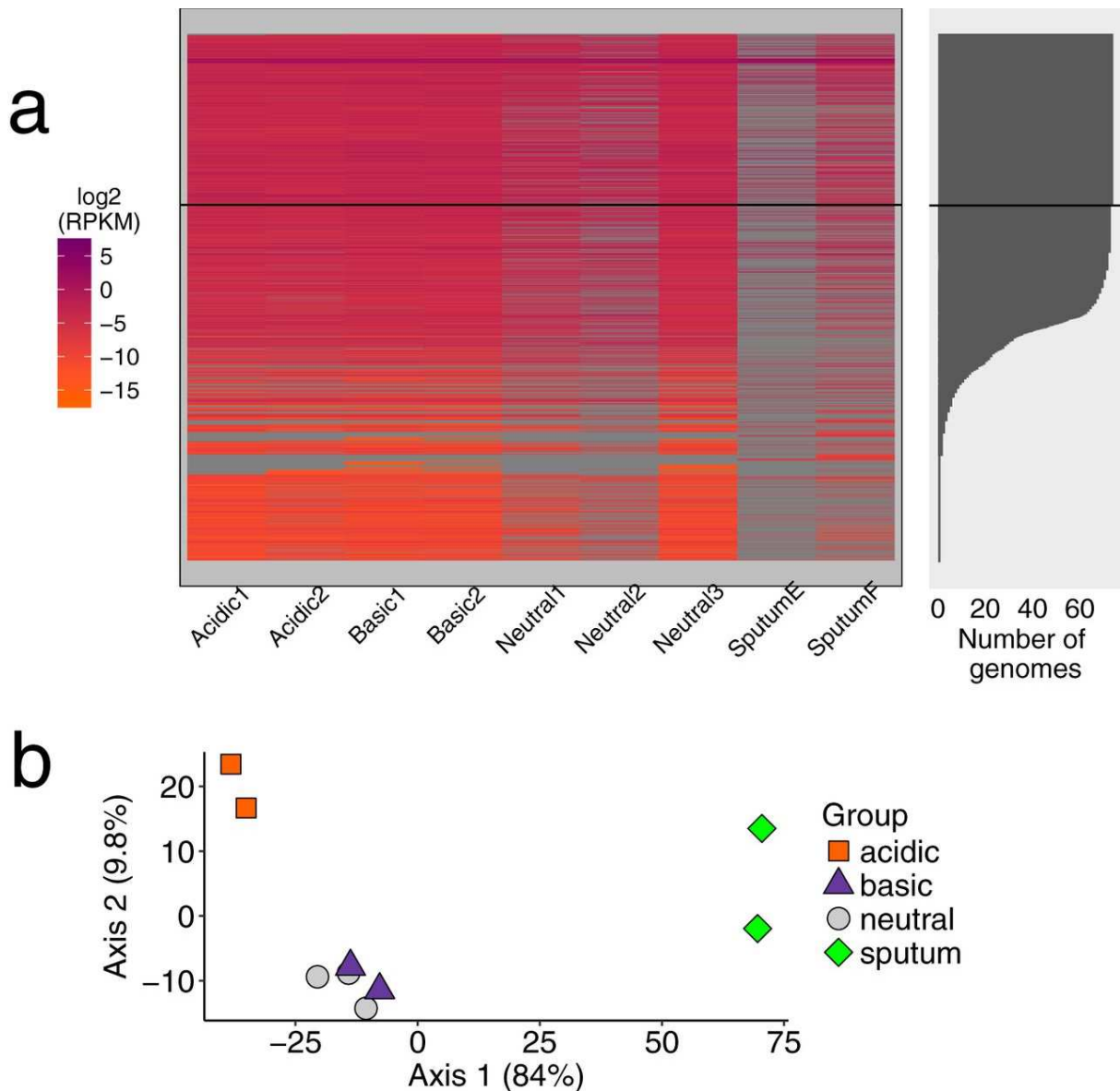


Fig. 2.5: Gene expression *in vitro* and in CF sputum. (a) Heat map of the \log_2 reads per kilobase of transcript per million mapped reads (RPKM) values of the transcriptome and metatranscriptome reads aligned to the *S. maltophilia* pangenome. Each row is one gene (95% AAI clusters from pangenome analyses). The number of *S. maltophilia* genomes which have that gene is indicated on the right. Any gene above the black horizontal line in both plots was part of the core genome (found in all 74 strains). (b) PCoA plot of the Euclidean distance matrix of RPKM values of 918 genes expressed in all samples.

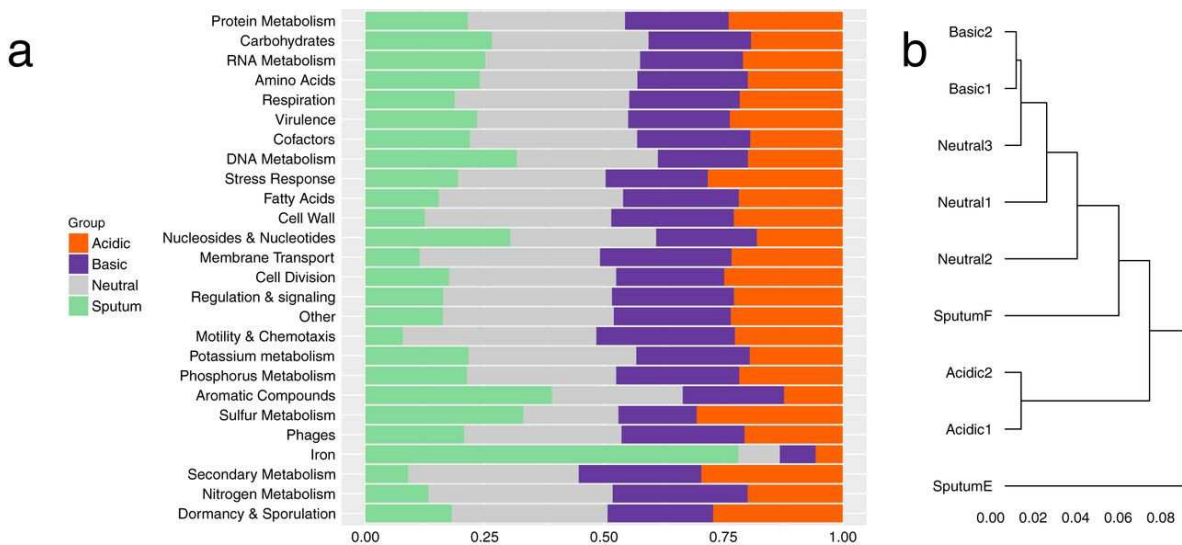


Fig. 2.6: Functional activities of FLR19 under a range of pH conditions and of *S. maltophilia* in CF sputum. (a) Relative proportion of RNA sequencing reads that aligned to 26 functional categories from the sputum transcriptomes ($n = 2$) and the *in vitro* acidic ($n = 2$), neutral ($n = 3$), and basic pH transcriptomes ($n = 2$). (b) Hierarchical clustering by sample of the Euclidean distance matrix of proportion of reads that aligned to a functional category.

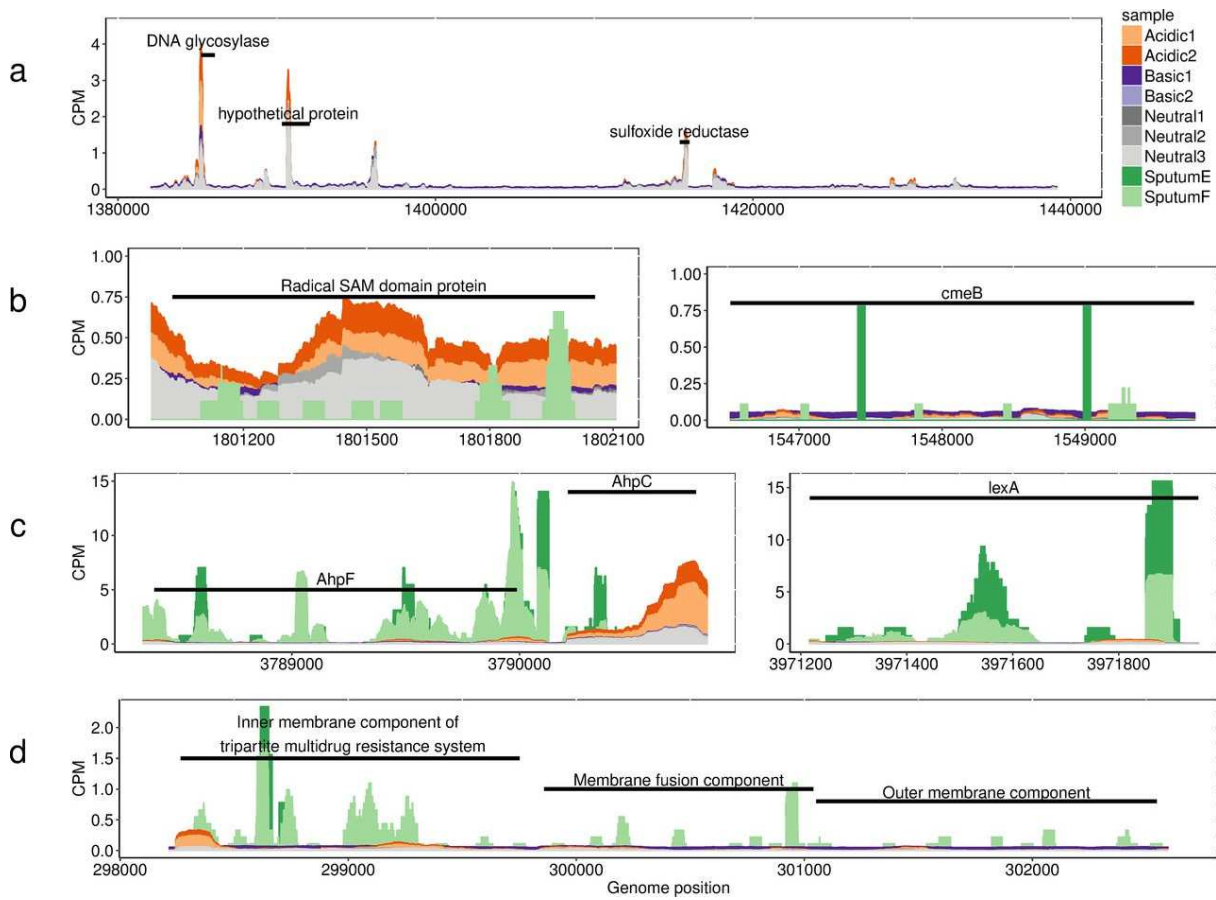


Fig. 2.7: Examples of genes expressed in acidic pH and CF sputum. The black bars in the plots depict the lengths of genes. CPM, counts per million. (a) Coverage of *S. maltophilia* FLR19 transcriptome reads across a 58,000-bp region which contained some genes unique to our strain. The labels indicate genes with higher expression in acidic pH. The DNA glycosylase was significantly upregulated in acidic pH compared to neutral pH. (b) FLR19 transcriptome reads and sputum metatranscriptome reads across a radical SAM domain protein (left panel) closely related to a DNA lyase and found in six *S. maltophilia* CF isolates and across the RND efflux pump CmeB (right panel). (c) FLR19 transcriptome reads and sputum metatranscriptome reads aligned to the genes for alkyl hydroperoxide reductases (AhpF and AhpC) and the SOS response repressor LexA, genes that were conserved across all 74 *S. maltophilia* strains. (d) FLR19 transcriptomes and sputum metatranscriptomes across three components of the tripartite multidrug efflux system.

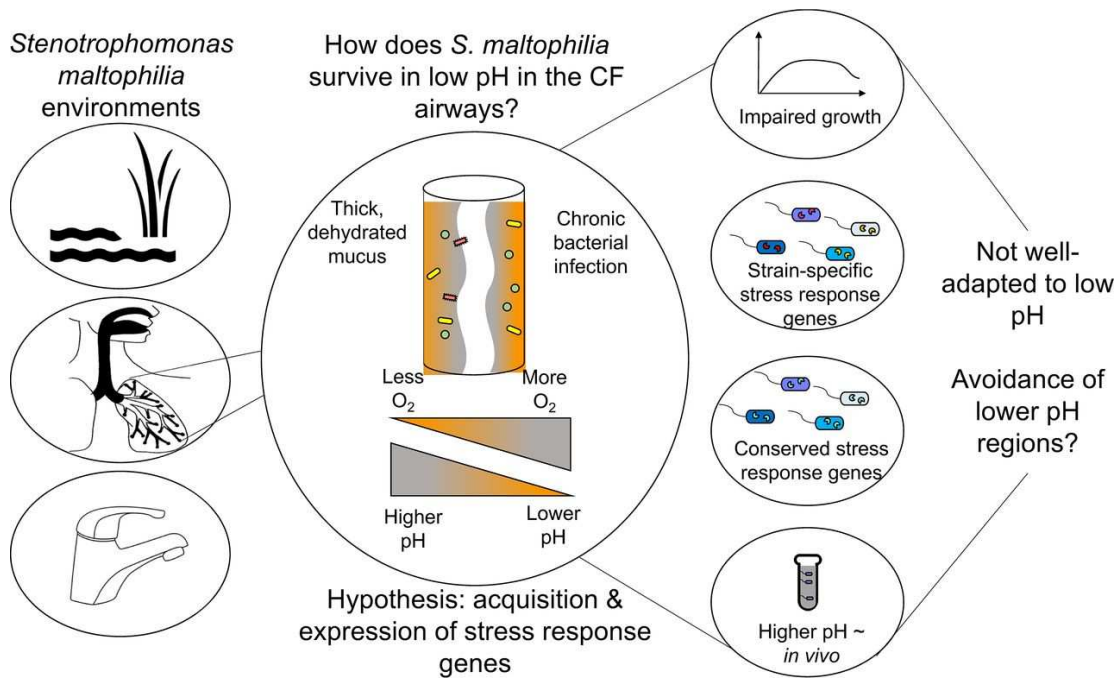


Fig. 2.8: Conceptual overview of study. *S. maltophilia* is a ubiquitous organism, found in aquatic and soil environments and in cystic fibrosis (CF) infections. Because CF sputum is characterized by gradients of pH (reported to range from 2.9 to 6.5) and oxygen (9), we wanted to determine how *S. maltophilia* survives under low-pH conditions. Growth assays indicate that low pH is stressful for both CF and non-CF strains. While *S. maltophilia* can cope with low pH by expressing conserved and adapted stress response genes, our *in vitro* and *in vivo* transcriptomics analyses suggest that *S. maltophilia* may survive in the airways by avoiding lower-pH microenvironments. Taken together, the results of our study highlight that pH can drive *S. maltophilia* physiology by inducing stress response mechanisms and controlling the physical colonization of *S. maltophilia*.

Chapter 3:

Visualization of *Pseudomonas aeruginosa* pyocyanin reduction at the surface of biofilms

Authors: T. Gallagher*, S.W. Leemans*, A. Dvornikov, K. Perinbam, J. Fong, C. Kim, J. Kapcia, M. Kagawa, A. Grosvirt-Dramen, A. Hochbaum, M. Digman, E. Gratton, A. Siryaporn, K. Whiteson

* T.G. and S.W.L. contributed equally

Abstract:

Understanding bacterial physiology in real-world environments is a challenging, yet necessary endeavor to effectively treat infection. The environments of many chronic infections are characterized by steep chemical gradients, yet the effect of hypoxia on opportunistic pathogens can be disregarded in clinical settings. *Pseudomonas aeruginosa* is a ubiquitous organism that infects wounds and the airways of persons with cystic fibrosis. *P. aeruginosa* produces pyocyanin, which has been traditionally classified as a toxin due to its redox-active properties, but can also facilitate anaerobic respiration. *P. aeruginosa* survival in low oxygen is dependent on pyocyanin electron cycling, but the utilization of pyocyanin throughout biofilms is not well-understood. To track pyocyanin reduction throughout a biofilm, we developed a fluorescence lifetime imaging microscopy (FLIM) unmixing approach that was compared to hyperspectral imaging microscopy (HIM). Pyocyanin fractional contribution predictions were similar with both approaches. Deep

imaging of colony biofilms was performed on a custom-made FLIM instrument designed for tissue imaging, called the DIVER. *P. aeruginosa* rapidly reduces pyocyanin at the surface of biofilms, where there is dense growth and possibly high oxygen consumption. Our FLIM unmixing approach paired with the DIVER acquisition can be used to track pyocyanin dynamics throughout biofilms and has promise as an application for assessing redox state in relevant chemical gradients.

Introduction

To persist in any environment, bacteria adapt to chemical and nutrient gradients. Understanding *in vivo* bacterial activity can improve treatment of infections. Chronic lung and wound infections consist of steep oxygen gradients that arise from low penetration and cellular consumption of oxygen (4, 160). These anaerobic conditions can reduce antibiotic efficacy, especially against organisms inactive in low oxygen (161).

Pseudomonas aeruginosa, an opportunistic pathogen that causes chronic wound and cystic fibrosis lung infections, is incapable of anaerobic growth via fermentation and employs alternative methods to survive in low oxygen. *P. aeruginosa* can respire anaerobically via denitrification (162, 163) and secrete phenazines (26, 164, 165) 6/4/2020 1:54:00 PM. Phenazines are colorful, redox-active molecules that recycle electrons. Pyocyanin, the final product in the phenazine synthesis pathway, has the highest affinity for oxygen out of the phenazine family (166). In the oxidized form, pyocyanin has a blue pigment and is toxic to other cells (167, 168). *P. aeruginosa* uses oxidized pyocyanin to

metabolize glucose into acetate, thereby generating more energy and reducing pyocyanin in the process. The reduced form of pyocyanin is fluorescent, but the emission spectrum of pyocyanin overlaps with other fluorescent metabolites, including NADH and apopyoverdine (169).

Hyperspectral imaging microscopy (HIM) can unmix pyocyanin fluorescence from other fluorophores and has been used to study dynamics of reduced pyocyanin in liquid cultures (169). The spatial production and reduction of pyocyanin has not been characterized, due to limits in the imaging depths of commercial microscopes. The DIVER (170, 171) is a custom-made fluorescence microscope designed for deep tissue imaging that can measure fluorescence lifetime with single-cell resolution. Fluorescence lifetime imaging microscopy (FLIM) can be used to determine the composition of multiple fluorophores contributing to a fluorescent signal. For example, FLIM is often used to image the relative amounts of enzyme-bound NADH to free NADH, which can indicate the respiratory state of a single cell (172–176).

FLIM and HIM data can be transformed and represented on phasors, a powerful approach to analyze fluorescence data (177, 178) (**Fig. 3.1**). For lifetime images, the response of the fluorophore to the excitation source is determined by Fourier transformation of exponential decay traces to obtain the modulation (M) and phase (φ) at different harmonics (177). The sine and cosine coefficients of the transform make up the y and x-axes of the lifetime phasor. Pure species (with single exponential decays) are located

on the universal semi-circle (**Fig. 3.1A**). For hyperspectral data, the modulation and phase are related to the width and mean wavelength of the spectrum (**Fig. 3.1B**) (178). Both the fluorescence lifetime and spectral phasor follow the same rule: samples containing a combination of the species fall on a line connecting the sample signal to the pure components. The distance from the signal to the pure component is proportional to the fractional contribution. The phasor is commonly used to unmix two or three fluorescent species using linear algebra (**Fig. 3.1**), but additional fluorescent species can be unmixed if additional harmonics are incorporated into the phasor analyses. The orthogonality of the Fourier transform guarantees that G and S components for each harmonic can be used as independent observations. This allows unmixing of a fluorescent signal into its constituent components using linear algebra (179) or least-squares optimization if the system is overdetermined. If the bandpass filter used for fluorescence lifetime imaging is the same as the hyperspectral acquisition window, the fractional contributions to the total signal will be same. This insight allows unmixing of fluorescent species present in each pixel in the image simultaneously using both spectral and lifetime data.

Redox state varies throughout biofilms, and understanding spatial changes in pyocyanin reduction can be used to assess bacterial activity, treatment susceptibility, and infection progression. We developed and compared our FLIM phasor unmixing approach to HIM phasor unmixing. DIVER FLIM acquisition and lifetime phasor unmixing can be used to track pyocyanin redox states throughout *P. aeruginosa* biofilms.

Results:

HIM and FLIM phasor characterization of *P. aeruginosa* fluorophores.

The two-photon fluorescence emission spectra of *P. aeruginosa* fluorophores were characterized (NADH, enzyme-bound NADH, FAD, pyoverdine, pyocyanin, 1-hydroxyphenazine, coproporphyrin) (**Fig. S3.1**) and agreed overall with previously published spectra (169). Different reduction methods of pyocyanin changed the fluorescence spectra and lifetime phasor results. The resulting pyocyanin population likely consisted of a mix of the radical and reduced form, but the FLIM phasor analysis suggests our FLIM setup primarily acquires the reduced form (**Fig. S3.2**).

Four of the seven species were captured by the FLIM DIVER acquisition parameters, which included an emission filter targeted towards NADH (400-500 nm): NADH, enzyme-bound NADH, and reduced pyocyanin, and apo-pyoverdine (**Fig. S3.1**). The FLIM and HIM phasor components for the pure fluorescent species were determined, and pyocyanin had a distinct FLIM and HIM phasor signature (**Fig. 3.2**). To compare the detected fluorescent species across both methods, the HIM spectral window was truncated to 410-500 nm to exclude measurements of species not captured with our FLIM acquisition settings (**Fig. S1**).

Comparison of HIM and FLIM unmixing results.

The spectral and fluorescence fractional contributions of NADH, enzyme-bound NADH, reduced pyocyanin, and apo-pyoverdine were determined at the surface of five-day old biofilms of WT *P. aeruginosa* PA14 and a phenazine knockout of the same strain (*Δphz*),

which does not synthesize any phenazines including pyocyanin (**Fig. 3.3**). To assess the robustness of the unmixing approaches across different systems, the *P. aeruginosa* strains were grown in two conditions, M9 succinate and artificial sputum medium. After imaging the aerobic cultures, the cultures were placed in an oxygen-limited environment for 2h, because we hypothesized that low oxygen would result in reduction of pyocyanin. WT *P. aeruginosa* PA14 shifted towards the reduced pyocyanin FLIM and HIM signal in hypoxic conditions,. This pyocyanin shift was not observed in the phenazine mutant cultures (**Fig. 3.4**). The FLIM and HIM phasor visualizations indicate reduced pyocyanin contributed to a higher proportion of the fluorescent signal when WT PA14 was grown in ASM and incubated in low oxygen conditions.

The HIM and FLIM data were unmixed to determine the fractional contribution of reduced pyocyanin, apo pyoverdine, NADH, and enzyme-bound NADH. The fluorescence lifetime of enzyme-bound NADH depends on local factors, including enzyme type and pH (180), and is not well-characterized in bacterial systems. The FLIM NADH phasor trajectory of *P. aeruginosa* cultures shifts in different media backgrounds and suggested NADH bound to certain enzymes may have a lifetime shorter than 3.4 ns (**Fig. S3.5**). We used 2.8 ns as the fluorescence lifetime representation for enzyme-bound NADH in *P. aeruginosa* (**Fig. S3.3**). Although Δphz does not produce pyocyanin, both the FLIM and HIM unmixing methods still detected low fractional contributions from pyocyanin (**Fig. 3.5**).

Overall, HIM and FLIM unmixing did not correlate for the M9 succinate cultures and moderately correlated for ASM cultures (**Fig. 3.5**). Pyoverdine and enzyme-bound NADH have similar spectra and lifetimes, and our unmixing method could not accurately

distinguish these two fluorophores with the narrow spectral band of acquisition (**Fig. 3.2, S3.1**). The HIM and FLIM fractional contributions predictions of pyocyanin were similar in cultures with high pyocyanin production (WT PA14 in ASM) (**Fig. 3.5B**).

Fluorescence lifetime and pyocyanin measurements throughout *P. aeruginosa* biofilms with the DIVER microscope.

The fluorescence intensity and lifetime were acquired throughout different depths of five-day old *P. aeruginosa* biofilms grown in artificial sputum medium using the DIVER (170, 171). Laser power was increased with deeper imaging in the sample to compensate for signal attenuation from scattering and absorption. The measured total fluorescence intensity was similar throughout the biofilm depths, suggesting effective excitation delivery (**Fig. 3.6**). Cell density decreased with biofilm depth, indicating more growth at the biofilm surface (**Fig. 3.6**). The FLIM phasor signal of masked cells or aggregates shifted with biofilm depth (**Fig. 3.6, 3.7A**). The biofilm surface FLIM signal was dominated by a longer lifetime species, and the sample phasor coordinates were near the coordinates of reduced pyocyanin. Worth nothing, this long lifetime signal was observed when a coverslip was placed on top of the biofilm sample. FLIM of the biofilm surface without a cover slip was acquired with an air objective, and indicated oxygen limitation was driving the formation of the long lifetime species believed to be reduced pyocyanin (data not shown). Lifetime unmixing of the biofilm samples (imaged with a coverslip) indicated higher contributions from reduced pyocyanin at the biofilm surface (**Fig. 3.6, 3.7**).

Discussion

Oxygen is scarce in many environments, and in the context of chronic infections, hypoxia drives microbes to produce redox-active metabolites that can act as alternative electron acceptors but are also toxic and may contribute to disease progression. Bacterial biofilms have little oxygen beneath the surface. *P. aeruginosa* synthesizes and secretes redox-active pyocyanin to recycle electrons in low-oxygen (165). We sought to determine the redox state of *P. aeruginosa*-produced pyocyanin throughout biofilms, and developed a fluorescence imaging unmixing approach to calculate reduced pyocyanin fluorescence contributions relative to other fluorescent metabolites.

FLIM and HIM unmixing results varied for fluorophores.

FLIM phasor unmixing of the first harmonic was used to determine the contribution of four species - reduced pyocyanin, apo-pyoverdine, NADH, and enzyme-bound NADH - to fluorescent signals in *P. aeruginosa* biofilms (**Fig. 3.2**). To validate the FLIM unmixing results which is an underdetermined system for four fluorophores, we implemented an orthogonal method with HIM phasor-based unmixing of two harmonics. By incorporating additional harmonics, the system is sufficiently constrained and can theoretically be solved with HIM unmixing. However, there was very little modulation of intensity in the emission acquisition window (410-500 nm). The HIM data was truncated for two reasons: (1) to directly compare predictions from the HIM and FLIM approaches and (2) to avoid introducing additional fluorescent species, such as FAD and other phenazines (169), and potentially confounding the HIM analyses (**Fig. S3.1**).

The HIM and FLIM-predicted fractional contributions did not correlate overall (**Fig. 3.4-3.5**). Pyoverdine and NADH FLIM predictions contradicted with that of HIM. FLIM predicted large contributions from pyoverdine, while HIM predicted larger contributions from NADH in the same samples. The spectral phasor positions of pyoverdine and free NADH are close, likely contributing to the discordance between HIM and FLIM predictions. In addition, the fluorescence lifetime of pyoverdine (4 ns) and enzyme-bound NADH (reported to range from 1.7-9 ns (176, 180)) could overlap depending on local conditions. In contrast, reduced pyocyanin had a distinct HIM spectral phasor position and FLIM phasor fingerprint with a long fluorescence lifetime (>10 ns) (**Fig. 3.2**). We proceeded with the FLIM unmixing method to determine if pyocyanin fractional contributions shift throughout *P. aeruginosa* biofilms.

Reduced pyocyanin was localized at the biofilm surface in our system.

To recapitulate slower bacterial growth observed in infections (16, 181), colony biofilms were radially grown for five days in artificial sputum medium with soft agar. The radial center of the colony was imaged axially to capture the different depths in the oldest population of the biofilm. Reasoning that natural gradients would form with less oxygen exposure deeper in the biofilm, we initially hypothesized that *P. aeruginosa* would produce more pyocyanin in the hypoxic core of the biofilm (164, 165, 182). However, in our system, reduced pyocyanin dominated the FLIM signal at the surface of the biofilm (**Fig. 3.6, 3.7**), and the pyocyanin-dominant signal was only observed when imaging with a coverslip placed on top of the sample.

The highest density of *P. aeruginosa* growth was at the surface and was associated with the reduced pyocyanin FLIM signal (**Fig. 3.6**). After oxygen was limited by the introduction of a coverslip at the surface, it is likely dense bacterial populations utilized a pool of pyocyanin for electron recycling. Our biofilm pyocyanin model agrees with previous studies showing that population density controls phenazine biosynthesis (183, 184) and oxygen is required for pyocyanin biosynthesis (185). Although it may seem counterintuitive that oxygen is necessary to synthesize an alternative electron acceptor, pyocyanin has the highest affinity for oxygen out of other studied phenazines (166). In locally anoxic conditions, *P. aeruginosa* couples pyocyanin reduction with oxidation of glucose and pyruvate, which generates ATP and increases anaerobic survival (165, 186, 187). The reduced pyocyanin is secreted and oxidized extracellularly (165, 182). A portion of the pyocyanin can be retained in the biofilms by *P. aeruginosa*-derived extracellular DNA that binds to phenazines (188, 189), distributing pyocyanin both inside and outside of the biofilm and enabling electron cycling.

Limitations and future directions.

The phasor approach has several benefits, including a clear visualization of the data and reliable deconvolution of the instrument response function (190). The phasor transform effectively applies a bandpass filter to the data, compressing the complete time-domain (or wavelength-domain) signal into two numbers, the G and S components. The first harmonic contains the low frequency components of the signal, representing an approximation to the shape of the lifetime (or spectrum) trace with a single sine or cosine

function. The addition of higher harmonics further refines the shape of the signal. The approach decreases the influence of high-frequency noise, giving an advantage over direct least-squares unmixing approaches.

A consideration in the application of the simultaneous spectral-lifetime unmixing method is that the spectral range of acquisition must be nearly identical for the two measurements. For accurate unmixing, the spectral ranges need to have broad enough modulation in the pure species. If the spectral range is too narrow (as in our measurements), the difference in the shape between pure species is negligible.

One of the challenges in unmixing the FLIM and HIM images using spectrum and lifetime simultaneously is that each pixel in the FLIM image must be aligned with the HIM image. With our instrument, the Zeiss LSM 880, acquisition of FLIM images was delayed by a couple minutes relative to spectral acquisition due to the need to switch to a different data acquisition software. During this time, bacteria in the sample can produce new metabolites.

The unmixing method yields the fractional contributions of fluorophores in each pixel in an image, and its accuracy is dependent on the fluorophores used as the references. While several studies on bacterial FLIM have been conducted, the lifetime of NADH when bound to bacteria enzymes has not been well-characterized. We used 2.8 ns to represent all enzyme-bound NADH in our unmixing program, but the lifetime of NADH changes in different enzymes and local environments and poses a challenge to NADH FLIM studies (176, 180, 191).

Finally, the fractional contributions are proportional to the relative concentrations of various metabolites. With appropriate instrumentation and characterization of fluorophores, it is possible measure the absolute concentration of molecules (192).

Conclusions.

Here, we compared two orthogonal measurements to determine the presence and relative amount of reduced pyocyanin in *P. aeruginosa* biofilms. Although our implementation is far from perfect, it puts forward a framework to combine hyperspectral imaging and lifetime imaging and map out the concentrations of different fluorophores in a sample with high molecular specificity.

Methods and Materials

Chemicals and bacterial media.

HPLC-grade pyocyanin was ordered from Sigma-Aldrich (P0046). 10 mM stocks were dissolved in 20% ethanol and stored at -20°C. Artificial sputum and M9 minimal media with 40 mM succinate soft agar were used to grow *P. aeruginosa* biofilms. The recipes for both media types were modified from Gao et al. (100) to include 0.28% final agar concentration. To visualize biofilm colony growth over time, the agar was prepared in large petri dishes (150x15 mm).

Bacterial strains and growth.

P. aeruginosa PA14 and the phenazine knockout *phzA1-G1/A2-G2* were obtained from Dianne Newman's lab at California Institute of Technology. For biofilm imaging, the bacteria were grown overnight on Todd-Hewitt agar, and individual colonies were inoculated into the center of the artificial sputum or M9 succinate soft agar plates. The biofilm colonies were grown aerobically at 37°C for 5 days.

Chemical reduction of 1-hydroxyphenazine and pyocyanin and electrochemical reduction of pyocyanin.

Five hundred micromolar stocks of pyocyanin were diluted in 1X MOPS buffer with concentration gradients of TCEP ranging from 0.1 mM to 125 mM (pH 7). A fresh stock of 821 μM of pyocyanin was prepared in ammonium acetate 0.1M KCl MOPS buffered solution in and electrochemically reduced following the protocol developed by Wang and Newman (166). The electrochemical cell consisted of a glassy carbon working electrode, platinum wire counter electrode, and Ag/AgCl₂ reference electrode. The voltage was set to -0.345V, and the reaction proceeded in an anaerobic chamber overnight until the current reached zero. For 1-hydroxyphenazine, 500 micromolar stocks were prepared and diluted in 1XMOPS buffer with pH 7-buffered DTT as the reducing agent (193).

Hyperspectral and fluorescence lifetime imaging on Zeiss LSM-880.

To characterize the emission spectra and fluorescence lifetime of NADH, FAD, pyoverdine, reduced pyocyanin, and reduced 1-hydroxyphenazine, solutions were transferred to a clean slide. The reduced pyocyanin and 1-hydroxyphenazine were prepared in a Coy anaerobic chamber and sealed with iSpacers to avoid oxygen exposure (<https://www.sunjinlab.com/>).

WT PA14 and *Δphz* biofilms grown in the artificial sputum and M9 succinate soft agar were cut with a sterile razor and placed onto a MATTEK dish (Part No: P35G-1.5-14-C) with the surface of the biofilm on the coverslip. To compare the impact of oxygen on the spectral and lifetime signal, the biofilm samples were (1) placed in a dish open to air and immediately imaged or (2) were placed in between two coverslips and sealed in the dish with tape for 2h at RT to promote oxygen consumption.

The pure fluorophore solutions and biofilm surfaces were imaged on an inverted Zeiss LSM-880 with an ISS Spartan3 FLIMbox, BH HPM-100-40-Hybrid detector, and a Spectra Physics Mai Tai titanium sapphire laser. The fluorophores were excited with 2-photon excitation at 740 nm and laser power ranging from 1-10 mW. For the hyperspectral imaging, emission ranging from 410-695 nm was collected with 9 nm step resolution over 32 channels. One frame was collected per sample with a pixel dwell time of 4 μ s. The spectra were analyzed on Zeiss Zen software, and .lsm files were exported for downstream unmixing steps. After collecting the spectra, fluorescence lifetime of the same sample was obtained by switching the light path to the FLIMbox detectors. The sample was excited with the same wavelength and laser power as the spectral images. The emission was filtered with a 495 nm LP dichroic and Semrock 442/46 nm BrightLine single-band bandpass filter

(CFW-BP01-Clin-25). The fluorescence lifetime data was acquired using simFCS software v4. To obtain enough fluorescence lifetime signal for the downstream analysis, 10-30 frames were collected per sample, with a frame size of 256x256 pixels and pixel dwell time of 32 μ s.

Z-stack fluorescence lifetime of WT PA14 biofilms on the DIVER microscope.

Intact WT *P. aeruginosa* PA14 biofilms were grown in ASM for five days and prepared for z-stack imaging by adding a large coverslip on top of the surface of the biofilm, and then imaged with a 0.8 NA 40x Water objective. Z-stacks were obtained on a custom-made microscope at the Laboratory for Fluorescence Dynamics, the DIVER (Deep Imaging Via Enhanced Recovery) (170, 171, 194). The DIVER is a Nikon Eclipse TE2000-U microscope equipped with a wide-area 18x18 mm photomultiplier tube (PMT) (Hamamatsu R7600P-300) which enhances photon collection. Samples were excited with 2-photon excitation at 740 nm using a Tsunami Spectra-Physics Ti:Sapphire laser (80 MHz). The emission was filtered with a Schott BG-39 filter and NADH-targeted optical bandpass filter (400-500 nm). The fluorescence lifetime data was collected with SimFCS v4 software. Z-stacks were automatically acquired every 100 μ m from the surface of the biofilm to 1 mm deep. The laser power was increased with an exponential function for deeper sample imaging, with the power ranging from 1-58 mM.

Fluorescence lifetime analysis and visualization.

The fluorescence lifetime data was analyzed in SimFCS v4 software using the phasor approach (174). The phasor approach uses a cosine-sine discrete fast Fourier transform to transform raw fluorescence lifetime traces onto a two-coordinate polar phasor plot. The resulting G and S coordinates are the cosine and sine components of the transform for a given frequency (80 MHz). For the FLIM phasor analyses, images were processed following Ranjit et al (190). The images were first masked using fluorescence intensity thresholds to exclude pixels with background signal. The resulting images contain the fluorescence lifetime phasor coordinates for each pixel. For the single cell or cluster analyses, individual cells or group of cells were selected as regions of interest, and the average g and s values were calculated.

Unmixing of fluorescence lifetime and hyperspectral data.

To represent the fluorescence lifetime data in phasor space, the intensity trace is Fourier transformed to obtain the s and g coordinates at a harmonic n,

$$s_t(n) = \frac{\int_0^T I(t)\sin(2\pi nt)dt}{\int_0^{2\pi} I(t)dt}$$

$$g_t(n) = \frac{\int_0^1 I(t)\cos(2\pi nt)dt}{\int_0^1 I(t)dt}$$

Similarly, the spectrum is transformed with the equations

$$s_\lambda(n) = \frac{\int_{\lambda_0}^{\lambda_1} I(\lambda)\sin(2\pi n \frac{\lambda - \lambda_0}{\lambda_1 - \lambda_0})d\lambda}{\int_{\lambda_0}^{\lambda_1} I(\lambda)d\lambda}$$

$$g_{\lambda}(n) = \frac{\int_{\lambda_0}^{\lambda_1} I(\lambda) \cos(2\pi n \frac{\lambda - \lambda_0}{\lambda_1 - \lambda_0}) d\lambda}{\int_{\lambda_0}^{\lambda_1} I(\lambda) d\lambda}$$

The pure fluorophores predicted to be present in the sample are characterized by spectral and lifetime imaging, creating a basis set of k - pure components in the lifetime and spectral phasor space, at each harmonic n :

$$S(n), G(n) = \{(s_{t1}, g_{t1}), \dots (s_{ti}, g_{tk}), (s_{\lambda 1}, g_{\lambda 1}), \dots (s_{\lambda k}, g_{\lambda k})\}_n$$

The measured signal in each pixel of the image is given by

$$S_{\text{signal}}(n), G_{\text{signal}}(n) = \{(s_{t\text{signal}}, g_{t\text{signal}}), (s_{\lambda\text{signal}}, g_{\lambda\text{signal}})\}_n$$

In the absence of FRET or other non-linear effects, and if the spectral window for FLIM acquisition is the same as the spectral window for hyperspectral acquisition, the measured signal is modeled as the sum of the each of the components of the basis set, multiplied by the fractional contribution f_j , (193),

$$S_{\text{model}}(f, n) = \sum_{j=1}^k S_{j,n} f_j = f_1 s_{t1} + \dots f_k s_{tk} + f_1 s_{\lambda 1} + \dots f_k s_{\lambda k}$$

$$G_{\text{model}}(f, n) = \sum_{j=1}^k G_{j,n} f_j = f_1 g_{t1} + \dots f_k g_{tk} + f_1 g_{\lambda 1} + \dots f_k g_{\lambda k}$$

The fractional contributions best describing the signal are found by least squares global optimization:

$$\vec{f} = \underset{f}{\operatorname{argmin}} \left\{ \sum_n \left(S_{\text{model}}(f, n) - S_{\text{signal}}(n) \right)^2 + \sum_n \left(G_{\text{model}}(f, n) - G_{\text{signal}}(n) \right)^2 \right\}$$

With the constraint that the sum of all fractions f is 1,

$$\sum_i f_i = 1$$

The optimization routine used in this work is simplicial homology global optimization (196). The number of harmonics that can be used in the unmixing algorithm is determined by the resolution of the spectral or lifetime instrument. If too many harmonics are used, the data becomes too noisy and the model breaks down. The maximum number of harmonics that can be used is limited by the Nyquist frequency of the instrument as well as the signal modulation. If there is no modulation in the signal, the phasor coordinates become smaller than the variance introduced by the noise, and unmixing becomes impossible.

The unmixing program is open-source and available at:

[https://github.com/tgallagh/PhaseUnmix.](https://github.com/tgallagh/PhaseUnmix)

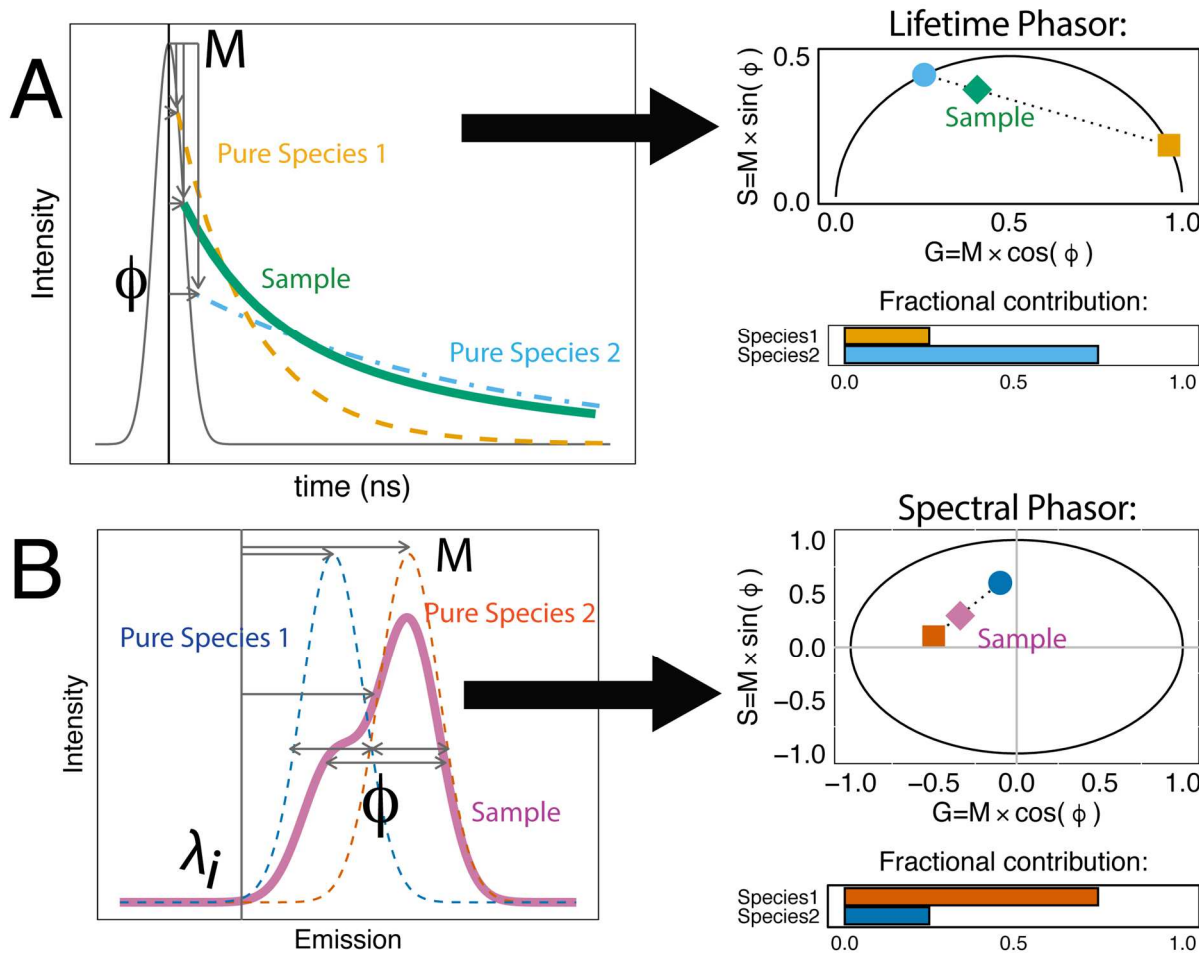


Figure 3.1: The phasor families are a powerful approach for analyzing and visualizing fluorescence data and facilitate calculations of relative abundances of fluorescent species in samples. (A) A simplified representation of the transformation of fluorescence exponential decays (left) into the fluorescence lifetime phasor (right). A Fourier transform is used to calculate the modulation (M) and phase shift (ϕ) relative to the laser pulse excitation source. M and ϕ are represented graphically for two pure fluorophores (orange dash line, blue dash-dot line) and a sample containing a mix of the two species (green solid line). The phasor G and S coordinates are the cosine and sine components of the Fourier transforms. Species closer to the origin of the phasor have long lifetimes, whereas species on the right corner of the phasor have short lifetimes. The fractional contribution of fluorescent species 1 (orange square) and species 2 (blue circle) to a sample (green diamond) can be determined if the lifetime of the pure species is known. **(B)** Example emission spectra from three fluorescent samples, including pure species and a sample with a mix of the two species (middle spectrum). A Fourier transform of the spectra gives ϕ , which represents the spectrum width, and M , which represents the spectral shift relative to the first wavelength measurement (λ). Species closer to the inner circle have broader emission spectra.

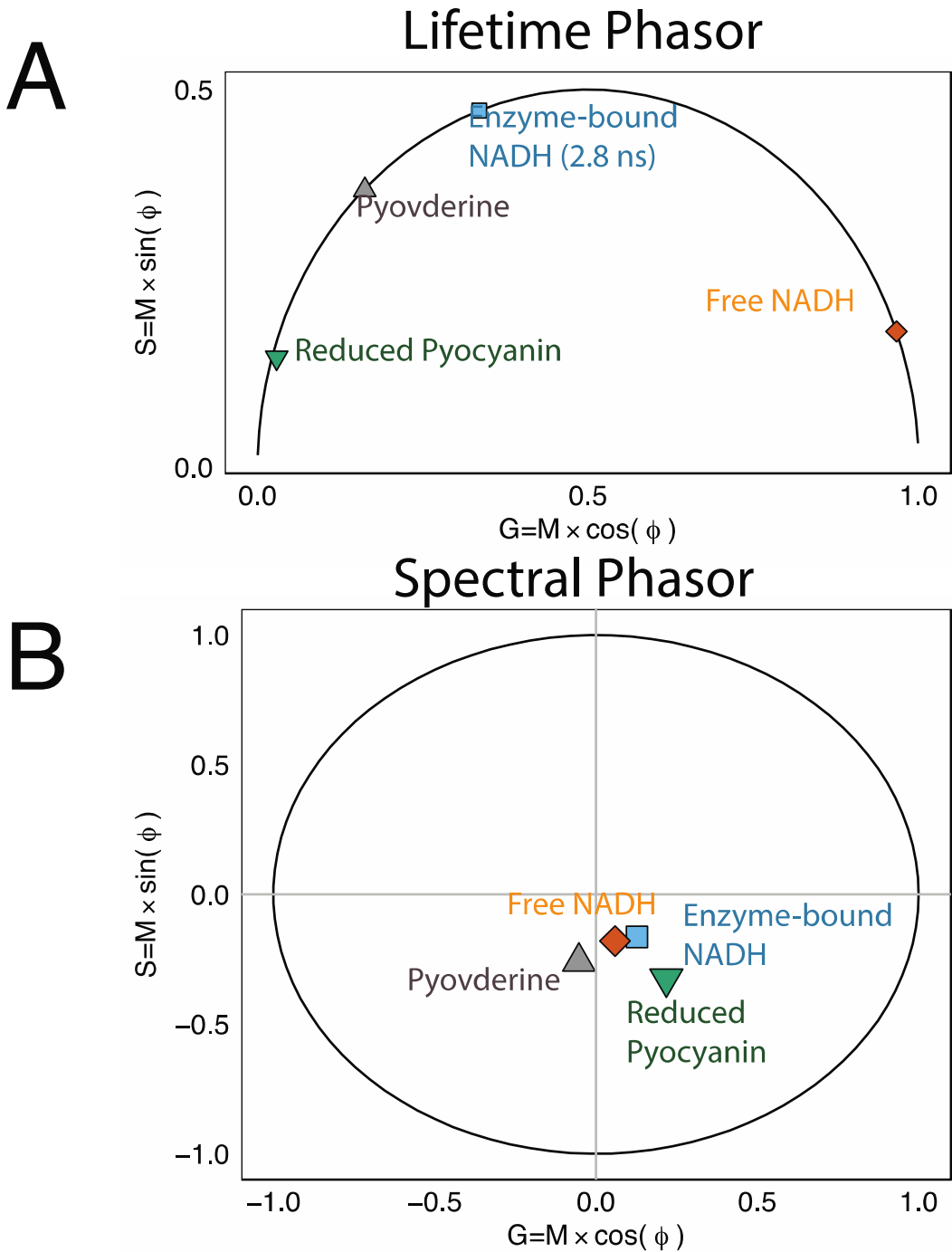


Figure 3.2: (A) Fluorescence lifetime and (B) spectral phasor of pure fluorescent species (first harmonics). For the fluorescence lifetime phasor, the S and G components were calculated for a lifetime of 2.8 ns and used as the reference for enzyme-bound NADH (Fig. S3.2). For the spectral phasor, the emission spectra were obtained over 9 channels from 410-486 nm.

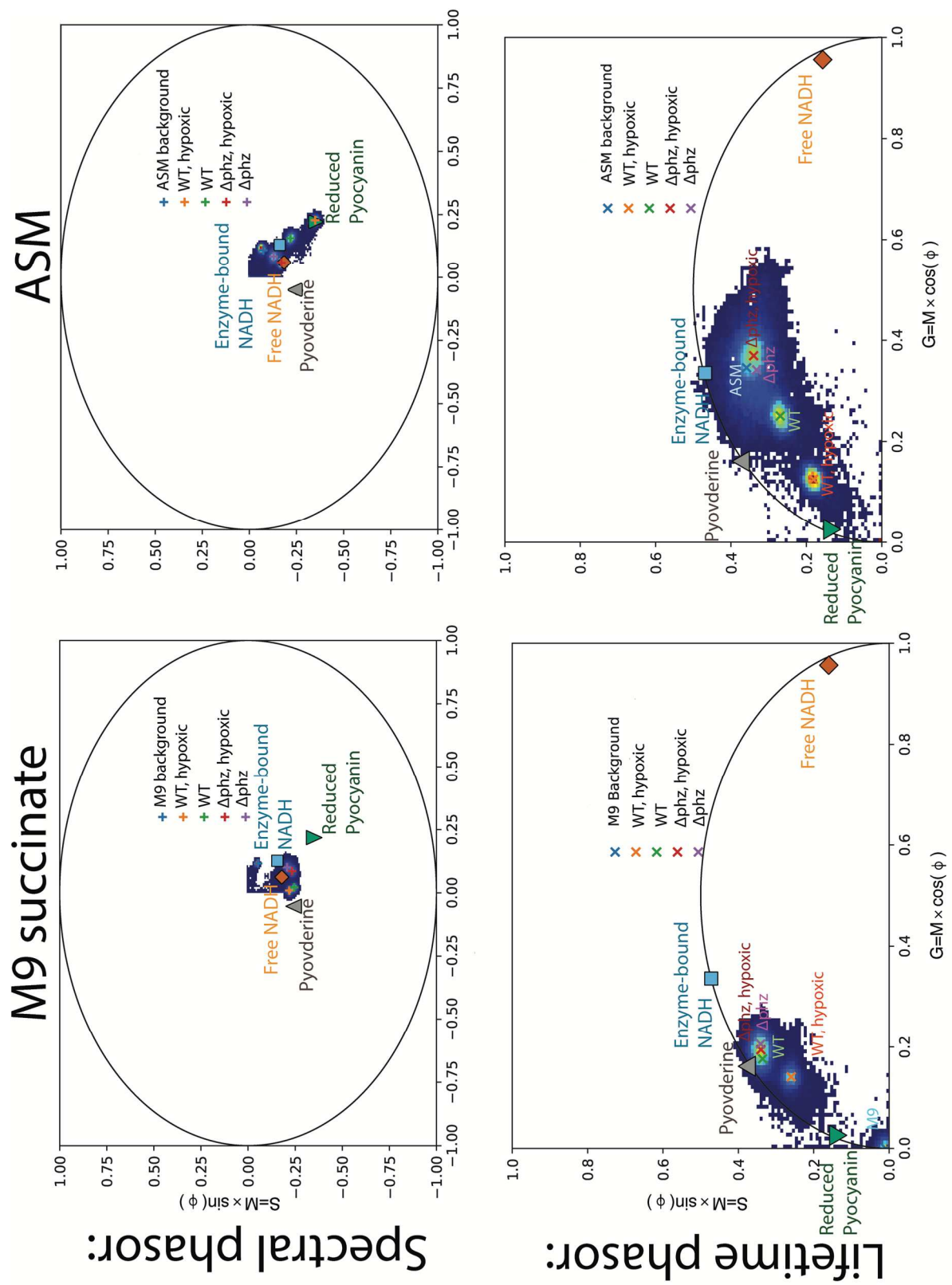


Figure 3.3: Fluorescence lifetime and spectral phasor of WT *P. aeruginosa* PA14 and the null phenazine mutant (Δphz) incubated in aerobic and or 2h hypoxic conditions in M9

succinate and artificial sputum medium. The displayed data is from one replicate representative of the biological replicates (N=2-3). Images were acquired on the Zeiss LSM 880 with a 2-photon excitation of 740 nm. HIM emission window: 410-500 nm with 9 nm steps. FLIM emission filter window: 410-470 nm.

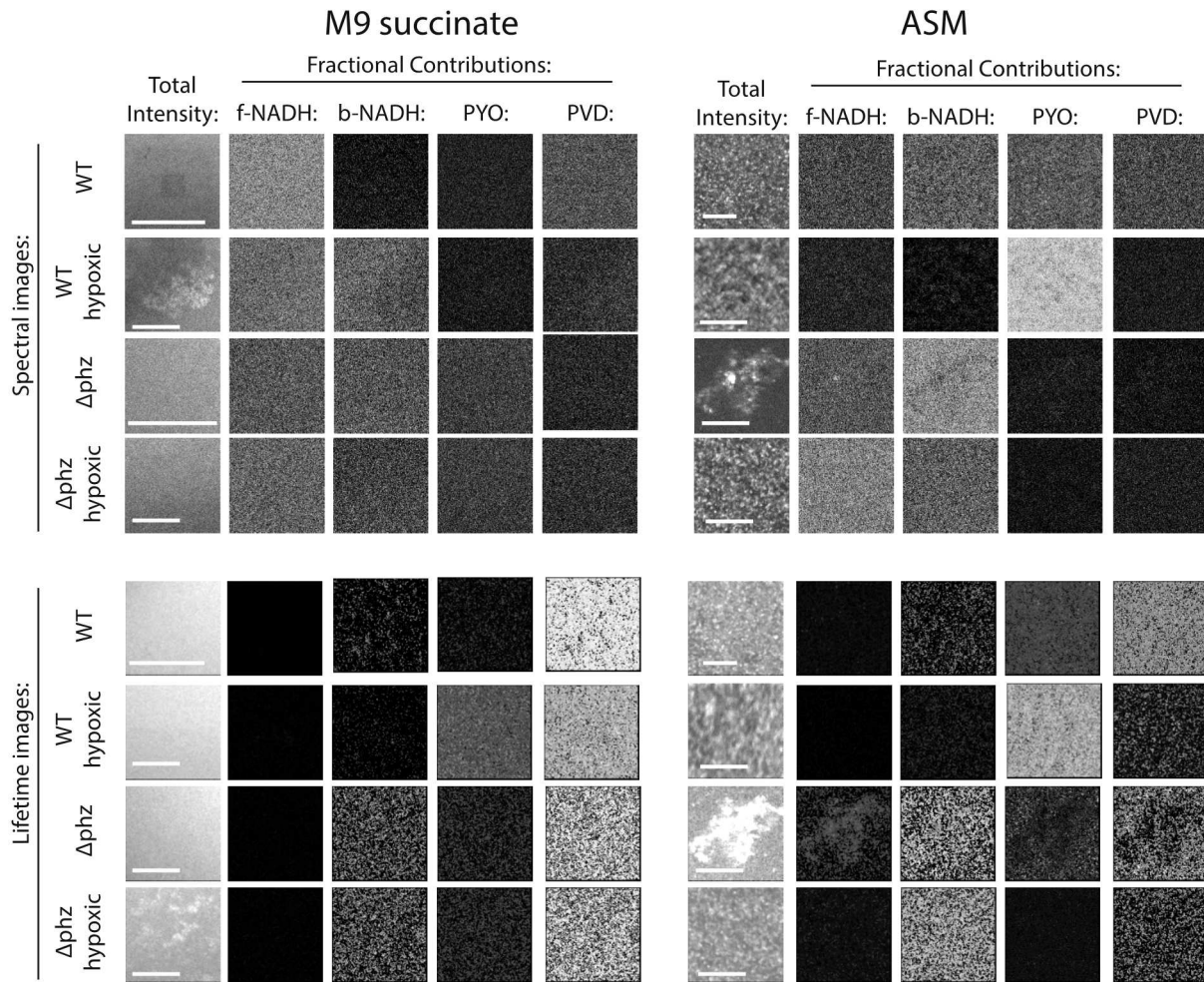


Figure 3.4. WT *P. aeruginosa* and null phenazine mutant (Δphz) grown in aerobic and low oxygen conditions in M9 succinate and artificial sputum medium. The fluorescence intensity of the images are depicted in the 1st columns. The next four columns represent the predicted fractional contributions of four fluorophores (free NADH, enzyme-bound NADH, reduced pyocyanin, and apo-pyoverdine) from lifetime and spectral phasor data. Scale bar=20 μ m. The displayed data is from one replicate representative of the biological replicates (N=2-3). Images were acquired on the Zeiss LSM 880 with a 2-photon excitation of 740 nm. HIM emission window: 410-500 nm with 9 nm steps. FLIM emission filter window: 410-470 nm. ASM= artificial sputum medium. f-NADH = free NADH. b-NADH = bound NADH.

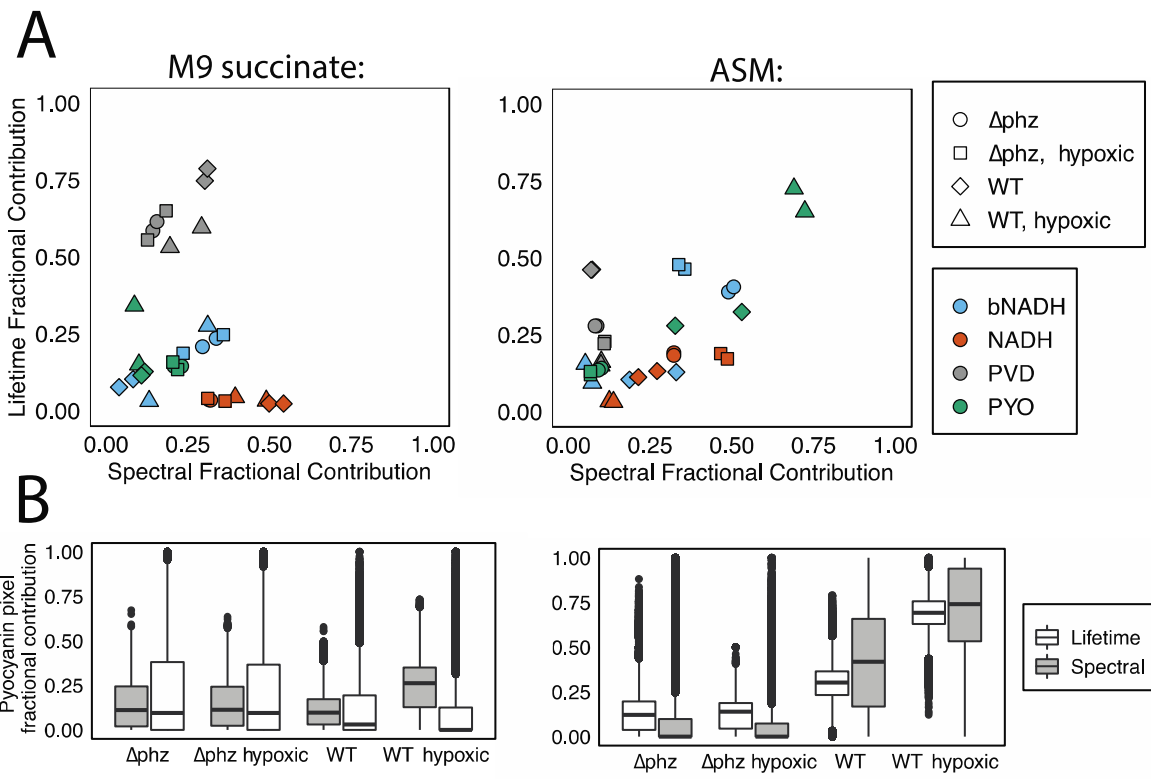


Figure 3.5. (A) The spectral and fluorescence lifetime fractional contribution predictions do not correlate for M9 succinate cultures ($r=-0.22$, $df = 30$, $p\text{-value} = 0.2$) and moderately correlate ($r=0.6$, $df = 30$, $p\text{-value} < 0.05$) for artificial sputum medium cultures. **(B)** In cultures with high pyocyanin production (WT and WT hypoxic in ASM), the lifetime and spectral predicted fractional contributions of pyocyanin were similar.

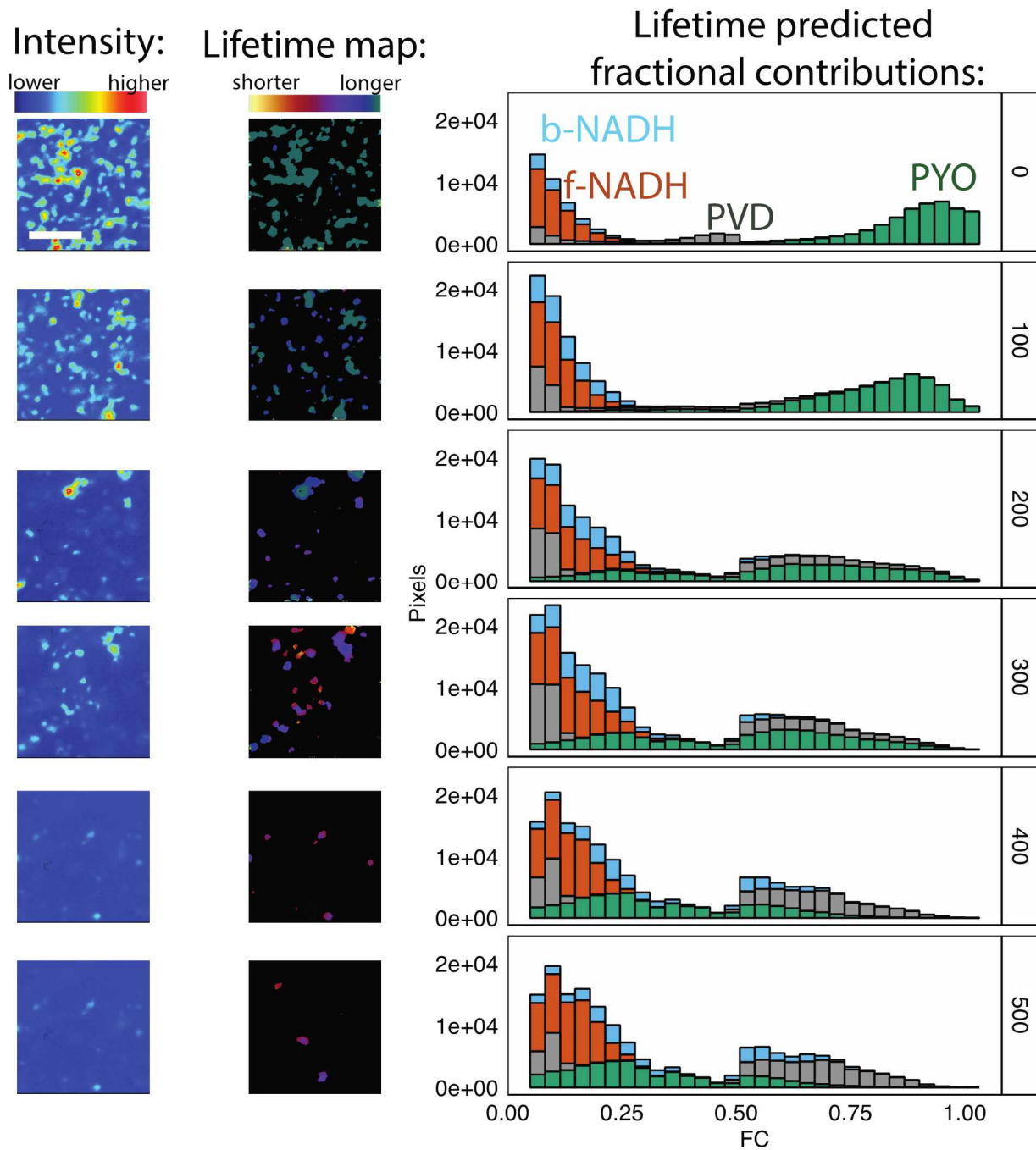


Figure 3.6. Example of WT PA14 biofilms grown in ASM. Fluorescence intensity of the biofilm at different depths - surface or 0 μm to 500 μm deep (column 1). The fluorescence lifetime color map projections, where cooler colors are indicative of longer lifetimes (column 2). The predicted fractional contributions of the four fluorophores indicates high abundance of reduced pyocyanin at the surface relative to the other species. Scale bar = 20 μM . Z-stacks acquired on the DIVER with two-photon excitation of 740 nm. Emission filter: 400-500 nm.

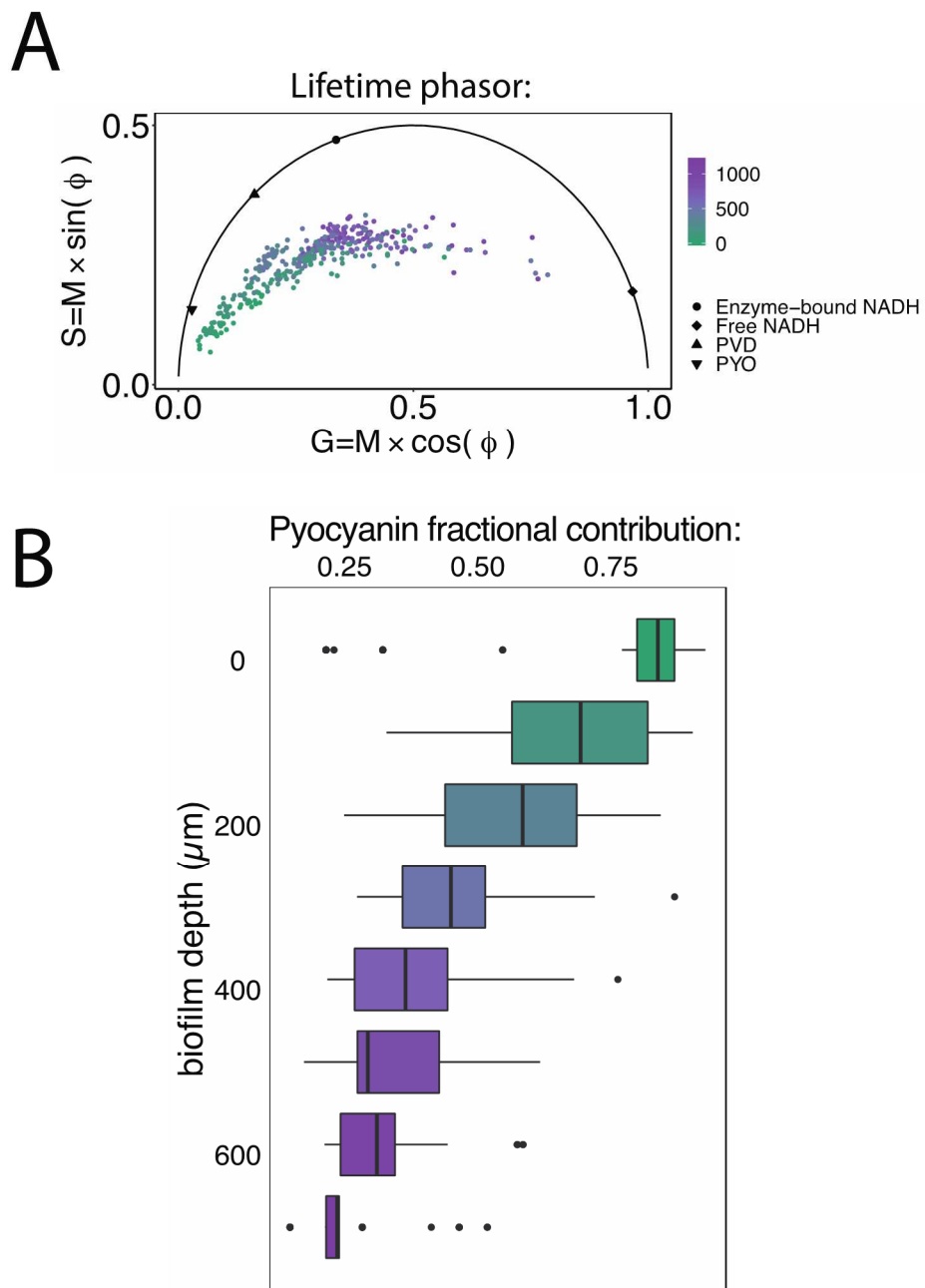


Figure 3.7. (A) Fluorescence lifetime phasor of WT PA14 biofilms grown in ASM at different depths (0=surface). The individual points represent the mean G and S coordinates for a single cell or cluster, where the background intensity is masked out. All of the biofilms had bacterial growth up to 500 μM deep, with one replicate imaged down to 1 mm. (B) Pyocyanin fractional contributions at different depths in the biofilm. N=5 biofilm plates.

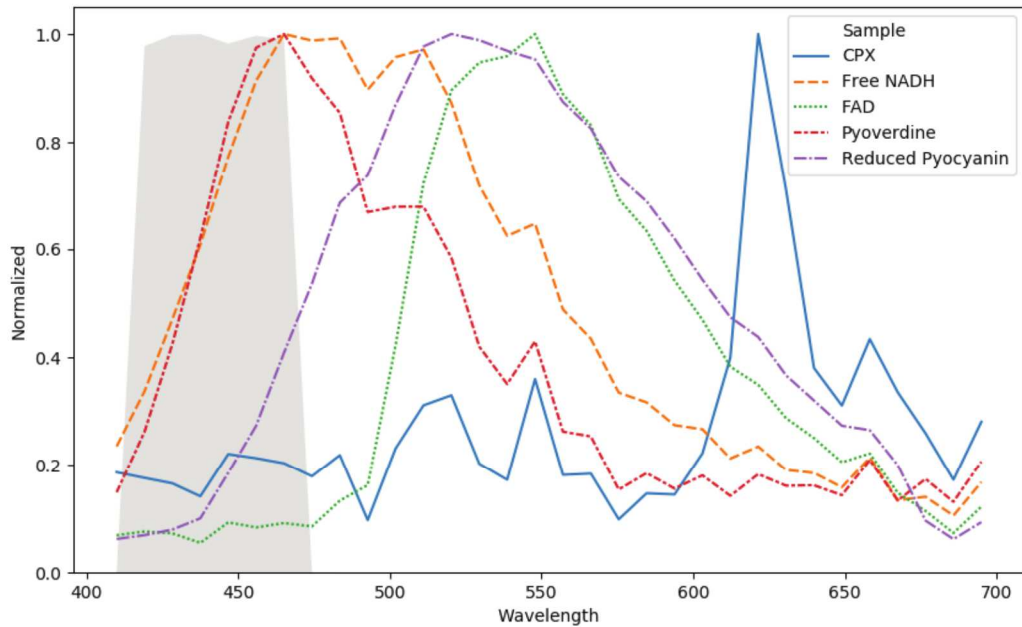
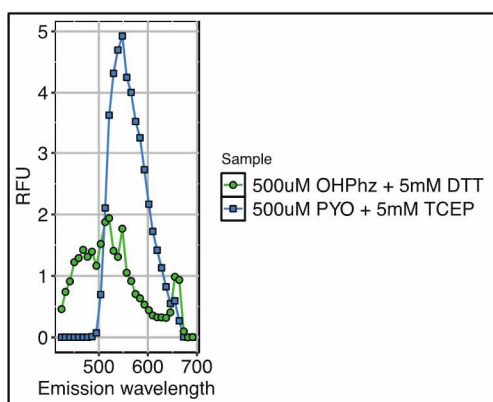
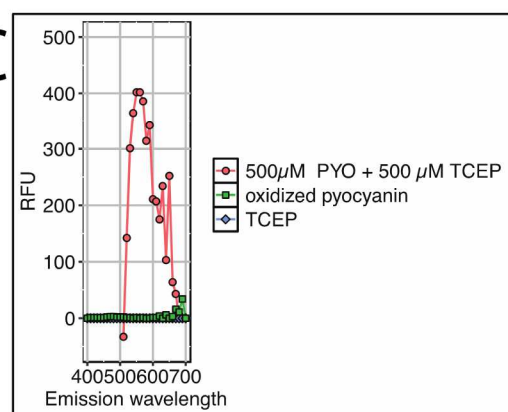
A**B****C**

Fig. S3.1 **(A)** Two-photon emission spectra, normalized by the max peak intensity, of some of the fluorescent metabolites produced by *P. aeruginosa*. The Zeiss LSM-880 FLIM emission filter is shaded in gray. The DIVER FLIM emission filter is wider: 400-500 nm. **(B)** Emission spectrum of chemically reduced 1-hydroxy-phenazine and pyocyanin (0.5 mM of phenazine with 5 mM of reducing agent). **(C)** Emission spectra of reduced pyocyanin (0.5 mM pyocyanin with 0.5 mM TCEP), oxidized pyocyanin (0.5 mM), and background from buffer (TCEP). Oxidized pyocyanin had negligible fluorescent with two-photon excitation at 740 nm.

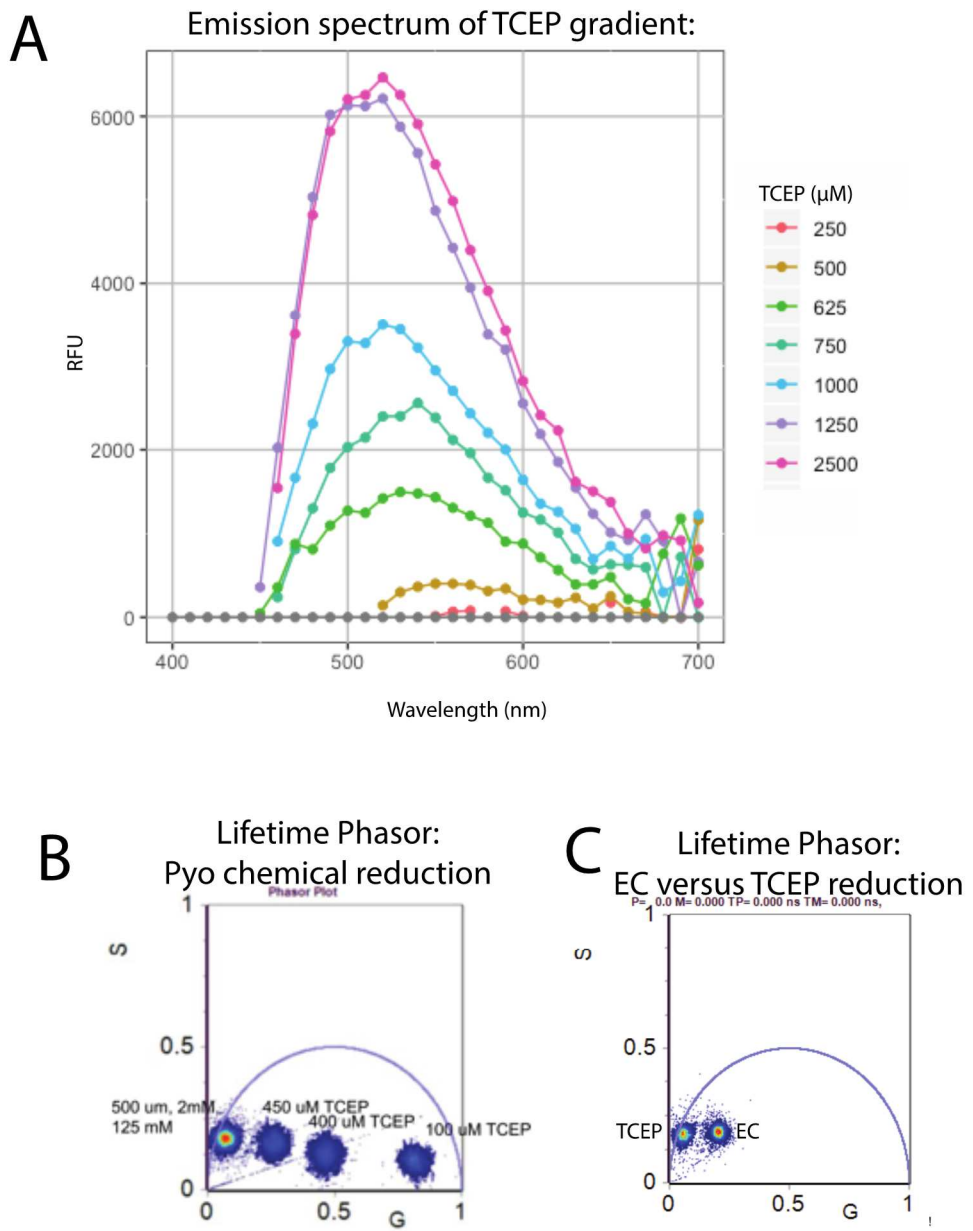


Fig. S3.2 (A) The emission spectra of pyocyanin shifts to the right with higher concentrations of reducing agent (TCEP). The samples were prepared in a 96-well plate with 0.5 mM of pyocyanin and titrations of TCEP in an anaerobic chamber. The spectra were acquired using 1-photon fluorescence excitation (370 nm) on a fluorometer. **(B)** The FLIM phasor position of pyocyanin (0.5 mM) varies with different concentrations of TCEP reducing agent. **(C)** FLIM phasor positions of electrochemically-reduced pyocyanin (0.821 mM) compared to 1 mM TCEP reduced pyocyanin (0.5 mM). FLIM data in B and C were

acquired with 2-photon fluorescence excitation at 740 nm and an emission filter of 442/46 nm on the LSM 880.

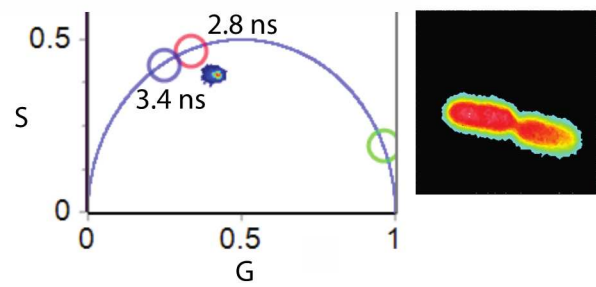


Fig. S3.3. The fluorescence lifetime of *P. aeruginosa* grown in aerobic M9 glucose for 24h, acquired on the DIVER with two-photon fluoresce excitation at 740 nm and an emission filter of 400-500 nm.

Supplemental Materials: FLIM of oxygen and cross-feeding experiments

*** The below materials are modified from presentations given at Pacific AAAS (2018), Lake Arrowhead Microbial Genomics (2018), and American Society for Microbiology Microbe 2019! The complete experimental design and stable isotope metabolomics results are described in Chapter 1 (100).

Abstract:

The airways of people with Cystic Fibrosis become chronically infected with slow-growing, antibiotic-resistant opportunistic pathogens such as *Pseudomonas aeruginosa*. At the same time, anaerobes associated with the oral cavities have been identified in patients' airway secretions, yet these bacteria can be overlooked in a clinical setting. While oral anaerobes are rarely destructive in healthy individuals with effective airway clearance, they can become dangerous in airway infections. For example, oral microbes produce volatile fermentation products that are both toxic to the patient and affect the physiology of opportunistic pathogens. One major environmental factor that drives bacterial fermentation and respiration is oxygen. Although CF sputum contains steep oxygen gradients, most CF microbiology studies disregard the effect of hypoxia on microbial interactions and physiology. We hypothesized that oxygen impacts the metabolic interactions between two CF isolates with different metabolic capabilities: *P. aeruginosa* and the oral facultative anaerobe, *Rothia mucilaginosa*. Using stable-isotope metabolomics, we found that *P. aeruginosa* utilized labeled substrates derived from *R. mucilaginosa* to generate different primary metabolites in low oxygen. Furthermore, fluorescence lifetime imaging of NADH was used to track changes in sub-cellular metabolism of

P. aeruginosa and indicated a shift in bacterial central metabolism in different oxygen levels and during cross-feeding interactions. Taken together, our results indicated oxygen was the biggest driver of *P. aeruginosa* physiology and affects how *P. aeruginosa* utilizes *R. mucilaginosa*-derived metabolites. This work was supported as a pilot project from the UC Davis West Coast Metabolomics Center funded by NIH DK097154, and T.G. is supported through the BEST IGERT program funded by the National Science Foundation DGE-1144901.

Main:

In order to determine the impact of oxygen on cross-feeding interactions, we grew a cystic fibrosis isolate *P. aeruginosa* FLR01 (43) in different liquid media types (M9 glucose, pyruvate, and succinate and ASM) with or without *Rothia*-derived supernatant in hypoxic or aerobic conditions. After 24, 72, or 120h incubation, bacteria were transferred to a slide and suspended in 1% warm agar. FLIM was acquired with the DIVER using two-photon fluorescence excitation and an NADH-targeted emission filter (400-500 nm), and the mean FLIM phasor G and S coordinates were calculated for single, masked cells (**Fig. S3.4-S3.5**). We found that for the earliest timepoint, most of the variation the FLIM signals arose from oxygen (**Table S3.1**). Over time, more of the variation was explained by single cells, and not the experimental conditions (**Fig. S3.6, Table S3.1**). In other experiments, our group later determined that the hypoxic chamber itself was affecting bacterial physiology (based on phenotypic assays performed in our chamber set to ambient oxygen). These chamber effects motivated us to start studying the oxygen gradients that naturally form in *P. aeruginosa* biofilms in Chapter 3! While the oxygen comparisons are imperfect, our results demonstrated that FLIM is a powerful tool for assessing metabolic heterogeneity.

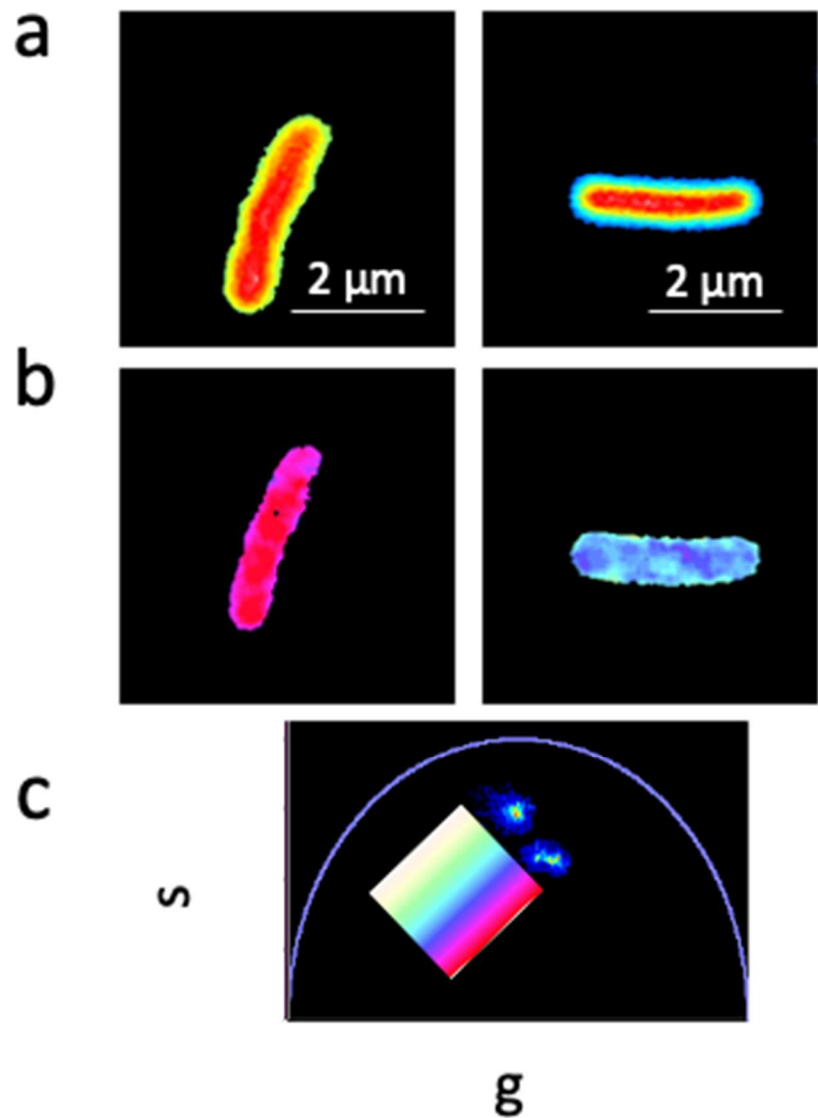


Figure S3.4. Examples of *Pseudomonas* lifetime images. (a) Fluorescence intensity of NADH and other endogenous fluorophores (2-Photon Excitation = 740 nm) from a CF strain (FLR01). (b) Color map of lifetime g and s coordinates onto the cells from phasor in panel c. (c) Distribution of lifetimes in both cells. Each dot represents 1 pixel.

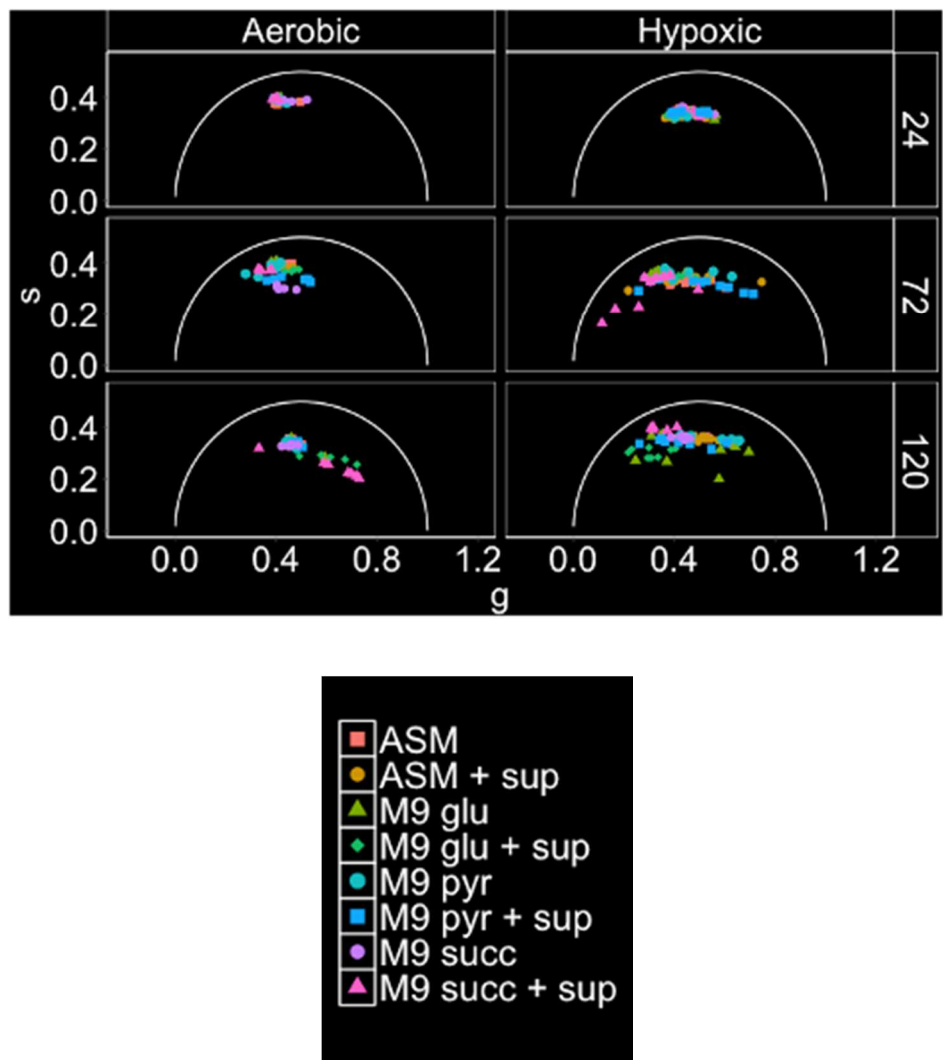


Fig. S3.5. Fluorescence lifetime of NADH and other endogenous fluorophores in *Pseudomonas* grown in ASM or minimal media (2-Photon Excitation = 740 nm). Each dot represents the mean lifetime coordinates of one cell.

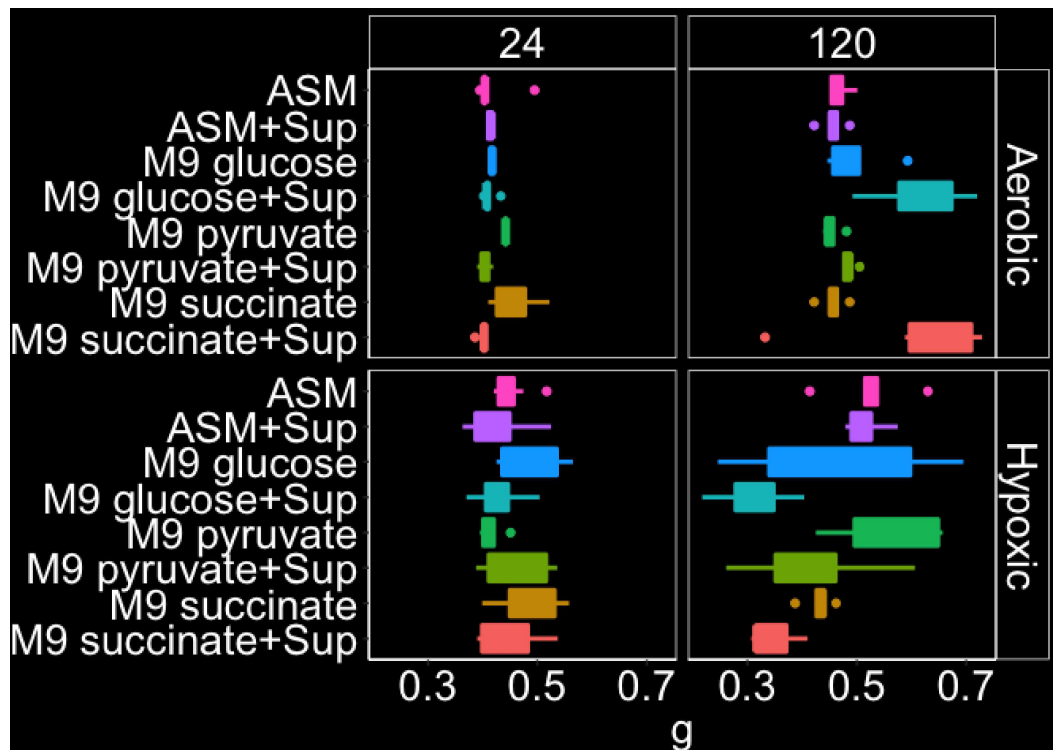


Fig. S3.6. Boxplot of fluorescence lifetime g-coordinate indicates increasing population heterogeneity for hypoxic and older cultures.

Table S3.1: PerMANOVA of lifetime data (g and s coordinates) suggests oxygen drives changes in lifetime in earlier cultures. In biofilms (120h), most of the variation is likely explained by cellular heterogeneity.

24h:	DF	F	R²	p
Media	3	1.6	0.02	0.15
Oxygen	1	74.8	0.05	0.001
Sup	1	9.9	0.38	0.001

120h:	DF	F	R²	p
Media	3	2.7	0.07	0.027
Oxygen	1	12	0.10	0.001
Sup	1	1.2	0.01	0.254

Chapter 4:

LC-MS detection of antibiotic agents in sputum from persons with cystic fibrosis

Authors: Tara Gallagher, Stefan Riedel, Joseph Kapcia, Lindsay J. Caverly, Lisa Carmody, Linda M. Kalikin, Junnan Lu, Joann Phan, Matthew Gargus, Miki Kagawa, Simon W. Leemans, Jason A. Rothman, Felix Grun, John J. LiPuma, Katrine L. Whiteson

ABSTRACT

Antibiotic therapy is expected to impact host microbial communities considerably, yet many studies focused on microbiome and health are often confounded by limited information about antibiotic exposure. Given that antibiotics have diverse pharmacokinetic and antimicrobial properties, investigating the type and concentration of these agents in specific host specimens would provide much needed insight into their impact on the microbes therein. Here, we developed liquid chromatography mass spectrometry (LC-MS) methods to detect 18 antibiotic agents in sputum from persons with cystic fibrosis. Antibiotic spike-in control samples were used to compare three liquid extraction methods on the Waters Acuity Quattro Premier XE. Extraction with dithiothreitol captured the most antibiotics and was used to detect antibiotics in sputum samples from 11 people with cystic fibrosis, with results being compared to the individuals' self-reported antibiotic use. For the sputum samples, two LC-MS assays were used; the Quattro Premier detected nanomolar or micromolar concentrations of 16 antibiotics, whereas the Xevo TQ-XS

detected all 18 antibiotics, most at sub-nanomolar levels. In 71 of the 158 tested sputum samples, at least one antibiotic that was not reported by the subject was detected by both LC-MS methods, a discordance largely explained by the thrice weekly administration and long half-life of azithromycin. For ~37% of samples, antibiotics reported as being taken by the individual were not detected by either instrument. Our results provide an approach for detecting a variety of antibiotics at the site of infection, thereby providing a means to include antibiotic usage data into microbiome studies.

INTRODUCTION

Antibiotic usage is expected to alter host microbial composition in the treatment of infectious diseases (62, 197). It is, however, challenging to account for the impact of antibiotics on microbial community composition during the course of therapy without determining which antibiotics microbes encounter at the site of infection or elsewhere in the host. Obtaining reliable information to account for antibiotic use is particularly challenging in persons with chronic infections where antibiotic therapy is often intermittent and adherence to treatment recommendations is uncertain (65, 99). The levels of antibiotics at the actual infection-site are often unknown, as most pharmacokinetic studies measure antibiotics in serum (**Table S4.1**) (66–87) with a very few assessing antibiotic levels at the infection site (74, 78, 88, 89).

Insofar as bacterial survival and gene expression are affected by antibiotic type and the local antibiotic concentration (90), there is a need for quantitative and objective

methods to account for antibiotics in assessing the dynamics of microbial communities in infectious diseases. To quantify antibiotics in clinical samples, we developed two low-cost, high throughput Ultra Performance Liquid Chromatography tandem Mass Spectrometry (UPLC-MS/MS) methods. We investigated the utility of these methods by examining sputum samples from persons with cystic fibrosis (CF), a condition where incomplete antibiotic use data contributes to confounding assessment of treatment outcomes (57, 59, 62, 64, 93, 95–98, 198). Individuals with CF experience chronic polymicrobial airway infections (59, 62, 94–96, 98, 199–203), and intensive antibiotic use is often poorly documented in the medical record. We assessed our results in the context of self-reporting of antibiotic use by these individuals.

RESULTS

Detection of antibiotics on the Waters Quattro Premier XE and Xevo TQ-XS UPLC-MS/MS. We compared two UPLC-MS/MS instruments for their ability to separate and quantitate 18 antibiotics commonly prescribed to individuals with CF (**Table 4.1**). Run conditions were first optimized on a pool of 18 pharmaceutical-grade antibiotics on the Waters Quattro Premier XE UPLC-MS/MS at the University of California, Irvine Mass Spectrometry Facility. Using a water:methanol gradient with 2 mM ammonium acetate and 0.1% acetic acid as the mobile phase (204), 16 of 18 antibiotics separated chromatographically with peak areas at least 100 times higher than background (**Figure 4.1**). Water:methanol with 2 mM ammonium acetate and 0.1% acetic acid produced a more robust signal for the majority of antibiotics compared to a water:acetonitrile gradient with

0.2 % acetic acid, another common mobile phase for hydrophilic compounds (**Table S4.2**). However, neither vancomycin nor colistin were consistently detected with either mobile phase solvent on the Quattro Premier due to low response from the protonated molecular ion ($M+H$). The lower limits of detection (LODs) of the external standards ranged from 5 nM (levofloxacin) to 29 μ M (cefepime) (**Table S4.3**).

Antibiotic standards were also optimized on the Xevo TQ-XS at the Waters Corporation Demo Laboratory (Beverly, MA). Colistin and vancomycin parameters were manually optimized on the Xevo by scanning and identifying multiple protonated forms ($M+2H$). While the Xevo parameters were different than the Quattro Premier and comparisons in the LODs between the two instruments are imperfect, the Xevo LODs were on average 10,000 fold lower than the Quattro Premier. The Xevo LODs ranged from 5 pM (amoxicillin, ampicillin, azithromycin, piperacillin, sulfamethoxazole) to 5 nM (colistin) (Table S3). Multiple reaction monitoring (MRM) parameters for both instruments are listed in Table 4.1.

Comparison of antibiotic extraction protocols for detection on the Quattro Premier.

We next compared three extraction solvents for efficiency in recovering antibiotics from sputum. Artificial sputum medium (ASM) was used as the matrix because antibiotic-free sputum was unavailable. Most individuals who expectorate sputum regularly take antibiotics. ASM was spiked with a pool of 16 antibiotics (excluding colistin and vancomycin). Using a water:methanol gradient mobile phase on the Quattro Premier, 1%

dithiothreitol (DTT) as the extraction solvent (204) yielded the most accurate recovered concentrations for the majority of the 16 antibiotics compared to methanol or acetonitrile/acetic acid mix solvents (**Figure 4.3A**). Coefficients of variation (COVs) were < 30% for 11 of 16 antibiotics spiked-in at 10 μM or less (amoxicillin, ampicillin, azithromycin, ceftazidime, ciprofloxacin, levofloxacin, linezolid, piperacillin, sulfamethoxazole, tobramycin, trimethoprim) (**Figure 4.3B, Table 4.2**). All of the antibiotics tested, except for amikacin, aztreonam, cefepime, ceftriaxone, and meropenem, were reproducibly measured with the Quattro Premier method (**Figure 4.3B, Table 4.2**). The apparent limit of detection (ALOD) values from the ASM recovery experiments were calculated (**Table S4.4**) and used as the lower threshold for the Quattro Premier detection of antibiotics from sputum samples to mitigate detection of false positives.

Detection of antibiotics in sputum samples. Optimized antibiotic extraction and chromatography conditions were initially tested on three replicate aliquots from each of three CF sputum samples on the Quattro Premier (**Figure 4.4**). Azithromycin, trimethoprim-sulfamethoxazole and tobramycin were reported as taken by the source subject on the days these samples were collected. The COVs for azithromycin and trimethoprim were at or below 30% for the tested samples. Similar to the ASM experiments, the COV for trimethoprim (30%) was lower than that of sulfamethoxazole (48%), suggesting trimethoprim quantification is more accurate than sulfamethoxazole. Tobramycin was detected by the Quattro Premier in one of three aliquots. The detected concentration (0.091 μM) was near the Quattro Premier ALOD (0.064 μM) (**Table S4.4**). In

addition, ceftriaxone was detected in two replicate aliquots from two samples. Although ceftriaxone was not provided as an option on the daily self-reporting survey, it may be prescribed to individuals with CF.

The optimized LC-MS antibiotic assays were then tested on 171 sputum samples from 11 subjects with CF. Antibiotic use was reported by subjects on the same day as sample collection for 158 of the sputum samples. Subjects took 11 of 18 antibiotics detected by the LC-MS assays by oral, inhaled or intravenous (IV) routes (azithromycin, aztreonam, ceftazidime, ciprofloxacin, colistin, levofloxacin, linezolid, trimethoprim-sulfamethoxazole, tobramycin, and vancomycin) (**Figure 4.5, Table 4.2**). Oral azithromycin was the most common antibiotic reported as taken (10 subjects, 75 samples), followed by inhaled aztreonam (8 subjects, 53 samples) and oral ciprofloxacin (5 subjects, 23 samples) (**Figure 4.5**). The most common combination taken on the same day was oral azithromycin and inhaled aztreonam (7 subjects, 22 samples) (Figure S1). Of the remaining seven antibiotics in the LC-MS assay, ampicillin and ceftriaxone were not a survey option but were included because these antibiotics could be prescribed to individuals with CF.

To reduce technical variability in our extraction method, all 171 samples were processed and run in one batch (total run time of 23.5 hours, including washes). As a technical quality control (QC), a pool of the 18 antibiotics was run every 57 samples. The intensity of the QC pools declined 50% on average by the end of the Quattro Premier run, and the intensity of the internal standards in samples also trended downwards (**Figure**

S4.2). The reduction in intensity could be explained by contamination of the column with protein, even though a centrifugation step was used to partially remove protein prior to running samples. In order to increase assay throughput, a more thorough protein-removal step, such as size-exclusion filtration, was excluded. The levels of protein post-extraction were high (mean=0.50 mg/mL, N=5 sputum samples) (**Figure S4.2B**). After completing the sample run on the Quattro Premier at the University of California, Irvine Mass Spectrometry Facility, the leftover material was shipped to Waters Corporation (Beverly, MA) to detect antibiotics on the Xevo TQ-XS. The Xevo run did not have a drop in the internal standard response over time, likely due to lower injection volume and less protein input on the column (0.25 mg versus 5 mg per sample) (**Figure S4.2C**).

LC-MS concordance with subject self-reported usage.

To assess the performance of the LC-MS platforms, we compared the results of the sputum assays with source subjects' self-reported antibiotic usage. For each antibiotic, we calculated sensitivity, specificity, positive predictive value and negative predictive value (using self-report as the gold standard) for both platforms (**Table 4.3**). Among the 10 antibiotic treatments reported as taken by the subjects, we analyzed trimethoprim and sulfamethoxazole separately, in addition to inhaled and IV tobramycin and aztreonam.

For both the Quattro Premier and Xevo, inhaled tobramycin had the lowest sensitivity (detected in 0/20 samples). Intravenous aztreonam and oral levofloxacin had the highest sensitivity (100%) but the sensitivity is likely inflated due to low number of samples

(Table 4.3). The Quattro Premier and Xevo had similar sensitivities for azithromycin, ciprofloxacin, levofloxacin, sulfamethoxazole, IV tobramycin, and trimethoprim. The Xevo was able to detect colistin (1/2) and vancomycin (6/6), whereas both of these antibiotics were not detectable with the Quattro Premier method. The Xevo also had higher sensitivity rates than the Quattro Premier for ceftazidime and linezolid, although both of these antibiotics were reported in only 6 and 2 samples, respectively. In contrast, the Quattro Premier had higher sensitivity for IV aztreonam than the Xevo. The Quattro Premier and Xevo specificities for nine of the antibiotics were 100%, the exception being azithromycin, which had specificities of 16% and 13%, respectively.

The Xevo detection of antibiotic concentrations were overall lower than that of the Quattro Premier, likely due to declining stability of the antibiotics while shipping the extracted material to the Xevo lab (**Figure 4.6**). Specifically, azithromycin and ciprofloxacin had statistically significant lower concentrations when the sample was run on the Xevo (paired Wilcoxon rank sum test P<0.05; azithromycin Quattro Premier mean=288 µM, azithromycin Xevo mean=43 µM, V = 9591; ciprofloxacin Quattro Premier mean=6.3 µM, ciprofloxacin Xevo mean= 4.8 µM, V=197). In addition, the Quattro Premier method detected aztreonam and tobramycin in more samples than the Xevo (N=9, 2). Antibiotics in several samples were detected only by the Xevo, including azithromycin (N=2), ceftazidime (N=1), and trimethoprim (N=1). In addition, the Xevo detected colistin (N=1) and vancomycin (N=1), antibiotics that were not measured with the Quattro Premier method (**Tables 4.3, S4.4**).

Detection of antibiotics on days without self-reported usage.

The Quattro Premier and Xevo both detected antibiotics reported as not taken on the day of sample collection. The percent of samples containing at least one unreported antibiotic was approximately 46% (72/158) for both LC-MS approaches. The top antibiotics detected with LC-MS but reported as not taken on that specific sampling day were: azithromycin (Quattro Premier N=70; Xevo N=72) and levofloxacin (Quattro Premier N=1; Xevo N=1) (Figure 6; Table 3). In all of the samples where azithromycin was detected, the subjects reported taking azithromycin in the last 8 days prior to sample collection. Levofloxacin was detected by both methods in one sample (**Figure 4.6, Table 4.3**).

The Quattro Premier alone also detected piperacillin in one sample (**Figures 4.6, S4.3**); ceftriaxone in five sputum samples; and ampicillin in one sample (**Figures 4.4, 4.6**). Ceftriaxone and ampicillin were not included as an option on the antibiotic usage survey. Electronic medical records indicate the subjects were not prescribed ceftriaxone or ampicillin around the time of sample collection and suggests these antibiotics were false-positives.

We wanted to determine if detection of unreported antibiotics correlated with subject symptom score, with the reasoning that subjects may take additional antibiotics during periods of worsening symptoms. However, samples with detected antibiotics did

not correlate with symptom score (**Figure S4.3A**) (Pearson correlation. Quattro Premier: $t=0.78$, $df=205$, $P=0.44$, $r=0.05$. Xevo: $t=-0.19$, $df=210$, $P=0.85$, $r=-0.01$).

Impact of antibiotic half-life, storage condition, and route of delivery.

The antibiotics with the lowest incidence of detection were inhaled tobramycin and inhaled aztreonam which had sensitivities of 0-36% (**Table 4.3**). It is unlikely that instrument limitation reduced the detection rate for most of the antibiotics. The LODs from the Xevo (0.005-5 nM) did not significantly correlate with the agreement rate, and the Quattro Premier LODs were weakly, but not significantly, negatively correlated with agreement rate (**Figure S4.3B**) (Pearson correlation. Xevo: $t=0.75$, $df=9$, $P=0.47$, $r=0.24$. Quattro Premier: $t=-1.6$, $df=7$, $P=0.14$, $r=-0.53$). The one antibiotic potentially impacted by instrumentation limits is tobramycin, which had the worst detection rate for the Quattro Premier (90 nM) and second worst for the Xevo (0.1 nM) (**Table S4.3**). In addition, instances of antibiotics being undetected by the LC-MS method were not due to the number of days sputum samples were stored at 4°C at subjects' homes (**Figure S4.3C**) (Pearson correlation. Acuity: $t=1.6$, $df=284$, $P=0.1$. Xevo: $t=0.95$, $df=285$, $P=0.343$).

Undetected antibiotics could be due to inadequate delivery to the airways or clearing of the antibiotic by the time of sampling as subjects reported usage within a 24h window of collection. In support of this antibiotics with shorter half-lives, as determined from cystic fibrosis pharmacokinetic studies of serum (Table S1), were less likely to be detected (**Figure S3D**) (Pearson's correlation. Quattro Premier: $t=-9.8$, $df=262$, $P<0.05$, $r=-$

0.51. Xevo: $t = -13.6$, $df = 263$, $P < 0.05$, $r = -0.64$). Aztreonam was the second most undetected antibiotic and has a short half-life (70, 71) (**Table 4.3**).

Two of the 11 antibiotics were taken by subjects through inhaled or IV routes. IV-administered tobramycin was detected more often by the LC-MS than inhaled tobramycin (**Table 4.3**). A similar trend was seen with aztreonam, although there were not enough IV-administered samples to confirm this statistically.

DISCUSSION

Although antibiotics are expected to be drivers for shaping the human microbiome, studies of human microbial ecology rarely account for the effect of antibiotics on changes in microbial community composition. An obstacle to a better understanding of the impact of antibiotics in this regard is the difficulty inherent in reliably ascertaining antibiotic usage, particularly in the context of prolonged or chronic therapy, and determining antibiotic presence in human tissues of interest. With respect to studies of the airway microbiome in persons with CF, antibiotic therapy is often not taken into account at all or is derived from prescribing information gleaned from the medical record (57, 59, 62, 64, 93–98), which is recognized as marginally reliable (65, 99). We therefore sought to investigate the utility of LC-MS to objectively determine the presence of antibiotics, which could, in turn, be taken

into account in analyses of microbial community dynamics in studies of the CF airway microbiome.

LC-MS performance and extraction efficiencies are antibiotic-dependent.

We explored the utility of two LC-MS methods and observed that these differed in terms of reliability in detecting the antibiotics included in our study. The Quattro Premier method detected levofloxacin and meropenem with the highest signals, while the Xevo assay performed best in the detection of ampicillin and sulfamethoxazole. Both instruments performed poorly in the detection of cefepime and ceftazidime, likely due to low-binding of these hydrophilic cephalosporins to the reverse-phase column (**Table S4.3**). The extraction efficiencies from ASM (represented by the ALOD) correlated with the LOD of the external standards. However, some of the antibiotics with low external standard detection limits had poor extraction efficiencies, including meropenem (**Table S4.4, Figure 4.3A**). This may have been due to the use of ASM which contains major sputum components, including extracellular DNA, ferritin, chloride ions, sugars, and mucin sourced from porcine stomach. Our extraction protocol did not precipitate total protein content out of the sample, which could have reduced the extraction of antibiotics that interact with mucin or other proteins. On the other hand, the use of ASM over sputum could have inflated extraction efficiency for certain antibiotics, since ASM does not contain immune cells. Azithromycin is known to accumulate in polymorphonuclear leukocytes, which likely impacts its delivery to the airways and decreases extraction efficiency from sputum (205).

Persistence of antibiotics with long half-lives.

We a priori hypothesized that antibiotics detected in sputum but reported as not taken would be associated with subject symptom scores, because persons with CF may take non-prescribed antibiotics when experiencing worsening symptoms (65, 206). However, the LC-MS data did not support this hypothesis, as unreported antibiotics were not correlated with subject symptom scores (**Figure S4.3A**). Oral antibiotics taken by subjects, including levofloxacin, trimethoprim-sulfamethoxazole, ciprofloxacin, and azithromycin, were detected in sputum around the time of reported usage except for a few examples. Indeed, discordance between self-reporting surveys and LC-MS data was primarily due to azithromycin detected in a sample collected one or two days after the subject reported taking oral azithromycin. The common dosage for azithromycin for people with CF is an oral tablet three times a week (207, 208). While most instances of discordance were due to persistence of azithromycin a couple of days after taking the antibiotic, some samples contained azithromycin 7-8 days after a subject last reported taking it. Azithromycin has the longest reported half-life of the 18 antibiotics (**Table S4.1**) and has been reported to persist in CF sputum days after administration (209). The persistence of azithromycin can be attributed to its high tissue penetration, accumulation in phagocytes, and lack of metabolism by the liver (205, 210).

Undetected antibiotics could reflect ineffective concentrations throughout the infection-site.

A high proportion of antibiotics, particularly inhaled aztreonam and tobramycin, were reported as taken by the subject but not detected by either method (**Table 4.3**). We first wanted to determine if sample storage conditions impacted the detection rate, because the stability of antibiotics decreases (211), and the metabolite profiles in CF sputum change significantly, from storage at 4°C (152). However, the number of days a sample was stored at 4°C was not correlated with lack of detection, suggesting adequate sample storage conditions (**Figure S4.3A**). Instead, undetected antibiotics were inversely correlated with the antibiotic pharmacokinetic half-lives. In support of this, aztreonam has a short half-life in serum of 2h for inhaled and 1.5h for IV (70, 71); however, tobramycin has a longer half-life of 13h for inhaled and 2.2h for IV (85, 86, 212) (**Table S4.1, Figure S4.3D**).

Inhaled tobramycin was not detected by either LC-MS method, even during periods of repeated usage, likely due to heterogeneous delivery throughout the CF airways (213). Sputum samples are not a global representation of the entire airway, and secretions from different physical locations in the lungs vary in metabolite, antibiotic, and microbial composition (4, 105, 214). The undetected antibiotics might also be explained by subject non-adherence, which was as high as 20% in one cohort of adult CF patients (206). Reported reasons for skipping antibiotics included forgetting or for social reasons (206). It is also possible that undetected antibiotics were degraded by the time of sputum collection in our study, as the enrolled subjects were asked to report antibiotics taken anytime on the same day of sample collection.

Discordance between LC-MS and usage data is not due to instrument limitation, because the undetected antibiotics (tobramycin, aztreonam and azithromycin) had sub-micromolar or sub-nanomolar limits of detection (**Table S4.4**). Antibiotic concentrations that fall below our limits of detection need to be further studied to determine their effect (if any) on microbial physiology. There is no exact threshold that determines if an antibiotic concentration impacts microbes *in vivo*; however, our sub-nanomolar thresholds are still below sub-inhibitory concentrations reported to impact bacterial physiology (215). For instance, the Quattro Premier ALOD for tobramycin after extraction from artificial sputum was 0.06 μ M (**Table S4.3**), and the Xevo LOD of the tobramycin standard was 0.1 nM. Both of these thresholds are lower than sub-inhibitory concentrations reported to affect *Pseudomonas aeruginosa* physiology (4 μ M) (216) and the CLSI minimum inhibitory concentration break-points (217) (**Table S4.3**). The impact of physiologically-relevant concentrations of antibiotics on the microbiome is poorly understood, and future efforts will determine if sub-inhibitory concentrations of antibiotics measured in sputum drive changes in bacterial composition.

Study limitations & recommendations.

The subjects in this study agreed to participate in the antibiotics survey, and their adherence to antibiotic-usage and accurate completion of the self-reported antibiotic surveys is likely not representative of all individuals. It is also possible that the subjects inflated antibiotic-usage in the surveys. In addition, the subjects provided survey responses

within a 24h window of expectorating. Antibiotics not detected by either LC-MS could have degraded by the time of sampling.

Certain antibiotics were taken more frequently than others, which likely impact the LC-MS sensitivities and specificities. While we optimized the LC-MS method for 18 antibiotics, only 11 antibiotics were reported as taken by the subjects in this cohort. Notably, azithromycin was the most common antibiotic reported as taken in this study period. Oral azithromycin is typically taken by persons with cystic fibrosis three times a week, which contributed to the high discordance between the LC-MS data and daily self-reported usage.

The Quattro Premier and Xevo methods were optimized in different facilities and are imperfect comparisons for antibiotic LODs. The ASM antibiotic spike-in extraction experiments were only performed on the Quattro Premier, and we also have more information about the Quattro Premier parameters since it is our in-house instrument. We also reiterate that the Quattro Premier method was unable to detect vancomycin and colistin and could only detect cefepime and ceftazidime at high concentrations (Table S1). However, the newer instrument, the Xevo, could detect all four of these antibiotics at nanomolar levels. In addition, the lower injection volume for the Xevo contributed to cleaner chromatography. Excluding these examples, the detection profiles of the Quattro Premier aligned with the Xevo for frequently-taken antibiotics. Given that the Quattro Premier platform at the UC Irvine Mass Spec Facility is accessible to the authors, one future

direction is to improve the sensitivity of this approach, with improved chromatography and cleaner extraction methods.

The data for antibiotic half-lives came from pharmacokinetic studies in serum (Table S1). While we acknowledge that the half-lives in serum are likely different than in sputum, there are few studies characterizing antibiotic pharmacokinetics in sputum.

Conclusion

We aimed to develop a high-throughput method that would allow for detection of antibiotics present at the infection site such as sputum from the CF airways. Direct observations of antibiotics are needed to be related to microbial composition measures along with other clinical data. Incorporating antibiotic data into microbial community composition models is challenging in the context of CF due to many factors, including the lack of a standardized antibacterial treatment regimen, the impact of individual subject factors on antibiotic efficacy, and the diverse properties of CF antibiotics. Our LC-MS approach has inherent limitations but is the first step towards including objective antibiotic data in CF studies. Future endeavors will determine how the local presence of antibiotics impacts the microbial community with paired quantitative LC-MS and microbiome data.

METHODS AND MATERIALS

Chemicals. Pharmaceutical-grade or HPLC-grade antibiotics were dissolved in water, methanol, or an acetonitrile/acetic acid solution to make 1 mM or 10 mM stocks (see **Table S4.1**). Stocks of the external standards were made directly before each run due to reported low stability of some antibiotics at -20°C and -80°C (204, 211). The antibiotics were then diluted with water and pooled to make a 10 µM stock. For the external standard curve, a three-fold dilution series was used: 10 µM, 3.3 µM, 1.1 µM, 0.37 µM, 0.123 µM, 0.041 µM, 0.014 µM. Internal standards linezolid-d₃ and levofloxacin-d₈ (Toronto Research Chemicals Inc., Ontario Canada) were dissolved in water and methanol, respectively. Aliquots of the internal standards were stored at -80°C.

Quattro Premier XE optimization. Standards, optimization samples, and sputum samples were first run on the Quattro Premier XE UPLC-MS/MS (Waters Corp., Milford, MA) at the University of California, Irvine's Mass Spectrometry Facility. An Acquity UPLC BEH C18 column (2.1 x 50 mm, 1.7 µM particle size) and Waters Quattro Premier XE MS were used to separate and analyze the compounds. The MS was operated in positive ion mode using electrospray ionization (ESI). Waters MassLynx 4.1 and QuanLynx 4.1 software were used for data acquisition and analysis. The mobile phases consisted of 0.1% v/v formic acid and 2 mM ammonium acetate in water (solvent A) and 0.1% v/v formic acid and 2 mM ammonium acetate in methanol (solvent B). The flow rate was 0.3 mL/min. The mobile phase gradient started at 90% solvent A and 10% solvent B. The mobile phase was then changed to 90% solvent B in 3 min with the following power-law function (curve 9 in Waters MassLynx software):

$$C(t) = Ci + [(Cf - Ci) * (X^N)] \quad (\text{equation 1})$$

Where $X = (t - Ti) / (Tf - Ti)$

$N=5$ (for curve 9)

$C(t)$ is the instantaneous composition at time "t"

Ci is the composition of B at the beginning of the segment

Cf is the composition at the end of the segment

T is time

Finally, the mobile phase was abruptly switched to 90% A and 10% B for 1.5 min.

The column temperature was 50°C, and the auto-sampler temperature was 10°C. For all samples, the injection volume was 10 µL. For the MS/MS, the detector capillary voltage was 3.3kV, and the extractor voltage was 3V. The source and desolvation temperatures were 125°C and 400 °C, respectively. Nitrogen was used as the cone and desolvation gas and set at flow rates of 150 L/h and 800 L/h, respectively. The retention times (RT) and MS/MS parameters for each antibiotic were determined using the QuanOpt function in the Waters Masslynx software (Table 1). The limits of detection (LOD) and limit of quantification (LOQ) of the external standards was calculated as:

$$\text{LOD or LOQ} = X\sigma/S \quad (\text{equation 2})$$

Where $X=3$ for the LOD or $X=10$ for the LOQ

σ =the standard deviation of the response from three independent LC-MS runs

S =the slope of the calibration curve

Xevo TQ-XS optimization. Standards were shipped overnight on wet ice to the Waters Demo Laboratory (Beverly, MA) to optimize on the Acquity UPLC Xevo TQ-XS. The Xevo column was the same (Acquity UPLC BEH C18, 1.7 µm; 2.1 mm x 50 mm), but the mobile phase consisted of 0.3% formic acid in water (solvent A) and 0.3% formic acid in acetonitrile (solvent B). The mobile phase gradient started at 98% solvent A and 2% solvent B. The mobile phase was then switched to 10% solvent A and 90% solvent B in 3 minutes with curve 6 in Waters MassLynx (N=1 in equation 1). The mobile phase was abruptly switched to 98% A and 2% B for the last 1.5 min. The injection volume was 0.5 µL and the detector gain was set to 0.1. The positive ion capillary was 0.5 kV, and the cone voltage was 50V. The desolvation gas and cone gas (nitrogen) flow rates were 1000 L/h and 150 L/h. The desolvation temperature was 600°C, and the source temperature was 150°C. The LC-MS parameters of all the antibiotics, except for colistin and vancomycin, were determined with IntelliStart optimization with Waters MassLynx software. The MS methods for colistin and vancomycin were determined by manually adjusting the cone voltage and capillary voltage and scanning the product ion spectra. The M+2H ions were used for MRM of colistin and vancomycin (Table 1).

Comparison of extraction solvents in artificial sputum media. To compare the extraction efficiency of three solvents, antibiotics were spiked into ASM (100) at concentrations of 0, 0.14, 0.41, 0.123, 0.370, 1.1, 3.3, and 10 µM. The three extraction solvents were 1% DTT, methanol, or 16/84 acetonitrile/2% acetic acid. Each solvent was

spiked with 1.33 μ M of both internal standards, linezolid-d₃ and levofloxacin-d₈. Solvent (150 μ L) was added to 50 μ L of ASM. The samples were vortexed for 30 seconds, shaken at 4°C on a shaking platform with moderate agitation for 15 minutes, and centrifuged at 13,200 RCF for 10 minutes at 4°C. The supernatant was pipetted into amber glass vials and injected directly into the LC-MS.

The apparent limit of detection (ALOD) was calculated for each antibiotic with each extraction solvent. The ALOD was calculated similarly as the LOD (equation 2), where σ is the standard deviation of the response from the spiked-in antibiotics, and S is the slope of the linear fit for the antibiotic spike-in response versus spiked-in concentration. To visualize the relationship between the recovered antibiotic concentration and the known spiked-in concentration, a linear model was fitted to the recovery data from three independent experiments for each extraction solvent. The coefficient of variation (COV) for three experiments was calculated as the standard deviation of the recovered concentrations divided by the mean of the recovered concentrations. A COV threshold of 30% was used to identify antibiotics that were reproducibly measured (218).

Sputum collection and extraction. Sputum samples from 11 subjects with CF were selected from a larger airway microbiome study that was approved by the University of Michigan Medical School Institutional Review Board (HUM00037056). Subjects were 6 males and 5 females, age 21 to 56 years (median 37). Sputum samples were collected by subjects at home and stored at 4°C for up to 23 days. Subjects also completed a daily survey

reporting symptoms and antibiotic-use of both chronic use maintenance antibiotics and episodic treatment antibiotics prescribed to treat pulmonary exacerbations (10). Samples and surveys were regularly shipped in batches to the University of Michigan. Sputum samples were shipped on ice packs for subsequent aliquoting and storage at -80°C. Sputum aliquots were shipped from the University of Michigan to the University of California, Irvine on dry ice, thawed on ice, partitioned into 50 µl aliquots, and refrozen at -80°C. Fifty microliter aliquots of sputum were thawed on ice and extracted using the same method described for the artificial sputum medium spike-in experiments and 1% DTT for extraction solvent. Symptom scores were calculated from the daily surveys as previously described (10).

UPLC-MS/MS data filtering. Peaks acquired on the Quattro Premier were automatically picked and filtered using QuanLynx software. Data were imported into R and the following criteria for filtering were applied: minimum peak area under the curve of 20 and signal to noise ratio of 10. Because several of the antibiotics had high carry-over rates (including ciprofloxacin, levofloxacin, and trimethoprim), sample peaks were also filtered out when the AUC was lower than the wash ran before the sample. Scripts can be found at the following: https://github.com/tgallagh/LCMS_Antibiotics. The Xevo TQ-XS peaks were manually picked and filtered using TargetLynx software.

Data Analysis. Contingency tables were constructed to compare the LC-MS and survey data. The surveys were treated as the standard, and sensitivity, specificity, PPV, and NPV

were calculated for each antibiotic. Specifically, the sensitivity is the number of samples where the antibiotic was detected and reported divided by total number of reported samples. Specificity is the number of samples where the antibiotic was undetected and unreported divided by the total number of unreported samples. PPV is the number of samples where the antibiotic was detected and reported divided by the number of times an antibiotic was detected; and NPV is the number of samples where an antibiotic was unreported and undetected divided by the number of undetected instances. To determine if the means of detected antibiotic concentrations were significantly different between the two instruments, paired Wilcoxon rank sums tests were performed on azithromycin, aztreonam, ceftazidime, ciprofloxacin, sulfamethoxazole, tobramycin, and trimethoprim using the “wilcox.test” function in R. Pearson’s correlations between negatives or positives with subject and sample data were completed using the “cor.test” function.

Data Availability. The raw Quattro Premier LC-MS data files can be found on Metabolomics Workbench: ST001365. Intermediate data files for the Quattro Premier and Xevo are available at this github link: https://github.com/tgallagh/LCMS_Antibiotics.

ACKNOWLEDGEMENTS

We thank the subjects for their participation and dedication to this study. We acknowledge Benjamin Katz from the Mass Spectrometry facility at UC Irvine for his input on the LC-MS experiments and Arnie Aistars and Jinxi Li from the Waters Company for their help organizing the LC-MS demo. We thank Gordon Murray from the Waters Company for developing and running the samples on the Xevo TQ-XS LC-MS. Finally, we acknowledge Heather Maughan for help with editing.

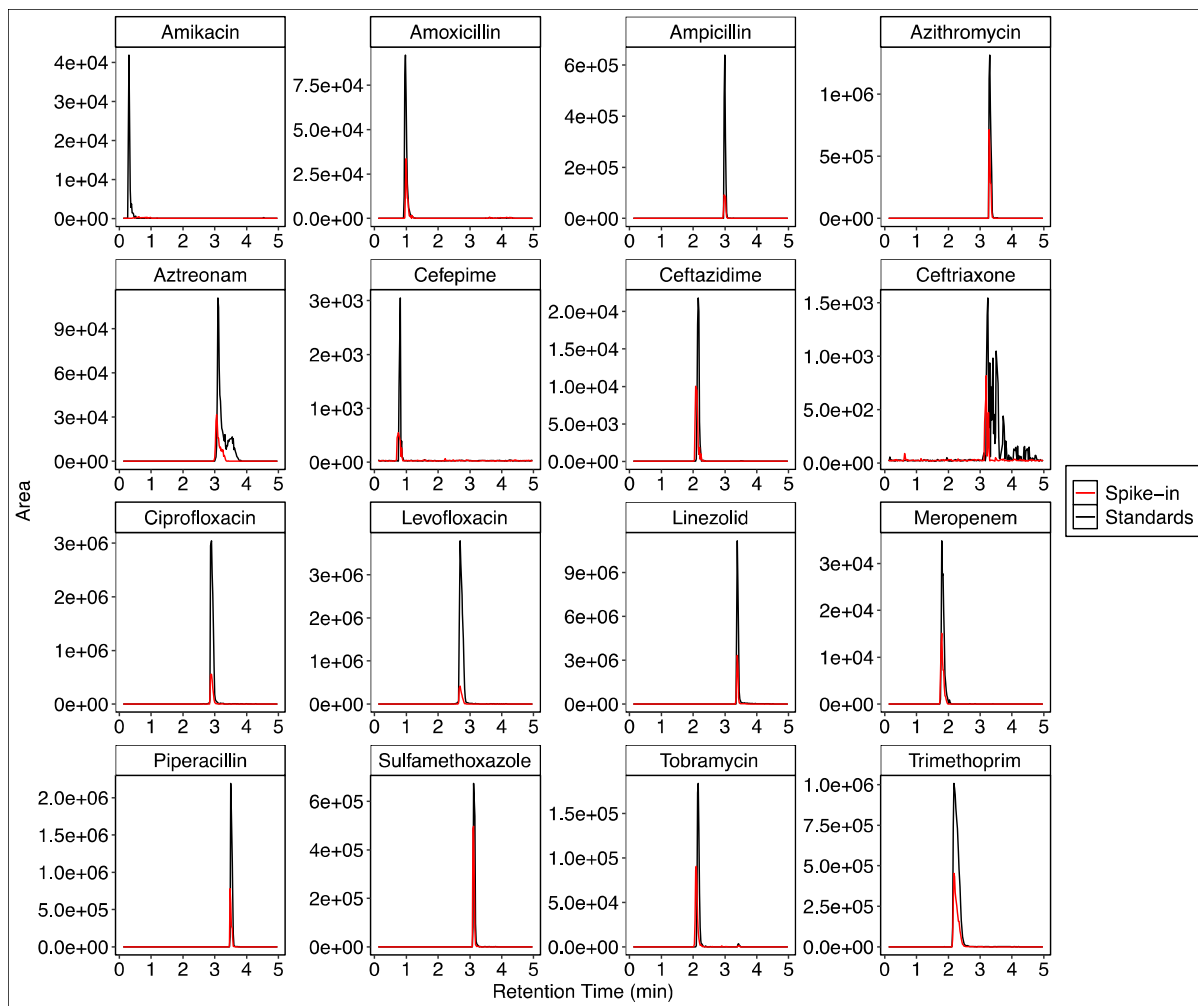


Fig. 4.1. Quattro Premier XE extracted ion chromatograms (XIC) of each antibiotic from the 10 μM pool of external standards (black line) and from the artificial sputum medium spike-in experiments (red line) using water:methanol gradient + 2 mM ammonium acetate and 0.1% acetic acid mobile phase method. XICs are ordered by retention time. No Quattro Premier XICs are shown for vancomycin and colistin due to inconsistent detection.

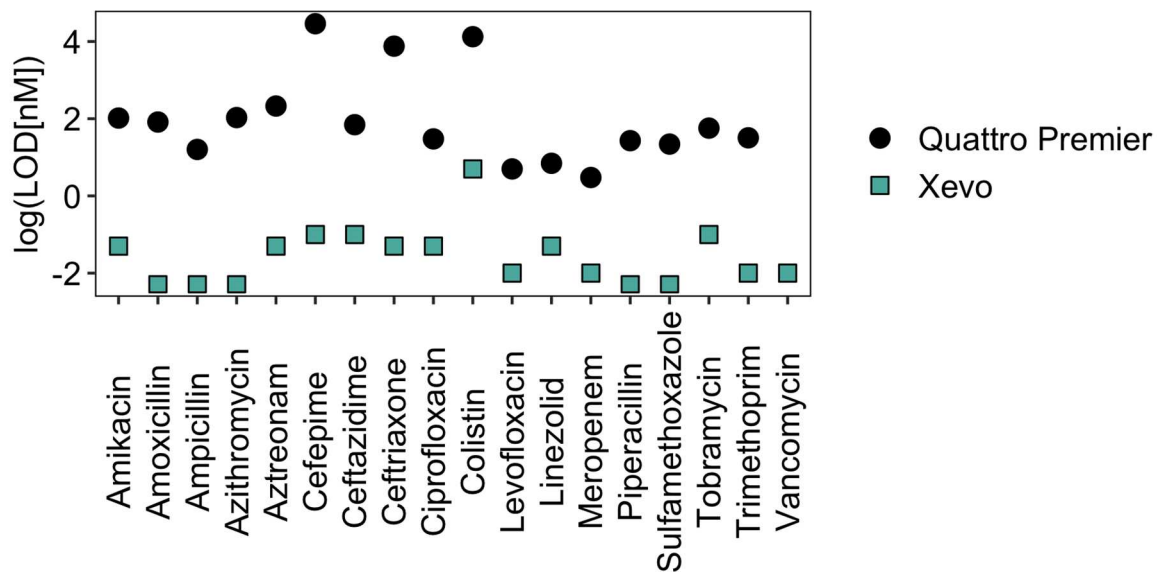


Fig. 4.2. Comparison of the log-transformed limits of detection (LOD) for antibiotic standards on the Quattro Premier XE and the Xevo TQ-XS. On average, the Xevo TQ-XS LOD was 9,500-fold lower than that of the Quattro Premier.

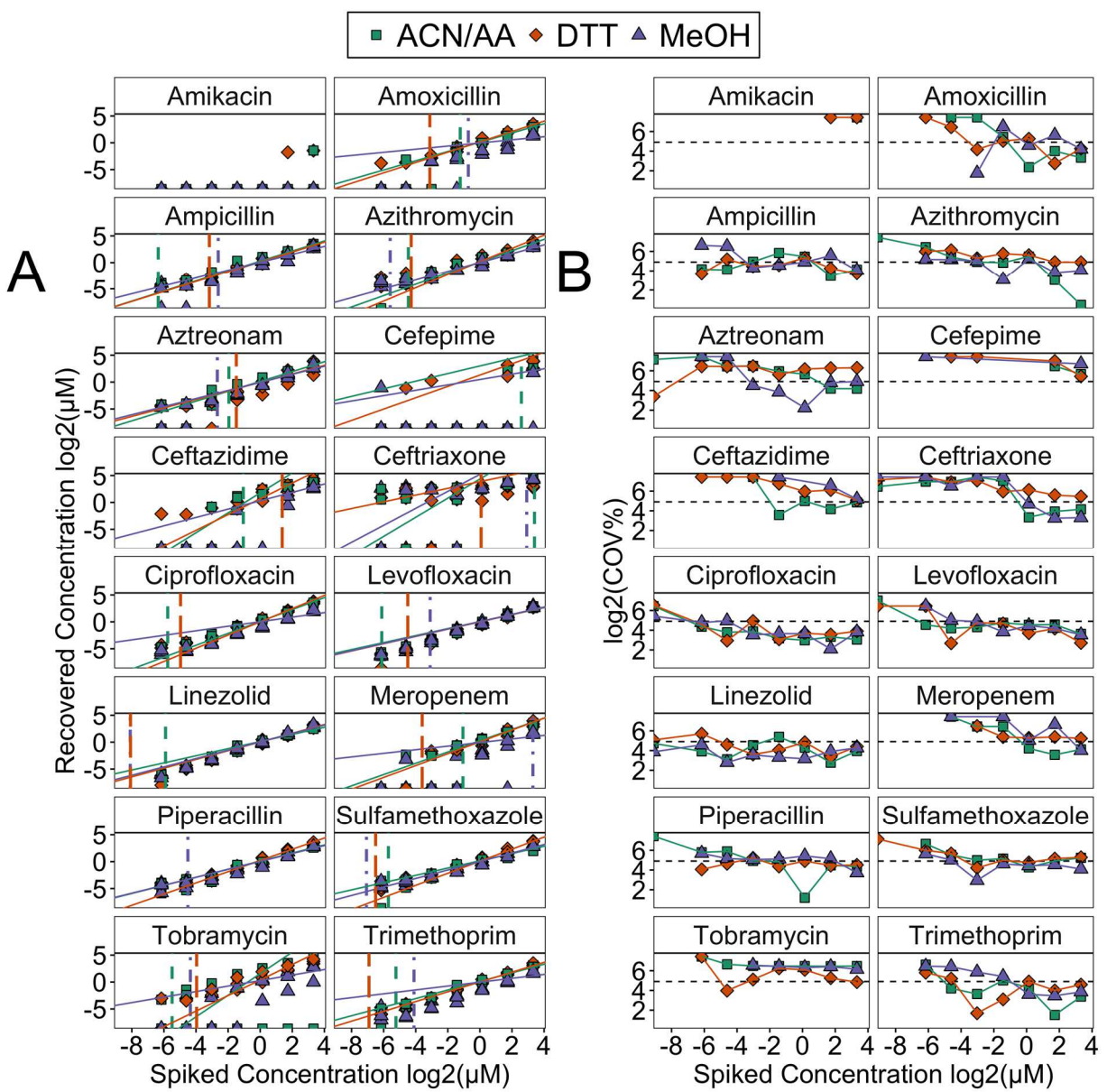


Fig. 4.3. Comparison of three solvents in the extraction of 16 antibiotics spiked into artificial sputum medium and analyzed on the Quattro Premiere. Vancomycin and colistin were excluded due to low response from the Quattro Premier method. (A) Dose response curve of antibiotics spiked into artificial sputum media, extracted with MeOH (methanol), DTT (1% DTT in water), or ACN/AA (16:84 acetonitrile:2% acetic acid). Each point represents the detected concentration from three independent experiments that were conducted on separate weeks. The solid lines represent the linear fit of the averages at each concentration. The dashed lines indicate the apparent lower limit of detection (ALOD) calculated for each antibiotic with each extraction solvent. (B) Coefficient of variation (COV) was used as a measure of reproducibility for quantifying antibiotic concentrations

from the dose response experiments. Eleven antibiotics had a COV below 30% (represented by dotted line) for concentrations less than 10 μ M: amoxicillin, ampicillin, azithromycin, ceftazidime, ciprofloxacin, levofloxacin, linezolid, piperacillin, sulfamethoxazole, tobramycin, and trimethoprim.

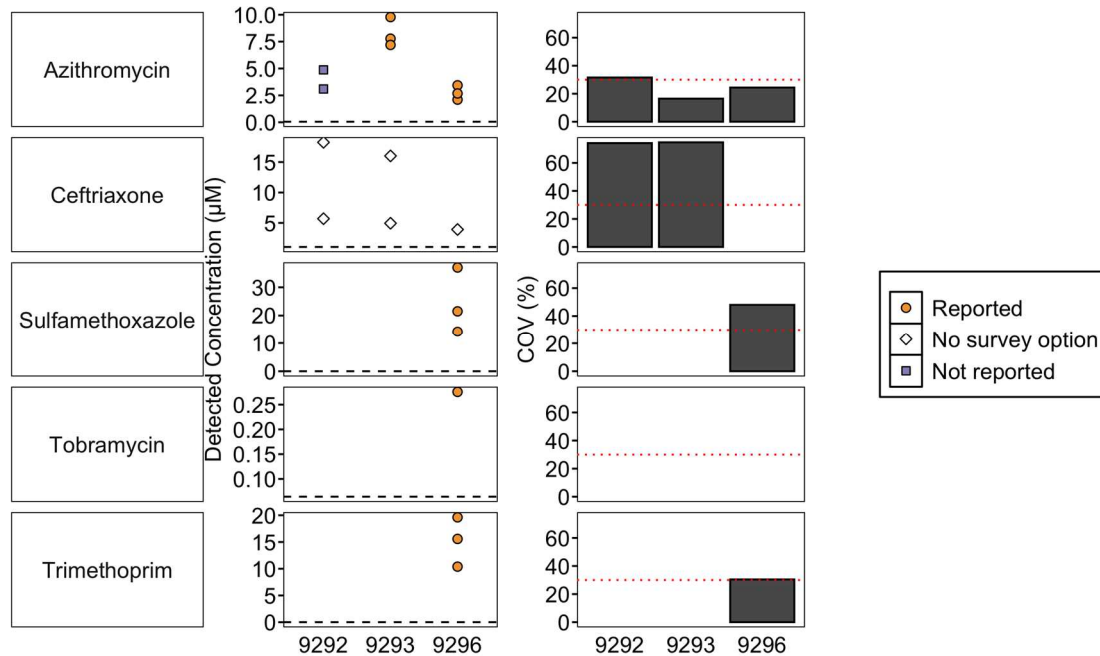


Fig. 4.4. Antibiotics detected by the Quattro Premier method in three aliquots from the same three sputum samples (9292, 9293, 9296). The concentration (μM) of detected antibiotics are on the left. Antibiotics were reported as taken (orange circle), not taken (purple square), or not provided as a survey option (ceftriaxone, white diamond). The apparent limit of detection (ALOD) from the artificial sputum experiments are indicated by black dashes. The coefficient of variation (COV) of the detected concentrations for each sample is represented on the right. The COV threshold (30%) is indicated with a red dotted line.

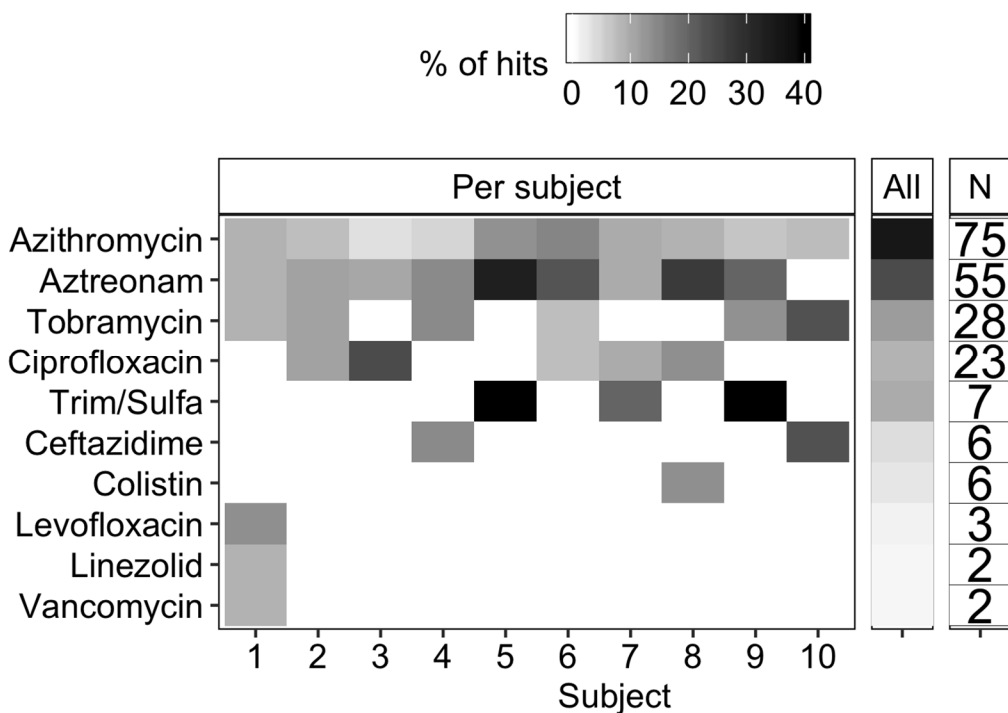
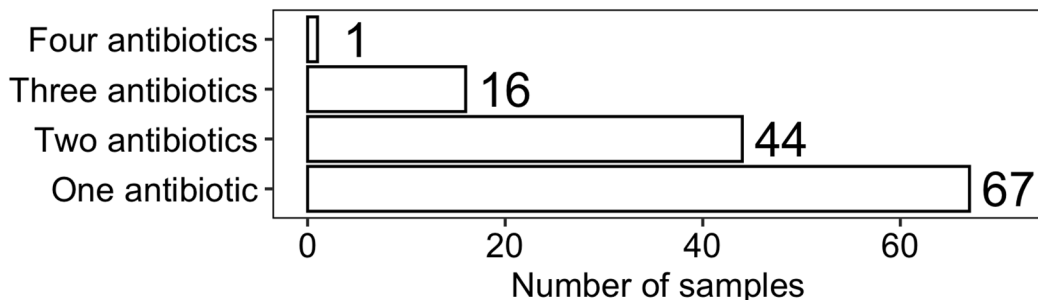
A**B**

Fig. 4.5. Daily self-reported antibiotic usage by ten subjects with cystic fibrosis on the same day that sputum samples were collected. (A) Cells are shaded on the grayscale heat map based on: number of times a subject reported taking the specified antibiotic divided by the total number times a subject reported taking any antibiotics (Per subject columns); and across the entire cohort (All column). N=the number of times an antibiotic was reported as taken on the sampling day (207 total reports of antibiotic usage for 128 sputum samples). Trim=trimethoprim, Sulfa=sulfamethoxazole. Subject 11 reported taking none of the antibiotics in this study set. (B) The number of sampling days where a subject reported taking 1-4 antibiotics on the same day.

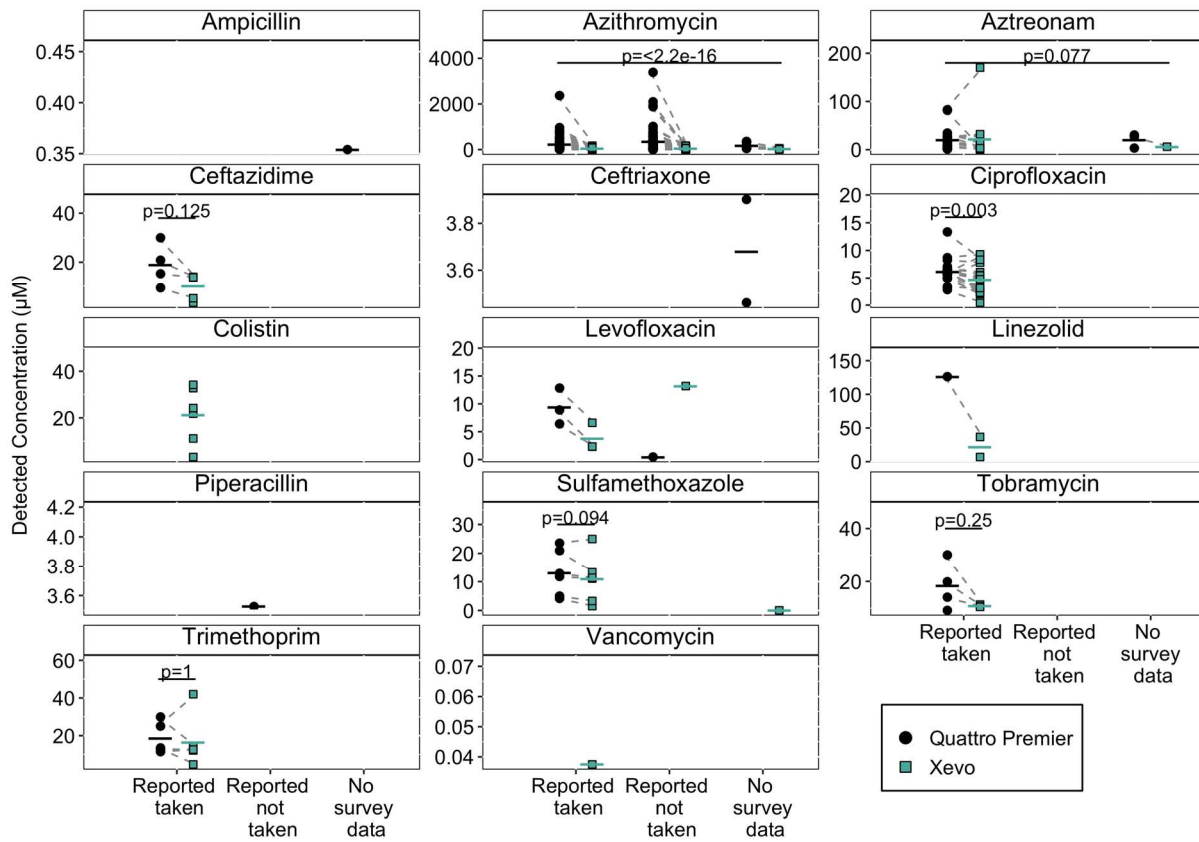


Fig. 4.6. Concentration (μM) of detected antibiotics reported as taken or not taken by a subject in 158 sputum samples. Subjects did not provide any antibiotics usage data for 13 samples. Ampicillin and ceftriaxone were not included as an option in the antibiotic usage survey. Points are concentrations of the individual samples for the Quattro Premier (black circle) and the Xevo (turquoise square). Samples containing antibiotics detected by both instruments are connected by a dashed gray line. A Wilcoxon rank sum test was used to determine if the Quattro Premier and Xevo detected concentrations were significantly different for seven antibiotics (with $n>3$ paired samples). Azithromycin and ciprofloxacin had significantly different mean detected concentrations detected by the two instruments (paired Wilcoxon rank sum test; azithromycin Quattro Premier mean=288 μM , azithromycin Xevo mean=43 μM , $V = 9591$, $P<0.05$; ciprofloxacin Quattro Premier mean=6.3 μM , ciprofloxacin Xevo mean= 4.8 μM , $V=197$, $P<0.05$).

Table 4.1: Multiple reaction monitoring (MRM) parameters for the Acquity Quattro Premier XE and Xevo TQ-XS. CV = cone voltage, CE = collision energy, RT = retention time, * indicates low response from the M+H ions for vancomycin and colistin on the Quattro Premier. Levofloxacin-d₈ and linezolid-d₃ are the internal standards.

Analyte	Quattro Premier XE TQ				Xevo TQ-XS	
	MS/MS:	CV (V)	CE (V)	RT (min)	MS/MS:	RT (min)
Amikacin	585.98 > 163.36	30	30	0.39	585.1 > 163	0.19
Amoxicillin	365.98 > 349.25	20	10	1.08	366.1 > 208	1.05
Ampicillin	350.00 > 106.36	20	20	3.14	350.1 > 106	1.34
Azithromycin	749.25 > 591.75	50	30	3.44	749.5 > 591.2	1.57
Aztreonam	435.94 > 313.27	20	20	2.61	436.1 > 313	1.23
Cefepime	480.99 > 123.35	20	50	0.81	481.1 > 167	1.01
Ceftazidime	546.91 > 468.22	30	20	2.08	547.1 > 396	1.19
Ceftriaxone	554.85 > 167.39	20	30	2.95	555.1 > 167	1.31
Ciprofloxacin	332.08 > 231.25	30	40	3.04	332.1 > 288	1.37
Colistin	1155.41 > 729.34 *	80	40	2.1	587.72 > 456.4	1.4
Levofloxacin	362.07 > 318.33	30	20	2.93	362.1 > 318	1.35
Linezolid	338.10 > 296.29	40	20	3.34	338.1 > 296	1.65
Meropenem	384.07 > 68.54	30	40	2.34	384.1 > 141	1.22
Piperacillin	518.04 > 143.37	30	20	3.46	518.1 > 160	1.93
Sulfamethoxazole	254.03 > 92.39	30	30	3.04	254.1 > 156	1.6
Tobramycin	467.96 > 167.22	40	20	2.08	468.1 > 167	1.19
Trimethoprim	291.11 > 230.24	40	20	2.89	291.1 > 230	1.34
Vancomycin	448.38 > 1305.91 *	40	20	1.63	725.63 > 1307.23	1.17
Levofloxacin-d ₈	371.10 > 326.38	40	20	2.93	370.1 > 326.1	1.35
Linezolid-d ₃	341.10 > 297.29	40	20	3.34	341.1 > 297.1	1.65

Table 4.2: Survey options for the 18 antibiotics optimized for LC-MS detection. Ampicillin and ceftriaxone were not provided as an option on the survey. Out of the 16 remaining antibiotics, 11 antibiotics were reported as taken. Fourteen antibiotics were detected in sputum on one or both of the LC-MS platforms. Antibiotics reproducibly measured on the Quattro Premier with COV<30% from the artificial sputum medium recovery experiments are indicated (see Figure 4.3). Trim=trimethoprim, Sulfa=sulfamethoxazole.

Antibiotic	Class	Survey Option	Reported by subjects	Detected by LC-MS	COV <30%?
Amikacin	Aminoglycoside	Amikacin Inhaled			
Amoxicillin	B-lactam	Amoxicillin Clavulanate Oral			Yes
Ampicillin	B-lactam	*Not provided	*Not provided	Yes	Yes
Azithromycin	Macrolide	Azithromycin IV or Oral	Oral	Yes	Yes
Aztreonam	B-lactam	Aztreonam IV or Inhaled	IV, Inhaled	Yes	
Cefepime	Cephalosporin	Cefepime IV			
Ceftazidime	Cephalosporin	Ceftazidime IV	IV	Yes	Yes
Ceftriaxone	Cephalosporin	*Not provided	*Not provided	Yes	
Ciprofloxacin	Fluoroquinolone	Ciprofloxacin IV or Oral	Oral	Yes	Yes
Colistin	Polymyxin	Colistin Inhaled or IV	Inhaled	Yes	
Levofloxacin	Fluoroquinolone	Levofloxacin Oral	Oral	Yes	Yes
Linezolid	Oxazolidinone	Linezolid Oral	Oral	Yes	Yes
Meropenem	B-lactam	Meropenem Inhaled			
Piperacillin	B-lactam	Piperacillin IV or Piperacillin Tazobactam IV		Yes	Yes
Sulfamethoxazole	Sulfonamide	Trim/Sulfa Oral	Oral	Yes	Yes
Tobramycin	Aminoglycoside	Tobramycin IV or inhaled	IV, Inhaled	Yes	Yes
Trimethoprim	Trimethoprim	Trim/Sulfa Oral	Oral	Yes	Yes
Vancomycin	Glycopeptide	Vancomycin Inhaled or IV	IV	Yes	

Table 4.3: Contingency tables comparing LC-MS data to subject self-reported surveys for each antibiotic reported as taken by at least one subject. Aztreonam and Tobramycin were reported as taken inhaled or intravenously (IV). Sens=sensitivity. Spec=Specificity. PPV=Positive predictive value. NPV= Negative predictive value.

Azithromycin	QUATTRO: SURVEY: XIVO: Yes Yes No No	Sens=92% Spec=16% PPV=50% NPV=68%	Aztreonam (Inhaled)	QUATTRO: SURVEY: XIVO: Yes Yes No No	Sens=36% Spec=100% PPV=100% NPV=74%	Aztreonam (IV)	QUATTRO: SURVEY: XIVO: Yes Yes No No	Sens=100% Spec=100% PPV=100% NPV=100%
Ceftazidime	QUATTRO: SURVEY: XIVO: Yes Yes No No	Sens=67% Spec=100% PPV=100% NPV=99%	Ciprofloxacin	QUATTRO: SURVEY: XIVO: Yes Yes No No	Sens=96% Spec=100% PPV=100% NPV=99%	Colistin	QUATTRO: SURVEY: XIVO: Yes Yes No No	Sens=0% Spec=100% PPV=100% NPV=96%
Levofloxacin	QUATTRO: SURVEY: XIVO: Yes Yes No No	Sens=100% Spec=100% PPV=75% NPV=99%	Linezolid	QUATTRO: SURVEY: XIVO: Yes Yes No No	Sens=50% Spec=100% PPV=100% NPV=99%	Sulfamethoxazole	QUATTRO: SURVEY: XIVO: Yes Yes No No	Sens=86% Spec=100% PPV=100% NPV=99%
Tobramycin (Inhaled)	QUATTRO: SURVEY: XIVO: Yes Yes No No	Sens=0% Spec=100% PPV=0% NPV=80%	Tobramycin (IV)	QUATTRO: SURVEY: XIVO: Yes Yes No No	Sens=50% Spec=100% PPV=100% NPV=87%	Trimethoprim	QUATTRO: SURVEY: XIVO: Yes Yes No No	Sens=71% Spec=100% PPV=100% NPV=99%
Vancomycin	QUATTRO: SURVEY: XIVO: Yes Yes No No	Sens=0% Spec=100% PPV=0% NPV=99%						Sens=86% Spec=100% PPV=100% NPV=99%

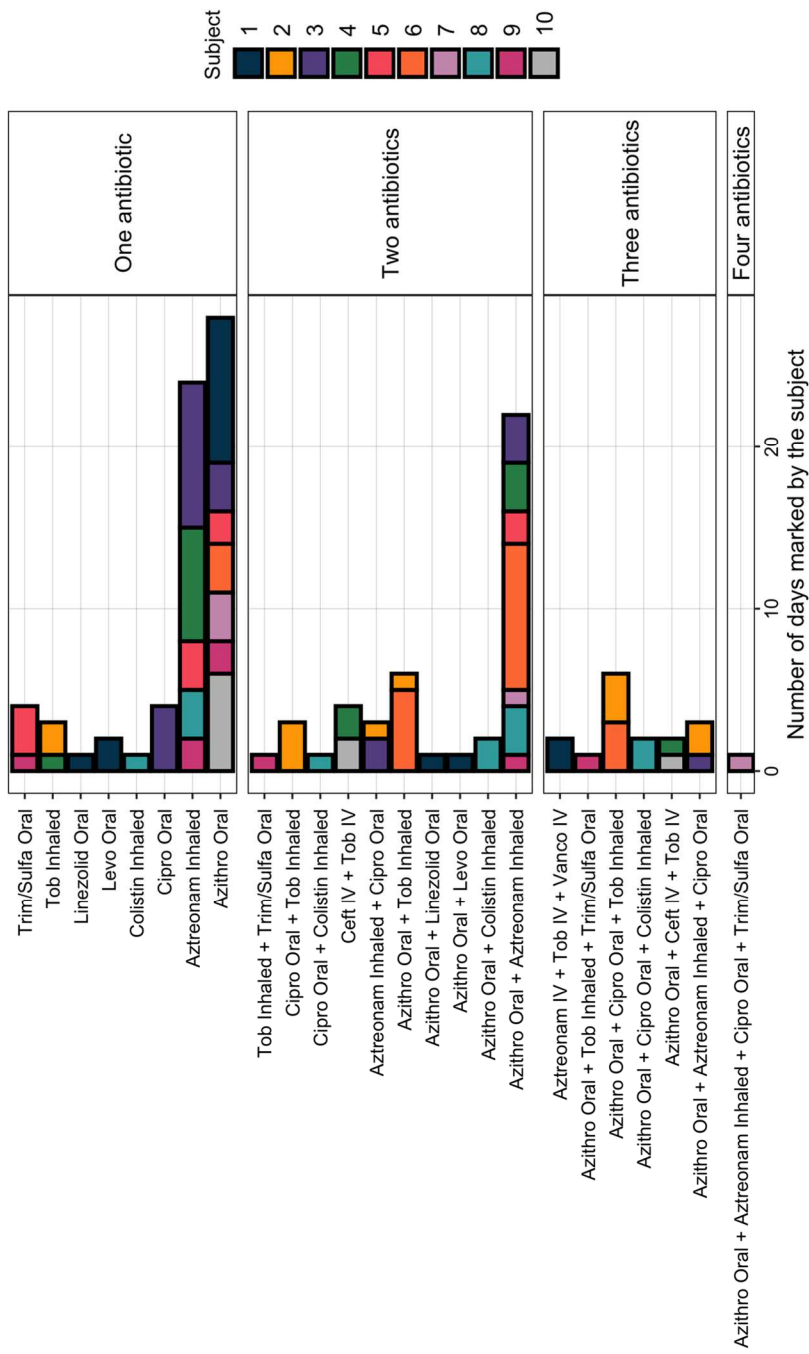


Figure S4.1. Number of samples where a subject marked taking an antibiotic (N=158 samples from 10 subjects with antibiotic usage reported) categorized by the number of marked antibiotics per day (1-4 antibiotics). Tob=Tobramycin. Levo=Levofloxacin. Cipro=Ciprofloxacin. Azithro=Azithromycin. Trim=Trimethoprim. Sulfa=Sulfamethoxazole. Ceft=Ceftazidime. Vanco=Vancomycin. Subject 11 did not record taking any antibiotics of interest on the days sputum samples were collected.

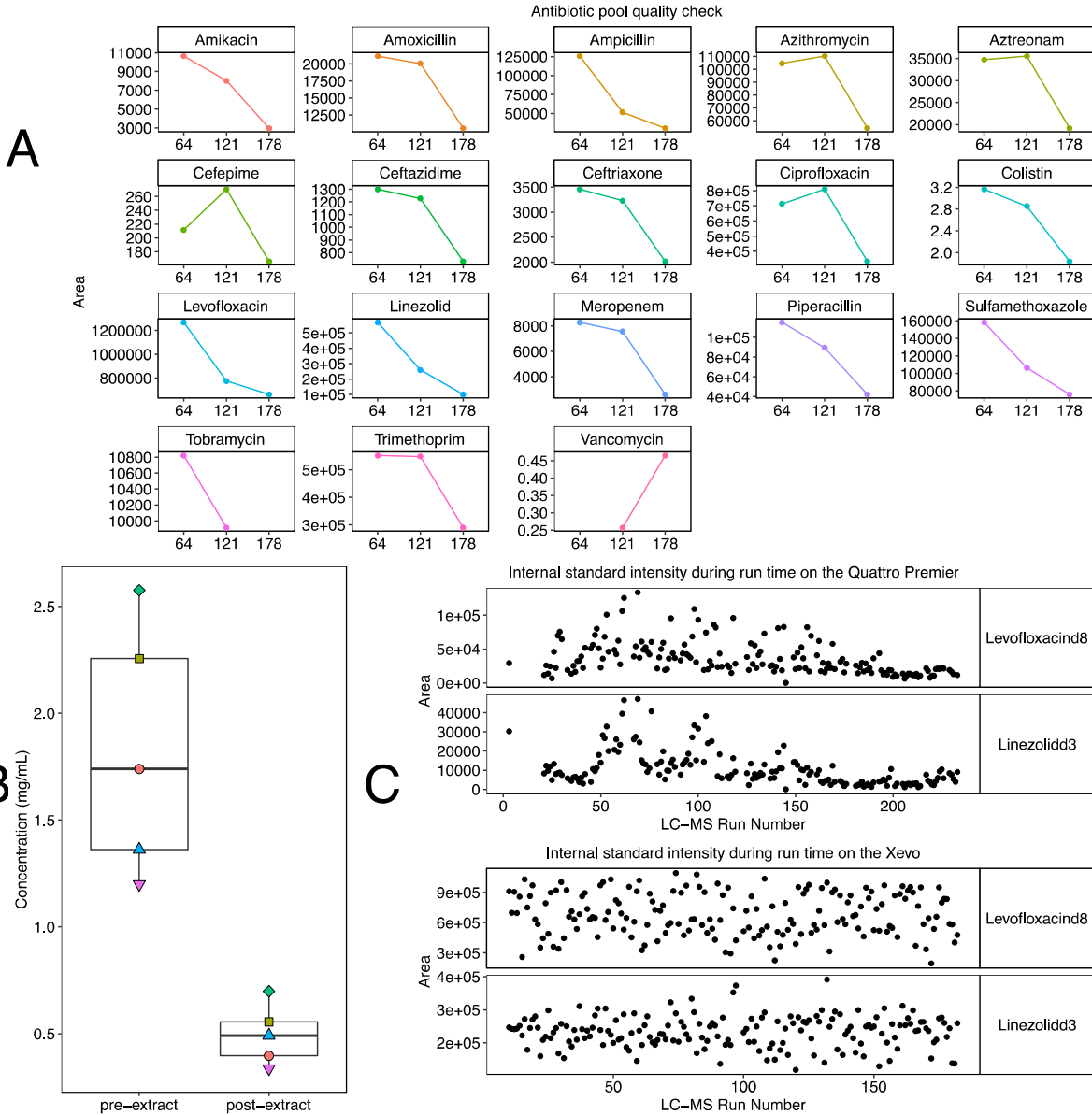


Figure S4.2. (A) The area of the external QC antibiotic pool dropped during the Quattro Premier XE run. (B) The protein levels before and after the DTT liquid-liquid extraction for five sputum samples. (C) The Quattro Premier internal standard intensity in CF sputum samples dropped during the LC-MS run, while the Xevo internal standard intensity did not have a decreasing trend.

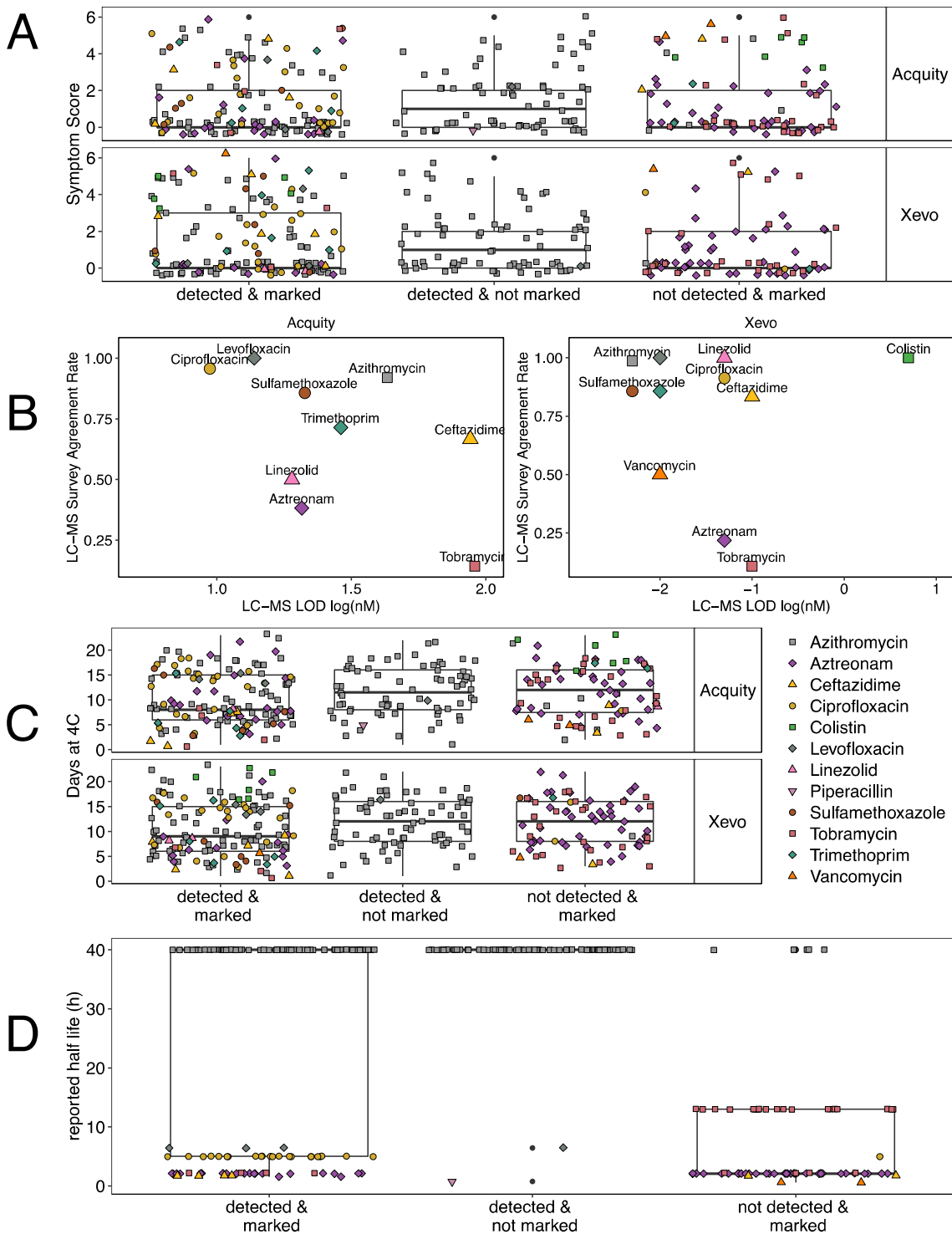
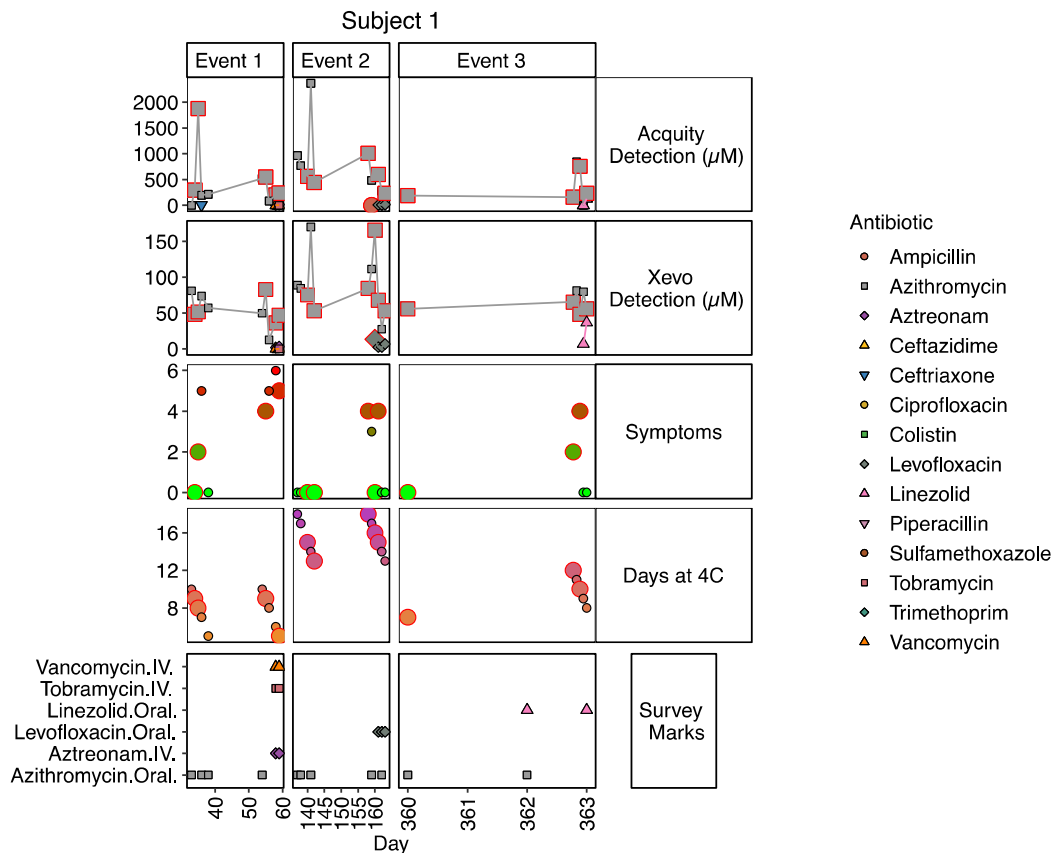


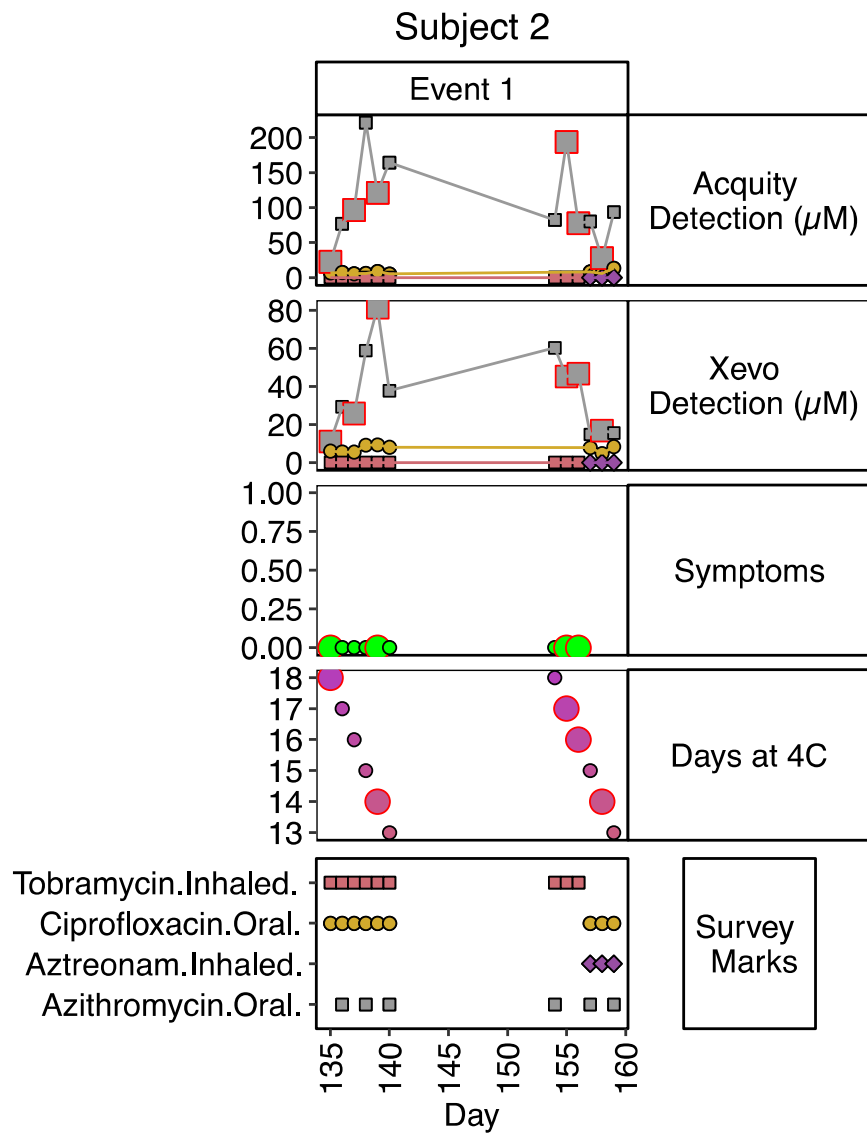
Figure S4.3: (A) Symptom score was not correlated with taking additional antibiotics (detected & not marked). (B) The Acuity Quattro Premier LC-MS LOD (limit of detection) was slightly negatively correlated with agreement rate, while the Xevo was not LOD was not correlated with agreement rate. (C) Days that samples were stored at 4°C did not impact the agreement rate with the subject surveys. (D) Antibiotics with longer half-lives (azithromycin, colistin, levofloxacin, piperacillin, vancomycin) were more likely to be detected in the 'not detected & marked' group.

green square) had higher detection rates than antibiotics with shorter half-lives (tobramycin, pink square).

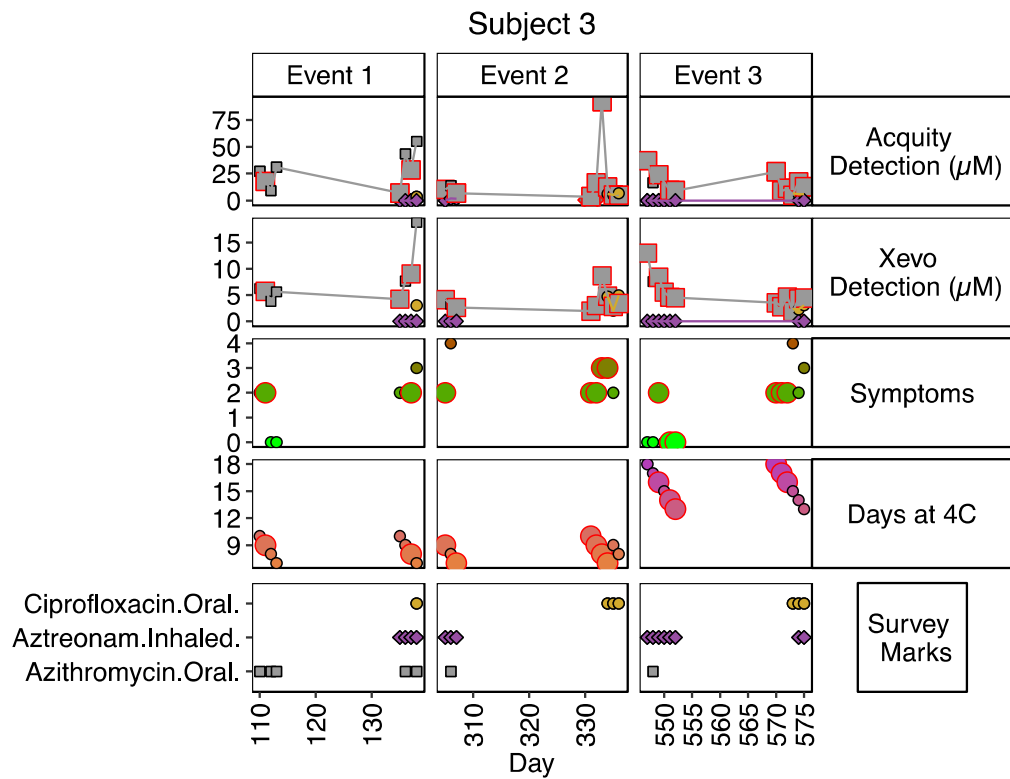
A



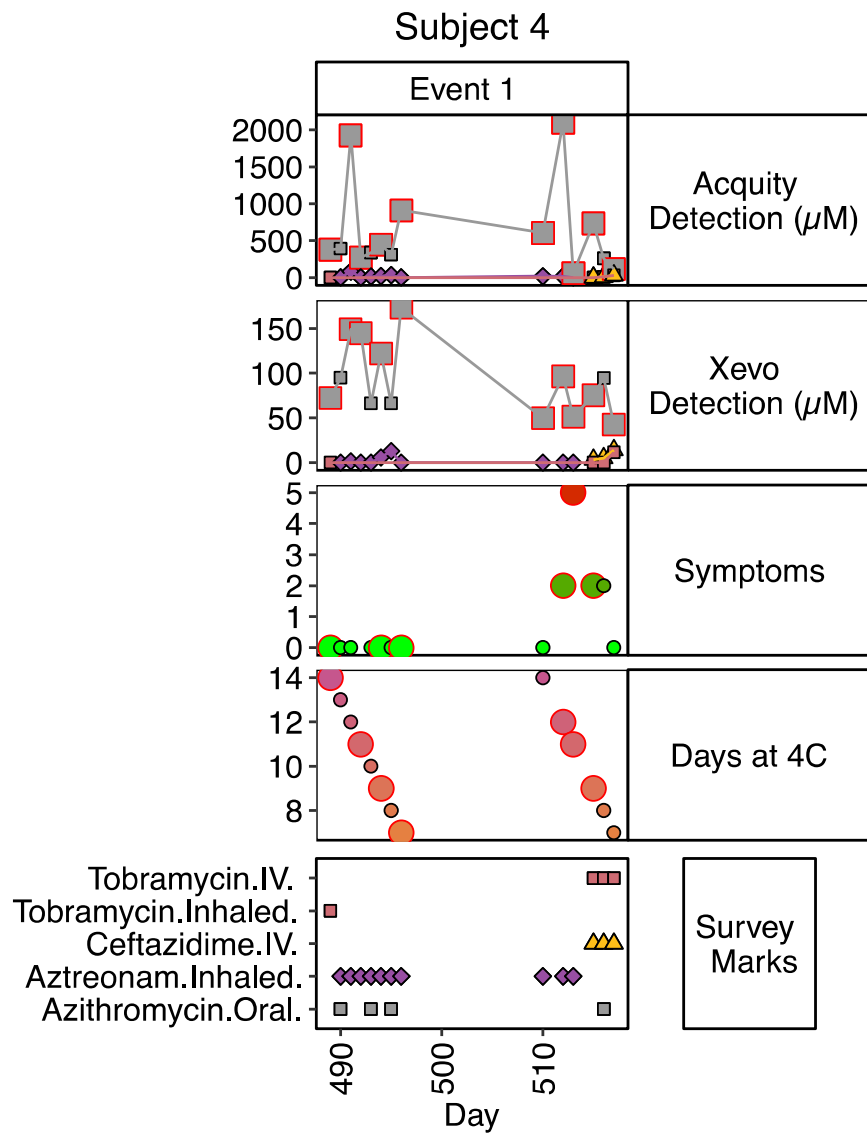
B

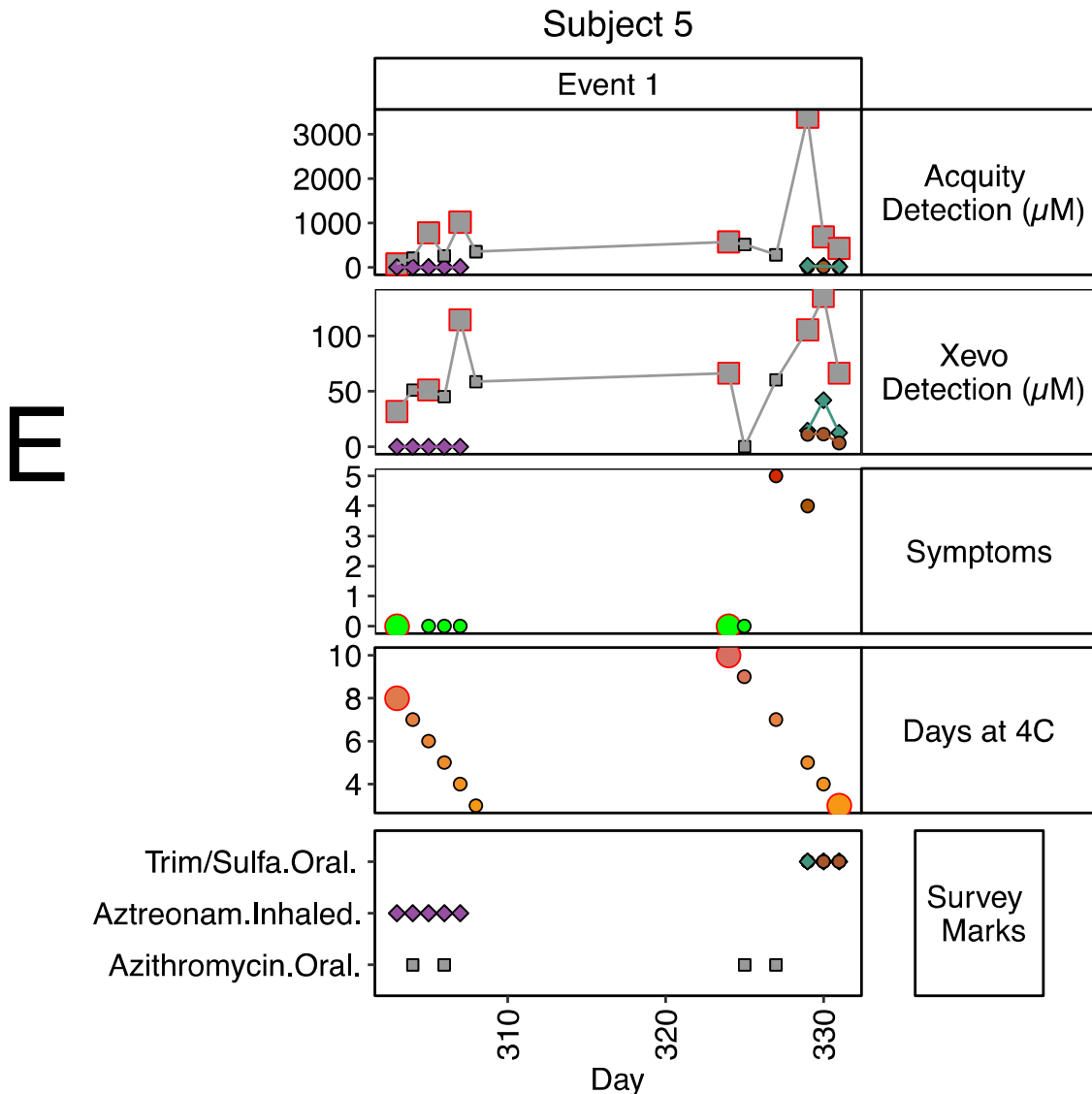


C

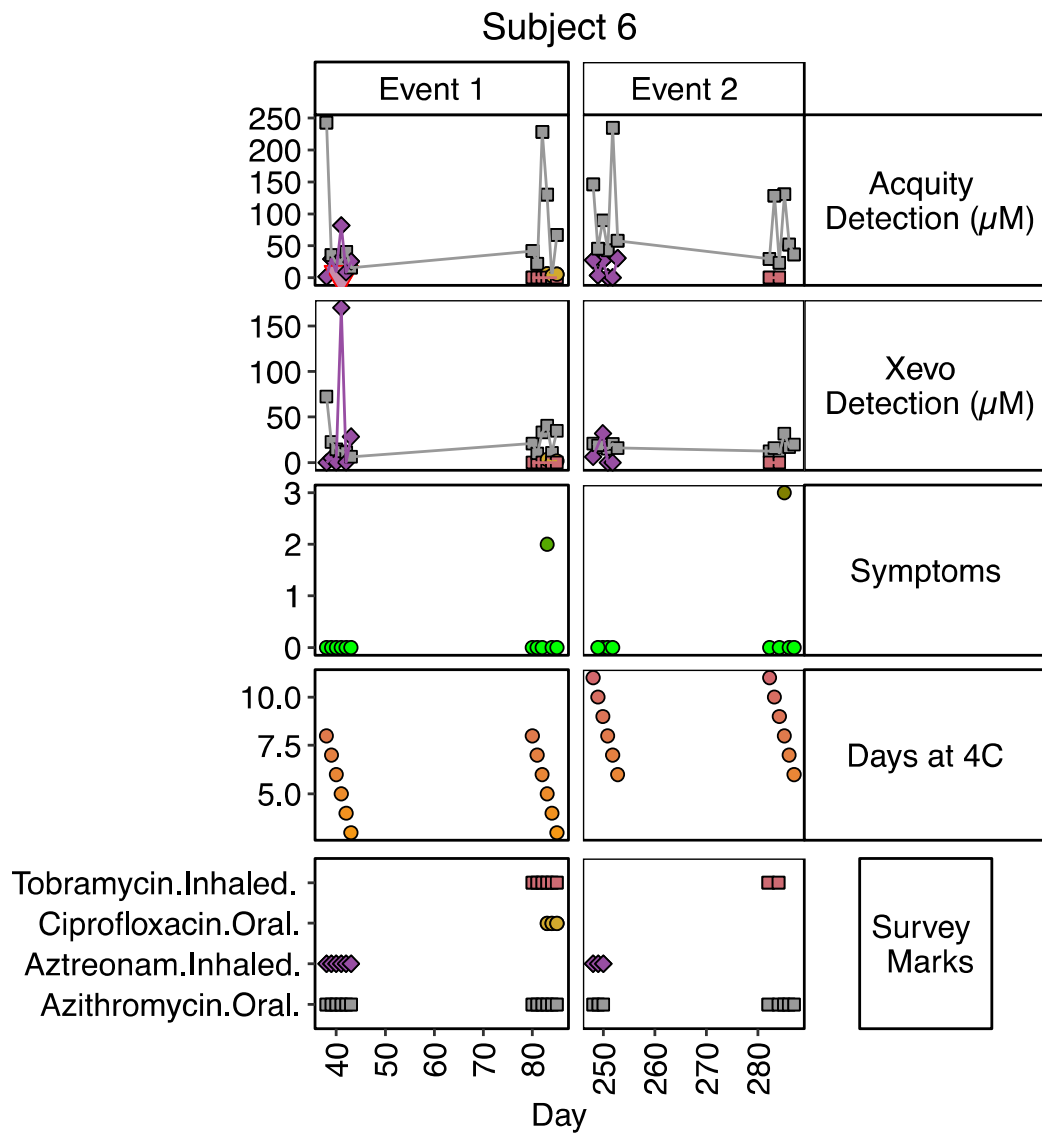


D

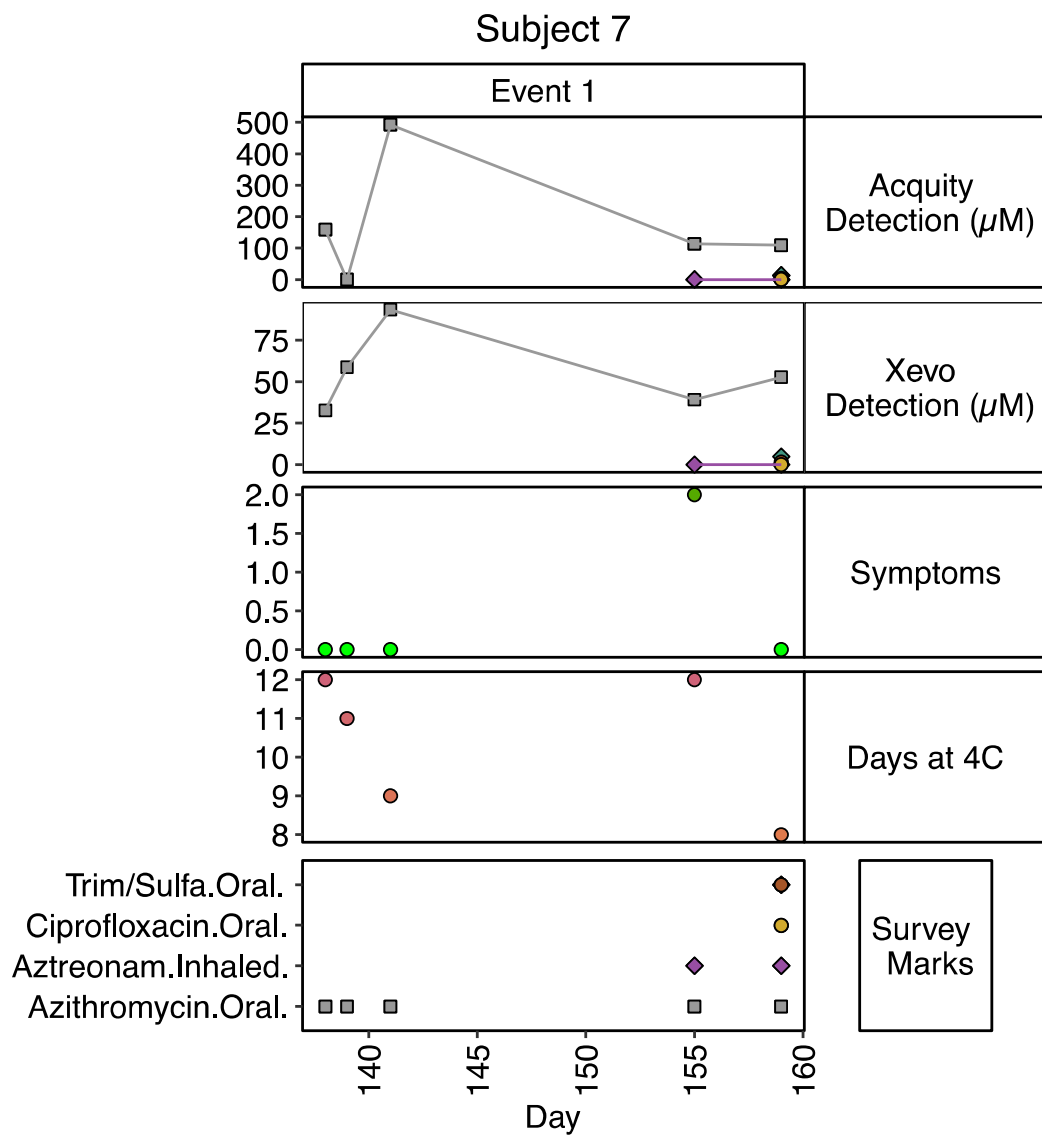




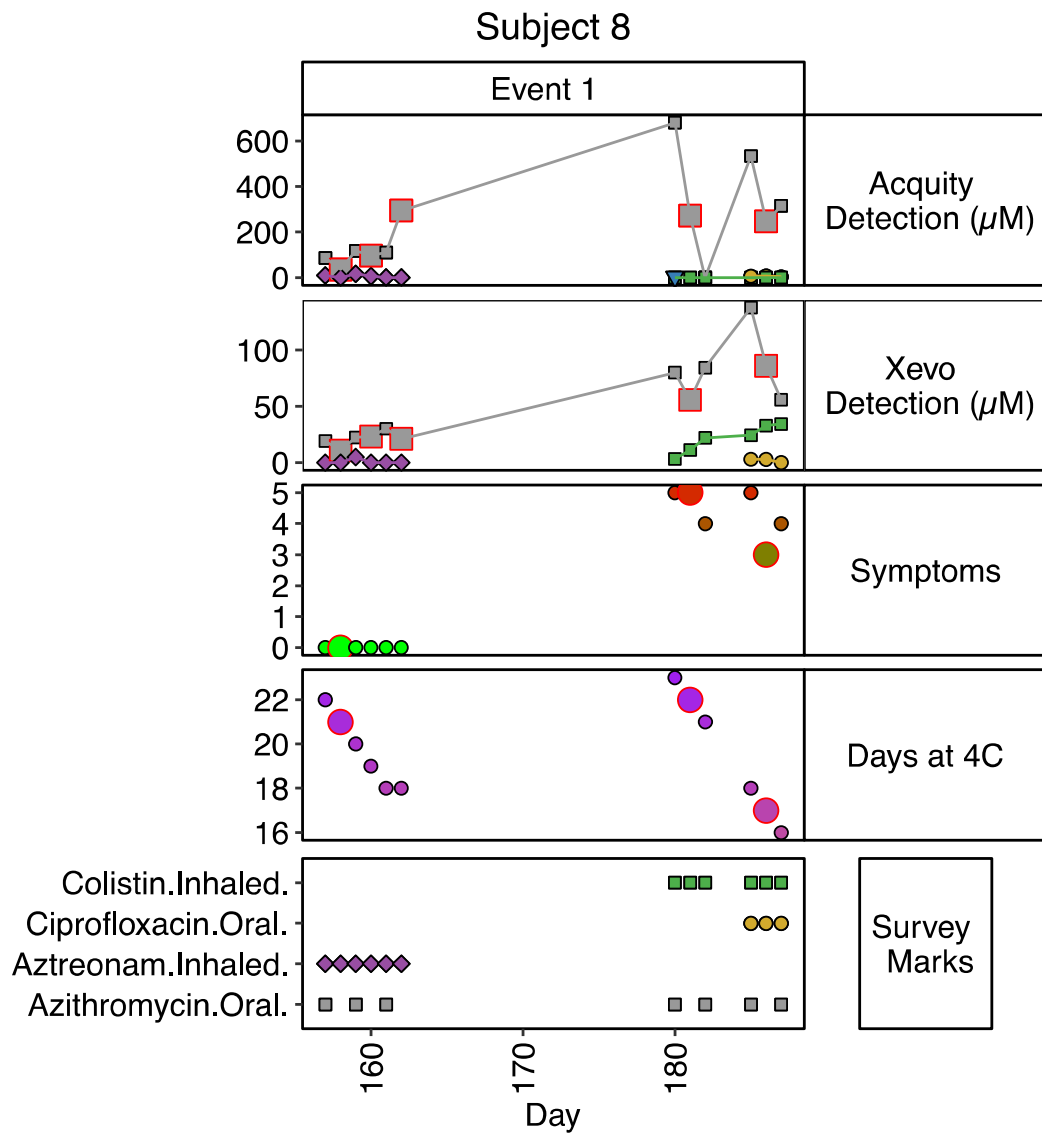
F



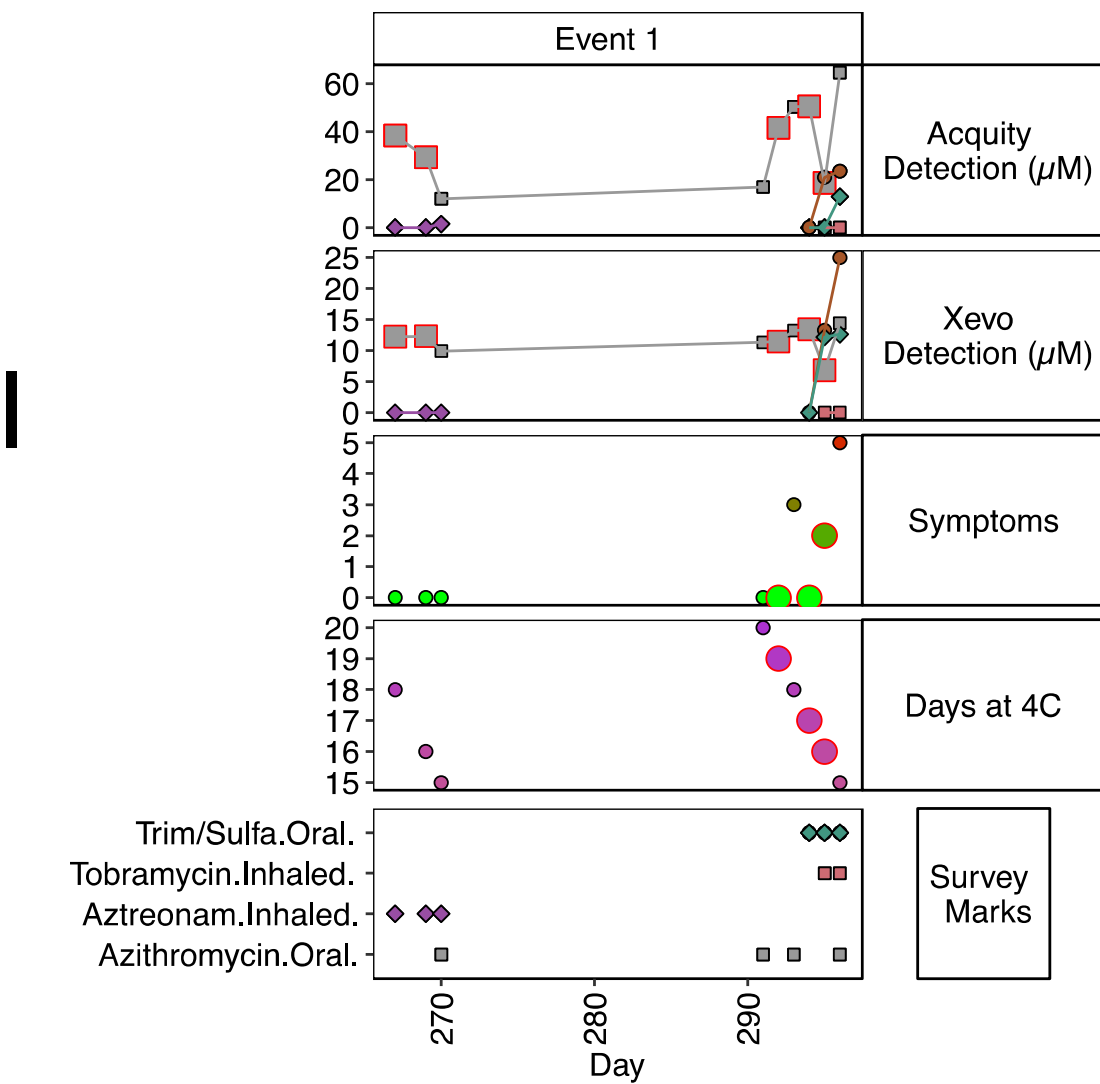
G



H



Subject 9



J

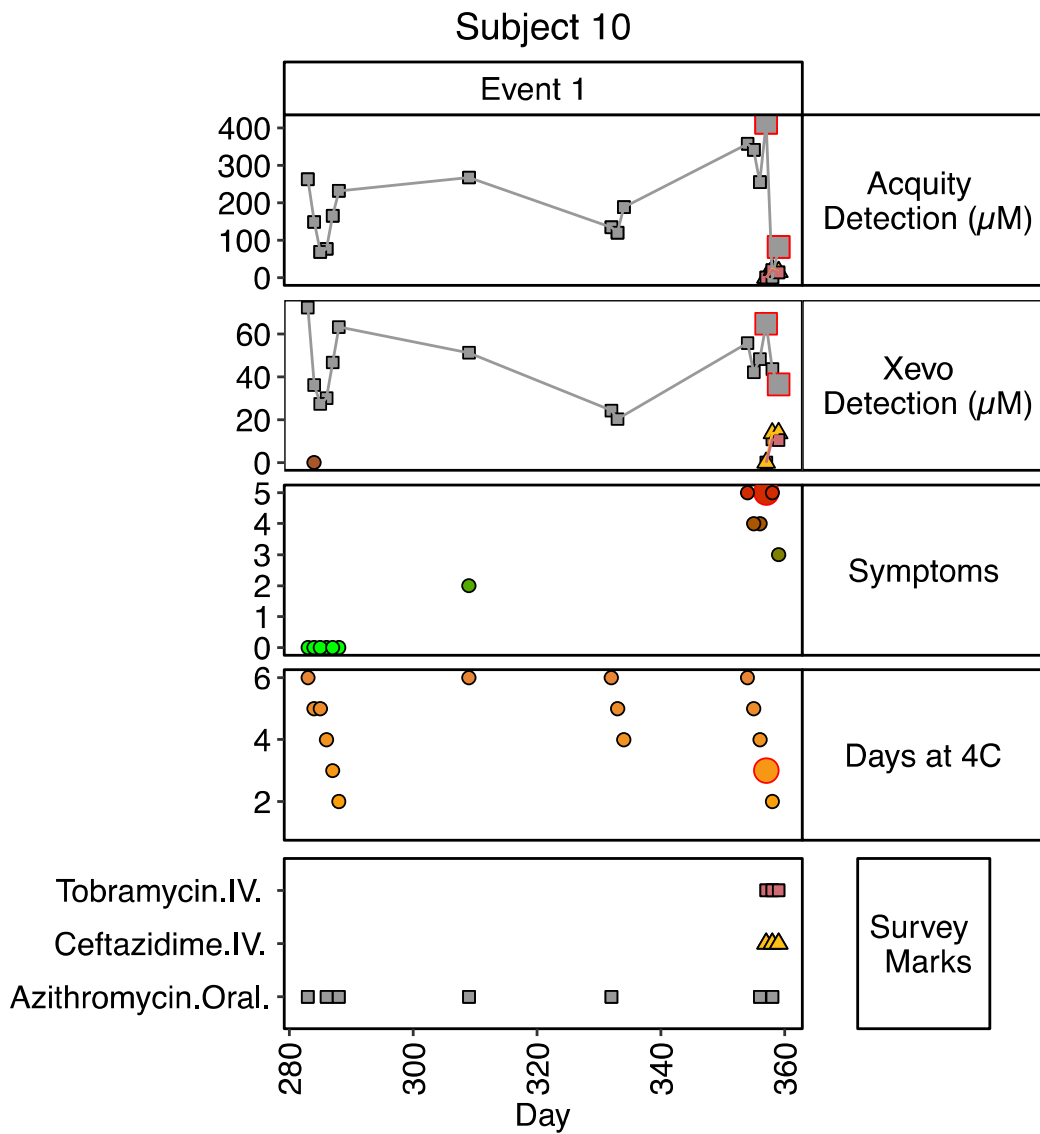


Figure S4.4. Antibiotics and sample data for all subjects (subjects 1-10 represented in panels A-J), except for subject 11 who reported taking no antibiotics during the study period. Antibiotics were detected and quantified with the Acquity Quattro Premier LC-MS method for each sputum sample. The subject symptom scores, days stored at 4°C, subject antibiotic survey marks, and clinical stage (baseline, exacerbation, or treatment) are also depicted. Antibiotics detected by the LC-MS but not marked by the subject are indicated with a red outline and larger shape size in all grids.

Table S4.1: Antibiotic preparation and properties. Pharmaceutical-grade or HPLC-grade antibiotics were dissolved in the specific solvent to make concentrated stocks of 10 mM or 1 mM. The included biological half-lives were determined primarily from short-term dosage (1-3 doses) pharmacokinetic studies in CF subjects, with a few exceptions noted below. IV= intravenous.

Antibiotic	Catalogue #	Solvent for suspension of concentrated stocks	Reported mean biological half-lives (h) in serum
Amikacin	Sigma-Aldrich PHR1654	Water	1.1 for IV* (Autret <i>et al.</i>)
Amoxicillin	Sigma-Aldrich PHR1127	Water	1.7 for IV (Lovering <i>et al.</i>)
Ampicillin	Sigma-Aldrich PHR1424	Water	1.5 for IV (Lovering <i>et al.</i>)
Azithromycin	Sigma-Aldrich PZ0007	Water	65.2 for IV* (Jacobs <i>et al.</i>); 40 for oral** (Foulds <i>et al.</i>)
Aztreonam	Sigma-Aldrich PHR1785	Water	1.54 for IV (Vinks, <i>et al.</i>) ; 2.1 for inhalation (Gibson, <i>et al.</i>)
Cefepime	Sigma-Aldrich PHR1763	Water	1.59 (Arguesadas, <i>et al.</i>)
Ceftazidime	Sigma-Aldrich PHR1847	Water	1.74 for IV (Kercsmar <i>et al.</i>), 1.57 for oral (Turner <i>et al.</i>)
Ceftriaxone	Sigma-Aldrich PHR1382	Water	7.09 for IV* (Michalson <i>et al.</i>)
Ciprofloxacin	Sigma-Aldrich 17850-5G-F	Acetonitrile, acetic acid mix	4.8h for IV, 5h for oral (Davis <i>et al.</i>)
Colistin	Sigma-Aldrich PHR1605	Water	4.5 for IV (Li <i>et al.</i>)
Levofloxacin	Sigma-Aldrich PHR1697	Methanol	6.44 for oral after steady state(Lee <i>et al.</i>); 7.4 for IV** (Chien <i>et al.</i>)
Linezolid	Sigma-Aldrich PZ0014	Water	4.4 (Bossu <i>et al.</i>)
Mereopenem	Fisher Scientific AK161987	Water	0.74 (Christensson <i>et al.</i>)
Piperacillin	Sigma-Aldrich PHR1805	Methanol	0.75* (Hoogkamp-Korstanje <i>et al.</i>)
Sulfamethoxazole	Sigma-Aldrich PHR1126	Methanol	6 (Reed <i>et al.</i>)
Tobramycin	Fisher Scientific AC455430050	Water	2.2 for IV (Beringer <i>et al.</i>); 13h for inhaled (Touw <i>et al.</i>)
Trimethoprim	Sigma-Aldrich T7883	Methanol	5.7 (Reed <i>et al.</i>)
Vancomycin	Sigma-Aldrich PHR1732	Water	0.6 (Albrecht <i>et al.</i>)

** healthy individuals

* pediatric patients

Table S4.2: Comparison of two mobile phases to detect 16 antibiotics on the Quattro Premier XE.

	Method 1: Water:Acetonitrile gradient phase area (10 µM standards Area)	Method 2: Water:methanol gradient (formic acid, 2 mM ammonium acetate) (10 µM standards Area)
Meropenem	5.01E+01	4.60E+04
Levofloxacin	5.43E+05	4.74E+05
Linezolid	4.06E+06	1.85E+05
Ampicillin	7.36E+04	6.60E+05
Piperacillin	1.76E+05	4.89E+04
Ciprofloxacin	2.27E+05	6.60E+05
Tobramycin	5.12E+03	1.84E+04
Ceftazidime	1.33E+04	5.38E+04
Amoxicillin	2.61E+04	2.37E+04
Amikacin	3.76E+01	9.68E+03
Azithromycin	3.93E+02	8.51E+05
Aztreonam	4.56E+02	4.99E+04
Ceftriaxone	6.59E+03	2.20E+04
Colistin	1.26E+04	3.54E+03
Cefepime	3.29E+04	3.11E+04
Vancomycin	5.20E+00	7.84E+03

Table S4.3: The Acuity and Xevo LOD (lower limits of detection) for the pooled external standards, compared to the MIC (minimum inhibitory concentration) break points for common cystic fibrosis opportunistic pathogens.

	MIC break points		Quattro Premier		Xevo	
	Example organism	CLSI MIC for susceptibility [ref. 61]	LOD (μM)	Fold change in MIC/LOD	LOD (nM)	Fold change in MIC/LOD
Amikacin	<i>Pseudomonas</i>	27 μM (16 $\mu\text{g/ml}$)	0.104	260	0.050	5.40E+05
Amoxicillin	<i>Staphylococcus</i>	5.5 μM (2 $\mu\text{g/ml}$)	0.082	67	0.005	1.10E+06
Ampicillin	<i>Staphylococcus</i>	6 μM (2 $\mu\text{g/ml}$)	0.016	375	0.005	1.20E+06
Azithromycin	<i>Staphylococcus</i>	3 μM (2 $\mu\text{g/ml}$)	0.107	28	0.005	6.00E+05
Aztreonam	<i>Pseudomonas</i>	9 μM (4 $\mu\text{g/ml}$)	0.213	42	0.050	1.80E+05
Cefepime	<i>Pseudomonas</i>	16 μM (8 $\mu\text{g/ml}$)	28.908	0.6	0.100	1.60E+05
Ceftazidime	<i>Pseudomonas</i>	15 μM (8 $\mu\text{g/ml}$)	0.070	214	0.100	1.50E+05
Ceftriaxone	<i>Haemophilus</i>	3.6 μM (2 $\mu\text{g/ml}$)	7.579	0.5	0.050	7.20E+04
Ciprofloxacin	<i>Pseudomonas</i>	3 μM (1 $\mu\text{g/ml}$)	0.030	100	0.050	6.00E+04
Colistin	<i>Pseudomonas</i>	2 μM (2 $\mu\text{g/ml}$)	13.325	0.15	5.000	4.00E+02
Levofloxacin	<i>Pseudomonas</i>	6.5 μM (2 $\mu\text{g/ml}$)	0.005	1300	0.010	6.50E+05
Linezolid	<i>Staphylococcus</i>	12 μM (4 $\mu\text{g/ml}$)	0.007	1700	0.050	2.40E+05
Meropenem	<i>Pseudomonas</i>	5 μM (2 $\mu\text{g/ml}$)	0.003	1670	0.010	5.00E+05
Piperacillin	<i>Pseudomonas</i>	31 μM (16 $\mu\text{g/ml}$)	0.027	1150	0.005	6.20E+06
Sulfamethoxazole	<i>Staphylococcus</i>	0.1 μM (0.05 $\mu\text{g/ml}$) with trimethoprim	0.022	4.5	0.005	2.00E+04
Tobramycin	<i>Pseudomonas</i>	9 μM (4 $\mu\text{g/ml}$)	0.057	158	0.100	9.00E+04
Trimethoprim	<i>Staphylococcus</i>	28 μM (8 $\mu\text{g/ml}$)	0.032	875	0.010	2.80E+06
Vancomycin	<i>Staphylococcus</i>	1.4 μM (2 $\mu\text{g/ml}$)	NA	NA	0.010	1.40E+05

Table S4.4: The Quattro Premier LOD (limit of detections) and LLOQ (lower limits of quantification) for the pooled external standards and apparent LOD (ALOD) and LLOQ (ALLOQ) for antibiotics spiked into artificial sputum media and extracted with three solvents: DTT (1% dithiothreitol), ACN/AA (16% acetonitrile:84% of 2% acetic acid), and MeOH (methanol). The antibiotics are ordered by increasing external standard LODs. NA=not available due to poor detection.

	External Standards		Artificial Sputum - DTT		Artificial Sputum - ACNAA		Artificial Sputum - MeOH	
	LOD (μ M)	LLQ (μ M)	ALOD (μ M)	ALLQOQ (μ M)	ALOD (μ M)	ALLQOQ (μ M)	ALOD (μ M)	ALLQOQ (μ M)
Meropenem	0.003	0.009	0.0825	0.2751	0.4805	1.6016	9.87	32.88
Levofloxacin	0.005	0.015	0.0443	0.1478	0.0144	0.0480	0.12	0.39
Linezolid	0.007	0.022	0.0037	0.0123	0.0168	0.0559	0.00	0.01
Ampicillin	0.016	0.053	0.111	0.371	0.0112	0.041	0.16	0.54
Sulfamethoxazole	0.022	0.075	0.0110	0.0368	0.0192	0.0639	0.01	0.02
Piperacillin	0.027	0.091	0.0687	0.2290	0.0257	0.0857	0.04	0.15
Ciprofloxacin	0.030	0.101	0.032	0.107	0.018	0.061	0.02	0.07
Trimethoprim	0.032	0.107	0.0083	0.0277	0.0266	0.0885	0.06	0.19
Tobramycin	0.057	0.191	0.0641	0.2137	0.0222	0.0741	0.05	0.16
Ceftazidime	0.070	0.234	2.589	8.629	0.482	1.606	NA	NA
Amoxicillin	0.082	0.272	0.115	0.383	0.427	1.424	0.61	2.02
Amikacin	0.104	0.347	NA	NA	NA	NA	NA	NA
Azithromycin	0.107	0.358	0.051	0.171	0.046	0.152	0.02	0.07
Aztreonam	0.213	0.709	0.356	1.188	0.258	0.861	0.16	0.52
Ceftriaxone	7.579	25.262	1.053	3.511	10.574	35.246	7.56	25.19
Colistin	NA	NA	NA	NA	NA	NA	NA	NA
Cefepime	28.908	96.359	14.678	48.928	6.001	20.002	NA	NA
Vancomycin	NA	NA	NA	NA	NA	NA	NA	NA

SUMMARY & FUTURE DIRECTIONS

Assessing the physiology of bacteria in their natural environment is essential for understanding natural microbial interactions and antibiotic efficacy. In the context of cystic fibrosis, steep chemical gradients drive bacterial physiology and antibiotic tolerance (4, 92). Reductionist experiments are powerful for assessing the impact of relevant conditions on microbes in a controlled setting. With *in vitro* methods, we were able to identify relevant cross-feeding interactions between *Rothia* and *P. aeruginosa* that would be impossible to track in an *in vivo* setting. We also determined that acidic pH is stressful for *S. maltophilia* and utilized fluorescence lifetime imaging microscopy (FLIM) to visualize changes in pyocyanin reduction throughout *P. aeruginosa* biofilms. We know there is a lack of overlap between laboratory conditions and CF sputum. This is evidenced by differences in bacterial growth rates, with estimates of bacterial doubling times being 100-fold times lower in sputum than in laboratory cultures (53). The question still remains: How are fermentation and chemical gradients impacting the physiology of opportunistic pathogens *in vivo*?

Future directions in fluorescence

The depth limits of fluorescence imaging are continuously advanced with the introduction of new technologies, like the DIVER (170, 194) and adaptive optics (219). FLIM, especially when combined with deep imaging technologies, shows promise as a method to assess bacterial metabolism in sputum and eventually directly in the airways (220). We

sought to visualize *P. aeruginosa* utilization of pyocyanin, a redox active molecule that can be used as an alternative electron accepter in low oxygen (165). We took the first step in developing a tool that can unmix multiple fluorescent metabolites from FLIM and hyperspectral images. The unmixing process can measure reduced pyocyanin, which has a fluorescence lifetime and spectral modulation unique from NADH and pyoverdine. Future directions will be to expand this approach to unmix NADH, pyoverdine, and other phenazines. In the next few paragraphs, I discuss future directions for improving our FLIM unmixing approach.

1: A priori identification of fluorescence lifetime species

FLIM has been extensively used in eukaryotes to measure relative abundances of fluorescent metabolites (174, 192, 192, 195, 221, 222) but there have been few published applications in microbes (172, 173). To calculate the contribution or shift in the fluorescence lifetime of one species in a complex system, all pure components potentially contributing to that signal must be characterized. A perfect model of the system will incorporate all fluorescent species, including variations in the lifetime that may arise from local conditions. Accounting for changes in the lifetime of NADH alone is complicated. The fluorescence lifetime of NADH varies depending on the enzyme it is bound to and other local factors such as pH (180). We, along with others (172, 173), found that bacteria do not always fall on the phasor trajectory connecting free NADH to enzyme-bound NADH observed in many eukaryotic FLIM studies. The shift from the classical NADH trajectory is likely due to the different and diverse enzymes produced by bacteria but may also arise

from the presence of other fluorophores in the sample, as was the case with our *P. aeruginosa* cultures. Blind unmixing approaches can guide the search for the number of contributing fluorophores. Further characterization of the individual molecular components contributing to the fluorescence in sample is necessary to answer biological questions about the dynamics of those fluorescent compounds in a system.

2: Incorporation of wider spectral ranges and characterization of additional fluorophores, including phenazine-1-carboxylic acid and phenazine-1-carboxamide

We did not obtain fluorescence spectra of other *P. aeruginosa* phenazines, such as phenazine-1-carboxylic acid (PCA) and phenazine-1-carboxamide (PCN). The one and two-photon excitation fluorescence spectra of these phenazines were described by Sullivan *et al.* (169) and suggested we were not capturing the emission of these phenazines with our DIVER FLIM emission filter (400-500 nm). The resolution and accuracy of the hyperspectral imaging unmixing routine can be improved by incorporating a wider spectral window. Although the hyperspectral microscope we used is capable of detecting emission ranges from ~400-700 nm, we decided to incorporate a narrower window consistent with the DIVER and LSM-880 FLIM acquisition settings. It is possible to acquire FLIM on the DIVER with a bandpass filter for visible light (meaning a broad range of light ~350-650 nm can pass through to the detector). However, acquiring a broader emission window with either spectral or FLIM systems will require characterization of additional compounds fluorescing at those ranges, including additional phenazines.

3. Incorporation of additional harmonics in the unmixing process

Sampling additional frequencies increases the accuracy of the Fourier series approximation from the FLIM and hyperspectral data, which can improve specificity for unmixing fluorophores (179). However, addition of harmonics also increase noise, and implementation of higher harmonics into unmixing processes will require higher resolution instruments.

4: Deep hyperspectral imaging on the DIVER

Dvornikov and Gratton (223) implemented cosine-sine shaped optical filters that act as single-harmonic spectral phasor transforms into the DIVER and can be used to resolve spectra in a highly-scattering matrix and collagen in mouse bone (170). The cosine-sine filters could be used to acquire time-resolved spectral information throughout biofilms and sputum, and when paired with FLIM analysis will be a powerful approach for resolving bacterial community structure and activity.

5: Incorporation of quantum yields into the model

The FLIM phasor transformation provides a fit-free method to visualize the fluorescence lifetime of the pixels in an image. The position of a signal in the phasor plot depends on the fluorescence intensity of contributing components, which means the predicted fractional contributions are proportional to the fluorophore concentration. However, each fluorophore species can have a different quantum yield. In order to

calculate the fluorophore concentration, the quantum yields of each fluorophore must be determined and incorporated into the interpretation of the unmixing model results.

Future directions in CF microbiome studies

We measured antibiotics in 171 longitudinal sputum samples from 11 individuals with CF using two LC-MS assays and found that the detection rates did not align with subject reported usage, likely due to antibiotic pharmacokinetics. Notably, azithromycin, which has a long half-life (68, 205), was detected in samples up to 8 days after a subject stopped usage. In preliminary analyses, the concentrations of orally-administered azithromycin correlated with the individual and with microbiome diversity (data not shown). In addition, individuals with higher concentrations of azithromycin repeatedly measured also had lower levels of anaerobes in their sputum. There are many factors that could explain why sputum concentrations of azithromycin were subject-specific, including differences in *in vivo* drug delivery and disease severity among subjects in the study cohort. The next goal is to unravel this complex relationship between patient health, the microbiome, and antibacterial efficacy. Are higher levels of antibiotics in sputum actually driving changes in microbiome, or is this observed correlation arising from the individualistic nature of CF and drug delivery?

Appendix A: DNA Extraction Method

Method: DNA extraction from human saliva and sputum

Purpose: to lyse human cells with hypotonic lysis (water) and remove human DNA and extracellular DNA (such as from biofilms)

This method was adapted from Nelson *et al.* (224)

<https://www.sciencedirect.com/science/article/pii/S2211124719301287>

Modified version of “benzonase 2” extraction protocol

Materials:

- Benzonase (Sigma E-1014), endonuclease enzyme in aqueous glycerol, stored in -20 freezer. KEEP ON ICE OR IN ICE BLOCK AT ALL TIMES

All other materials should be stored in BSL-2 room shelves:

- Sterile (filtered) 10X Benzonase buffer (200 mM Tris-HCl, 10 mM MgCl₂)
 - How to make 150 mL of 10X Buffer:
Pipette 60 mL of 500 mM Tris-HCl stock, 88.5 mL of UPW, and 1.5 mL of 1M MgCl₂ stock into bottle
Filter sterilize
- Sterile (filtered) 100 mM EDTA
- Sterile (filtered or autoclaved) 1X PBS
- 1M NaCl (filtered)
- 1X TE

Steps (~4h total)

1. Thaw sputum at room temp for a few minutes
2. Transfer 200 µL of the sputum into 2 mL tubes (if not aliquoted already)
3. Add 1 mL of DI Water. Incubate at room temp for 1h with “gentle agitation” (use shaking platform, low speed; platform has “DNA” written in Sharpie on speed meter).
4. Add 0.12 mL of 10X Benzonase Buffer and 1 uL of Benzonase stock (final concentration of 250U Benzonase; can make a M.M. here!). KEEP Benzonase enzyme on ICE BLOCK. Avoid taking it out of freezer prematurely.
5. Incubate sample at 37 C for 2h with gentle agitation (in warm room, use shaking platform, put box over)
6. Pellet the bacteria by centrifuging at 8,000 g for 10 minutes in BSL-2 room

7. Remove and discard supernatant (or save for virome)
 8. Pipette ~1.5 mL of 1x PBS for wash.
 9. Pellet again by centrifuging at 8,000 g for 10 minutes in BSL-2 room
 10. Remove and discard supernatant
- ** Safe step to stop, and store pellet in -20 freezer****

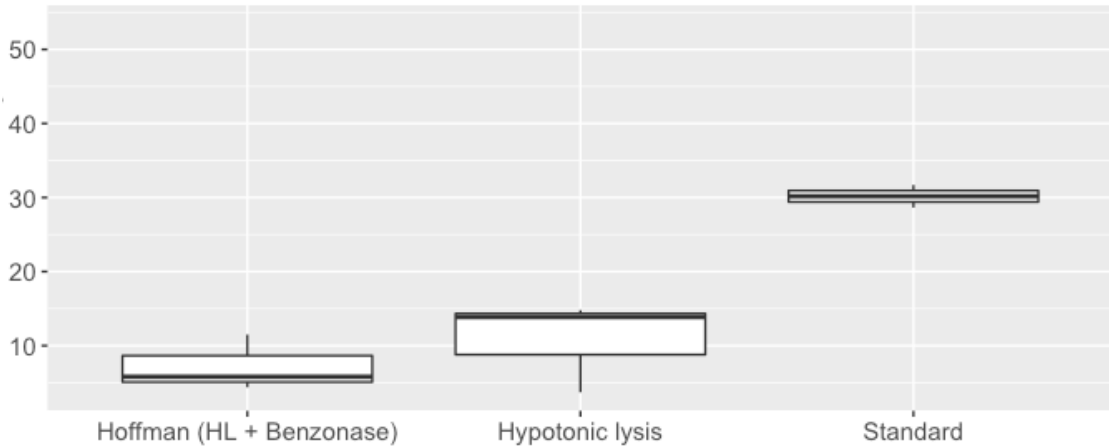
11. Suspend the pellet in 250 μ L of TE
12. Add 12.5 μ L of 100 mM EDTA and 40 μ L of 1M NaC (can make a M.M. here!) l, Vortex. (inactivates endonuclease)
13. Proceed to standard DNA extraction (Hoffman did phenol chloroform extraction), but we use zymo microbiome kits if high enough yield

Purpose of zymo DNA extraction kit: to lyse bacteria, fungi, and phage, and extract the intracellular DNA

The protocol steps are below. Here is a link to the full product info:

https://files.zymoresearch.com/protocols/_d4301_d4305_zymobiomics_dna_microprep_kit.pdf

Results:



With saliva from a healthy human, the percent of DNA sequencing reads that aligned to the human genome decreased from 30% using standard methods (ZYMO kit) to 8% with the benzoate two approach (N=3 saliva samples).

Appendix B: A tutorial on using UCI HPC to assemble and analyze genomes from wound isolates

Contributors: Josh Fong, Christina Kim, many others in the Whiteson Lab

**This is a work in progress. We update the tutorial and include example datasets here:
<https://github.com/tgallagh/UndergradStuff>*

Resources

- Google
- In person classes offered by UCI Data Science Initiative:
<http://datascience.uci.edu/education/short-courses/>
- Forum and discussion boards: <https://stackoverflow.com/>
- Dr. Rob Edwards metagenomics workshop manual:
<https://edwards.sdsu.edu/SDSU2017/WorkshopManual.pdf>
- Edwards lab blog: <https://edwards.sdsu.edu/research/category/lab-blog/>
- Beginners guide to comparative bacterial genome analysis:
<https://microbialinformaticsj.biomedcentral.com/articles/10.1186/2042-5783-3-2>
- Dr. Kevin Thornton github for advanced informatics class:
<https://github.com/ThorntonLab/AdvancedInformatics2017>

Requesting an HPC Account

Instructions here: <http://hpc-trac.oit.uci.edu/wiki/HowTo/Signup>

Make sure to indicate you are part of Dr. Katrine Whiteson's group and a biological sciences student.

HPC Tutorial

Read through and follow tutorial here: https://hpc.oit.uci.edu/HPC_USER_HOWTO.html

How to connect

Working on the HPC

Read through: <https://github.com/ThorntonLab/biocluster>

After reading through all the dense stuff, check out Prof. Thornton's HPC "cheat sheet":
<https://github.com/ThorntonLab/AdvancedInformatics2017/blob/master/materials/HPC.md>

Starting the *P. aeruginosa* Bacterial Genomes Analysis

- **Bioinformatics Tip 1: Keep your notes and data organized!**

There are multiple electronic notebooks you can use to save notes and scripts you write for bioinformatics project. I like github. You don't need to worry about learning github for now, but if you continue doing bioinformatics analyses, I would recommend learning it. Here is a great tutorial on using github from Prof. Kevin Thornton:

<https://github.com/ThorntonLab/intro2github>

In addition to documenting what you are doing with an electronic notebook, you want to make sure you are well-organized for a number of reasons:

- (1) In this day and age, bioinformatics data is becoming mainstream in biology journals. If you publish a bioinformatics project, the journal will most likely ask for scripts or code you used for your project. Having a well-organized project directory will make it much easier to find and share these scripts.
- (2) To make redoing an analysis or reusing scripts from a project easier!
- (3) so that your collaborator won't get lost in a sea of messy data and scripts if you end up doing a collaborative bioinformatics project

So before we even get started on the *P. aeruginosa* project, we are going to make a nice parent directory for your project filled with empty subdirectories.

- **Make an empty, well-organized project directory using a pre-written bash script**

From here on out, I am assuming you read through the linux tutorial and are somewhat familiar with unix commands. If you have no idea what is going on, reread the linux chapter.

When you initially log into the HPC, you are connected to a "login node". The function of these nodes are to let people into the HPC, so avoid doing any computationally intensive work in them. Request a "compute" node with the command:

`qrsh`

Then, do the following:

1. *cd* into my directory: /dfs3/bio/tgallagh/GenomicsTutorial/code/scripts
2. *ls* to see what files are there
3. copy (*scp*) the “create_project.sh” file into your /dfs3/bio/<USERNAME> directory

*Note, anytime you see “<>” this signifies user input

Next, we are going to run the “create_project.sh” script. This script was written by Prof. JJ Emerson, it basically sets up an empty shell of nicely named directories for the user.

After *cd-ing* into your /dfs3/bio/<USERNAME> directory, if you enter “bash create_project.sh” into the commandline, the usage of this script should appear:

```
[tgallagh@compute-1-13 scripts]$ bash create_project.sh
```

usage: create_project.sh name path

We need to give the bash script a directory name and path to where you want the directory to be located. For example, if I want to make a new project directory named “Cheetos” in my /bio/tgallagh folder:

```
[tgallagh@compute-1-13 scripts]$ bash create_project.sh Cheetos /dfs5/bio/tgallagh
```

Project Cheetos created at /dfs3/bio/tgallagh.

As you look throughout your new project directory and subdirectories, you’ll notice each subdirectory has an empty “README.md” files. These files are great for putting notes for yourself or potentially other users.

There are a couple of different linux text editors you can use to make edits to text files. I like using “vim” but it takes some getting used to... definitely not as intuitive as microsoft word, and you can only use your keyboard to edit and save!

<http://www.vim.org/about.php>.

- **Copy the raw sequencing data into your directory**

Background information on the sequencing data:

This sequencing data you will be working with in this tutorial consists of DNA from 4 *Pseudomonas aeruginosa* strains. Specifically, the names of the strains are *P. aeruginosa* FLR01 (sometimes nicknamed “P1” in our lab) and 3 “substrains” of *P. aeruginosa* PA14 (all derived from different labs: Dorrestein, Siryaporn, Hochbaum). FLR01 was isolated from cystic fibrosis sputum. The other 3 substrains are basically the same lab strain of *P. aeruginosa* that have been passaged in other labs, and we want to see if there are any noticeable genome changes as these 3 substrains adapted to different lab environments.

To see the data, first “cd” into my directory:

```
cd /dfs3/bio/tgallagh/GenomicsTutorial/data/raw
```

And then “ls” to see what is in there:

```
[tgallagh@compute-1-13 raw]$ ls
```

```
PA14_Dorresteин.read1.fastq.gz  
PA14_Hochbaum.read2.fastq.gz  
PAnmFLR01_S10_L001_R1_001.fastq  
PA14_Dorresteин.read2.fastq.gz  
PA14_Siryaporn.read1.fastq.gz  
PAnmFLR01_S10_L001_R2_001.fastq  
PA14_Hochbaum.read1.fastq.gz  
PA14_Siryaporn.read2.fastq.gz  
README.md
```

The most common sequencing file formats you will probably encounter are “.fastq” or “.fastq.gz” (compressed fastq) and “.fasta.” Sometimes this file extensions are shortened to “.fq”, “.fa”, “.fna”, etc. To read about fastq files:

https://en.wikipedia.org/wiki/FASTQ_format

Use the *scp* command to copy all 8 fastq files from my directory into your new project directory. I would recommend copying these new files into your “raw” data directory, e.g. /bio/<USER>/<PROJECTNAME>/data/raw

Some bioinformatics programs do not allow you to use compressed (.gz or .zip) files as input, so you can unzip the 6 “PA14” files:

```
gunzip PA14*
```

Note: that asterisk is a wildcard. It basically tells linux to replace the asterisk with any character, number, whitespace, etc. So it lets us unzip all 6 files that begin with “PA14” at once. Be careful when you are using wildcards! You can easily make mistakes, like unintentionally delete certain files.

This sequencing data is illumina paired end sequencing data, so we have two reads per sequenced DNA fragment. Let’s look at the first ten lines of one of the uncompressed files:

```
[tgallagh@compute-1-13 raw]$ head -10 PAnmFLR01_S10_L001_R1_001.fastq
```

```
@M00285:18:000000000-A611E:1:1101:9210:1117 1:N:0:10
```

```
CCACGAAGAACAGCATCGAGCCNAAGGTCTGGCCAGGATGAATATATTGATGGAGCTGATGTGGAG  
+  
CCCCCGGGGGGGGGGGCGGGG#:CFGFGGGGGGGGGGGGGAGFGFGGGGGGGGGGGGGGGGGGGGGGGGG  
@M00285:18:000000000-A611E:1:1101:19487:1117 1:N:0:10  
GTACAAGGCGGTGCCGCACGCGCTGGTCTACATGCACCCGGAGGATGCGCAGCTCAAGCTGCGCCGCGCAGCGA  
GGTCAAGGNGNNNNNNNNNNNNNGANNNNCGCGCGGGTCGAGACCCGCGGGCGAACAAAGCCGCCAGGG
```

```

GCTGGTGGTGTGCCGTTCTCGACGCCAACAGCTGATCACCAAGTACACCCTGGACGCCACCGACCCGATTCCAA
GCAGACCGACTACAAGAAGTTCGCCGCTGCCACGAACCTGCTCAACCTGGCCTGAAGAG
+
CCCCCGDGGGC@FEDFD@F@FCFEEGDGFFGGGDGCDFGGFECGGG7FFGGGGGFFEGGGFG@FGGGGEGGGG
>FFGGGGGF#:######+#+#+#+#::@<7C@B1><FGGDGCCFFECCB88>EE*,65CEE58?E8E58C*A>F
EC5@EGCEGDCGEFFF*;=8CEG58CCFFGGC9C*AFGF++0<?C*:7CFDGG<DFDDDECD)05.?>*<5>?D7>>D5B
F6=*7<6**1.>D5471).)(.)40,(.6)).5(4(.).3581).60

```

```

@M00285:18:000000000-A611E:1:1101:9237:1117 1:N:0:10
GCCGAGGCCAGGCCAAGGTTNGGAGGCCTGCACCGCAACTCGCGAGGTCGACCCGAATCGGCTGCGCGTATC
CACCNAANNNNNNNNNNNNNNNNNNNGCNNNCGCTCGAGGTGTATGCCCTCGCGGGGTGTCGATGAGCGACCTG
CGTCGCCGCAAAGCGCTGAAAAGGCGGATTTGCTGCGTCAGGCGGAATCAATTGCCGTATACTGTCGCGCAGCTG
GCGATTGGTCCCAGCGGCCAAGATTGCAGACGCGGATTGCGCAGCGTTTCGCCACGTGCCGAA

```

- Quality filtering the reads and assembling the filtered data into genomes**

We will first quality filter the sequencing data using a program called “trimmomatic”. Then, we will assemble the filtered reads into the genomes of the 4 strains using a bioinformatics tool called “spades.” You can either run the “trimmomatic” and “spades” programs in an Interactive node, which allows you to watch any output from the programs in real time in your shell. Or, a safer and typically more efficient option, is to write a batch of code and submit it to the HPC task scheduler to run on a compute node.

Before getting started, review the rules for running jobs on the HPC here:
<https://hpc.oit.uci.edu/running-jobs>

We already have a skeleton script which contains most of the code needed to run the sequencing files through trimmomatic and then spades.

- First, copy the script into your own scripts directory. You already learned how to copy files. Here is the full file path to the script: *w*
- After copying the scripts file into your own directory, look at the contents of the file using “cat” to print it to your screen or the text editor “vim”.

\$ vim filter_spades.sh

And you’ll see the script:

```

#!/bin/bash
## -N filterspadesPA14
## -q free64,pub64,bio

```

```

#\$ -m e
#\$ -ckpt restart

#####
##### USER MUST PROVIDE THEIR INPUT HERE:
BASE_DIR=<FULL PATH TO THE DIRECTORY WITH YOUR SEQ READS>
# e.g: BASE_DIR=/dfs3/bio/tgallagh/GenomicsTutorial/data/raw/
#####

cd $BASE_DIR
## Use trimmomatic to quality filter sequencing reads
#make a new directory to put all the quality filtered reads
mkdir qualityfiltered

# make variable with path to output directory
TRIMMED=${BASE_DIR}/qualityfiltered/

# load modules
module load trimmomatic/0.35
module load SPAdes/3.8.2

java -jar /data/apps/trimmomatic/0.35/trimmomatic-0.35.jar PE -phred33
PA14_Dorrestein.read1.fastq
PA14_Dorrestein.read2.fastq $TRIMMED\PA14_Dorrestein.paired.read1.fastq
$TRIMMED\PA14_Dorrestein.unpaired.read1.fastq
$TRIMMED\PA14_Dorrestein.paired.read2.fastq
$TRIMMED\PA14_Dorrestein.read2.fastq ILLUMINACLIP:/dfs3/bio/tgallagh/alladaptors.fa:
2:30:10 LEADING:25 TRAILING:25 SLIDINGWINDOW:4:20 MINLEN:50

java -jar /data/apps/trimmomatic/0.35/trimmomatic-0.35.jar PE -
phred33 PA14_Hochbaum.read1.fastq PA14_Hochbaum.read2.fastq $TRIMMED\PA14_Hoc
hbaum.paired.read1.fastq $TRIMMED\PA14_Hochbaum.unpaired.read1.fastq
$TRIMMED\PA14_Hochbaum.paired.read2.fastq
$TRIMMED\PA14_Hochbaum.unpaired.read2.fastq ILLUMINACLIP:/dfs3/bio/tgallagh/alla
daptors.fa:2:30:10 LEADING:25 TRAILING:25 SLIDINGWINDOW:4:20 MINLEN:50

java -jar /data/apps/trimmomatic/0.35/trimmomatic-0.35.jar PE -phred33
PA14_Siryaporn.read1.fastq PA14_Siryaporn.read2.fastq
$TRIMMED\PA14_Siryaporn.paired.read1.fastq
$TRIMMED\PA14_Siryaporn.unpaired.read1.fastq
$TRIMMED\PA14_Siryaporn.paired.read2.fastq
$TRIMMED\PA14_Siryaporn.unpaired.read2.fastq ILLUMINACLIP:/dfs3/bio/tgallagh/allad
aptors.fa:2:30:10 LEADING:25 TRAILING:25 SLIDINGWINDOW:4:20 MINLEN:50

java -jar /data/apps/trimmomatic/0.35/trimmomatic-0.35.jar PE -phred33
PAnmFLR01_S10_L001_R1_001.fastq PAnmFLR01_S10_L001_R2_001.fastq
$TRIMMED\PAnmFLR01.paired.read1.fastq $TRIMMED\PAnmFLR01.unpaired.read1.fastq
$TRIMMED\PAnmFLR01.paired.read2.fastq
$TRIMMED\PAnmFLR01.unpaired.read2.fastq ILLUMINACLIP:/dfs3/bio/tgalla
gh/alladaptors.fa:2:30:10 LEADING:25 TRAILING:25 SLIDINGWINDOW:4:20 MINLEN:50

```

```

# assemble the quality filtered reads with SPAdes
mkdir spades
$SPADES=${BASE_DIR}/spades/
spades.py --pe1-1 $TRIMMED\PA14_Dorrestein.paired.read1.fastq --pe1-2
$TRIMMED\PA14_Dorrestein.paired.read2.fastq -o $SPADES\PA14_Dorrestein
spades.py --pe1-1 $TRIMMED\PA14_Hochbaum.paired.read1.fastq --pe1-2
$TRIMMED\PA14_Hochbaum.paired.read2.fastq -o $SPADES\PA14_Hochbaum
spades.py --pe1-1 $TRIMMED\PA14_Siryaporn.paired.read1.fastq --pe1-2
$TRIMMED\PA14_Siryaporn.paired.read2.fastq -o $SPADES\PA14_Siryaporn
spades.py --pe1-1 $TRIMMED\PAnmFLR01.paired.read1.fastq --pe1-2
$TRIMMED\PAnmFLR01.paired.read2.fastq -o $SPADES\PAnmFLR01

```

Note at the top, the script has a bunch of comments (lines starting with “#”, meaning the computer won’t run it).

In order to get the script to run and work with the data in your directory, you need to copy the full path of your directory. There is an example right below (with a comment so the computer doesn’t run it). To edit the file, use “vim” and type in “i” to go into “insert” mode. You can now use your keyboard to edit the file. When you are done editing, hit escape and type in “wq” to save the edits and quit vim.

You can now submit the script to the HPC task scheduler to run on a compute node. You do this with the “qsub” command. For example:

```
$ qsub filter_spades.sh
```

You can check the status of your run by typing:

```
qstat -u <INPUT your username>
```

for example, to see all of my current running jobs:

```
$ qstat -u tgallagh
```

job-ID	prior	name	user	state	submit/start at	queue	slots	ja-task-ID
1493082	0.50010	QRLOGIN	tgallagh	r	01/29/2020 12:31:04	interactive@hpc-interactive-1-		1
1493094	0.50007	filterspad	tgallagh	r	01/29/2020 12:48:14	pub64@compute-7-6.local		1

which prints information about the running jobs, including the job ID (first number) and the job start time. The ‘r’ indicates the job is currently running. If the job has been submitted and is in the queue to run, you will see a ‘qw’

If it takes only a minute or less to “run” your job, it’s likely there is an error in your script!

In which case, you will need to fix the bug in your script. You can start by going to the directory where your script is saved and typing ‘ls’. You should see two new files:

- <your job name>.e<your job ID>
- <your job name>.o<your job ID>

For example, in my project directory:

```
$ cd /dfs3/bio/tgallagh/GenomicsTutorial/code/scripts/
$ ls -l
-rwxr-xr-x 1 tgallagh bio      1766 Jul 17 2017 create_project.sh
-rw-r--r-- 1 tgallagh tgallagh 5616 Jan 29 12:54 filterspadesPA14.e1493094
-rw-r--r-- 1 tgallagh tgallagh 12526 Jan 29 13:31 filterspadesPA14.o1493094
-rw-r--r-- 1 tgallagh bio      2944 Jan 29 13:31 filter_spades.sh
-rw-r--r-- 1 tgallagh bio      0 Jul 17 2017 README.md
```

To read any “errors” from my job, I will use cat or vim to look at the error output file.

```
$ cat filterspadesPA14.e1493094
```

Another way to determine if your script ran properly is to simply look in the directories where you expect to see your output and check to see if the files are OK. The script tells spades to save the output in BASE_DIR/spades. So check the files in your project directory to see if they’re there and not empty (can use ls -l to check file size).

/dfs3/bio/tgallagh/genomes_wound/filenames.txt

Running job arrays:

Job arrays:

https://github.com/tgallagh/UndergradStuff/blob/master/Linux/PE_jobarray.md

- make change to t line--->tells how many files there are
- input--->assigns task ID 1-39 for the job, specifically going to make a file a list of all the files--->orders 1-39--->assigns task ID number to each file
- make a file name with with only the prefix for 39 files
- to escape a file---->Vim [file name]
- \$SPADES\$input--->to create new directory

- **PATRIC to annotate genomes and compare genomes**

URL to PATRIC :<https://www.patricbrc.org/>

Make an account and upload your assembled genomes

Annotating a genome: <https://www.patricbrc.org/public/pdfs/Workshop-Genome-Annotation.pdf>

REFERENCES:

1. Tate S, MacGregor G, Davis M, Innes JA, Greening AP. 2002. Airways in cystic fibrosis are acidified: detection by exhaled breath condensate. *Thorax* 57:926–929.
2. Bensel T, Stotz M, Borneff-Lipp M, Wollschläger B, Wienke A, Taccetti G, Campana S, Meyer KC, Jensen PØ, Lechner U, Ulrich M, Döring G, Worlitzsch D. 2011. Lactate in cystic fibrosis sputum. *J Cyst Fibros* 10:37–44.
3. Whiteson KL, Meinardi S, Lim YW, Schmieder R, Maughan H, Quinn R, Blake DR, Conrad D, Rohwer F. 2014. Breath gas metabolites and bacterial metagenomes from cystic fibrosis airways indicate active pH neutral 2,3-butanedione fermentation. *ISME J* 8:1247–1258.
4. Cowley ES, Kopf SH, LaRiviere A, Ziebis W, Newman DK. 2015. Pediatric cystic fibrosis sputum can be chemically dynamic, anoxic, and extremely reduced due to hydrogen sulfide formation. *mBio* 6:e00767-15.
5. Cystic Fibrosis Foundation. 2015 Patient Registry Annual Data Report.
6. Knowles MR, Stutts MJ, Spock A, Fischer N, Gatzky JT, Boucher RC. 1983. Abnormal ion permeation through cystic fibrosis respiratory epithelium. *Science* 221:1067–1070.
7. Quinton PM. 1983. Chloride impermeability in cystic fibrosis. *Nature* 301:421–422.
8. Lyczak JB, Cannon CL, Pier GB. 2002. Lung Infections Associated with Cystic Fibrosis. *Clin Microbiol Rev* 15:194–222.

9. Carmody LA, Caverly LJ, Foster BK, Rogers M a. M, Kalikin LM, Simon RH, VanDevanter DR, LiPuma JJ. 2018. Fluctuations in airway bacterial communities associated with clinical states and disease stages in cystic fibrosis. *PLoS One* 13:e0194060–e0194060.
10. Carmody LA, Zhao J, Kalikin LM, LeBar W, Simon RH, Venkataraman A, Schmidt TM, Abdo Z, Schloss PD, LiPuma JJ. 2015. The daily dynamics of cystic fibrosis airway microbiota during clinical stability and at exacerbation. *Microbiome* 3:12.
11. Quinn RA, Whiteson K, Lim YW, Zhao J, Conrad D, LiPuma JJ, Rohwer F, Widder S. 2016. Ecological networking of cystic fibrosis lung infections. *Npj Biofilms Microbiomes* 2:4.
12. Quinn RA, Lim YW, Maughan H, Conrad D, Rohwer F, Whiteson KL. 2014. Biogeochemical Forces Shape the Composition and Physiology of Polymicrobial Communities in the Cystic Fibrosis Lung. *mBio* 5:e00956-13.
13. Coburn B, Wang PW, Caballero JD, Clark ST, Brahma V, Donaldson S, Zhang Y, Surendra A, Gong Y, Tullis DE, Yau YCW, Waters VJ, Hwang DM, Guttman DS. 2015. Lung microbiota across age and disease stage in cystic fibrosis. *Sci Rep* 5:10241.
14. Rubin JL, Thayer S, Watkins A, Wagener JS, Hodgkins PS, Schechter MS. 2017. Frequency and costs of pulmonary exacerbations in patients with cystic fibrosis in the United States. *Curr Med Res Opin* 33:667–674.

15. Sanders DB, Bittner RCL, Rosenfeld M, Hoffman LR, Redding GJ, Goss CH. 2010. Failure to Recover to Baseline Pulmonary Function after Cystic Fibrosis Pulmonary Exacerbation. *Am J Respir Crit Care Med* 182:627–632.
16. Neubauer C, Kasi AS, Grahl N, Sessions AL, Kopf SH, Kato R, Hogan DA, Newman DK. 2018. Refining the Application of Microbial Lipids as Tracers of *Staphylococcus aureus* Growth Rates in Cystic Fibrosis Sputum. *J Bacteriol* 200.
17. Gallagher T, Phan J, Whiteson K. 2018. Getting Our Fingers on the Pulse of Slow-Growing Bacteria in Hard-To-Reach Places. *J Bacteriol* 200.
18. Stressmann FA, Rogers GB, Gast CJ van der, Marsh P, Vermeer LS, Carroll MP, Hoffman L, Daniels TWV, Patel N, Forbes B, Bruce KD. 2012. Long-term cultivation-independent microbial diversity analysis demonstrates that bacterial communities infecting the adult cystic fibrosis lung show stability and resilience. *Thorax* 67:867–873.
19. Lam JC, Somayaji R, Surette MG, Rabin HR, Parkins MD. 2015. Reduction in *Pseudomonas aeruginosa* sputum density during a cystic fibrosis pulmonary exacerbation does not predict clinical response. *BMC Infect Dis* 15:145.
20. Stressmann FA, Rogers GB, Marsh P, Lilley AK, Daniels TWV, Carroll MP, Hoffman LR, Jones G, Allen CE, Patel N, Forbes B, Tuck A, Bruce KD. 2011. Does bacterial density in cystic fibrosis sputum increase prior to pulmonary exacerbation? *J Cyst Fibros* 10:357–365.

21. Whiteson KL, Bailey B, Bergkessel M, Conrad D, Delhaes L, Felts B, Harris JK, Hunter R, Lim YW, Maughan H, Quinn R, Salamon P, Sullivan J, Wagner BD, Rainey PB. 2014. The upper respiratory tract as a microbial source for pulmonary infections in cystic fibrosis. Parallels from island biogeography. *Am J Respir Crit Care Med* 189:1309–1315.
22. Carmody LA, Zhao J, Schloss PD, Petrosino JF, Murray S, Young VB, Li JZ, LiPuma JJ. 2013. Changes in cystic fibrosis airway microbiota at pulmonary exacerbation. *Ann Am Thorac Soc* 10:179–187.
23. Caverly LJ, LiPuma JJ. 2018. Cystic fibrosis respiratory microbiota: unraveling complexity to inform clinical practice. *Expert Rev Respir Med* 0:1–9.
24. Twomey KB, Alston M, An S-Q, O'Connell OJ, McCarthy Y, Swarbreck D, Febrer M, Dow JM, Plant BJ, Ryan RP. 2013. Microbiota and Metabolite Profiling Reveal Specific Alterations in Bacterial Community Structure and Environment in the Cystic Fibrosis Airway during Exacerbation. *PLOS ONE* 8:e82432.
25. Caverly LJ, LiPuma JJ. 2018. Good cop, bad cop: anaerobes in cystic fibrosis airways. *Eur Respiratory Soc.*
26. Bergkessel M, Basta DW, Newman DK. 2016. The physiology of growth arrest: uniting molecular and environmental microbiology. *Nat Rev Microbiol* 14:549–562.

27. Lagier J-C, Edouard S, Pagnier I, Mediannikov O, Drancourt M, Raoult D. 2015. Current and past strategies for bacterial culture in clinical microbiology. *Clin Microbiol Rev* 28:208–236.
28. Lim YW, Haynes M, Furlan M, Robertson CE, Harris JK, Rohwer F. 2014. Purifying the Impure: Sequencing Metagenomes and Metatranscriptomes from Complex Animal-associated Samples. *J Vis Exp JoVE*.
29. Whitchurch CB, Tolker-Nielsen T, Ragas PC, Mattick JS. 2002. Extracellular DNA Required for Bacterial Biofilm Formation. *Science* 295:1487–1487.
30. Wilkinson DJ. 2018. Historical and contemporary stable isotope tracer approaches to studying mammalian protein metabolism. *Mass Spectrom Rev* 37:57–80.
31. Schoenheimer R, Rittenberg D. 1935. Deuterium as an Indicator in the Study of Intermediary Metabolism. *Science* 82:156–157.
32. Radajewski S, Ineson P, Parekh NR, Murrell JC. 2000. Stable-isotope probing as a tool in microbial ecology. *Nature* 403:646–649.
33. McLean JS, Fansler SJ, Majors PD, McAtee K, Allen LZ, Shirtliff ME, Lux R, Shi W. 2012. Identifying Low pH Active and Lactate-Utilizing Taxa within Oral Microbiome Communities from Healthy Children Using Stable Isotope Probing Techniques. *PLOS ONE* 7:e32219.
34. Atherton JC, Spiller RC. 1994. The urea breath test for *Helicobacter pylori*. *Gut* 35:723–725.

35. Wikoff WR, Anfora AT, Liu J, Schultz PG, Lesley SA, Peters EC, Siuzdak G. 2009. Metabolomics analysis reveals large effects of gut microflora on mammalian blood metabolites. *Proc Natl Acad Sci U S A* 106:3698–3703.
36. Aksenov AA, Silva R da, Knight R, Lopes NP, Dorrestein PC. 2017. Global chemical analysis of biology by mass spectrometry. *Nat Rev Chem* 1:0054.
37. Dorrestein PC, Mazmanian SK, Knight R. 2014. Finding the missing links among metabolites, microbes, and the host. *Immunity* 40:824–832.
38. Patterson AD, Turnbaugh PJ. 2014. Microbial determinants of biochemical individuality and their impact on toxicology and pharmacology. *Cell Metab* 20:761–768.
39. Berry D, Loy A. 2018. Stable-Isotope Probing of Human and Animal Microbiome Function. *Trends Microbiol*.
40. Palmer KL, Mashburn LM, Singh PK, Whiteley M. 2005. Cystic fibrosis sputum supports growth and cues key aspects of *Pseudomonas aeruginosa* physiology. *J Bacteriol* 187:5267–5277.
41. Basta DW, Bergkessel M, Newman DK. 2017. Identification of Fitness Determinants during Energy-Limited Growth Arrest in *Pseudomonas aeruginosa*. *mBio* 8:e01170-17.

42. Sagel SD, Wagner BD, Anthony MM, Emmett P, Zemanick ET. 2012. Sputum biomarkers of inflammation and lung function decline in children with cystic fibrosis. *Am J Respir Crit Care Med* 186:857–865.
43. Phan J, Gallagher T, Oliver A, England WE, Whiteson K. 2018. Fermentation products in the cystic fibrosis airways induce aggregation and dormancy-associated expression profiles in a CF clinical isolate of *Pseudomonas aeruginosa*. *FEMS Microbiol Lett* 365.
44. Chen AI, Dolben EF, Okegbe C, Harty CE, Golub Y, Thao S, Ha DG, Willger SD, O'Toole GA, Harwood CS, Dietrich LEP, Hogan DA. 2014. *Candida albicans* Ethanol Stimulates *Pseudomonas aeruginosa* WspR-Controlled Biofilm Formation as Part of a Cyclic Relationship Involving Phenazines. *PLOS Pathog* 10:e1004480.
45. Hunter RC, Klepac-Ceraj V, Lorenzi MM, Grotzinger H, Martin TR, Newman DK. 2012. Phenazine content in the cystic fibrosis respiratory tract negatively correlates with lung function and microbial complexity. *Am J Respir Cell Mol Biol* 47:738–745.
46. Flynn JM, Niccum D, Dunitz JM, Hunter RC. 2016. Evidence and Role for Bacterial Mucin Degradation in Cystic Fibrosis Airway Disease. *PLOS Pathog* 12:e1005846.
47. Sønderholm M, Kragh KN, Koren K, Jakobsen TH, Darch S, Alhede M, Jensen PØ, Whiteley M, Kühl M, Bjarnsholt T. 2017. Aggregate formation of *Pseudomonas aeruginosa* in an alginate bead model system exhibits in vivo like characteristics. *Appl Env Microbiol AEM*.00113-17.

48. Quinn RA, Whiteson K, Lim Y-W, Salamon P, Bailey B, Mienardi S, Sanchez SE, Blake D, Conrad D, Rohwer F. 2015. A Winogradsky-based culture system shows an association between microbial fermentation and cystic fibrosis exacerbation. *ISME J* 9:1024–1038.
49. Dickson RP, Huffnagle GB. 2015. The Lung Microbiome: New Principles for Respiratory Bacteriology in Health and Disease. *PLoS Pathog* 11.
50. Bos LD, Sterk PJ, Fowler SJ. 2016. Breathomics in the setting of asthma and chronic obstructive pulmonary disease. *J Allergy Clin Immunol* 138:970–976.
51. DePas WH, Starwalt-Lee R, Sambeek LV, Kumar SR, Grdinaru V, Newman DK. 2016. Exposing the Three-Dimensional Biogeography and Metabolic States of Pathogens in Cystic Fibrosis Sputum via Hydrogel Embedding, Clearing, and rRNA Labeling. *mBio* 7:e00796-16.
52. Welch JLM, Rossetti BJ, Rieken CW, Dewhurst FE, Borisy GG. 2016. Biogeography of a human oral microbiome at the micron scale. *Proc Natl Acad Sci* 113:E791–E800.
53. Kopf SH, Sessions AL, Cowley ES, Reyes C, Sambeek LV, Hu Y, Orphan VJ, Kato R, Newman DK. 2016. Trace incorporation of heavy water reveals slow and heterogeneous pathogen growth rates in cystic fibrosis sputum. *Proc Natl Acad Sci* 113:E110–E116.
54. Kopf SH, McGlynn SE, Green-Saxena A, Guan Y, Newman DK, Orphan VJ. 2015. Heavy water and ¹⁵N labelling with NanoSIMS analysis reveals growth rate-dependent metabolic heterogeneity in chemostats. *Environ Microbiol* 17:2542–2556.

55. Adamowicz EM, Hunter RC, Flynn J, Harcombe WR. 2018. Cross-feeding modulates antibiotic tolerance in bacterial communities. *bioRxiv* 243949.
56. Bacci G, Taccetti G, Dolce D, Armanini F, Segata N, Di Cesare F, Lucidi V, Fiscarelli E, Morelli P, Casciaro R. 2019. The personalized temporal dynamics of microbiome in the airways of cystic fibrosis patients. *bioRxiv* 609057.
57. Jorth P, Ehsan Z, Rezayat A, Caldwell E, Pope C, Brewington JJ, Goss CH, Benscoter D, Clancy JP, Singh PK. 2019. Direct lung sampling indicates that established pathogens dominate early infections in children with cystic fibrosis. *Cell Rep* 27:1190-1204.e3.
58. Heirali AA, Acosta N, Storey DG, Workentine ML, Somayaji R, Laforest-Lapointe I, Leung W, Quon BS, Berthiaume Y, Rabin HR, Waddell BJ, Rossi L, Surette MG, Parkins MD. 2019. The effects of cycled inhaled aztreonam on the cystic fibrosis (CF) lung microbiome. *J Cyst Fibros.*
59. Goddard AF, Staudinger BJ, Dowd SE, Joshi-Datar A, Wolcott RD, Aitken ML, Fligner CL, Singh PK. 2012. Direct sampling of cystic fibrosis lungs indicates that DNA-based analyses of upper-airway specimens can misrepresent lung microbiota. *Proc Natl Acad Sci* 109:13769–13774.
60. Fodor AA, Klem ER, Gilpin DF, Elborn JS, Boucher RC, Tunney MM, Wolfgang MC. 2012. The adult cystic fibrosis airway microbiota is stable over time and infection type, and highly resilient to antibiotic treatment of exacerbations. *PLOS ONE* 7:e45001.

61. Zhao J, Schloss PD, Kalikin LM, Carmody LA, Foster BK, Petrosino JF, Cavalcoli JD, VanDevanter DR, Murray S, Li JZ, Young VB, LiPuma JJ. 2012. Decade-long bacterial community dynamics in cystic fibrosis airways. *Proc Natl Acad Sci* 109:5809–5814.
62. Caverly LJ, Lu J, Carmody LA, Kalikin LM, Shedd K, Opron K, Azar M, Cahalan S, Foster B, VanDevanter DR, Simon RH, LiPuma JJ. 2019. Measures of cystic fibrosis airway microbiota during periods of clinical stability. *Ann Am Thorac Soc* 16:1534–1542.
63. Whelan FJ, Heirali AA, Rossi L, Rabin HR, Parkins MD, Surette MG. 2017. Longitudinal sampling of the lung microbiota in individuals with cystic fibrosis. *PLOS ONE* 12:e0172811.
64. Hahn A, Burrell A, Fanous H, Chaney H, Sami I, Perez GF, Koumbourlis AC, Freishtat RJ, Crandall KA. 2018. Antibiotic multidrug resistance in the cystic fibrosis airway microbiome is associated with decreased diversity. *Heliyon* 4.
65. Caverly LJ, Caverly TJ, Kalikin LM, Foster BK, Simon RH, LiPuma JJ. 2016. Episodic oral antibiotic use in CF: Discordance between the electronic medical record and self-report. *J Cyst Fibros* 15:630–633.
66. Autret E, Marchand S, Breteau M, Grenier B. 1986. Pharmacokinetics of amikacin in cystic fibrosis: a study of bronchial diffusion. *Eur J Clin Pharmacol* 31:79–83.

67. Lovering AM, Pycock CJ, Harvey JE, Reeves DS. 1990. The pharmacokinetics and sputum penetration of ampicillin and amoxycillin following simultaneous i.v. administration. *J Antimicrob Chemother* 25:385–392.
68. Jacobs RF, Maples HD, Aranda JV, Espinoza GM, Knirsch C, Chandra R, Fisher JM, Kearns GL. 2005. Pharmacokinetics of intravenously administered azithromycin in pediatric patients. *Pediatr Infect Dis J* 24:34.
69. Foulds G, Shepard RM, Johnson RB. 1990. The pharmacokinetics of azithromycin in human serum and tissues. *J Antimicrob Chemother* 25 Suppl A:73–82.
70. Vinks AA, van Rossem RN, Mathôt RAA, Heijerman HGM, Mouton JW. 2007. Pharmacokinetics of aztreonam in healthy subjects and patients with cystic fibrosis and evaluation of dose-exposure relationships using monte carlo simulation. *Antimicrob Agents Chemother* 51:3049–3055.
71. Gibson RL, Retsch-Bogart GZ, Oermann C, Milla C, Pilewski J, Daines C, Ahrens R, Leon K, Cohen M, McNamara S, Callahan TL, Markus R, Burns JL. 2006. Microbiology, safety, and pharmacokinetics of aztreonam lysinate for inhalation in patients with cystic fibrosis. *Pediatr Pulmonol* 41:656–665.
72. Arguedas AG, Stutman HR, Zaleska M, Knupp CA, Marks MI, Nussbaum E. 1992. Cefepime: pharmacokinetics and clinical response in patients With cystic fibrosis. *Am J Dis Child* 146:797–802.

73. Kercsmar CM, Stern RC, Reed MD, Myers CM, Murdell D, Blumer JL. 1983. Ceftazidime in cystic fibrosis: pharmacokinetics and therapeutic response. *J Antimicrob Chemother* 12:289–295.
74. Turner A, Pedler SJ, Carswell F, Spencer GR, Speller DCE. 1984. Serum and sputum concentrations of ceftazidime in patients with cystic fibrosis. *J Antimicrob Chemother* 14:521–527.
75. Michalsen H, Bergan T. 1982. Pharmacokinetics of antibiotics in children with cystic fibrosis with particular reference to netilmicin. *Acta Paediatr* 71:101–105.
76. Davis RL, Koup JR, Williams-Warren J, Weber A, Heggen L, Stempel D, Smith AL. 1987. Pharmacokinetics of ciprofloxacin in cystic fibrosis. *Antimicrob Agents Chemother* 31:915–919.
77. Li J, Coulthard K, Milne R, Nation RL, Conway S, Peckham D, Etherington C, Turnidge J. 2003. Steady-state pharmacokinetics of intravenous colistin methanesulphonate in patients with cystic fibrosis. *J Antimicrob Chemother* 52:987–992.
78. Ratjen F, Rietschel E, Kasel D, Schwierz R, Starke K, Beier H, van Koningsbruggen S, Grasemann H. 2006. Pharmacokinetics of inhaled colistin in patients with cystic fibrosis. *J Antimicrob Chemother* 57:306–311.
79. Lee CKK, Boyle MP, Diener-West M, Brass-Ernst L, Noschese M, Zeitlin PL. 2007. Levofloxacin pharmacokinetics in adult cystic fibrosis. *Chest* 131:796–802.

80. Chien SC, Rogge MC, Gisclon LG, Curtin C, Wong F, Natarajan J, Williams RR, Fowler CL, Cheung WK, Chow AT. 1997. Pharmacokinetic profile of levofloxacin following once-daily 500-milligram oral or intravenous doses. *Antimicrob Agents Chemother* 41:2256–2260.
81. Bosso JA, Flume PA, Gray SL. 2004. Linezolid pharmacokinetics in adult patients with cystic fibrosis. *Antimicrob Agents Chemother* 48:281–284.
82. Christensson BA, Ljungberg B, Eriksson L, Nilsson-Ehle I. 1998. Pharmacokinetics of meropenem in patients with cystic fibrosis. *Eur J Clin Microbiol Infect Dis* 17:873–876.
83. Hoogkamp-Korstanje JAA, van der Laag J. 1983. Piperacillin and tobramycin in the treatment of *Pseudomonas* lung infections in cystic fibrosis. *J Antimicrob Chemother* 12:175–183.
84. Reed MD, Stern RC, Bertino JS, Myers CM, Yamashita TS, Blumer JL. 1984. Dosing implications of rapid elimination of trimethoprim-sulfamethoxazole in patients with cystic fibrosis. *J Pediatr* 104:303–307.
85. Beringer PM, Vinks AATMM, Jelliffe RW, Shapiro BJ. 2000. Pharmacokinetics of tobramycin in adults with cystic fibrosis: implications for once-daily administration. *Antimicrob Agents Chemother* 44:809–813.
86. Touw DJ, Vinks AA, Heijerman HG, Bakker W. 1993. Validation of tobramycin monitoring in adolescent and adult patients with cystic fibrosis. *Ther Drug Monit* 15:52–59.

87. Albrecht LM, Rybak MJ, Boike SC, Pancorbo S. 1988. Comparison of serum sampling methods for determining vancomycin dosage regimens. *Ther Drug Monit* 10:85–90.
88. Locatelli M, Ciavarella MT, Paolino D, Celia C, Fiscarelli E, Ricciotti G, Pompilio A, Di Bonaventura G, Grande R, Zengin G, Di Marzio L. 2015. Determination of ciprofloxacin and levofloxacin in human sputum collected from cystic fibrosis patients using microextraction by packed sorbent-high performance liquid chromatography photodiode array detector. *J Chromatogr A* 1419:58–66.
89. Geller DE, Flume PA, Griffith DC, Morgan E, White D, Loutit JS, Dudley MN. 2011. Pharmacokinetics and safety of MP-376 (levofloxacin inhalation solution) in cystic fibrosis subjects. *Antimicrob Agents Chemother*.
90. Kidd TJ, Canton R, Ekkelenkamp M, Johansen HK, Gilligan P, LiPuma JJ, Bell SC, Elborn JS, Flume PA, VanDevanter DR, Waters VJ. 2018. Defining antimicrobial resistance in cystic fibrosis. *J Cyst Fibros* 17:696–704.
91. Akiyoshi Tsuji, Yasuko Kaneko, Kuniko Takahashi, Masatoshi Ogawa, Sachiko Goto. 1982. The effects of temperature and pH on the growth of eight enteric and nine glucose non-fermenting species of Gram-negative rods. *Microl Immunolg* 26:15–24.
92. Quinn RA, Comstock W, Zhang T, Morton JT, da Silva R, Tran A, Aksakov A, Nothias L-F, Wangpraseurt D, Melnik AV. 2018. Niche partitioning of a pathogenic microbiome driven by chemical gradients. *Sci Adv* 4:eaau1908.

93. Heirali AA, Acosta N, Storey DG, Workentine ML, Somayaji R, Laforest-Lapointe I, Leung W, Quon BS, Berthiaume Y, Rabin HR, Waddell BJ, Rossi L, Surette MG, Parkins MD. 2019. The effects of cycled inhaled aztreonam on the cystic fibrosis (CF) lung microbiome. *J Cyst Fibros* 18:829–837.
94. Carmody LA, Caverly LJ, Foster BK, Rogers MAM, Kalikin LM, Simon RH, VanDevanter DR, LiPuma JJ. 2018. Fluctuations in airway bacterial communities associated with clinical states and disease stages in cystic fibrosis. *PLOS ONE* 13:e0194060.
95. Whelan FJ, Heirali AA, Rossi L, Rabin HR, Parkins MD, Surette MG. 2017. Longitudinal sampling of the lung microbiota in individuals with cystic fibrosis. *PLOS ONE* 12:e0172811.
96. Cuthbertson L, Rogers GB, Walker AW, Oliver A, Green LE, Daniels TWV, Carroll MP, Parkhill J, Bruce KD, van der Gast CJ. 2016. Respiratory microbiota resistance and resilience to pulmonary exacerbation and subsequent antimicrobial intervention. *ISME J* 10:1081–1091.
97. Fodor AA, Klem ER, Gilpin DF, Elborn JS, Boucher RC, Tunney MM, Wolfgang MC. 2012. The adult cystic fibrosis airway microbiota is stable over time and infection type, and highly resilient to antibiotic treatment of exacerbations. *PLOS ONE* 7:e45001.
98. Zhao J, Schloss PD, Kalikin LM, Carmody LA, Foster BK, Petrosino JF, Cavalcoli JD, VanDevanter DR, Murray S, Li JZ, Young VB, LiPuma JJ. 2012. Decade-long bacterial community dynamics in cystic fibrosis airways. *Proc Natl Acad Sci U S A* 109:5809–5814.

99. Grigoryan L, Germanos G, Zoorob R, Juneja S, Raphael JL, Paasche-Orlow MK, Trautner BW. 2019. Use of antibiotics without a prescription in the U.S. population: A scoping review. *Ann Intern Med* 171:257.
100. Gao B, Gallagher T, Zhang Y, Elbadawi-Sidhu M, Lai Z, Fiehn O, Whiteson KL. 2018. Tracking polymicrobial metabolism in cystic fibrosis airways: *Pseudomonas aeruginosa* metabolism and physiology are influenced by *Rothia mucilaginosa*-derived metabolites. *mSphere* 3:e00151-18.
101. Blainey PC, Milla CE, Cornfield DN, Quake SR. 2012. Quantitative analysis of the human airway microbial ecology reveals a pervasive signature for cystic fibrosis. *Sci Transl Med* 4:153ra130–153ra130.
102. Lim YW, Schmieder R, Haynes M, Furlan M, Matthews TD, Whiteson K, Poole SJ, Hayes CS, Low DA, Maughan H. 2013. Mechanistic model of *Rothia mucilaginosa* adaptation toward persistence in the CF lung, based on a genome reconstructed from metagenomic data. *PLoS One* 8:e64285.
103. Ramsey MM, Rumbaugh KP, Whiteley M. 2011. Metabolite Cross-Feeding Enhances Virulence in a Model Polymicrobial Infection. *PLOS Pathog* 7:e1002012.
104. Flynn JM, Phan C, Hunter RC. 2017. Genome-Wide Survey of *Pseudomonas aeruginosa* PA14 Reveals a Role for the Glyoxylate Pathway and Extracellular Proteases in the Utilization of Mucin. *Infect Immun* 85:e00182-17.

105. Garg N, Wang M, Hyde E, da Silva RR, Melnik AV, Protsyuk I, Bouslimani A, Lim YW, Wong R, Humphrey G, Ackermann G, Spivey T, Brouha SS, Bandeira N, Lin GY, Rohwer F, Conrad DJ, Alexandrov T, Knight R, Dorrestein PC. 2017. Three-dimensional microbiome and metabolome cartography of a diseased human lung. *Cell Host Microbe* 22:705–716.e4.
106. Lee SA, Gallagher LA, Thongdee M, Staudinger BJ, Lippman S, Singh PK, Manoil C. 2015. General and condition-specific essential functions of *Pseudomonas aeruginosa*. *Proc Natl Acad Sci* 112:5189–5194.
107. Venkataraman A, Rosenbaum MA, Perkins SD, Werner JJ, Angenent LT. 2011. Metabolite-based mutualism between *Pseudomonas aeruginosa*PA14 and *Enterobacter aerogenes* enhances current generation in bioelectrochemical systems. *Energy Environ Sci* 4:4550–4559.
108. Bennett BD, Kimball EH, Gao M, Osterhout R, Van Dien SJ, Rabinowitz JD. 2009. Absolute metabolite concentrations and implied enzyme active site occupancy in *Escherichia coli*. *Nat Chem Biol* 5:593–599.
109. Somerville G, Mikoryak CA, Reitzer L. 1999. Physiological characterization of *Pseudomonas aeruginosa* during exotoxin A synthesis: glutamate, iron limitation, and aconitase activity. *J Bacteriol* 181:1072–1078.
110. Köhler T, Curty LK, Barja F, Delden C van, Pechère J-C. 2000. Swarming of *Pseudomonas aeruginosa* Is Dependent on Cell-to-Cell Signaling and Requires Flagella and Pili. *J Bacteriol* 182:5990–5996.

111. Basu Roy A, Sauer K. 2014. Diguanylate cyclase NicD-based signalling mechanism of nutrient-induced dispersion by *Pseudomonas aeruginosa*. *Mol Microbiol* 94:771–793.
112. Helling RB. 1998. Pathway Choice in Glutamate Synthesis in *Escherichia coli*. *J Bacteriol* 180:4571–4575.
113. Phan J, Meinardi S, Barletta B, Blake DR, Whiteson K. 2017. Stable isotope profiles reveal active production of VOCs from human-associated microbes. *J Breath Res* 11:017101.
114. Gallagher T, Phan J, Oliver A, Chase AB, England WE, Wandro S, Hendrickson C, Riedel SF, Whiteson K. 2019. Cystic Fibrosis-Associated *Stenotrophomonas maltophilia* Strain-Specific Adaptations and Responses to pH. *J Bacteriol* 201.
115. Rousk J, Bååth E, Brookes PC, Lauber CL, Lozupone C, Caporaso JG, Knight R, Fierer N. 2010. Soil bacterial and fungal communities across a pH gradient in an arable soil. *ISME J* 4:1340–1351.
116. Noyes N, Cho K-C, Ravel J, Forney LJ, Abdo Z. 2018. Associations between sexual habits, menstrual hygiene practices, demographics and the vaginal microbiome as revealed by Bayesian network analysis. *PLOS ONE* 13:e0191625.
117. Ilhan ZE, Marcus AK, Kang D-W, Rittmann BE, Krajmalnik-Brown R. 2017. pH-Mediated Microbial and Metabolic Interactions in Fecal Enrichment Cultures. *mSphere* 2.

118. Martiny JBH, Jones SE, Lennon JT, Martiny AC. 2015. Microbiomes in light of traits: A phylogenetic perspective. *Science* 350:aac9323.
119. García-Quintáns N, Repizo G, Martín M, Magni C, López P. 2008. Activation of the Diacetyl/Acetoin Pathway in *Lactococcus lactis* subsp. *lactis* bv. *diacetylactis* CRL264 by Acidic Growth. *Appl Environ Microbiol* 74:1988–1996.
120. Ratzke C, Gore J. 2018. Modifying and reacting to the environmental pH can drive bacterial interactions. *PLOS Biol* 16:e2004248.
121. Jaffar-Bandjee MC, Lazdunski A, Bally M, Carrère J, Chazalette JP, Galabert C. 1995. Production of elastase, exotoxin A, and alkaline protease in sputa during pulmonary exacerbation of cystic fibrosis in patients chronically infected by *Pseudomonas aeruginosa*. *J Clin Microbiol* 33:924–929.
122. Verhoogt HJ, Smit H, Abbe T, Gamper M, Driessen AJ, Haas D, Konings WN. 1992. *arcD*, the first gene of the *arc* operon for anaerobic arginine catabolism in *Pseudomonas aeruginosa*, encodes an arginine-ornithine exchanger. *J Bacteriol* 174:1568–1573.
123. Parkins MD, Floto RA. 2015. Emerging bacterial pathogens and changing concepts of bacterial pathogenesis in cystic fibrosis. *J Cyst Fibros* 14:293–304.
124. Salsgiver EL, Fink AK, Knapp EA, LiPuma JJ, Olivier KN, Marshall BC, Saiman L. 2016. Changing Epidemiology of the Respiratory Bacteriology of Patients With Cystic Fibrosis. *Chest* 149:390–400.

125. Kolpen M, Kragh KN, Bjarnsholt T, Line L, Hansen CR, Dalbøge CS, Hansen N, Kühl M, Høiby N, Jensen PØ. 2015. Denitrification by cystic fibrosis pathogens – *Stenotrophomonas maltophilia* is dormant in sputum. *Int J Med Microbiol* 305:1–10.
126. Pompilio A, Crocetta V, Ghosh D, Chakrabarti M, Gherardi G, Vitali LA, Fiscarelli E, Di Bonaventura G. 2016. *Stenotrophomonas maltophilia* Phenotypic and Genotypic Diversity during a 10-year Colonization in the Lungs of a Cystic Fibrosis Patient. *Front Microbiol* 7.
127. Waters V, Atenafu EG, Lu A, Yau Y, Tullis E, Ratjen F. 2013. Chronic *Stenotrophomonas maltophilia* infection and mortality or lung transplantation in cystic fibrosis patients. *J Cyst Fibros* 12:482–486.
128. Esposito A, Pompilio A, Bettua C, Crocetta V, Giacobazzi E, Fiscarelli E, Jousson O, Di Bonaventura G. 2017. Evolution of *Stenotrophomonas maltophilia* in Cystic Fibrosis Lung over Chronic Infection: A Genomic and Phenotypic Population Study. *Front Microbiol* 8.
129. Steinmann J, Mamat U, Abda EM, Kirchhoff L, Streit WR, Schaible UE, Niemann S, Kohl TA. 2018. Analysis of Phylogenetic Variation of *Stenotrophomonas maltophilia* Reveals Human-Specific Branches. *Front Microbiol* 9.
130. Cornforth DM, Dees JL, Ibberson CB, Huse HK, Mathiesen IH, Kirketerp-Møller K, Wolcott RD, Rumbaugh KP, Bjarnsholt T, Whiteley M. 2018. *Pseudomonas aeruginosa* transcriptome during human infection. *Proc Natl Acad Sci* 201717525.

131. Lim YW, Schmieder R, Haynes M, Willner D, Furlan M, Youle M, Abbott K, Edwards R, Evangelista J, Conrad D. 2013. Metagenomics and metatranscriptomics: windows on CF-associated viral and microbial communities. *J Cyst Fibros* 12:154–164.
132. Overbeek, R., Olson, R., Pusch, G.D., Olsen, G.J. 2013. SEED and the Rapid Annotation of microbial genomes using Subsystems Technology (RAST). *Nucleic Acids Res* 42:D206–D214.
133. Baudoux, P., Bles, N., Lemaire, S., Mingeot-Leclercq, M. P., Tulkens, P. M., Van Bambeke, F. Combined effect of pH and concentration on the activities of gentamicin and oxacillin against *Staphylococcus aureus* in pharmacodynamic models of extracellular and intracellular infections. *J Antimicrob Chemother* 59:246–253.
134. Stancik LM, Stancik DM, Schmidt B, Barnhart DM, Yoncheva YN, Slonczewski JL. 2002. pH-Dependent Expression of Periplasmic Proteins and Amino Acid Catabolism in *Escherichia coli*. *J Bacteriol* 184:4246–4258.
135. Romano A, Ladero V, Alvarez MA, Lucas PM. 2014. Putrescine production via the ornithine decarboxylation pathway improves the acid stress survival of *Lactobacillus brevis* and is part of a horizontally transferred acid resistance locus. *Int J Food Microbiol* 175:14–19.
136. Wattam AR, Abraham D, Dalay O, Disz TL, Driscoll T, Gabbard JL, Gillespie JJ, Gough R, Hix D, Kenyon R, Machi D, Mao C, Nordberg EK, Olson R, Overbeek R, Pusch GD, Shukla M, Schulman J, Stevens RL, Sullivan DE, Vonstein V, Warren A, Will R, Wilson MJC, Yoo

- HS, Zhang C, Zhang Y, Sobral BW. 2014. PATRIC, the bacterial bioinformatics database and analysis resource. *Nucleic Acids Res* 42:D581-591.
137. Kidd TJ, Ritchie SR, Ramsay KA, Grimwood K, Bell SC, Rainey PB. 2012. *Pseudomonas aeruginosa* Exhibits Frequent Recombination, but Only a Limited Association between Genotype and Ecological Setting. *PLOS ONE* 7:e44199.
138. Cramer N, Wiehlmann L, Tümmler B. 2010. Clonal epidemiology of *Pseudomonas aeruginosa* in cystic fibrosis. *Int J Med Microbiol* 300:526–533.
139. Marvig RL, Johansen HK, Molin S, Jelsbak L. 2013. Genome Analysis of a Transmissible Lineage of *Pseudomonas aeruginosa* Reveals Pathoadaptive Mutations and Distinct Evolutionary Paths of Hypermutators. *PLOS Genet* 9:e1003741.
140. Römling U, Wingender J, Müller H, Tümmler B. 1994. A major *Pseudomonas aeruginosa* clone common to patients and aquatic habitats. *Appl Environ Microbiol* 60:1734–1738.
141. Marvig RL, Damkiær S, Khademi SMH, Markussen TM, Molin S, Jelsbak L. 2014. Within-Host Evolution of *Pseudomonas aeruginosa* Reveals Adaptation toward Iron Acquisition from Hemoglobin. *mBio* 5:e00966-14.
142. Hunter RC, Asfour F, Dingemans J, Osuna BL, Samad T, Malfroot A, Cornelis P, Newman DK. 2013. Ferrous Iron Is a Significant Component of Bioavailable Iron in Cystic Fibrosis Airways. *mBio* 4:e00557-13.

143. Pezzulo AA, Tang XX, Hoegger MJ, Abou Alaiwa MH, Ramachandran S, Moninger TO, Karp PH, Wohlford-Lenane CL, Haagsman HP, van Eijk M, Bánfi B, Horswill AR, Stoltz DA, McCray PB, Welsh MJ, Zabner J. 2012. Reduced airway surface pH impairs bacterial killing in the porcine cystic fibrosis lung. *Nature* 487:109–113.
144. Finn RD, Clements J, Eddy SR. 2011. HMMER web server: interactive sequence similarity searching. *Nucleic Acids Res* 39:W29–W37.
145. Price MN, Dehal PS, Arkin AP. 2010. FastTree 2—approximately maximum-likelihood trees for large alignments. *PloS One* 5:e9490.
146. Hyatt D, Chen G-L, LoCascio PF, Land ML, Larimer FW, Hauser LJ. 2010. Prodigal: prokaryotic gene recognition and translation initiation site identification. *BMC Bioinformatics* 11:119.
147. Seemann T. 2014. Prokka: rapid prokaryotic genome annotation. *Bioinformatics* 30:2068–2069.
148. Page AJ, Cummins CA, Hunt M, Wong VK, Reuter S, Holden MT, Fookes M, Falush D, Keane JA, Parkhill J. 2015. Roary: rapid large-scale prokaryote pan genome analysis. *Bioinformatics* 31:3691–3693.
149. Sievers F, Higgins DG. 2014. Clustal Omega, Accurate Alignment of Very Large Numbers of Sequences, p. 105–116. *In* Multiple Sequence Alignment Methods. Humana Press, Totowa, NJ.

150. Stamatakis A. 2014. RAxML version 8: a tool for phylogenetic analysis and post-analysis of large phylogenies. *Bioinformatics* 30:1312–1313.
151. Letunic I, Bork P. 2006. Interactive Tree Of Life (iTOL): an online tool for phylogenetic tree display and annotation. *Bioinformatics* 23:127–128.
152. Wandro S, Carmody L, Gallagher T, LiPuma JJ, Whiteson K. 2017. Making it last: storage time and temperature have differential impacts on metabolite profiles of airway samples from cystic fibrosis patients. *MSystems* 2:e00100–17.
153. Fiehn O. 2016. Metabolomics by Gas Chromatography–Mass Spectrometry: Combined Targeted and Untargeted Profiling. *Current Protocols in Molecular Biology*. John Wiley & Sons, Inc.
154. Bolger AM, Lohse M, Usadel B. 2014. Trimmomatic: a flexible trimmer for Illumina sequence data. *Bioinformatics* 30:2114–2120.
155. Zhang J, Kobert K, Flouri T, Stamatakis A. 2013. PEAR: a fast and accurate Illumina Paired-End reAd mergeR. *Bioinformatics* 30:614–620.
156. Langmead B, Salzberg SL. 2012. Fast gapped-read alignment with Bowtie 2. *Nat Methods* 9:357–359.
157. Anders S, Pyl PT, Huber W. 2015. HTSeq—a Python framework to work with high-throughput sequencing data. *Bioinformatics* 31:166–169.

158. Robinson MD, McCarthy DJ, Smyth GK. 2010. edgeR: a Bioconductor package for differential expression analysis of digital gene expression data. *Bioinformatics* 26:139–140.
159. Schmieder R, Edwards R. 2011. Quality control and preprocessing of metagenomic datasets. *Bioinformatics* 27:863–864.
160. Worlitzsch D, Tarran R, Ulrich M, Schwab U, Cekici A, Meyer KC, Birrer P, Bellon G, Berger J, Weiss T, Botzenhart K, Yankaskas JR, Randell S, Boucher RC, Döring G. 2002. Effects of reduced mucus oxygen concentration in airway *Pseudomonas* infections of cystic fibrosis patients. *J Clin Invest* 109:317–325.
161. Kolpen M, Lerche CJ, Kragh KN, Sams T, Koren K, Jensen AS, Line L, Bjarnsholt T, Ciofu O, Moser C, Kühl M, Høiby N, Jensen PØ. 2017. Hyperbaric Oxygen Sensitizes Anoxic *Pseudomonas aeruginosa* Biofilm to Ciprofloxacin. *Antimicrob Agents Chemother* 61.
162. Line L, Alhede M, Kolpen M, Kühl M, Ciofu O, Bjarnsholt T, Moser C, Toyofuku M, Nomura N, Høiby N, Jensen PØ. 2014. Physiological levels of nitrate support anoxic growth by denitrification of *Pseudomonas aeruginosa* at growth rates reported in cystic fibrosis lungs and sputum. *Front Microbiol* 5.
163. Palmer KL, Brown SA, Whiteley M. 2007. Membrane-Bound Nitrate Reductase Is Required for Anaerobic Growth in Cystic Fibrosis Sputum. *J Bacteriol* 189:4449–4455.
164. Price-Whelan A, Dietrich LEP, Newman DK. 2006. Rethinking “secondary” metabolism: physiological roles for phenazine antibiotics. *Nat Chem Biol* 2:71–78.

165. Glasser NR, Kern SE, Newman DK. Phenazine redox cycling enhances anaerobic survival in *Pseudomonas aeruginosa* by facilitating generation of ATP and a proton-motive force. *Mol Microbiol* 92:399–412.
166. Wang Y, Newman DK. 2008. Redox reactions of phenazine antibiotics with ferric (hydr) oxides and molecular oxygen. *Environ Sci Technol* 42:2380–2386.
167. Hall S, McDermott C, Anoopkumar-Dukie S, McFarland AJ, Forbes A, Perkins AV, Davey AK, Chess-Williams R, Kiefel MJ, Arora D, Grant GD. 2016. Cellular Effects of Pyocyanin, a Secreted Virulence Factor of *Pseudomonas aeruginosa*. *Toxins* 8.
168. Lau GW, Ran H, Kong F, Hassett DJ, Mavrodi D. 2004. *Pseudomonas aeruginosa* Pyocyanin Is Critical for Lung Infection in Mice. *Infect Immun* 72:4275–4278.
169. Sullivan NL, Tzeranis DS, Wang Y, So PTC, Newman D. 2011. Quantifying the Dynamics of Bacterial Secondary Metabolites by Spectral Multiphoton Microscopy. *ACS Chem Biol* 6:893–899.
170. Dvornikov A, Malacrida L, Gratton E. 2019. The DIVER Microscope for Imaging in Scattering Media. *2. Methods Protoc* 2:53.
171. Crosignani V, Jahid S, Dvornikov A, Gratton E. 2014. Deep tissue imaging by enhanced photon collection. *J Innov Opt Health Sci* 07:1450034.
172. Perinbam K, Chacko JV, Kannan A, Digman MA, Siryaporn A. 2020. A Shift in Central Metabolism Accompanies Virulence Activation in *Pseudomonas aeruginosa*. *mBio* 11.

173. Bhattacharjee A, Datta R, Gratton E, Hochbaum AI. 2017. Metabolic fingerprinting of bacteria by fluorescence lifetime imaging microscopy. *1. Sci Rep* 7:1–10.
174. Stringari C, Cinquin A, Cinquin O, Digman MA, Donovan PJ, Gratton E. 2011. Phasor approach to fluorescence lifetime microscopy distinguishes different metabolic states of germ cells in a live tissue. *Proc Natl Acad Sci* 108:13582–13587.
175. Ranjit S, Malacrida L, Stakic M, Gratton E. 2019. Determination of the metabolic index using the fluorescence lifetime of free and bound nicotinamide adenine dinucleotide using the phasor approach. *J Biophotonics* 12:e201900156.
176. Lakowicz JR, Szmacinski H, Nowaczyk K, Johnson ML. 1992. Fluorescence lifetime imaging of free and protein-bound NADH. *Proc Natl Acad Sci* 89:1271–1275.
177. Digman MA, Caiolfa VR, Zamai M, Gratton E. 2008. The Phasor Approach to Fluorescence Lifetime Imaging Analysis. *Biophys J* 94:L14–L16.
178. Fereidouni F, Bader AN, Gerritsen HC. 2012. Spectral phasor analysis allows rapid and reliable unmixing of fluorescence microscopy spectral images. *Opt Express* 20:12729–12741.
179. Vallmitjana A, Dvornikov A, Torrado B, Jameson DM, Ranjit S, Gratton E. 2020. Resolution of 4 components in the same pixel in FLIM images using the phasor approach. *Methods Appl Fluoresc* 8:035001.

180. Jameson DM, Thomas V, Zhou D. 1989. Time-resolved fluorescence studies on NADH bound to mitochondrial malate dehydrogenase. *Biochim Biophys Acta BBA-Protein Struct Mol Enzymol* 994:187–190.
181. Kopf SH, Sessions AL, Cowley ES, Reyes C, Sambeek LV, Hu Y, Orphan VJ, Kato R, Newman DK. 2016. Trace incorporation of heavy water reveals slow and heterogeneous pathogen growth rates in cystic fibrosis sputum. *Proc Natl Acad Sci* 113:E110–E116.
182. Cierniecki JA, Newman DK. 2020. The Potential for Redox-Active Metabolites To Enhance or Unlock Anaerobic Survival Metabolisms in Aerobes. *J Bacteriol* 202.
183. Whiteley M, Lee KM, Greenberg EP. 1999. Identification of genes controlled by quorum sensing in *Pseudomonas aeruginosa*. *Proc Natl Acad Sci* 96:13904–13909.
184. Déziel E, Lépine F, Milot S, He J, Mindrinos MN, Tompkins RG, Rahme LG. 2004. Analysis of *Pseudomonas aeruginosa* 4-hydroxy-2-alkylquinolines (HAQs) reveals a role for 4-hydroxy-2-heptylquinoline in cell-to-cell communication. *Proc Natl Acad Sci* 101:1339–1344.
185. Parsons JF, Greenhagen BT, Shi K, Calabrese K, Robinson H, Ladner JE. 2007. Structural and Functional Analysis of the Pyocyanin Biosynthetic Protein PhzM from *Pseudomonas aeruginosa*. *Biochemistry* 46:1821–1828.

186. Eschbach M, Schreiber K, Trunk K, Buer J, Jahn D, Schobert M. 2004. Long-Term Anaerobic Survival of the Opportunistic Pathogen *Pseudomonas aeruginosa* via Pyruvate Fermentation. *J Bacteriol* 186:4596–4604.
187. Glasser NR, Wang BX, Hoy JA, Newman DK. 2017. The pyruvate and α -ketoglutarate dehydrogenase complexes of *Pseudomonas aeruginosa* catalyze pyocyanin and phenazine-1-carboxylic acid reduction via the subunit dihydrolipoamide dehydrogenase. *J Biol Chem* jbc.M116.772848.
188. Das T, Kutty SK, Kumar N, Manefield M. 2013. Pyocyanin Facilitates Extracellular DNA Binding to *Pseudomonas aeruginosa* Influencing Cell Surface Properties and Aggregation. *PLoS ONE* 8.
189. Saunders SH, Edmund CM, Yates MD, Otero FJ, Trammell SA, Stemp ED, Barton JK, Tender LM, Newman DK. 2019. Extracellular DNA promotes efficient extracellular electron transfer by pyocyanin in *Pseudomonas aeruginosa* biofilms. *bioRxiv*.
190. Ranjit S, Malacrida L, Jameson DM, Gratton E. 2018. Fit-free analysis of fluorescence lifetime imaging data using the phasor approach. *Nat Protoc* 13:1979–2004.
191. Chacko JV, Eliceiri KW. 2019. Autofluorescence lifetime imaging of cellular metabolism: Sensitivity toward cell density, pH, intracellular, and intercellular heterogeneity. *Cytometry A* 95:56–69.

192. Ma N, Digman MA, Malacrida L, Gratton E. 2016. Measurements of absolute concentrations of NADH in cells using the phasor FLIM method. *Biomed Opt Express* 7:2441–2452.
193. Neelakshi G. 2008. Studies on the structure and function of phenazine modifying enzymes PhzM and PhzS involved in the biosynthesis of pyocyanin. Department of Chemistry, University of Dortmund.
194. Crosignani V, Dvornikov AS, Gratton E. 2011. Enhancement of imaging depth in turbid media using a wide area detector. *J Biophotonics* 4:592–599.
195. Ranjit S, Malacrida L, Gratton E. 2018. Differences between FLIM phasor analyses for data collected with the Becker and Hickl SPC830 card and with the FLIMbox card. *Microsc Res Tech* 81:980–989.
196. 2018. A simplicial homology algorithm for Lipschitz optimisation | SpringerLink. *J Glob Optim* 72:181–217.
197. Abeles SR, Jones MB, Santiago-Rodriguez TM, Ly M, Klitgord N, Yooseph S, Nelson KE, Pride DT. 2016. Microbial diversity in individuals and their household contacts following typical antibiotic courses. *Microbiome* 4:39.
198. Bacci G, Taccetti G, Dolce D, Armanini F, Segata N, Cesare FD, Lucidi V, Fiscarelli E, Morelli P, Casciaro R, Negroni A, Mengoni A, Bevvivino A. 2019. Taxonomic and functional dynamics of lung microbiome in cystic fibrosis patients chronically infected with *Pseudomonas aeruginosa*. *bioRxiv* 609057.

199. Whiteson KL, Meinardi S, Lim YW, Schmieder R, Maughan H, Quinn R, Blake DR, Conrad D, Rohwer F. 2014. Breath gas metabolites and bacterial metagenomes from cystic fibrosis airways indicate active pH neutral 2,3-butanedione fermentation. ISME J 8:1247.
200. Tunney MM, Field TR, Moriarty TF, Patrick S, Doering G, Muhlebach MS, Wolfgang MC, Boucher R, Gilpin DF, McDowell A. 2008. Detection of anaerobic bacteria in high numbers in sputum from patients with cystic fibrosis. Am J Respir Crit Care Med 177:995–1001.
201. Lim YW, Schmieder R, Haynes M, Willner D, Furlan M, Youle M, Abbott K, Edwards R, Evangelista J, Conrad D, Rohwer F. 2013. Metagenomics and metatranscriptomics: Windows on CF-associated viral and microbial communities. J Cyst Fibros 12:154–164.
202. Pienkowska K, Wiehlmann L, Tümmeler B. 2019. Metagenome inferred bacterial replication rates in cystic fibrosis airways. J Cyst Fibros Off J Eur Cyst Fibros Soc 18:653–656.
203. Whelan FJ, Waddell B, Syed SA, Shekarriz S, Rabin HR, Parkins MD, Surette MG. 2020. Culture-enriched metagenomic sequencing enables in-depth profiling of the cystic fibrosis lung microbiota. Nat Microbiol 5:379–390.
204. Forier K, Van Heck V, Carlier M, Van Braeckel E, Van Daele S, De Baets F, Schelstraete P, Haerynck F, Stove V, Van Simaey L, Vaneechoutte M, Verstraete AG. 2018. Development and validation of an LC tandem MS assay for the quantification of β -

- lactam antibiotics in the sputum of cystic fibrosis patients. *J Antimicrob Chemother* 73:95–101.
205. Wilms, EB, Touw, DJ, Heijerman, HG. 2006. Pharmacokinetics of azithromycin in plasma, blood, polymorphonuclear neutrophils and sputum during long-term therapy in patients with cystic fibrosis. *Ther Drug Monit* 28:219–25.
206. Passero MA, Remor B, Salomon J. 1981. Patient-reported compliance with cystic fibrosis therapy. *Clin Pediatr (Phila)* 20:264–268.
207. Clement A, Tamalet A, Leroux E, Ravilly S, Fauroux B, Jais J-P. 2006. Long term effects of azithromycin in patients with cystic fibrosis: A double blind, placebo controlled trial. *Thorax* 61:895–902.
208. Mogayzel PJ, Naureckas ET, Robinson KA, Mueller G, Hadjiliadis D, Hoag JB, Lubsch L, Hazle L, Sabadosa K, Marshall B. 2013. Cystic fibrosis pulmonary guidelines. *Am J Respir Crit Care Med* 187:680–689.
209. McCormack J, Bell S, Senini S, Walmsley K, Patel K, Wainwright C, Serisier D, Harris M, Bowler S. 2007. Daily versus weekly azithromycin in cystic fibrosis patients. *Eur Respir J* 30:487–495.
210. Wildfeuer A, Laufen H, Zimmermann T. 1996. Uptake of azithromycin by various cells and its intracellular activity under in vivo conditions. *Antimicrob Agents Chemother* 40:75–79.

211. Riediker S, Rytz A, Stadler RH. 2004. Cold-temperature stability of five β -lactam antibiotics in bovine milk and milk extracts prepared for liquid chromatography–electrospray ionization tandem mass spectrometry analysis. *J Chromatogr A* 1054:359–363.
212. Touw DJ, Jacobs FA, Brimicombe RW, Heijerman HG, Bakker W, Briemer DD. 1997. Pharmacokinetics of aerosolized tobramycin in adult patients with cystic fibrosis. *Antimicrob Agents Chemother* 41:184–187.
213. Mukhopadhyay S, Staddon GE, Eastman C, Palmer M, Davies ER, Carswell F. 1994. The quantitative distribution of nebulized antibiotic in the lung in cystic fibrosis. *Respir Med* 88:203–211.
214. Melnik AV, Vázquez-Baeza Y, Aksnov AA, Hyde E, McAvoy AC, Wang M, Silva RR da, Protsyuk I, Wu JV, Bouslimani A, Lim YW, Luzzatto-Knaan T, Comstock W, Quinn RA, Wong R, Humphrey G, Ackermann G, Spivey T, Brouha SS, Bandeira N, Lin GY, Rohwer F, Conrad DJ, Alexandrov T, Knight R, Dorrestein PC, Garg N. 2019. Molecular and microbial microenvironments in chronically diseased lungs associated with cystic fibrosis. *mSystems* 4.
215. Odenholt I. 2001. Pharmacodynamic effects of subinhibitory antibiotic concentrations. *Int J Antimicrob Agents* 17:1–8.
216. Wright EA, Fothergill JL, Paterson S, Brockhurst MA, Winstanley C. 2013. Sub-inhibitory concentrations of some antibiotics can drive diversification of

Pseudomonas aeruginosa populations in artificial sputum medium. BMC Microbiol 13:170.

217. Clinical Laboratory and Standards Institute. 2018. Performance standards for antimicrobial disk susceptibility tests, 13th ed.
218. Want EJ, Masson P, Michopoulos F, Wilson ID, Theodoridis G, Plumb RS, Shockcor J, Loftus N, Holmes E, Nicholson JK. 2013. Global metabolic profiling of animal and human tissues via UPLC-MS. 1. Nat Protoc 8:17–32.
219. Leemans SW, Dvornikov A, Gallagher T, Gratton E. 2020. AO-DIVER Advances the Depth Limits of Multiphoton Microscopy in Scattering Media. Biophys J 118:307a.
220. Leung HM, Birket SE, Hyun C, Ford TN, Cui D, Solomon GM, Shei R-J, Adewale AT, Lenzie AR, Fernandez-Petty CM, Zheng H, Palermo JH, Cho D-Y, Woodworth BA, Yonker LM, Hurley BP, Rowe SM, Tearney GJ. 2019. Intranasal micro-optical coherence tomography imaging for cystic fibrosis studies. Sci Transl Med 11.
221. Sameni S, Syed A, Marsh JL, Digman MA. 2016. The phasor-FLIM fingerprints reveal shifts from OXPHOS to enhanced glycolysis in Huntington Disease. 1. Sci Rep 6:34755.
222. Trinh AL, Chen H, Chen Y, Hu Y, Li Z, Siegel ER, Linskey ME, Wang PH, Digman MA, Zhou Y-H. 2017. Tracking Functional Tumor Cell Subpopulations of Malignant Glioma by Phasor Fluorescence Lifetime Imaging Microscopy of NADH. 12. Cancers 9:168.
223. Dvornikov A, Gratton E. 2018. Hyperspectral imaging in highly scattering media by the spectral phasor approach using two filters. Biomed Opt Express 9:3503–3511.

224. Nelson MT, Pope CE, Marsh RL, Wolter DJ, Weiss EJ, Hager KR, Vo AT, Brittnacher MJ, Radey MC, Hayden HS, Eng A, Miller SI, Borenstein E, Hoffman LR. 2019. Human and Extracellular DNA Depletion for Metagenomic Analysis of Complex Clinical Infection Samples Yields Optimized Viable Microbiome Profiles. *Cell Rep* 26:2227-2240.e5.